INVESTIGATIONS INTO VIBRATION AND SOUND TRANSMISSION

CHARACTERISTICS OF CYLINDRICAL SHELLS

by

ANKIM VEERA SWAMY

A Thesis Submitted in Fulfilment of the

Requirement for the degree of

Doctor of Philosophy

Faculty of Engineering

The University of Aston in Birmingham

DECEMBER 1972

SUMMARY

This thesis describes an analytical and experimental study of the relationship between cylinder wall vibration and the resultant acoustic energy generated inside an enclosed stiffened cylinder representative of an aircraft fuselage.

The work included measuring vibration and noise transmission properties of models simulating a fuselage. The results from these tests were used in the analytical predictions.

Experimental facilities were developed for this work to measure parameters such as space average vibration and sound pressure levels, structural damping, transmission loss together with other relative parameters.

Three cylindrical shell configurations were tested. Extensive experimental measurements were carried out to study various effects which are reported on noise and vibration characteristics. An emphirical approach was taken, to account for the internal loss factor. With this approach, a significant improvement was obtained in the comparison between analysis and experiment.

A relationship between the cylinder wall vibration and noise transmission characteristics were measured for both acoustical and mechanical forms of excitation. Below the ring frequency there was no direct comparison between the two measurements.

Computer programs were developed for the theoretical study of natural frequencies of cylinders and plates, and results are presented in the form of graphs and tables.

Statistical energy analysis was used for the theoretical study of energy and noise transmission. A comparison of analytical and experimental results, whilst showing a good agreement between 2.5 kHz to 10 kHz did not give such a result in the vicinity of 600 Hz to 2.5 kHz.

ACKNOWLEDGEMENT

I wish to thank Professor E. Downham, Department of Mechanical Engineering, for his ready and willing help, valuable advice and encouragement throughout the course of this work, to his Secretary, Mrs. D. Scott, for her cooperation and typing of this thesis.

My thanks are also extended to the technical staff of the Department of Mechanical Engineering, in particular Ian Redfern for his contribution in the experimental work. To Mr. G. Noland of The Regional Computer Services, Manchester, and to Mr. N. Bilenky of the Institution of the Marine Engineers for their interest and help.

I acknowledge the financial support given to this project by the Ministry of Defence, Procurement Executive.

Sincere thanks are also due, to those closely associated with me, during the course of this work.

CONTENTS

Page

LIST OF FIGURES

LIST OF SYMBOLS

A	= Cross-sectional area of stiffener
A_s	= Structural surface area
a	= Length of cylinder of plate
b	= Width of plate
C_a	= Speed of sound in air
D	= Flexural stiffness of isotropic plate or isotropic cylinder wall, $Et^3/12(1-\mu^2)$
d	= Stringer spacing
E	= Young's modulus
E_i	= Total energy in i^{th} system
f	= Frequency = $\omega/2\pi$
f_c	= Critical or Coincidence frequency
f_r	= Ring frequency
G	= Shear modulus
g	= Acceleration due to gravity
I	= Moment of inertia of stiffener about its centroid
I_o	= Moment of inertia of stiffener about middle surface of plate or cylinder
J	= Torsional constant for stiffener.
K_o, K_1, K_2	= Coefficients in frequency equation (freely supported ends)
ℓ	= Ring spacing
M	= Mass per unit area of cylinder or plate
M_s	= Total mass of structure
M_2	= Total mass of System 2.
M_x, M_y, M_{xy}, M_{yx}	= Moment results

m,n = Integers

N = Number of stringers

n_i = Modal density of i^{th} system

$n_s(\omega)$ = Modal density of structure in radian frequency

N_x, N_y, N_{xy} = Stress resultants

NR = Noise reduction

P_{in_i} = Power supplied to i^{th} system

P_{ij} = Power flow from i^{th} to j^{th} system

P_{diss_i} = Power dissipated internally by i^{th} system

R = Mean radius of cylinder

$\bar{R}$ = Nondimensional parameter, $E_r A_r / Et\ell$

R_{2TOT} = Total resistance of structure (cylinder wall)

R_{2int} = Internal resistance of structure (cylinder wall)

R_{2rad} = Radiation resistance of cylinder wall to whole space

$\bar{S}$ = Nondimensional parameter, $(a^2/Rt)(1-\mu^2)^{\frac{1}{2}}$

S_{a_2} = Spectral density of cylinder wall acceleration

S_a = Spectral density of structural acceleration

S_{p_1} = Spectral density of sound pressure in reverberant room

S_{p_3} = Spectral density of sound pressure in space enclosed by cylinder wall

T_i = Reverberation time of i^{th} system

TL = Transmission loss

t = Thickness of cylinder or plate material

u, v, w = displacement in x-, y-, and z- directions, respectively

V_1 = Volume of reverberant room

V_3 Volume of space enclosed by cylinder wall

x, y, z	= Orthogonal coordinates defined in sketch of Appendix 'C' (x, and y lie in middle surface of cylinder or plate)
Z	= Curvature parameter, $E_s A_s/Etd$
$\bar{Z}$	= Distance from middle surface of plate or cylinder to centroid of stringer
Π	= Potential energy
η_i	= Internal loss factor for i^{th} system
η_{ij}	= Coupling loss factor from i^{th} to j^{th} system
η_{rad}	= Radiation loss factor for cylinder wall to half space
η_{int}	= Internal loss factor for cylinder wall
β_1	= Energy decay constant of reverberant room
β_3	= Energy decay constant of space enclosed by cylinder wall
ρ	= Density of material
ρ_a	= Density of air
μ	= Poisson's Ratio
α, β	= Wavelength parameters
Δ	$= \dfrac{\rho a^2(1-\mu^2)4\pi^2 f^2}{Eg}$, frequency factor
∇^4	$= \nabla^2\nabla^2$, where ∇^2 is the laplacian operator in two dimensions
$\langle\ \rangle$	= Space-time average
ω	= Angular frequency
e_x, e_y, ν	= Middle-surface normal and shearing strains
$e_{xT}, e_{yT}, \nu_{xyT}$	= Total normal and shearing strains

Subscripts

c = Cylinder

r = Stiffening in y direction

s = Stiffening in x direction

p = plate

ω = Inertial load

1,2,3 = Systems - (room, structure, enclosed space)

CHAPTER ONE

CHAPTER ONE

INTRODUCTION

To understand either the effect of sound on a structure or the transmission of sound through a structure it is necessary first to understand the vibration characteristics of the structure. Whatever the nature of 'sound' whether random, 'white' noise, pure tone, or excitation which is not acoustic; the response of structures to such an excitation and the subsequent vibration and either radiation, transmission or both of these parameters are central to the field of acoustics. The applications of structural response studies are very broad. They include the response of missiles to environmental sound, building vibrations resulting from shock and sonic boom(26), transmission of noise through walls, and many others. The missile and aircraft problems are primarily problems associated with the structural response, the main problem areas being concerned with the fatigue of structures and environmental loads on equipment mounted within the structures. There is also the problem of acoustic noise transmission to the interior of aircraft cabins that are used for passenger and personal accommodation. The structure may vibrate resonantly or may be forced into non-resonant vibration where stiffness reactions predominate; they may be formed of flat plate, curved plates or both, and various forms of stiffening (stringers or rings) configurations will also influence the form of vibrational modes involved(10).

Clasically, vibration engineers have focussed their attention on low-frequency oscillation, since the lowest few vibration modes are generally the ones which are associated with the greatest deflections. However, the analytical techniques which have been developed for dealing with low-frequency vibration problems contain none which can deal simply and effectively with most high-frequency problems, such as those of importance in relation to sonically induced fatigue, instrumentation performance, or sound transmission.

Although the classical methods are valid in principle at all frequencies, their use is in fact very often impractical for high frequencies, particularly for randomly excited complex structures. The classical approach consists of determining the natural modes, of calculating the responses of these modes to a specified excitation of interest, and of superposing these responses to determine the total structural response. Continuous structures have an infinite number of modes, but generally only the lowest few of these are of importance in low frequency vibrations, so that in these cases one needs to consider only those few modes. At high frequencies, however, a frequency band of interest usually encompasses the resonances of a large number of modes, and one must consider the responses of all of these modes in calculating the structural vibration in that band and hence sound transmission.

In order to understand and estimate the significant properties of multimodal vibrations of complex systems, the Statistical Energy Analysis approach, pioneered by Lyon, Smith,Jr., and Dyer (2 to 9,14) was developed. In this analysis, the structure and its environments are described in terms of such parameters as modal density, damping,and radiation properties; whereas the dynamical quantities of interest are energy, mean square acceleration and mean square pressure. This approach was spawned by the realization that averaging initially and then carrying out calculations in terms of average quantities, should lead to results much more readily than the classical approach, which involves much initial detailed calculation and subsequent averaging.

A plain and uniformly stiffened cylindrical shell structure on Page (11), approximating to an aircraft fuselage was chosen to be a suitable model for theoretical and experimental study. The structure consisted of a combination of panels, stringers and rings. It can be considered representative of a fair proportion of the practical structures involved in vibration and noise transmission problems, having sufficient complications, and yet still being amenable to theoretical analysis. If such a structure is immersed in a reverberant sound field and the sound field is maintained within the space then the amount of energy that flows into the structure will depend on the degree of coupling between the structure and the sound field. The amount of energy which the structure will accept in any frequency band depends on how many modes will resonate in that frequency band and accept energy. Therefore, an average modal density for the structure (average number of resonance frequencies per unit bandwidth) must be ascertained (Chapter 4).

Once the energy has been accepted by the structure, it will either be dissipated internally and converted to heat or re-radiated back into the space in the form of sound. This loss of energy is expressed through a total damping which has contributions from radiation and from internal dissipation. There is no theoretical method for the prediction of internal dissipation factor(internal loss factor), therefore this value is determined from total and radiation loss factor (Chapter 5). The internal dissipation usually occurs at welds and other forms of joints, although it may be due to metal friction or hysteresis damping(11) in some instances.

In recent years new techniques have been developed for predicting the acoustic response and radiation properties of complicated structures (1 and 3). These techniques based on "Statistical Energy Method" have been primarily applied to predicting the noise and vibration levels in aircraft and space craft structures. The classical sound transmission problem was approached by Crocker and Price(5) using statistical energy methods. This approach included panel stiffness and damping and the effects of finite panel size and they successfully predicted the panel vibration amplitude and the dip in the transmission loss curve at the coincidence frequency. Theory developed by Lyon (4, 6) and Ungar(8) was used by them to predict the partition transmission loss and vibration amplitude. The theory was extended by Crocker and Price to determine the partition radiation resistance and its coupling with the transmission rooms.

Using the statistical energy analysis, it is now possible to calculate the average response of a structure, assuming the exciting source to be random and diffuse. The vibrational energy can then be related to transmission loss as shown by Crocker and Price(5) and Lyon and Scharton(4). However, there are still some limitations to this type of analysis in that a good estimate of the acoustically induced vibrations is possible if one averages over a large number of modes and positions of observations. The accuracy of the estimated average will decrease if one is dealing with a few modes and positions of observations. In practice, quite often it is not possible to achieve this. A second limitation of the Statistical Energy Analysis is that the exciting source (either acoustical or mechanical) causing the structural vibrations is assumed to be random and diffused. An aircraft fuselage, for instance, is not limited to this kind of excitation only, in practice. This is also true for many other structures. It would seem that the most reasonable way of estimating the structural response and hence sound transmission is by a model test and then relating the results to a real structure. Any corrections necessary could then be estimated from this and applied in determining the final data.

There is no easy method available for estimating the natural frequencies of cylindrical shells of the type being considered in this thesis. An experimental estimate of the natural frequencies of shells and plates was possible in the lower frequencies only(11). Therefore, the natural frequencies for a plain cylinder were calculated using the expressions developed by Arnold and Warburton(12). The expressions developed by Arnold and Warburton were based on earlier work by Lord Rayleigh(15), Love(16) and Flugge(19).

Although the vibration of uniform cylindrical shells have been fairly extensively investigated by Arnold and Warburton(12), there was not much literature available on stiffened cylinders. In references (20 - 24) the effects of eccentricities on the buckling of stiffened cylinders have been treated analytically. An externally stiffened cylinder under axial compression has been shown experimentally to carry over twice the load sustained by its internally stiffened counterpart(25). In the paper by McElman and Mikulas(10), the differential equations of dynamic equilibrium are derived from energy considerations for the free vibrations of ring- and stringer-stiffened cylinders. The derivation is accomplished by utilizing Donell-type strain-displacement relations for the cylinder and beam-type strain-displacement relations for the stiffeners[Appendix c]. The differential equations are solved to obtain a closed-form frequency expression for ring- and stringer-stiffened cylinders for the case of simple support boundary conditions. Results from these expressions and that obtained from Arnold and Warburton's expressions are presented in the form of graphs and tables of natural frequencies. These results were also used in calculating transmission loss for the cylindrical shell.

The objective of this program, which was a sub-contract from the Ministry of Defence, Procurement Executive, was to study the vibration and sound transmission characteristics of cylindrical shell structures. This was to be achieved by deriving a relationship between the total vibrational energy in the cylinder wall and as a result, the total transmitted energy (sound energy) contained in the space enclosed by the cylinder. This was required as a function of frequency in the range 200 Hz to 10,000 Hz. Further, to investigate the effects of longitudinal and radial stiffeners, the effects of different forms of excitation, determination of the least area and an optimum number of transducers to be used, the best measurement and analysis techniques and various other effects on the parameters related to vibration and sound transmission characteristics. Finally, to predict sound energy inside the cylinder (simulating a fuselage) for a given vibrational energy. This was to be presented in the form of transmission loss

To meet the objectives, both theoretical and experimental investigations were carried out. The theoretical concept based on the statistical energy analysis of the form used by Crocker and Price(5) is outlined in Chapter(2). This was used for the theoretical calculations of vibration and sound transmission characteristics with some data obtained from the experiments.

The development of experimental techniques in the measurement and analysis of data, and their application is described in Chapter(3). An extensive experimental investigation which was carried out to meet the objectives and the results obtained from it are also given in this chapter.

A comparison between the measured results obtained by two forms of excitation (acoustical and mechanical) show that below the ring frequency (2.1 kHz) the mechanically excited response remains almost unchanged while the response obtained by acoustical excitation increases with frequency (figure 3.29).

The development of computer programs for calculating the natural frequencies of cylinder and plates are discussed in Chapter(4). A single program for the solution of each parameter was developed initially and then combined in one large program. Using this program it is possible to study various vibration characteristics of cylinders and plates.

Chapter(5) is devoted to the analysis of results for estimating vibration and sound transmission characteristics. Theoretical results on the transmission loss calculated using statistical energy concepts is presented in this chapter. A comparison between the experimental and analytical results are presented. A good agreement between the theory and experiment is shown in one case while this was not so, when the energy ratio was calculated using the measured loss factor data.

The main text concludes with discussion, conclusions and recommendations for further work.

CHAPTER TWO

CHAPTER TWO

SOUND TRANSMISSION THROUGH CYLINDRICAL SHELL WALL

2.1 Theoretical Analysis using Statistical Energy Concept

The statistical energy method of analysis has been developed (1-4) and applied to many problems in order to estimate the response of a complicated structure where many modes of vibration are present. This analysis has recently been applied to the problem of estimating the response and transmission loss of a single finite panel(5), including the effect of the panel stiffness and damping. This is now extended to the problem of a cylindrical shell structure constructed of panel or panels.

2.2 A Three Coupled Oscillator System

The single wall cylindrical shell sound transmission problem can be considered as a three coupled-oscillator system, arranged as room - cylindrical shell wall - space enclosed by the shell wall and is studied in this manner. If a set of oscillators is linearly coupled, then the power flow P_{ij} from one system to another is directly proportional to the difference of the modal energies of the system (4), that is

$$P_{ij} = \phi_{ij} \quad (< E_i > - < E_j >) \tag{2.1}$$

The proportionality constant ϕ_{ij} is called the coupling factor and can be determined if the coupling element is defined.

Consider a reverberant room in which a cylindrical shell is suspended as shown on page (11). The ends of the vessel are enclosed with sound absorbing material. The analytical model of this may be considered to consist of three coupled systems as shown in figure (2.1). below. The power flow balance for the three systems may be written as:

$$P_{in_1} = P_{diss_1} + P_{12} + P_{13} \tag{2.2}$$

$$P_{in_2} = P_{diss_2} - P_{12} + P_{23} \tag{2.3}$$

$$P_{in_3} = P_{diss_3} - P_{13} - P_{23} \tag{2.4}$$

Using equation (2.1) and following Lyon and Scharton(4) yields the following equations:

$$P_{in_1} = \omega\eta_1 E_1 + \omega\eta_{12} n_1 (E_1/n_1 - E_2/n_2) + \omega\eta_{13} n_1 (E_1/n_1 - E_3/n_3); \tag{2.5}$$

$$P_{in_2} = \omega\eta_2 E_2 - \omega\eta_{12} n_1 (E_1/n_1 - E_2/n_2) + \omega\eta_{23} n_2 (E_2/n_2 - E_3/n_3); \tag{2.6}$$

$$P_{in_3} = \omega\eta_3 E_3 - \omega\eta_{13} n_1 (E_1/n_1 - E_3/n_3) - \omega\eta_{23} n_2 (E_2/n_2 - E_3/n_3). \tag{2.7}$$

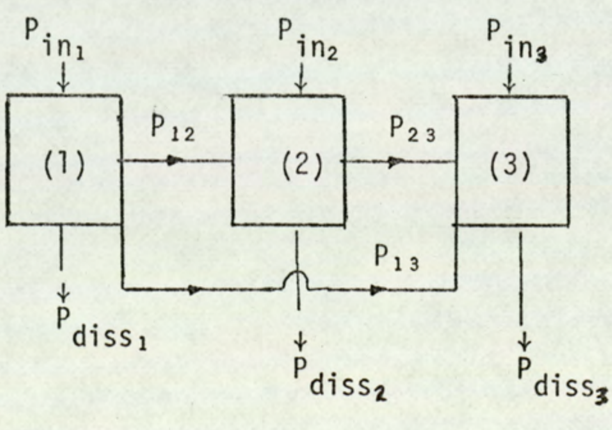

Fig. 2.1. Block Diagram Representing Energy Flow Between Coupled Systems.

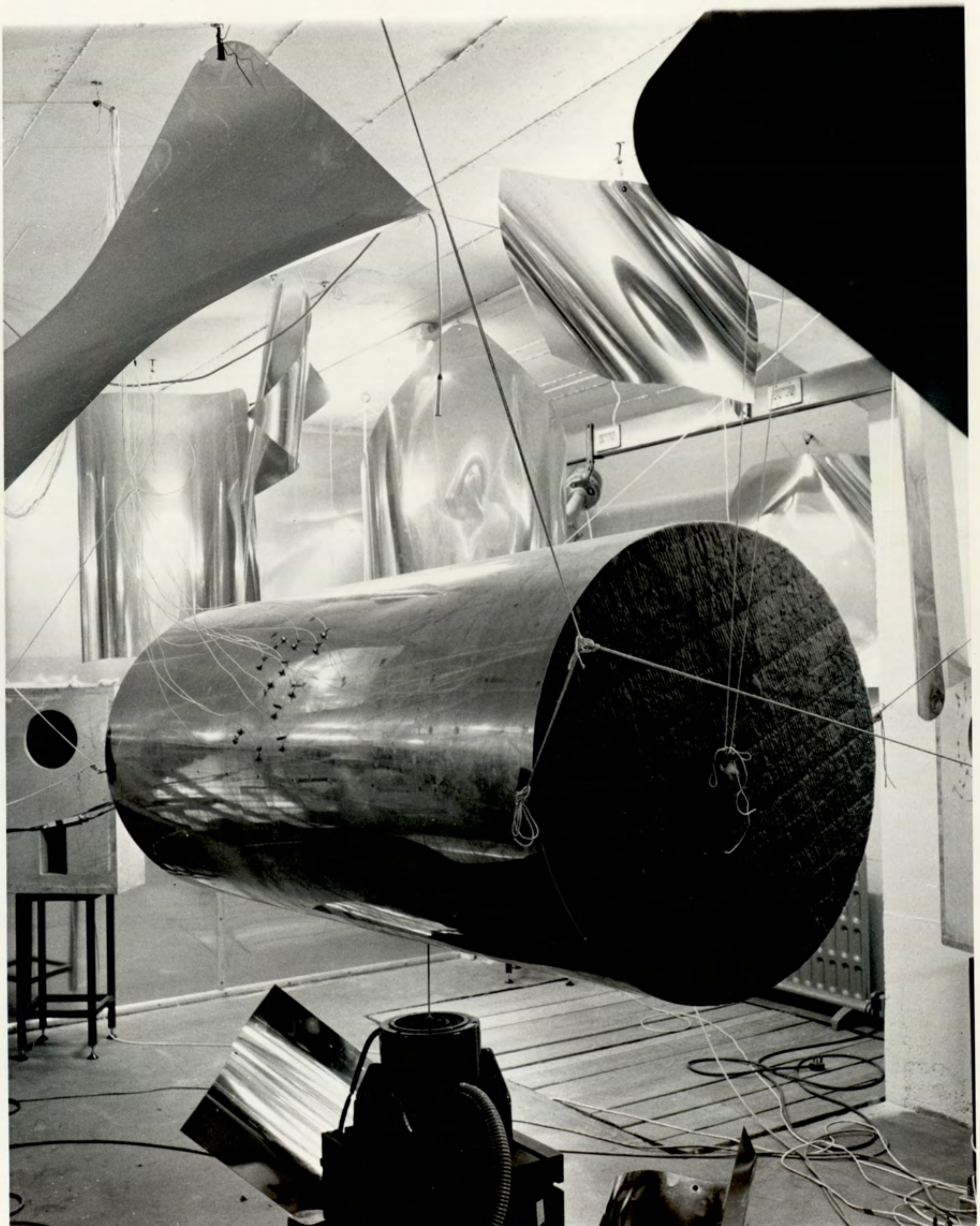

The P_{13} term represents power flow from system (1) to system (3) when there are no modes excited in system (2) in the frequency band under consideration. Thus the power flow P_{13} must be due to modes which are resonant outside of the frequency band under consideration. In this situation system (2) is non-resonant and acts only as a coupling element between system (1) and (3). Provided the coupling factor is defined (i.e. a limp mass giving "mass law", power flow) this non-resonant power flow can be calculated. Since, "mass law", transmission is derived assuming zero stiffness and damping in the partition and off resonance, these parameters are important to the response; then P_{13} can be derived from "mass law" transmission (6.7).

2.3 Shell radiation resistance and coupling with the room and enclosed space

2.3.1 Radiation resistance of cylinder wall between room and enclosed space

If the cylindrical shell structure (System 2) is excited by a vibrator, power flow is given by equations (2.2) to (2.7) with $P_{in_1} = 0$ and $P_{in_3} = 0$. Thus, with the substitution, equation (2.2) and (2.4) become equations (2.8) and (2.9) respectively:

$$0 = P_{diss_1} + P_{12} + P_{13} \tag{2.8}$$

$$0 = P_{diss_3} - P_{13} - P_{23} \tag{2.9}$$

Combining equations (2.8) and (2.9) and noting that power flow must be directional, $P_{21} = -P_{12}$, gives equation (2.10):

$$P_{diss_1} + P_{diss_2} = P_{21} + P_{23} \tag{2.10}$$

In this instance equation (2.3) is written as

$$P_{in_2} = P_{diss_2} + P_{21} + P_{23} \tag{2.11}$$

which becomes, on substituting equation (2.10),

$$P_{in_2} = P_{diss_2} + P_{diss_1} + P_{diss_3} \tag{2.12}$$

Thus equation (2.12) is written

$$(S_{a_2}/\omega^2)R_{2_{TOT}} = (S_{a_2}/\omega^2)R_{2_{int}} + (V_1 S_{p_1}\beta_1)/(\rho_a C_a^2) + (V_3 S_{p_3}\beta_3)/\rho_a C_a^2 \tag{2.13}$$

Equation (2.13) could also be obtained by considering the system as a whole. The power supplied to the whole system must be equal to the sum of the dissipated powers on each element of the system. The power supplied to the vibrator is

$$P_{in_2} = \beta_2 E_2 = (S_{a_2} R_{2_{TOT}})/\omega^2, \tag{2.14a}$$

$$P_{diss_i} = (S_{a_i} R_{int_i})/\omega^2, \text{ for } i = 2 \tag{2.14b}$$

and

$$P_{diss_j} = \beta_j \, [(V_j S_{p_j})/(\rho_a C_a^2)], \text{ for } j \;] \; 1 \text{ and } 3 \tag{2.14c}$$

Hence, equation (2.13)

$$\text{For the rooms, } \beta_i = 13.8/T_i \text{ and } \eta_i = \frac{2.2}{fT_i} \text{ for } i = 1 \text{ and } 3 \tag{2.15}$$

Since $R_{2TOT} = R_{2rad} + R_{2int}$ the equation (2.13) is written:

$$R_{2rad} = \frac{\omega^2}{S_{a_2}(\rho_a C_a^2)} [V_1 S_{p_1}\beta_1 + V_3 S_{p_3}\beta_3] \qquad (2.16)$$

But $n_i = (\omega^2 V_i)(2\pi^2 C_a^3)$ where $i = 1$ and 3

thus equation (2.16) may be written as

$$R_{2rad} = \frac{2\pi^2 C_a}{S_{a_2}\rho_a} [n_1 S_{p_1}\beta_1 + n_3 S_{p_2}\beta_3] \qquad (2.17)$$

The radiation resistance of a simply supported plate has been derived by Maidanik(3) and the equations are given in Appendix [A].

2.3.2 Coupling Factor for cylinder wall in a reverberant room

If the cylindrical shell vessel is excited on either side by noise field, then the power flow is given by equations (2.2) to (2.7) with $P_{in_2} = 0$. Thus equation (2.3) becomes

$$0 = P_{diss_2} - P_{12} - P_{32} \qquad (2.18)$$

$$\eta_2 E_2 = \eta_{12} n_1 (E_1/n_1 - E_2/n_2) + \eta_{32} n_3 (E_3/n_3 - E_2/n_2) \qquad (2.19)$$

It has been shown by Lyon and Scharton(4) and Ungar and Scharton(8) that under most conditions in practice,

$$\eta_{12} n_1 = \eta_{21} n_2 \qquad (2.20)$$

But $\eta_{21} = \eta_{rad}$ and $\eta_2 = \eta_{int}$ thus equation (2.19) is written:

$$\mu = \eta_{rad}/(\eta_{int} + 2\eta_{rad}) = (E_2/n_2)/[E_1/n_1 + E_3/n_3]; \tag{2.21}$$

$$\mu = [S_{a_2}/(S_{p_1} + S_{p_3})]\ \Gamma^{-1}, \tag{2.22}$$

$$\text{where}\quad \Gamma = 2\pi^2\ [n_2(\omega)/M_2](C_a\rho_a) \tag{2.23}$$

2.4 Sound Transmission and Cylinder wall response

For a cylindrical shell vessel suspended in the reverberant room and reverberant sound is produced in the room (System 1) by loudspeakers; the sound energy reduction, E_1/E_3, and consequently the sound energy transmission loss produced by the structure and also the structural vibration amplitude may be determined from equations (2.2) to (2.7) with $P_{in_2} = 0$ and $P_{in_3} = 0$.

2.4.1 Cylinder wall transmission loss

Using $\eta_{12}n_1 = \eta_{21}n_2$ and substituting P_{in_2} in equation (2.4) the next equation is obtained:

$$(E_2/n_2) = [(E_1/n_1)\eta_{21} - (E_3/n_3)\eta_{23}]/(\eta_2 + \eta_{21} + \eta_{23}) \tag{2.24}$$

But $\eta_{21} = \eta_{23} = \eta_{rad}$ and, except at low frequency where the present theory does not apply, $E_1/n_1 >> E_3/n_3$, thus equation (2.24) becomes

$$(E_2/n_2) = (E_1/n_1)\left[\frac{\eta_{rad}}{\eta_{int} + 2\,\eta_{rad}}\right] \tag{2.25}$$

Putting $P_{in_3} = 0$ in equation (7) yields:

$$E_3 = (E_1/\eta_{13} + E_2\eta_{23})/\eta_3 + \eta_{31} + \eta_{32} \qquad (2.26)$$

The term $E_1\eta_{13}$ represents the mass law or non-resonant transmission since it occurs without the modes resonant in the frequency band under consideration being excited. The term $E_2\eta_{23}$ represents the resonant transmission.

By substituting equation (2.25) into equation (2.26) gives:

$$\frac{E_1}{E_3} = \frac{\eta_3 \; (n_1/n_3)\eta_{13} + (n_2/n_3)\eta_{rad}}{\eta_{13} + \eta_{rad}^2(n_2/n_1)/(\eta_{int} + 2\eta_{rad})} \qquad (2.27)$$

equation (2.27) gave the noise reduction for the system and this is related to the transmission less (TL) by

$$TL = N.R. + 10 \; Log_{10} \; [(A_s C_a T_3)/(24V_3 \ell_n(10)] \qquad (2.28)$$

where $N.R.(\text{in db}) = 10 \; Log_{10} \; [\eta_3 + (n_1/n_3)\eta_{13} + (n_2/n_3)\eta_{rad}]$

$$10 \; log_{10} \; [\eta_{13} + \eta_{rad}^2 \; (n_2/n_1)/(\eta_{int} + 2\eta_{rad})] \qquad (2.29a)$$

or $\quad N.R.(\text{in db}) = 10 \; log \; (E_3/E_1) - 10 \; Log \; (V_3/V_1) \qquad (2.29b)$

The coupling loss factor η_{13}(room - enclosed space) due to non-resonant mass-law transmission is obtained from (5);

$$10 \; Log \; \eta_{13} = -TL_2 + 10 \; Log_{10} \; (\frac{A_s C_a}{AV_1\omega})$$

The internal loss factor for the 3rd system was:

$$\eta_3 = \frac{2.2}{f\,T_3} \qquad (2.30)$$

The modal densities of the reverberant room and the space enclosed by the cylindrical shell were taken as:

$$n\,(\omega)_1 = \frac{V_1\omega^2}{2\pi^2 C_a{}^3}$$

$$\text{modes/(rad Sec}^{-1}) \qquad (2.31)$$

$$n\,(\omega)_3 = \frac{V_3\omega^2}{2\pi^2 C_a{}^3}$$

The coupling loss factor from the cylindrical shell structure to the adjacent space was given by:

$$\eta_{21} = R_{2rad}/2\omega M_2 \qquad (2.32)$$

2.42 Response of cylindrical shell wall

The structural vibration amplitude is given by equation (2.25) For a reverberant field the total energy in a given bandwidth is $E_1 = S_{p_1}V_1/(\rho_a C_a^2)$, and the total panel energy is $E_2 = M_2 S_{a_2}/\omega^2$; and hence equation (2.33) becomes:

$$\frac{M_2 S_{a_2}}{n_2\omega^2} = S_{p_1}V_1/\rho_a C_a^2 n_1 \left[\frac{\eta_{rad}}{\eta_{int} + 2\eta_{rad}} \right] \qquad (2.34)$$

and

$$\frac{S_{a_2}}{S_{p_1}} = \frac{n_2\omega^2}{M_2} \left[V_1/\rho_a C_a^2 n_1 \left[\frac{\eta_{rad}}{\eta_{int} + 2\,\eta_{rad}} \right] \right] \qquad (2.35)$$

2.5 Non-resonant transmission

In a given frequency band, there are two types of modes; resonant modes, which have their natural frequencies in the band under consideration and hence have a high response, and non-resonant modes, which are excited such that their natural frequencies fall outside the band.

It is postulated that these non-resonant modes are responsible for the "mass law" transmission of sound(7,9). This would explain the ineffectiveness of damping at low frequencies, where the resonant modes are inefficient radiators, and thus the transmission must be mainly due to the non-resonant modes.

Hence, for non-resonant transmission, energy is shown to flow in figure (2.2) schematically, directly from Resonant System 1 to Resonant System 3, since system 2 is not resonant.

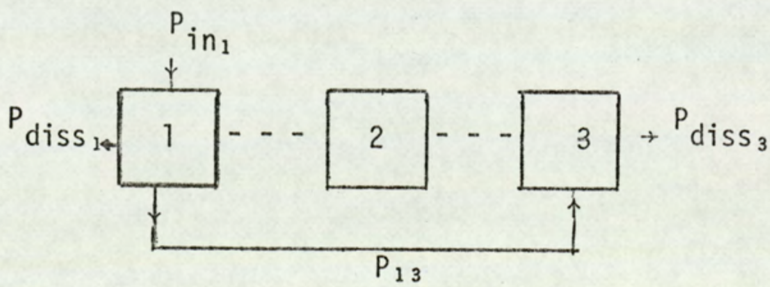

Fig. 2.2 Block diagram representing power flow through cylinder wall when the wall is non-resonant.

Considering the power flow equation for system 3, we have, from equation (2.4) (if the resonant transmission is neglected);

$$P_{in_3} = P_{diss_3} - P_{13} = 0 \qquad (2.37)$$

and $$0 = \omega\eta_3 E_3 - \omega\eta_{13} n_1 (E_1/n_1 - E_3/n_3) \qquad (2.38)$$

From equation (2.38) the ratio E_1/E_3 is obtained as

$$\frac{E_1}{E_3} = \left[\frac{n_1}{n_3} + \frac{\eta_3}{\eta_{13}} \right] \qquad (2.39)$$

Equation (2.39) gives the noise reduction for the non-resonant system and is related to the transmission loss (TL) by,

$$TL = N.R. + 10 \log_{10} \left(\frac{A_s C_a T_3}{24 V_3 \, n_{(10)}} \right) \qquad (2.40)$$

where $$N.R.(\text{in dB}) = 10 \log_{10} [n_1 - n_3] + 10 \log_{10} [\eta_3 - \eta_{13}] \qquad (2.41)$$

CHAPTER THREE

CHAPTER THREE

EXPERIMENTAL INVESTIGATIONS

3.1 Introduction

In order to investigate the vibration and noise transmission properties of cylindrical shells under conditions approximating a realistic aircraft structure (fuselage), a special instrument and data sampling facility was required. The automatic time and space averaging system was designed and developed specifically to meet the objectives of this research program. The test facility provided the capability to subject the test model to either mechanical or acoustical excitation in the pure tone, narrow band random or in the wide band random. Provisions were made to mount the transducers at various locations on the skin of the cylinder and inside the enclosed space so that the space average response could be studied in one sweep of the frequency spectrum.

The acoustical properties of the test chamber and the enclosed space could be measured for frequencies up to 20 kHz. For this measurement, the conventional technique was applied for frequencies up to 2 kHz. Above this frequency, improved techniques had to be developed.

The scope of the experimental program was extended in order that the best measurement and analysis techniques could be developed and applied for the verification of the more important parameters. This was then extended to obtain the data required for the present program of work and recommended, where suitable, for the measurement on a real structure. Therefore, an extensive investigation was carried out into the techniques of frequency analysis, instrumentation, room acoustics, effects of various structural configurations on vibration and noise transmission characteristics, methods of excitation, the optimum number of transducers to be used and the least area of the structure for the measurement. The details of this work are described in the sections that follow.

3.2 Use of instruments in the measurement and analysis of data

A block diagram showing the general layout of the main instruments used for the experimental work is given in figure (3.1). Use was made of the available instruments described in reference (11) by ensuring that the sensitivity, frequency response, signal to noise ratio and other characteristics were compatible with the kind of data reduced. The calibrations of the instruments were first made individually and then the whole system calibration was sorted before any measurements were recorded.

A special instrument to determine the mean square of the measured response at several stations of a continuous system both with respect to time and to the number of stations in the system was designed and developed for this work. Thus, if the acceleration response to random excitation at the r^{th} station in the system is $Ar(r = 1....n)$

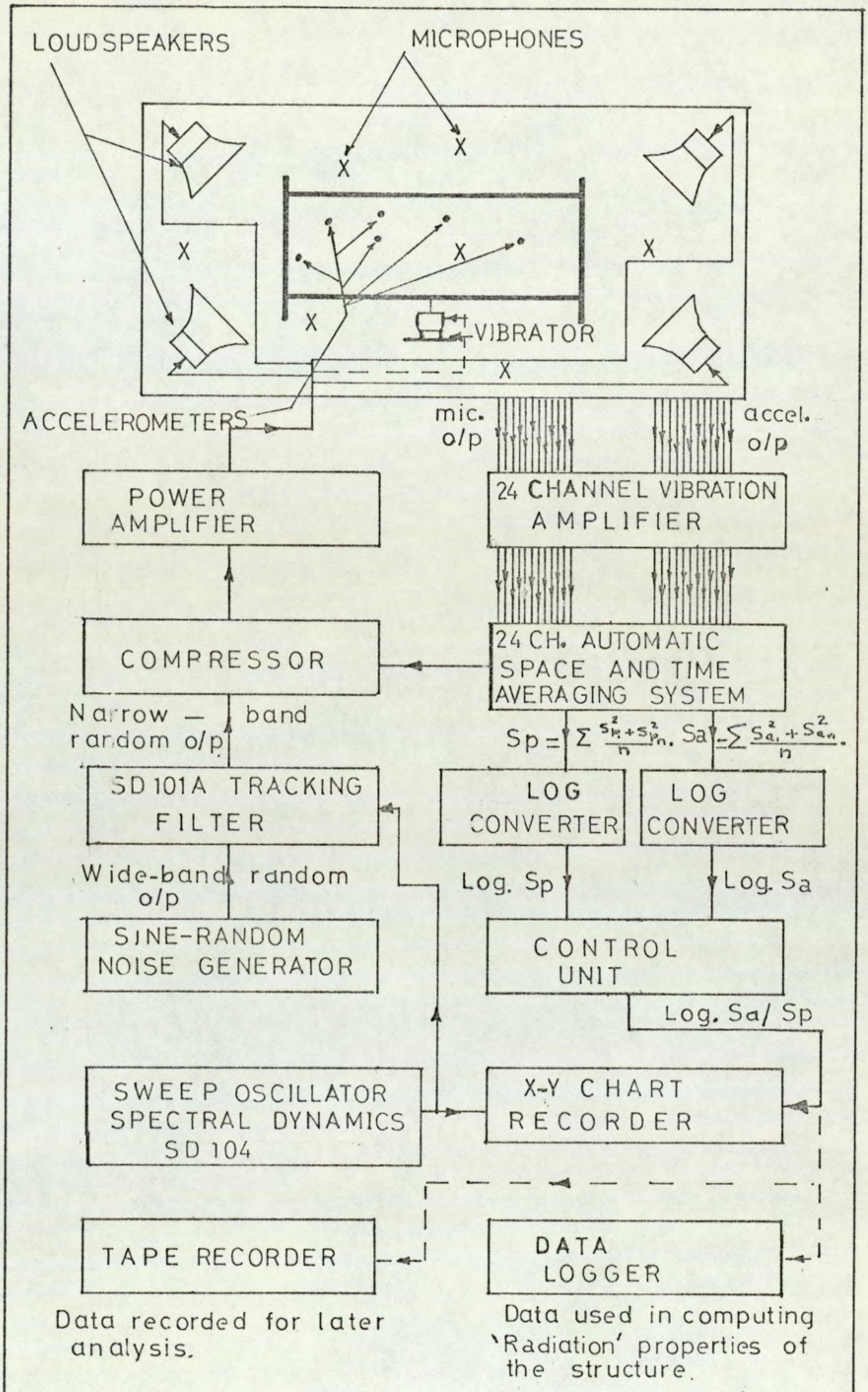

INSTRUMENTS USED IN MEASURING S_p/S_a AND S_a/S_p

FIG 3.1

at any instant, then the mean square acceleration $\bar{a}^2$ is given by:

$$\bar{a}^2 = \frac{1}{T_n} \int_o^T \{ \sum_{r=1}^{n} a_r^2 \} dt \text{ or } \frac{1}{n} \sum_{r=1}^{n} \{ \int_o^T a_r^2 dt \} \tag{3.1}$$

Thermal convertors were used in this instrument to perform the squaring and integration with respect to time. A total number of inputs to the instruments were 24 in two groups of 12. One side of the instrument was used for measuring the mean square sound pressure levels and the other side to measure the mean square acceleration. The outputs were either recorded on x-y chart recorder individually or where necessary, the values of the two output signals were obtained with the aid of log converting facility of the Spectral Dynamic Impedance Measuring System. Thus a ratio of space average of a number of inputs was obtained in one frequency sweep.

3.3 Experimental Model

3.3.1 Test Cylindrical Shells and Stiffeners

Three test cylinders were manufactured, all of a similar length and wall-thickness but of different diameters. All the cylinders were test--ed as an unstiffened shell first and then modified to longitudinal and radial stiffening conditions. All the three cylinders were fitted with identical end blanks and the same system for vibration and internal noise measurements was used.

The longitudinal and radial stiffeners were both of 'Z' section and manufactured from the same material as the cylinders. The details of a cylinder and the stiffeners are shown in figure [C1] of Appendix [C].

(i) Unstiffened Cylindrical Shells.

The cylinders were formed from one sheet of B.S. 2L 72 aluminium alloy 0.00122M thick, welded together having one longitudinal seam. The two three inches thick end blanks were a tight fit into the shell and the material used was rocksil which provided a non-reverberant end condition. For some tests the end blanks were replaced by reverberant material for which aluminium alloy sheets were used.

(ii) Stiffened Cylindrical Shells.

The plain cylinders were stiffened and the effects of stiffening examined by increasing the number of stiffeners. For the complete experimental studies, the stiffeners were fixed inside the shell by a thin layer of araldite and riveted to the skin of the shell to ensure a permanent and uniform fixture. The longitudinal and radial stiffeners were spaced in nearly equal intervals along the circumference and length of the shell. The radial stiffeners were fixed inbetween the longitudinal members as shown in the photograph on page (25).

3.4 Determination of Test Chamber Characteristics

(i) Test Facility

The Applied Dynamics laboratory number 4 at Aston University has a reverberant and a semi-reverberant room. There is a separate

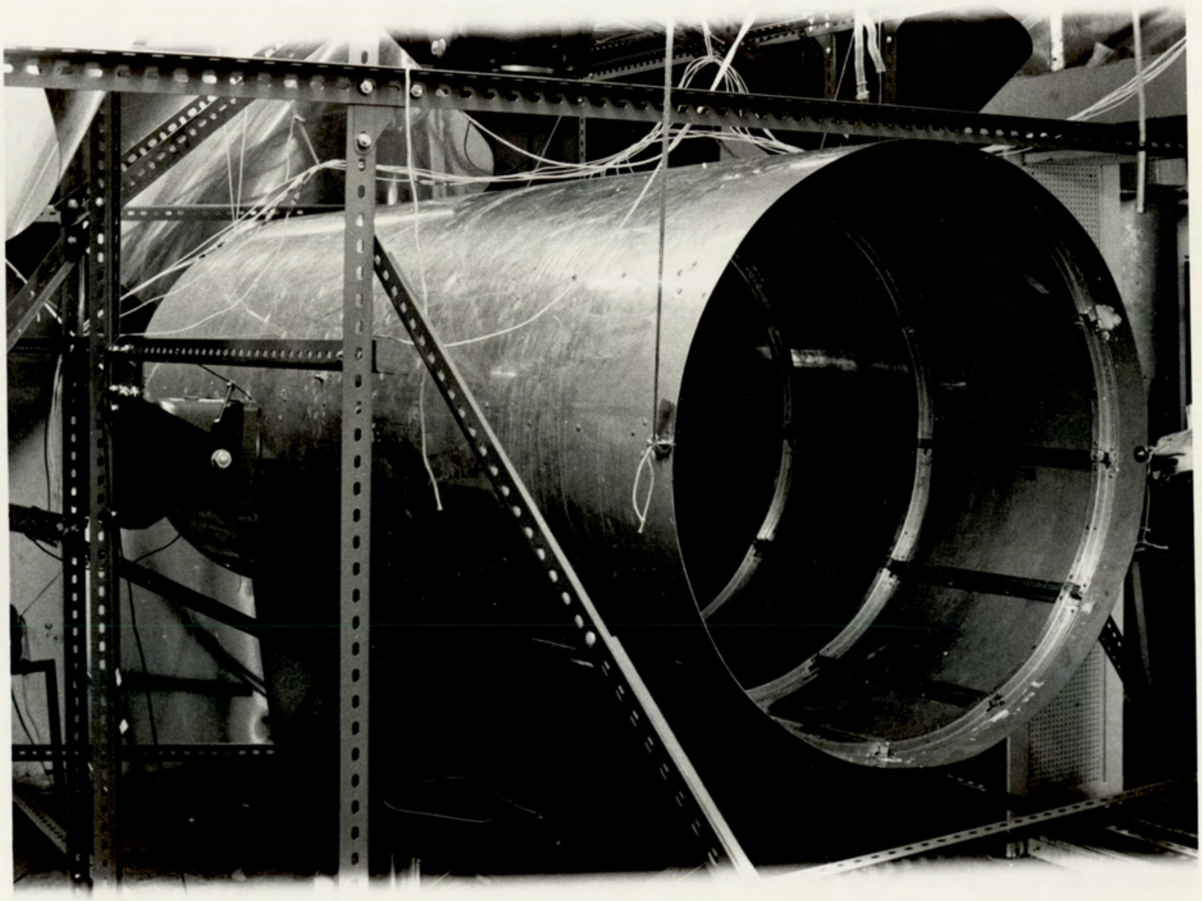

instrument room connecting these two chambers. The power supply to the exciting source and simultaneous recording of required data from transducers were controlled from the instrument room. The two types of noise generating facilities available were the Ling pneumatic noise generator and the Goodman loudspeakers. For the purpose of the present work and the frequency range of interest the Goodman loudspeakers were used for acoustical excitation and vibrators for mechanical excitation. All the experimental work was carried out in the reverberant room. The measurement of structural damping was made in the semi-reverberant room. The cylindrical shell was hung horizontally by cords in the middle of the room for all the tests.

(ii) Reverberant Room

The volume of this room was 68 m^3. The walls were lined with hard material to provide a reasonable reflective condition. Six loudspeakers were placed near the walls in such positions to give a uniform sound intensity around the test model. Aluminium reflectors of different size and dimension were also hung from the ceiling at different heights to break any standing wave pattern. The noise intensity variation level around the model was measured and found to be around ±3 dB when excited in the wide band (20 Hz 20 k Hz) random frequency. When excited in the other frequency band the diffusibility(11) was not so good.

(iii) Semi-Reverberant Room

The volume of this room was 32 m^3. The walls and the ceiling were lined with non-reflective material.

3.4.1 Acoustical properties of the test chamber and the enclosed space

(i) General

In determining the acoustic qualities of an enclosure, one of the important factors is the measurement of enclosure reverberation time. The accuracy with which it can be determined from the decay curve is limited by random fluctuating in it. A method to minimize the effects of the fluctuations in decay response on the measured reverberation time value is to repeat the reverberation experiment many times and to average the data obtained from the individual responses. The method takes quite a lengthy analysis time and often fails to reveal a true nature of the decay, especially when the response is subject to a multiple decay rate as shown in figure (3.2) which is the result from one of the actual measurements.

The high initial decay value containing much of the valuable information persists only for a few decibels and if the data is not carefully reduced, much of the information can be lost. Decays with multiple slopes, point to a lack of sound diffusion in the enclosure. In some reverberant rooms the diffusion decreases during the decay and therefore it is the initial decay rate that is important for the determination of the statistical absorption. To extract all the useful information from the decay curves, many such curves obtained under identical physical conditions should be averaged and not just the decay rates or reverberation times obtained from individual decay curves.

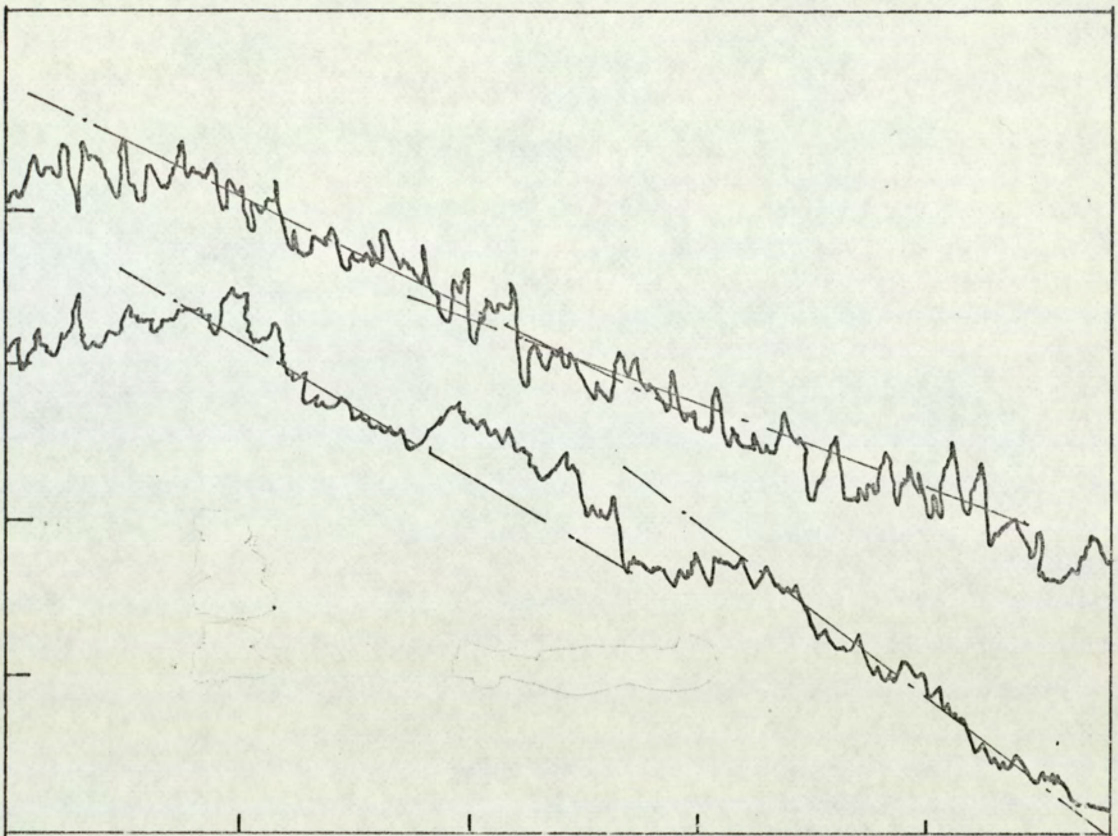

NOISE DECAY CURVES OBTAINED UNDER IDENTICAL TEST CONDITION.

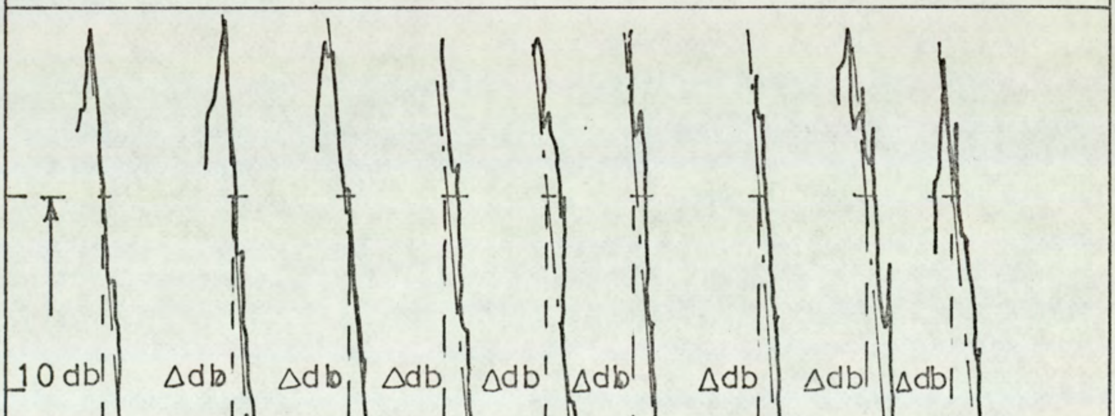

FILTERED RESPONSE OF NOISE DECAY CURVES AT DIFFERENT FILTER BAND CENTRE FREQUENCIES.

FIG. 3.2

A new method for measuring reverberation time is described by Schroeder(17), which, in a single measurement, yields the decay curves that are identical to the average over infinitely many decay curves that would be obtained from exciting the enclosure with band pass filtered noise. Thus, the difficulties mentioned in the conventional methods of determining the reverberation time could be reduced to some extent.

Rooms in which random sound fields can be established are important tools in applied acoustics. Two outstanding problems are the production of random sound fields and the determination of whether or not a given sound field is random. This can be determined and approximated from the point measurements in the room and from the method recommended by Cook and Associates(18) which considers a cross-correlation coefficient,R, the sound pressure at two different points in the sound field and from these the acoustic qualities of a room can be determined more accurately.

(ii) Methods of Reverberation Time Evaluation

(A) From the measurement of the decaying response

The two most commonly used methods in the measurement of reverberation time are outlined in this section. Common to both methods are the use of a sound source, a microphone, an amplifier and a recorder capable of responding to a quickly decaying response. By using a Sine Random Noise Generator, random or pure tone sound can be produced in its enclosure. The decaying output from the microphone may be filtered in the desired frequency band before recording. An example of such a measuring arrangement is shown in figure (3.3A) where a gun is used to produce a sound source instead of a noise generator. When the gun is fired, the sound level in the room will first rapidly increase and then decrease according to the reverberant properties of the room. The output from the microphone placed in the enclosure is filtered and recorded. The reverberation time is measured from the initial portion of the recorded decay curve.

The above method was found to be convenient when only a limited number of reverberation curves were to be measured. When a number of curves were to be recorded and sampled over a wide frequency range, the use of a gun as a sound source was unsatisfactory as it required one shot for every recording. It was then advantageous to employ the method where the sound source consisted of a noise generator and; one or more loudspeakers in the room, as shown in figure (3.3B). For this test, when a steady noise field in the room had been observed, the input source was cut off and the decaying response from a microphone was recorded as before.

(B) From the Measurement of the Integral of the Squared Impulses of the decaying response

The basis of Schroeder's(17), Integrated Impulse Method, was that the ensemble average of the square of the reverberation noise decay in an enclosure equals the time integral of the enclosure squared impulse response. To arrive at this result, it was considered

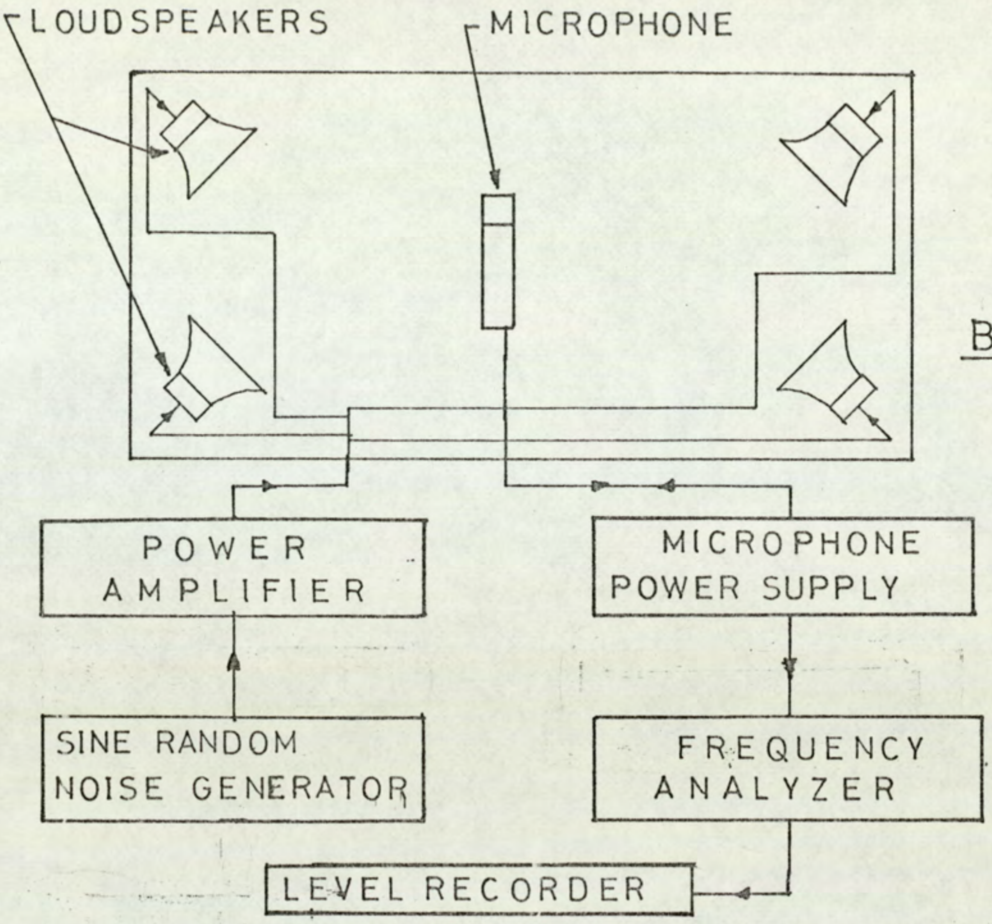

MEASUREMENT OF REVERBERATION TIME USING LOUDSPEAKERS AND SINE RANDOM NOISE GENERATOR.

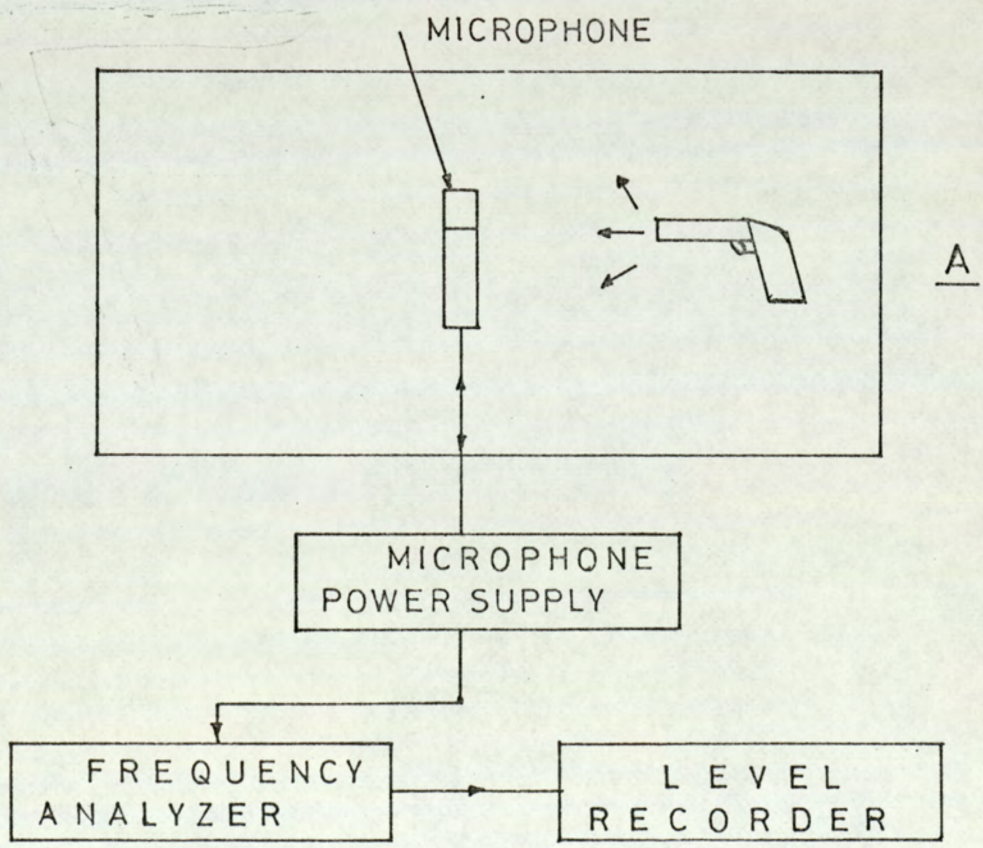

MEASUREMENT OF REVERBERATION TIME USING A GUN AS SOUND SOURCE.

FIG 3.3 A&B

that the room is excited by 'Stationary White Noise', and then suddenly shut off. The analytical approach to this is given in Appendix [B].

The practical method of obtaining the squared and integrated impulse response was from the tape recorder tone burst whose spectra covered the wide frequency bands which were radiated into the room from the loudspeakers. The response of the enclosure to each tone burst was picked up by a microphone, the response of which was recorded on tape. This was then played back in reverse-time direction, squared and integrated by means of an R.C. network shown in figure (3.4) and recorded once again on tape for later analysis. For an immediate analysis, the play back response signal was squared, integrated, frequency analysed in the required bandwidth and recorded all in one pass. A block diagram showing the measuring instruments is shown in figure (3.5).

From the measurement taken of the reverberation time using all the techniques, it was concluded that no immediate advantage is gained by using the, Integrated Impulse Method, as the variation in the determined values was so small that it could be dismissed as due to evaluation error. However, this technique proved to be a good check on the results measured by conventional method and is recommended where a very close study of a decay time is required.

In the final evaluation of the reverberation time, the wide band random response from a noise generator was radiated into the

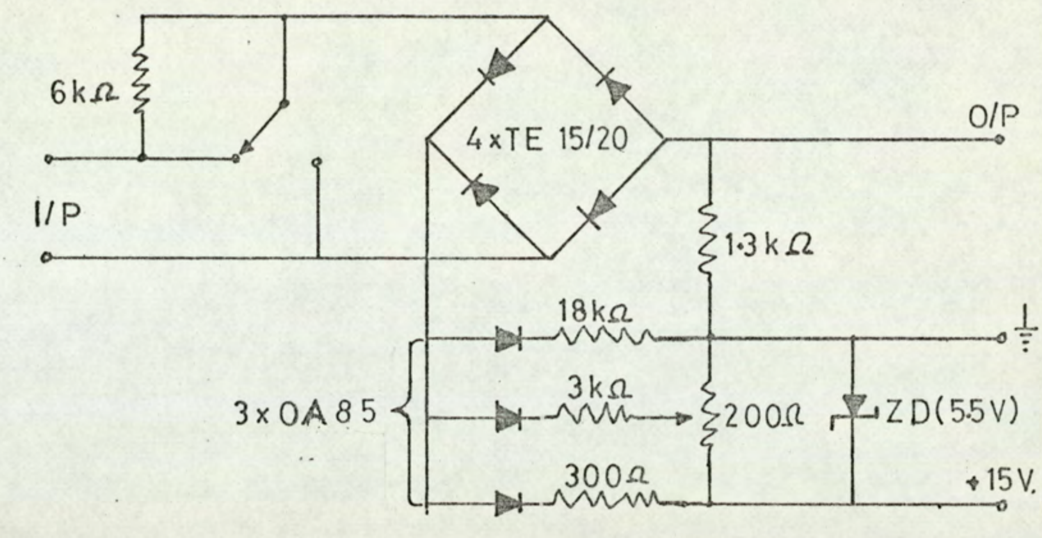

SCHEMATIC DIAGRAM OF THE SQUARING CIRCUIT

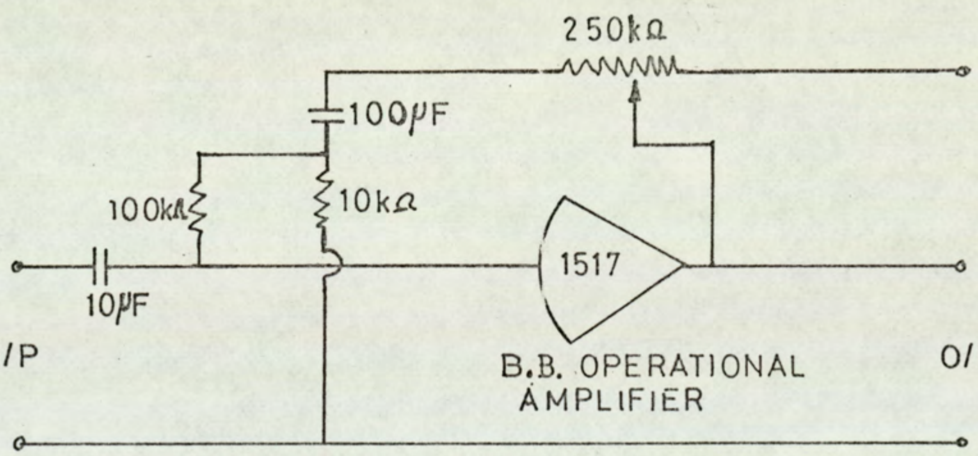

SCHEMATIC DIAGRAM OF THE AMPLIFIER CIRCUIT

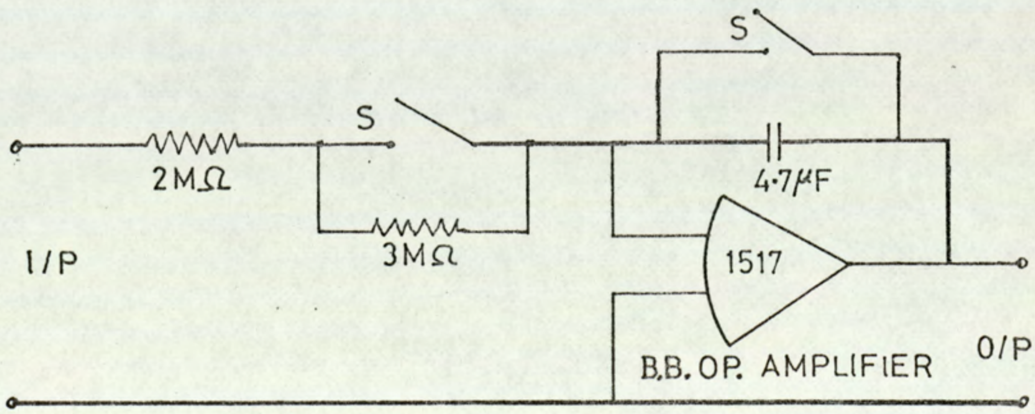

SCHEMATIC DIAGRAM OF THE INTEGRATING CIRCUIT

FIG. 3.4

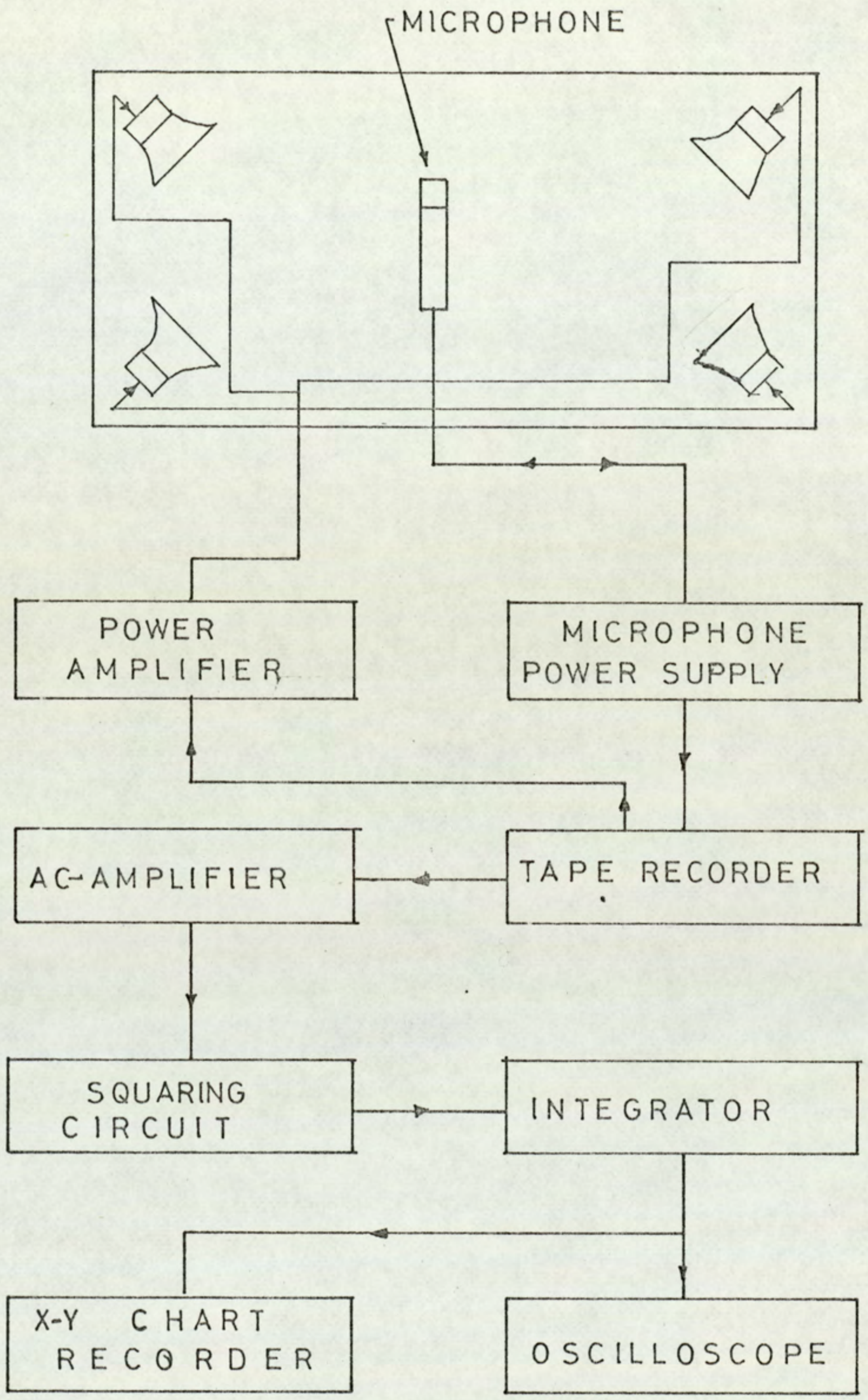

BLOCK DIAGRAM OF THE INSTRUMENTATION FOR THE MEASUREMENT OF REVERBERATION TIME ACCORDING TO THE "INTEGRATED IMPULSE METHOD"

FIG 3.5

room from the loudspeaker. The noise level distribution in the room was detected by microphones placed at different positions in the room. When the noise level had reached a steady condition, the input to the loudspeakers was suddenly cut off and the decaying response picked up by a microphone placed in the centre of the room was recorded on the magnetic tape recorder. The tape was then slowed down and the response passed through a 1/3 octave filter and recorded on a level recorder. The time to decay over 10 dB from the initial position of the decaying response was measured and then a decay time over 60 dB was computed.

For this kind of rapid decay measurement, it was found that the responses of the level recorder and other available x-y chart recorders were compatible only in the lower frequency range and above about 2 K Hz the actual response died down much faster than the pen response, even when subjected to the lowest averaging time. This problem was solved by either recording the response at a faster tape speed and then slowing down for recording or recording directly on the storage oscilloscope, the response time of which is in the order of 10^{-9} s. The former technique was used for the measurement and the result is given in figure (3.6). The experimental flow diagram is given in figure (3.7).

The damping of the room and enclosed space was then computed from the reverberation time and the equation,

$$10 \log_{10} \left[\frac{13.8}{T_{60}} \right] \text{ dB} \tag{3.1}$$

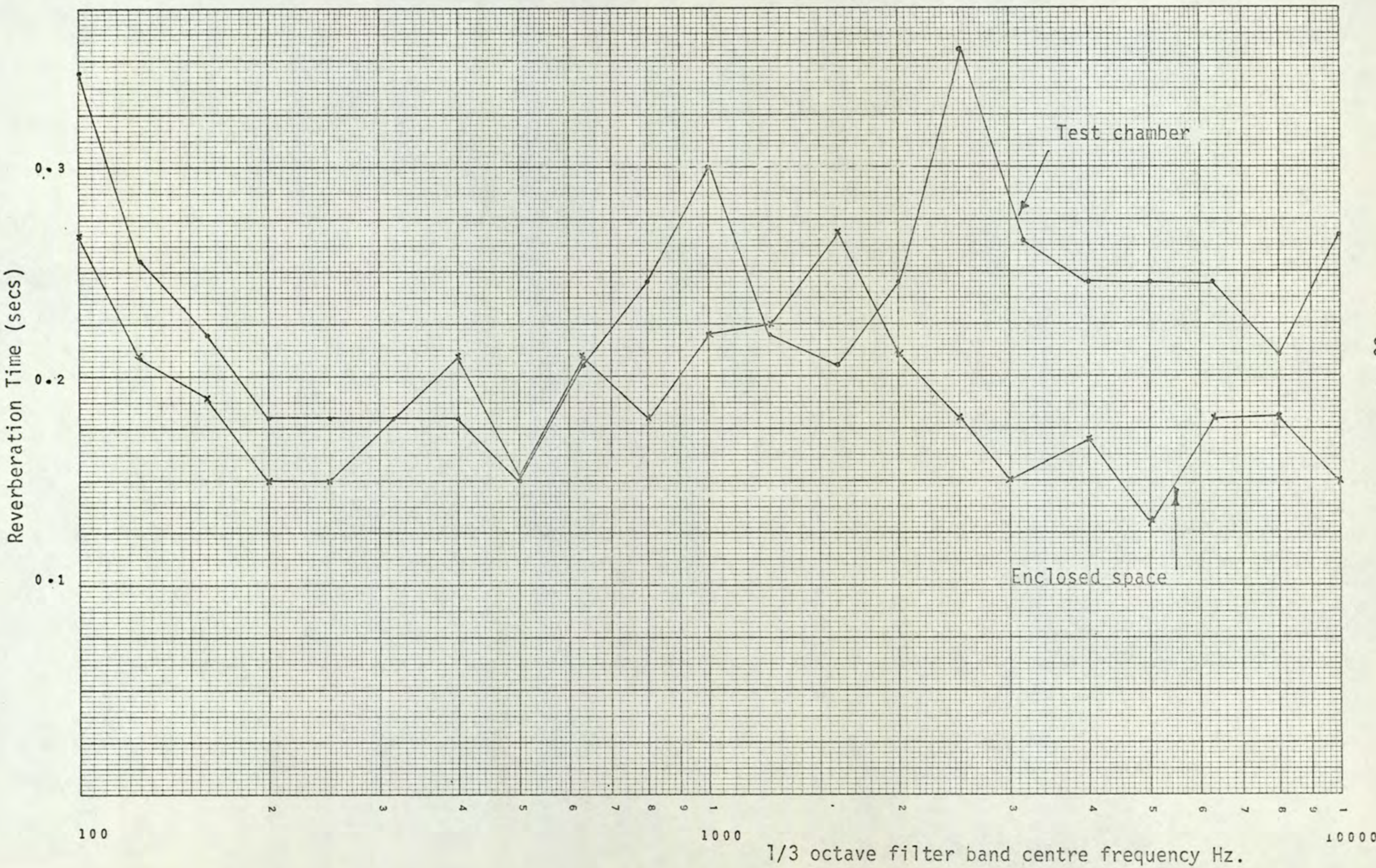
Reverberation Time (secs)
0.3
0.2
0.1
Test chamber
Enclosed space
2
3
4
5
6
7
8
9
1
2
3
4
5
6
7
8
9
1
100
1000
10000
1/3 octave filter band centre frequency Hz.

Fig.3.6

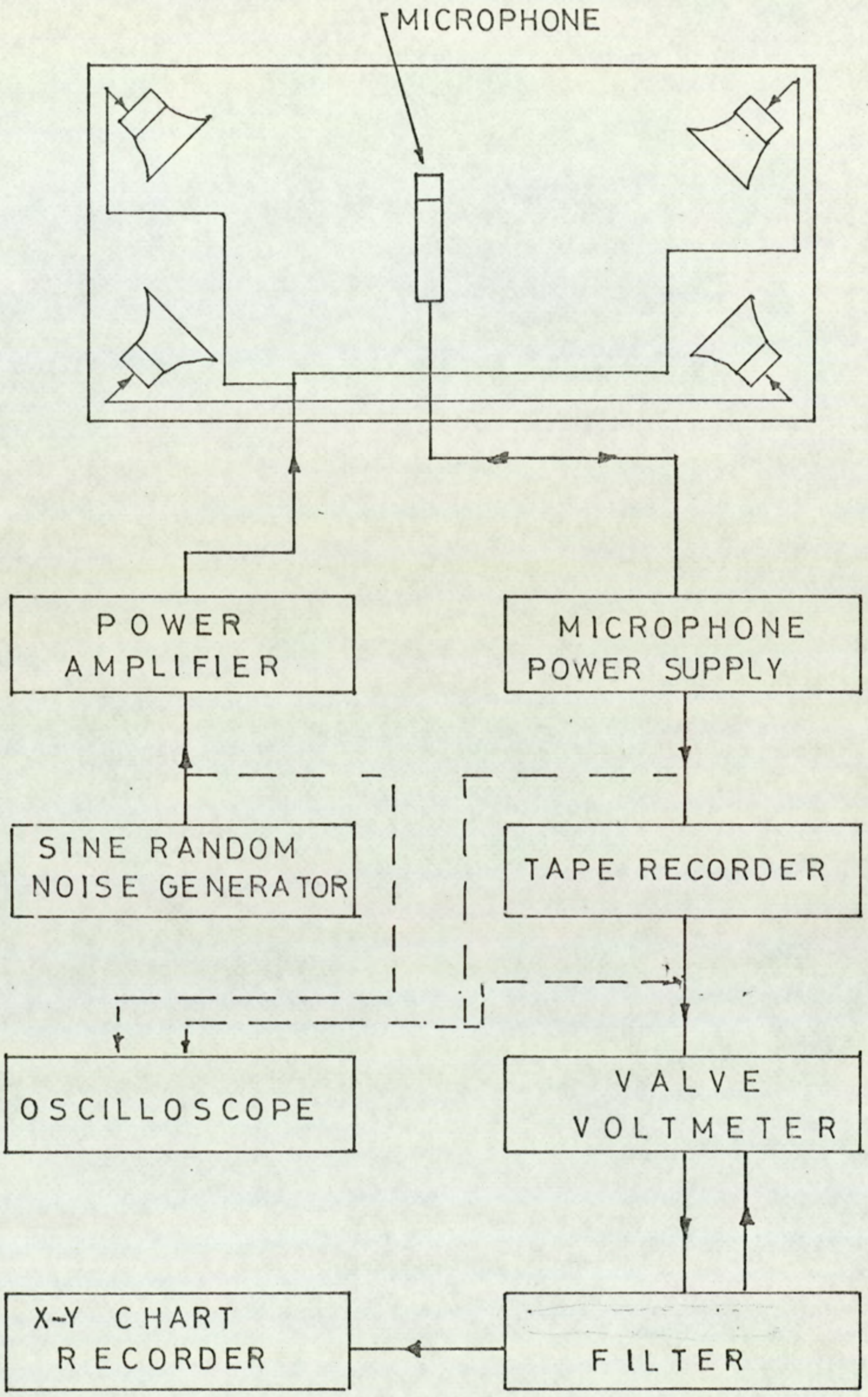

BLOCK DIAGRAM OF THE INSTRUMENTATION USED FOR THE MEASUREMENT OF THE REVERBERATION TIME.

FIG 3.7

The result of the above calculation is given in figures (3.8A) and Table (3.8B).

The reverberation contributes to the total noise existing in a room over a period of time, since it produces audible prolongation of noise during these intervals in which no noise is actually being emitted by the source. The reverberation time, T_{60} depends on the volume of the room and the total room absorption as is shown by the equation below.

$$T_{60} = 0.161 \frac{v}{a'}, \text{ sec} \tag{3.2}$$

$$a' = \frac{0.161\ v}{T_{60}} \tag{3.3}$$

where v = volume of enclosure in cubic meters

a' = absorption in square meters (Sabin units)

The room and enclosure absorption is shown in Table (3.9). It can be seen that the accuracy of this result depends on the accuracy of reverberation time measurement.

3.4.2 Determination of Diffusibility of the Reverberant Sound Field

(i) Basic Consideration

Reverberant chambers used for acoustical measurements should have completely random sound fields. In an ordinary room a great deal of sound is reflected from the walls. Thus, the sound at a given position in the room is made up of that which travels directly

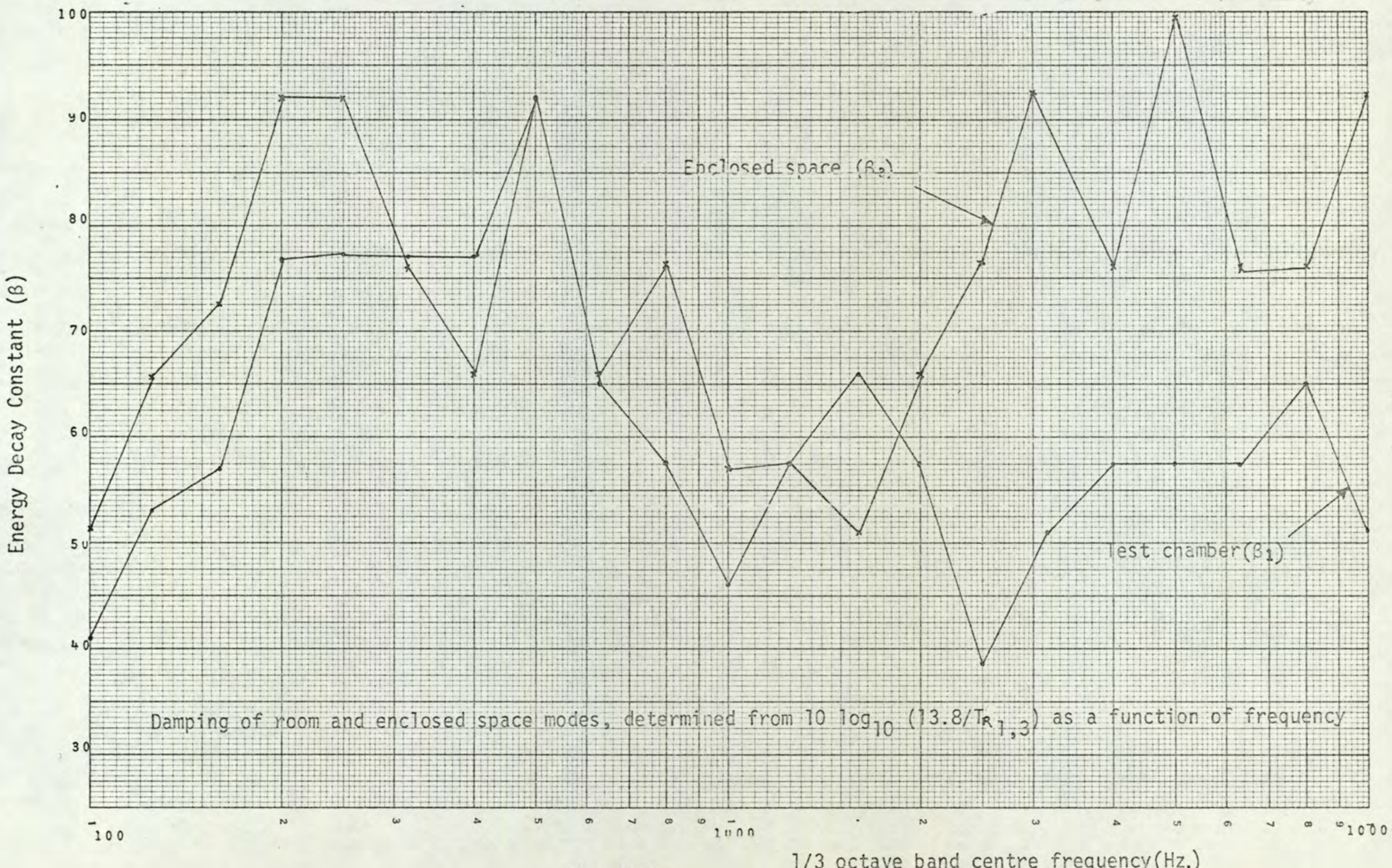
Energy Decay Constant (β)
1/3 octave band centre frequency(Hz.)
Enclosed space (β_2)
Test chamber(β_1)
Damping of room and enclosed space modes, determined from 10 $\log_{10}$ ($13.8/T_{R\,1,3}$) as a function of frequency
100
90
80
70
60
50
40
30
100
1000
10000

Fig. 3.8A

TABLE 3.8B

	Rev. Room	Enclosed space
f	Energy decay constant (β_1)	Energy decay constant (β_3)
100	40.58	51.1
125	53.07	65.7
160	57.5	72.63
200	76.66	92.32
250	76.66	92.45
315	76.66	76.6
400	76.66	65.7
500	92.0	92.12
630	65.7	65.7
800	57.5	76.6
1000	46.3	57.5
1250	57.5	56.8
1600	65.7	51.1
2000	57.5	65.7
2500	38.33	76.6
3150	51.1	92.18
4000	57.5	76.6
5000	57.5	106.1
6300	57.5	76.6
8000	65.7	76.6
10000	51.1	92.4

Damping of room and enclosed space modes.

TABLE 3.9

f	Reverberant room	Enclosed space
100	32.200	0.401
125	42.107	0.567
160	45.617	0.627
200	60.822	0.794
250	60.822	0.794
400	60.822	0.662
400	60.822	0.567
500	72.986	0.794
630	52.133	0.567
800	45.616	0.661
1000	36.493	0.496
1250	45.617	0.490
1600	52.133	0.441
2000	45.617	0.567
2500	30.411	0.661
3150	40.548	0.794
4000	45.616	0.662
5000	45.616	0.916
6300	45.616	0.662
8000	52.133	0.662
10,000	40.548	0.794

Absorption characteristics of reverberant room and enclosed space ($a' = 0.161v/T_{60}$

from the source plus the sound that comes from other directions as a result of reflection. Under such circumstances the sound pressure does not decrease so rapidly. Non uniformity of absorption and of shape of the room surfaces tend to increase the scattering of sound within the room when the conditions are such that the sound waves travel equally in all directions and the sound pressure is everywhere the same within the room then the sound field is perfectly diffused. As a consequence of reflection from the boundaries of a room the sound persists for some time after the source has stopped.

Two outstanding problems in applied acoustics are the production of random sound fields in reverberant rooms and the determination of whether or not a given sound field, once established, is random. A completely random sound field is defined such that at every point within the enclosure, plane waves near a particular frequency, having the same average intensity for all directions and phases, will have passed by after a sufficiently long time.

(ii) Measurement of diffusibility of the reverberant room

A reference microphone was placed in the centre of the room. Wide band random, (20 Hz - 20 kHz) noise was then radiated into the room from the loudspeakers placed randomly near the walls. Another microphone of identical sensitivity as the reference microphone was rotated round while point measurements were taken and compared with the results of reference microphone. This experiment was then repeated with the room being excited by band limited random noise.

It was found that when the enclosure was excited with the wide band random noise, the variation in the noise level was ± 1.5 dB. With the room excited in the narrow band, the fluctuation in the measured level depended very much on the frequency bandwidths and its centre frequency. The narrower the bandwidth of excitation, the greater were the fluctuations, although aluminium reflectors were used to reduce this to some extent. On an average, the noise level variation was in the order of ± 4 dB.

3.4.3 Determination of Modal Density

An attempt was made to determine the modal density of the transmission room and the space enclosed by the cylindrical shells, but because of very high concentration of resonances it was almost impossible to count the peaks. Therefore the modal density for each space was calculated from the following equation

$$n_R(\omega) = \frac{V\omega^2}{2\pi^2 C_a^{\,3}} \text{ modes/(rad sec}^{-1}\text{)}$$

The results of the above calculation are given in Table (3.10).

3.5 Selection of Analyser

In figure (3.1) is shown a typical noise and vibration analysis and measuring arrangements. Even though all the basic "elements" in a measuring arrangement are equally essential, the analyser may be considered the "central" unit. It determined, in general what signal properties are being measured and what kind of data can be

TABLE 3.10

f	Δf	N_{R_1}	$N_{R_1}\Delta f$	$N_{R_3}(f)$	$N_{R_3}\Delta f$
25	5.8	.0021	.0/22	.000023	.000134
31.5	7.3	.0033	.0244	.000036	.000268
40	9.2	.0053	.0496	.000059	.00054
50	11.6	.0084	.0977	.000092	.00107
63	14.5	.0133	.193	.000146	.0021
80	18.3	.0215	.394	.000236	.0043
100	23	.0337	.775	.00137	.0085
125	29	.052	1.527	.000578	.0167
160	37	.086	3.192	.00094	.035
200	46	.1348	6.2008	.00148	.068
250	58	.210	12.21	.0023	.134
315	73	.334	24.4	.0036	.268
400	92	.539	49.6	.0059	.544
500	116	.842	97.73	.0092	1.073
630	145	1.33	193.94	.0146	2.129
800	183	2.156	394.69	.023	4.33
1000	230	3.37	775.100	.037	8.51
1250	290	5.26	1527.03	.057	16.76
1600	370	8.62	3.92	.094	35.06
2000	460	13.48	6200.8	.148	68.08
2500	580	21.06	12216.25	.231	134.125
3150	730	33.43	24410.34	.367	268.008
4000	920	53.92	49606.4	.592	171.68
5000	1160	84.25	97730	.925	1073
6300	1450	133.7	193945	1.468	2129.36
8000	1830	215.68	394694	2.368	4333.44
10,000	2300	337	775100	3.7	8510

Modal density of transmission room and enclosed space obtained in the form of numbers or curves. The simplest analyser consists of a linear amplifier and a detection device which makes it possible to measure some characteristic signal values for instance the peak value, the RMS-value or the average absolute value of either the acceleration, the velocity or the displacement. In most practical cases it will be necessary at least to be able to determine the frequency composition of the signal and therefore use is made of a frequency analyser. There are two types of frequency analysers commonly available, namely the constant bandwidth type analyser and the constant percentage type analyser.

Since the signal to be analysed is of a schoastic nature (random vibration) which produces a continuous frequency spectrum, the preferred type of analysis will depend not only upon the spectrum itself but upon the ultimate use of the measured data. Where no detailed spectrum analysis is normally required, analysis in the form of 1/3 octave, or even 1/1 octave, frequency band will therefore suffice. On the otherhand, if the data are to be used for a close study of certain characteristics, an extremely detailed frequency analysis is required. For this, a constant bandwidth type of analyser may be preferred.

In order to select a most practical type of analyser best suited for the type of analysis required in the present work, the investigations described in this section were carried out.

3.5.1 Constant Percentage Bandwidth Analyser

The structure suspended in the centre of reverberant room was acoustically excited with wideband (20 Hz - 20 K Hz) random source fed from a Sine Random Noise Generator. The transducer-accelerator on the skin of the shell and microphones in the room and enclosed space - outputs were analysed using a 1/1 and 1/3 octave analyser. Since the analyser had only a single channel input facility; one transducer input at a time had to be analysed. The results of one of these tests are shown in figure (3.11).

The test was then repeated when the structure was mechanically excited by a vibrator. The results of this test are shown in figure (3.12).

The main disadvantages of this type of analysis for the particular application were that signals from only single transducers could be analysed at a time hence a great deal of time, effort and cost would be involved for a complete analysis of data. Secondly, it was observed that due to mechanical and other characteristics of the level recorder and the sweep generator, it was not possible every time to start and frequency match the signal.

This type of analysis was useful, however, in that a broad spectrum of the measured data could be obtained quite quickly. This will then enable one to narrow the areas that would require a thorough analysis.

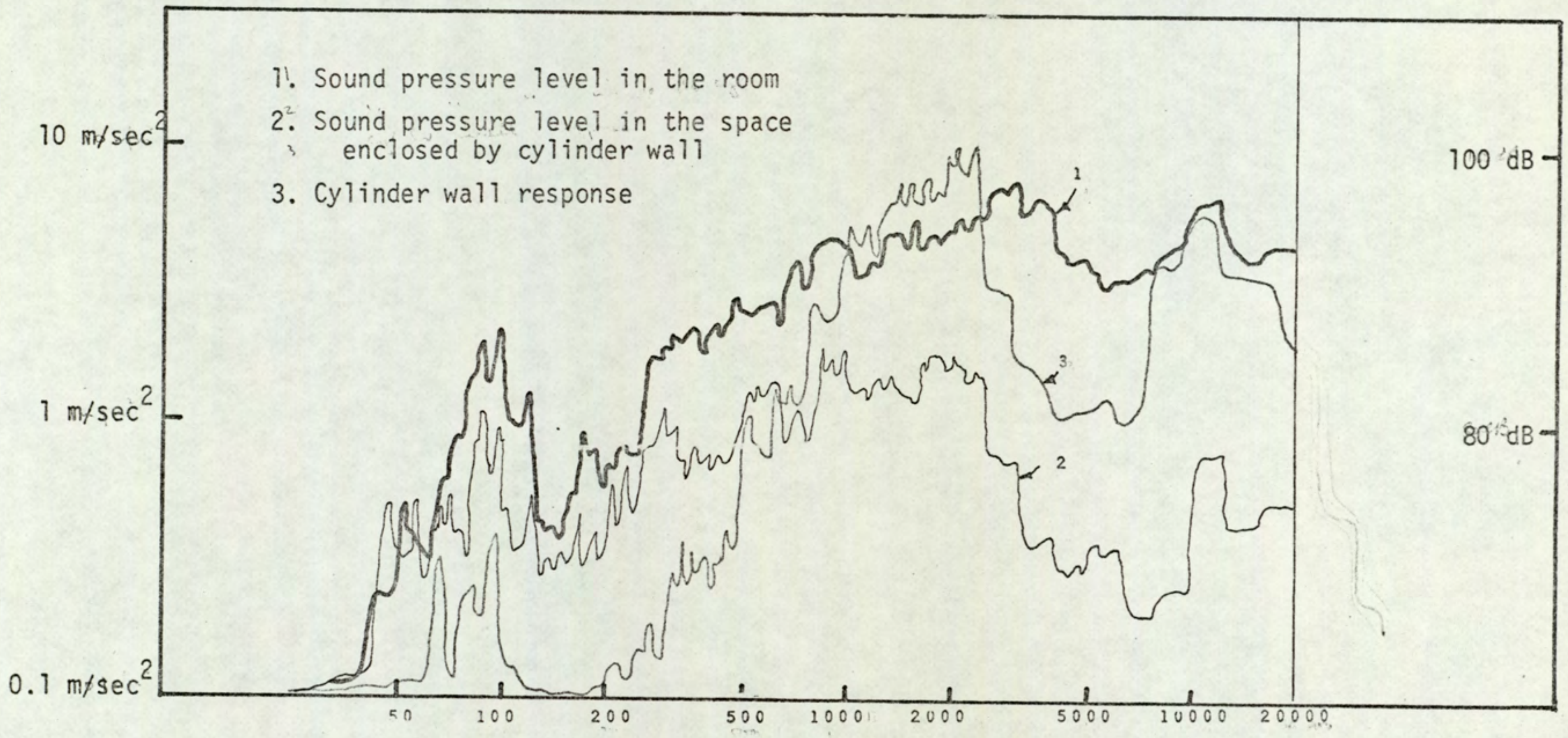

1/3 octave band centre frequency Hz.

Fig. 3.11

Graph showing sound pressure and acceleration levels to wideband random acoustical excitation.
Analysed in 1/3 octave.

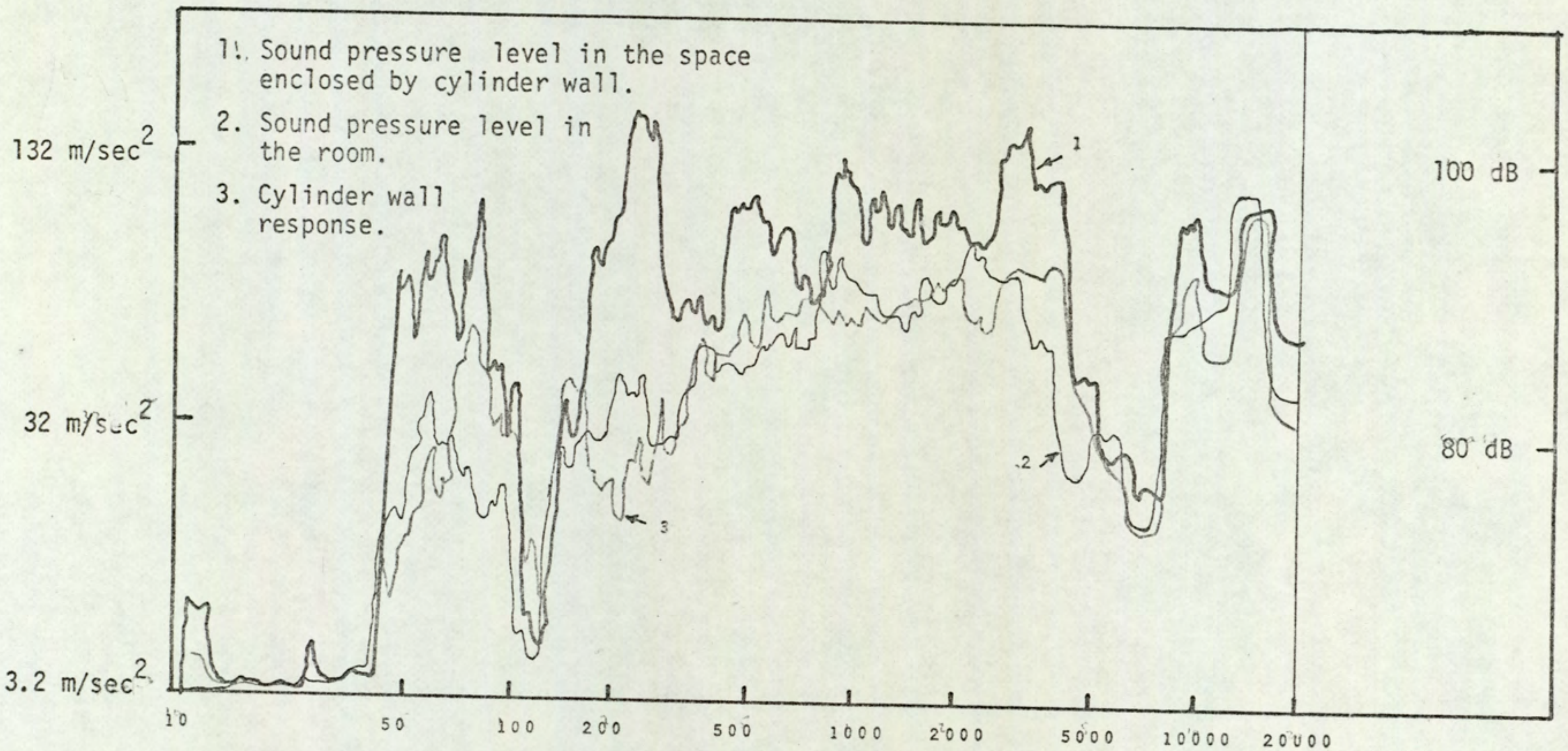

1/3 octave band centre frequency Hz.

Fig. 3.12

Graph showing the sound pressure and acceleration level to wideband random mechanical excitation. Analysed in 1/3 octave.

3.5.2 Constant Bandwidth Analysis

In view of the complex nature of the cylindrical shell vibration and noise transmission characteristics it was desirable to sample and space average a number of inputs simultaneously. Since the Automatic Time and Space Averaging instrument did not have the facility to frequency analyse the data; the best technique to be used was to excite the system in the required frequency band and record the space averaged data in one sweep from a number of transducers randomly positioned either on the shell or in the enclosure. An example of one of the measurements is shown in figure (3.13).

Since it was desired to draw a relationship between the space average sound pressure, Sp, inside the enclosed space and space average shell acceleration, Sa, the structure was acoustically excited in the frequency band of interest and the results sampled are shown in figure (3.14).

In figure (3.15) is shown the variation in the measured results obtained at various filter band centre frequencies. These results show that below 700 Hz and above 3 kHz the filter effects are more obvious.

According to the existing theory of hearing, the human ear responds to sound much in the same way as a constant percentage bandwidth analyser having a bandwidth of about 1/3 octave. Thus, in order to obtain a relationship between the space average subjective

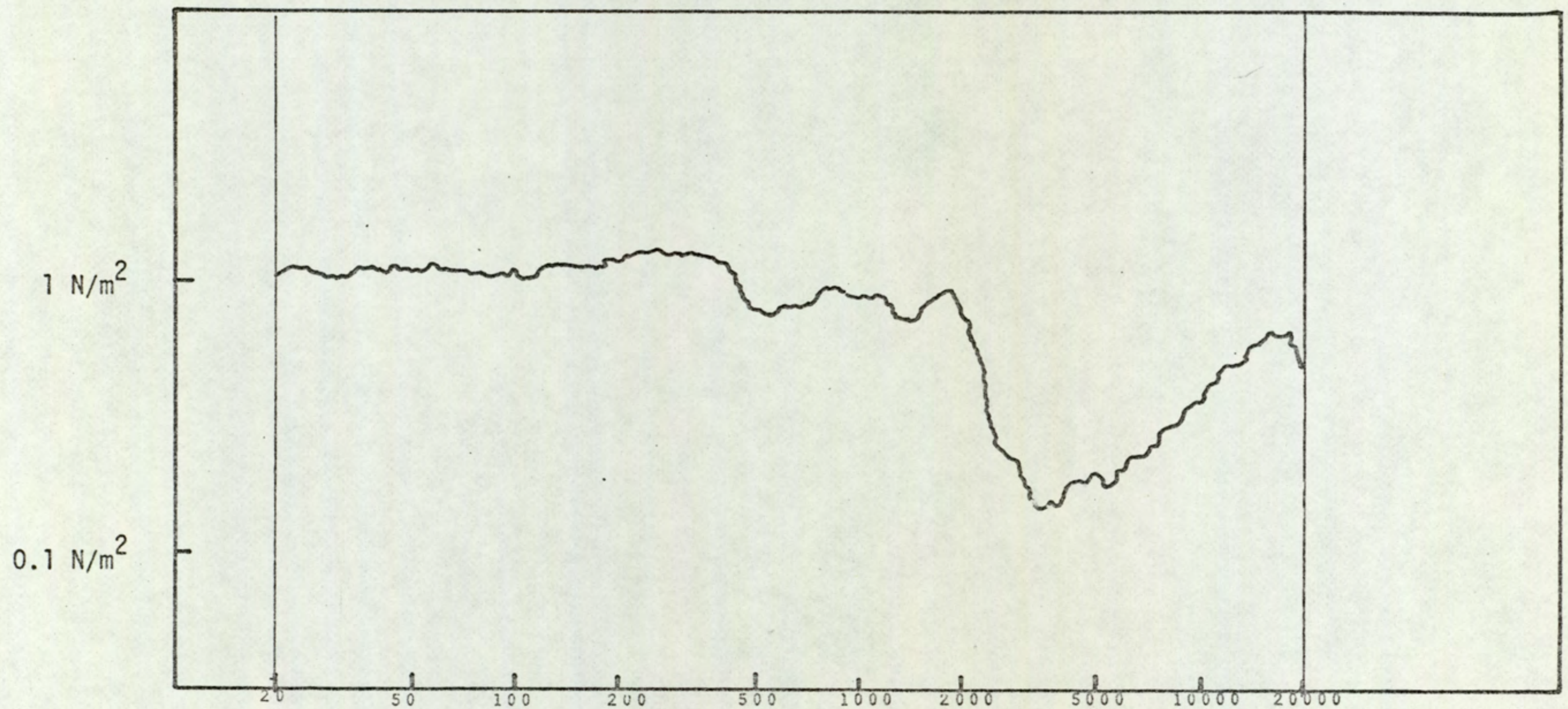

300 Hz band

FIG. 3.13

Graph showing space average sound pressure level inside the cylinder (Average of 3 microphones)

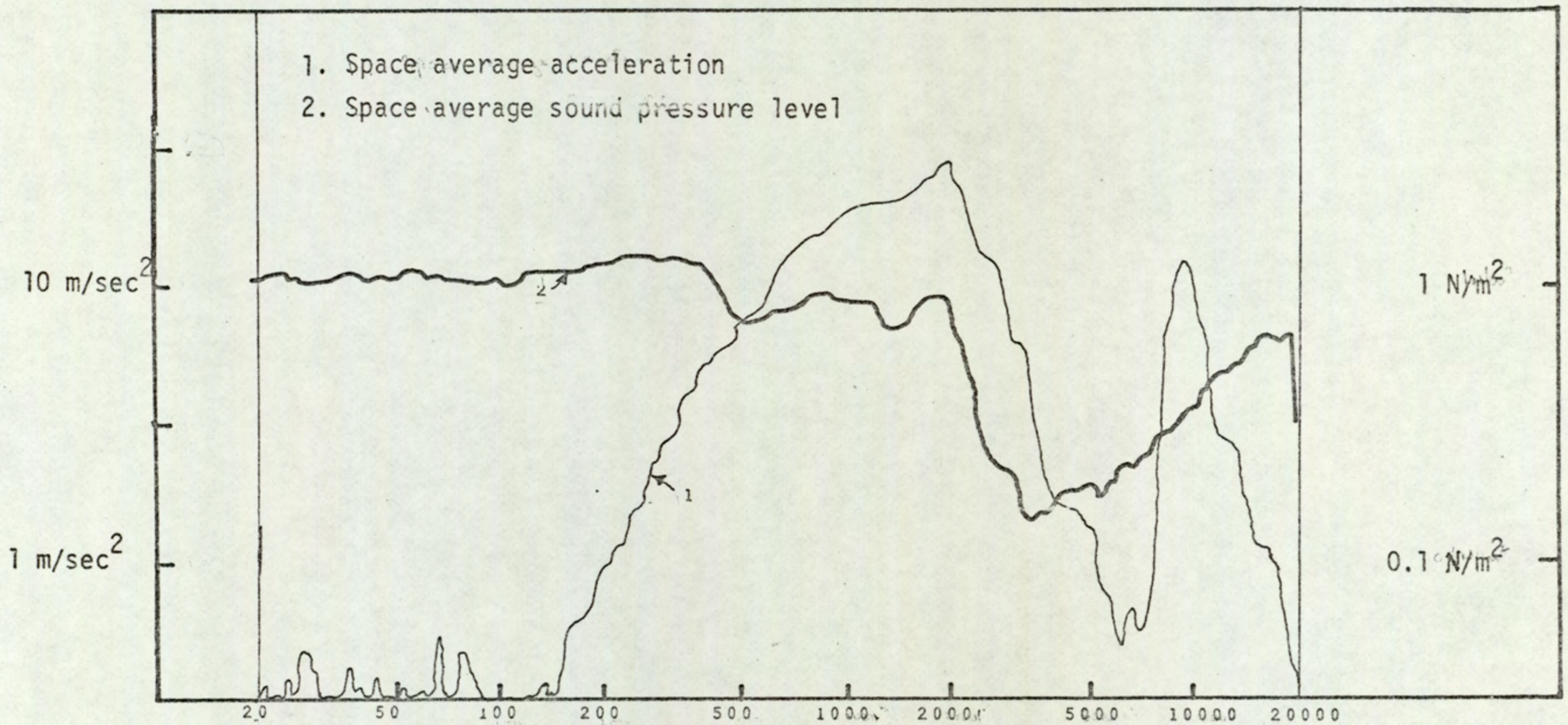

300 Hz band centre frequency Hz.

Fig. 3.14

Graph showing space average acceleration and sound pressure levels.

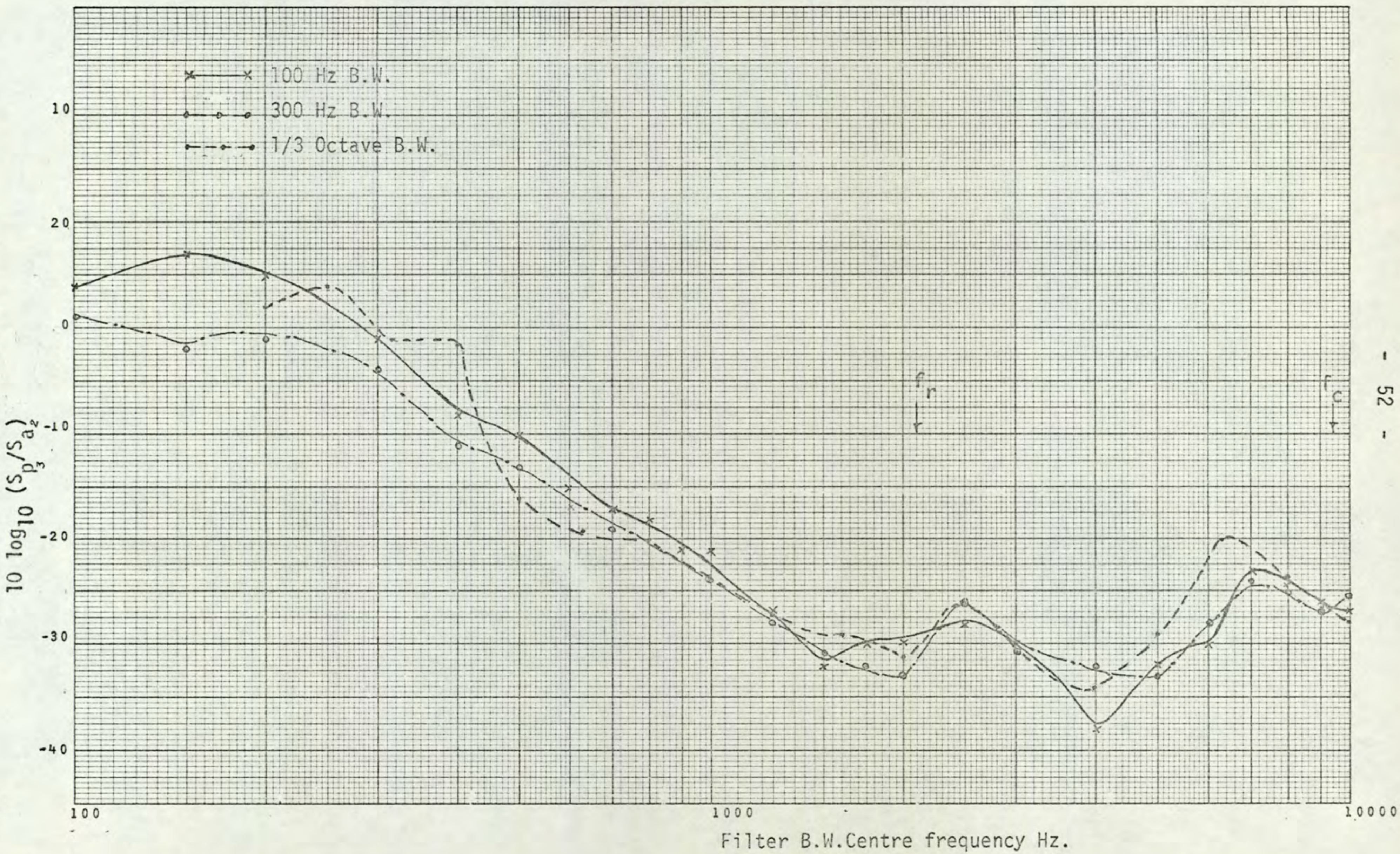
100 Hz B.W.
300 Hz B.W.
1/3 Octave B.W.
10
20
0
-10
-20
-30
-40
$10 \log_{10} (S_{p_3}/S_{a_2})$
f_r
f_c
100
1000
10000
Filter B.W.Centre frequency Hz.

Fig. 3.15

loudness of a measured sound inside the cylindrical vessel and the space average vibration level, it would be more convenient to have the data in the form of 1/3 octave band sound and vibration levels. Therefore, more measurements were taken when the structure was excited in the 1/3 octave band and the results compared with those obtained from a wideband random excitation and analysed in the 1/3 octave band.

Comparison of the results obtained by two methods of analysis are shown in figure (3.16) and (3.17). This shows a trend in the measured result and that the separation between the results obtained by the two methods of analysis were small when the structure was fully stiffened with 6 radial and 12 longitudinal stiffeners except above 6 K Hz. In figures (3.18) and (3.19) is shown more comparison of the results. This gives some confirmation in the trends of the measurement made under different stiffening and exciting conditions.

Selection of an analyser, therefore, seems to depend upon the amount of data to be analysed and the analysis equipment available. Even though the constant percentage bandwidth type of analysis seems, from the investigation, to offer many advantages where only a trend in the results are required, may not be sufficient when more detailed information is desired. For the study of noise transmission characteristics, analysis in the 1/3 octave should be sufficient but when studying vibration characteristics, analysis in the narrow band is recommended.

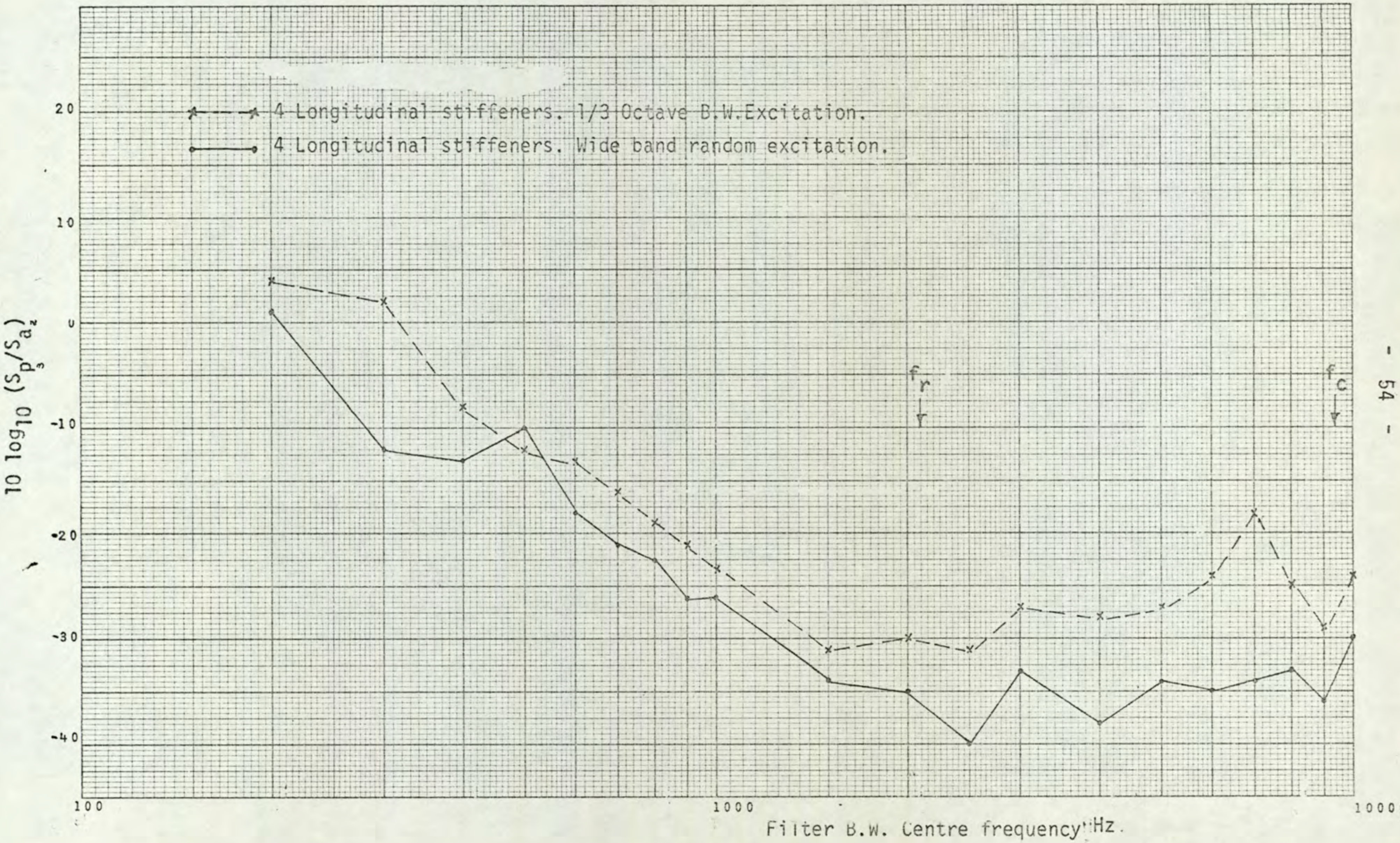
4 Longitudinal stiffeners. 1/3 Octave B.W.Excitation.
4 Longitudinal stiffeners. Wide band random excitation.
20
10
0
-10
-20
-30
-40
$10 \log_{10} (S_{p_3}/S_{a_z})$
100
1000
10000
Filter B.W. Centre frequency Hz.
f_r
f_c

Fig. (3.16)

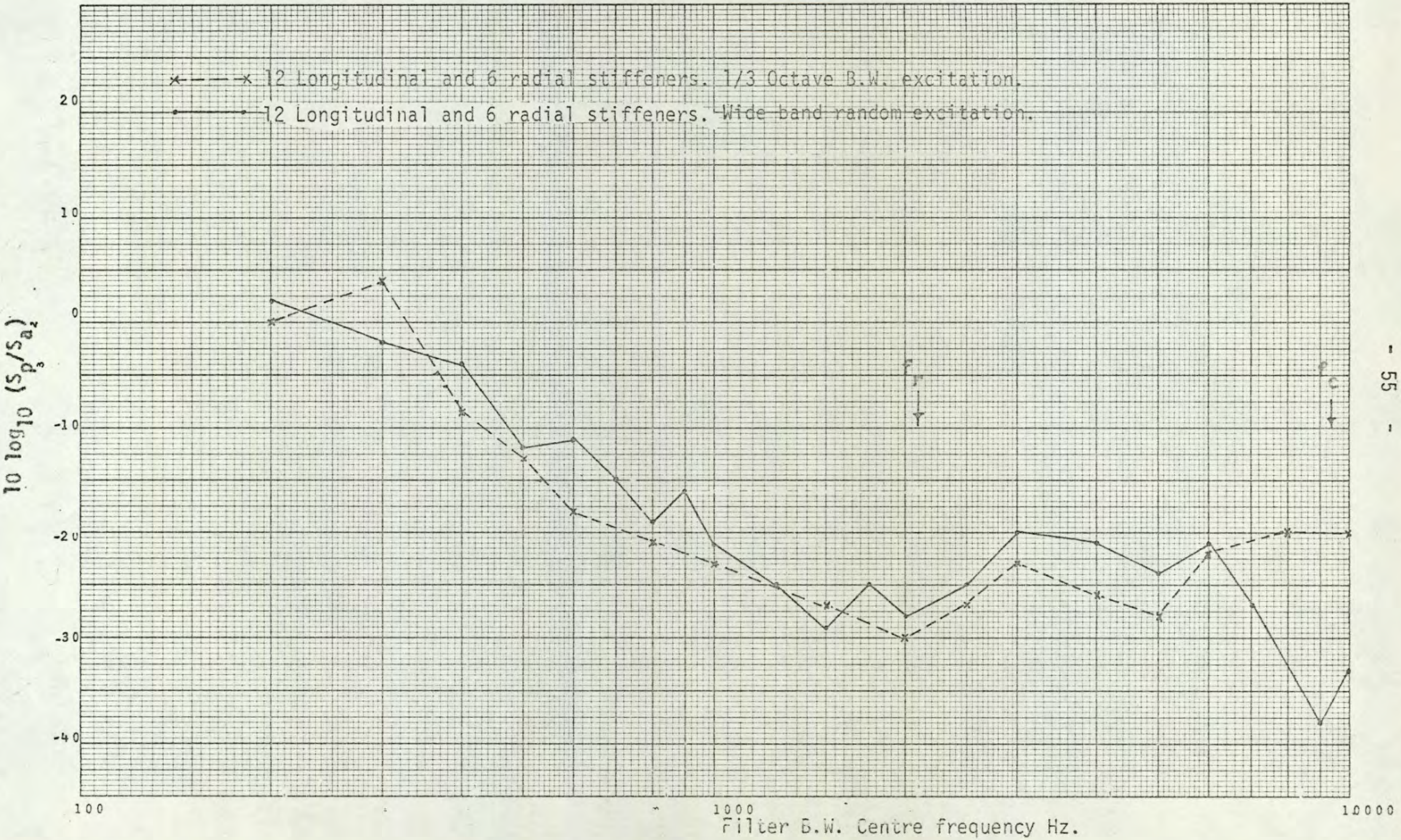

12 Longitudinal and 6 radial stiffeners. 1/3 Octave B.W. excitation.
12 Longitudinal and 6 radial stiffeners. Wide band random excitation.
20
10
0
-10
-20
-30
-40
$10 \log_{10} (S_{p_3}/S_{a_2})$
f_r
f_c
100
1000
10000
Filter B.W. Centre frequency Hz.

Fig. (3.17)

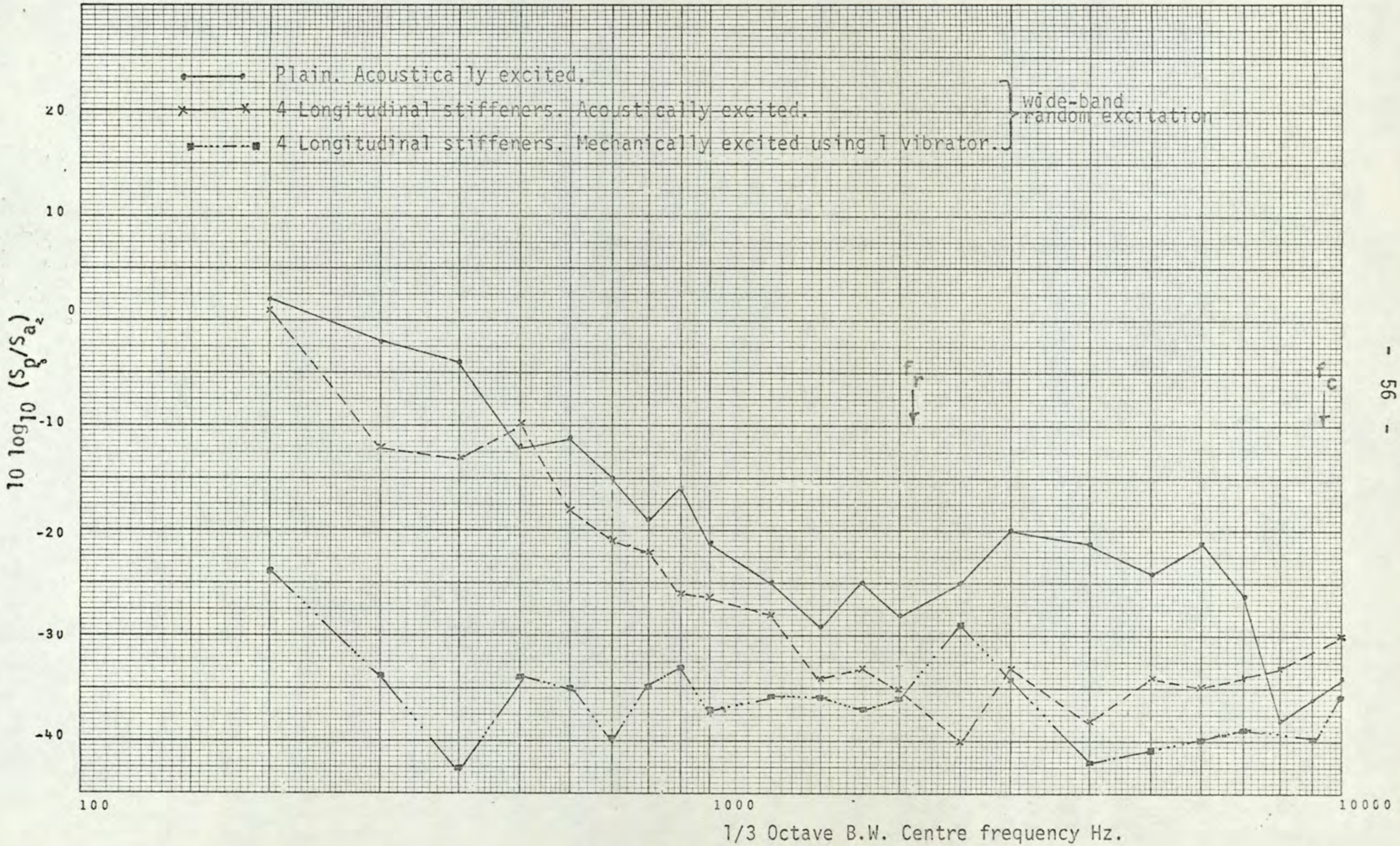

Plain. Acoustically excited.
4 Longitudinal stiffeners. Acoustically excited.
4 Longitudinal stiffeners. Mechanically excited using 1 vibrator.
wide-band random excitation
20
10
0
-10
-20
-30
-40
$10 \log_{10} (S_p/S_{a_2})$
f_r
$\frac{f_c}{r}$
100
1000
10000
1/3 Octave B.W. Centre frequency Hz.

Fig.(3.18)

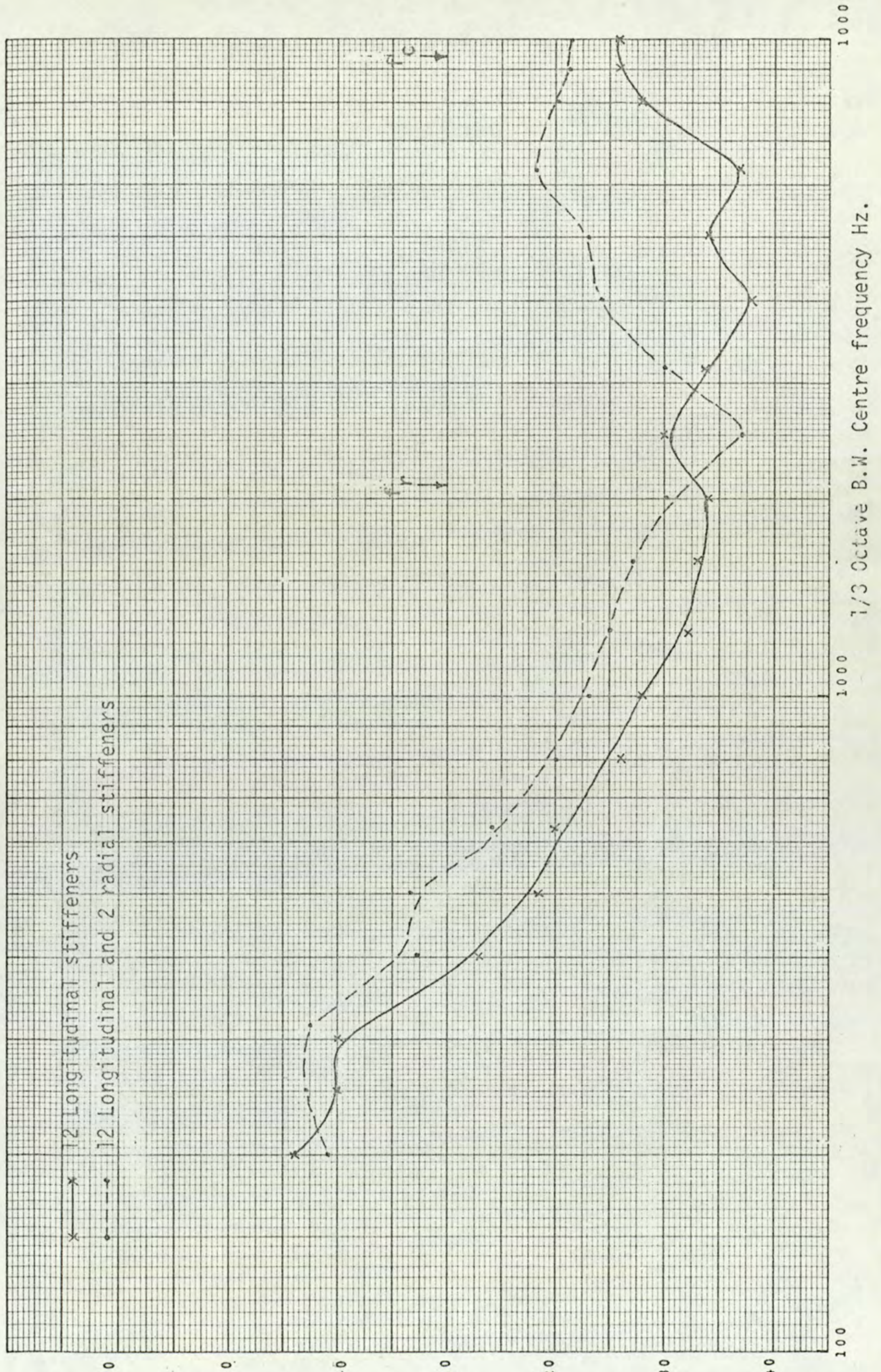
12 Longitudinal stiffeners
12 Longitudinal and 2 radial stiffeners
f_c
f_r
20
10
0
-10
-20
-30
-40
$10 \log_{10} (S_p/S_a)$
100
1000
10000
1/3 Octave B.W. Centre frequency Hz.

Fig. (3.19)

3.6 Transducers - Selection of an optimum number for the measurement

3.6.1 Accelerometers

Accelerometers were selected for vibration measurement in preference to velocity pick-ups because they were made smaller and their useful frequency range was wider. If the measured result was wanted in terms of velocity or displacement, rather than in terms of acceleration, use could have been made of electronic integrators at the output of acceleration.

The requirement of mechanically small vibration transducer originated from the fact that the transducer should load the structural member on which it is placed as little as possible. This requirement was important from the fact that any extra load might change the original motion of the structure and thus invalidate the measured result. Since measurements were made on thin shells, use was made of the available light weight accelerometers (D.J.Birchall).

The accelerometers were cemented on the shell skin by a thin layer of wax to give the possibility of removing them when necessary. The accelerometer cables were firmly clamped to the shell skin in order to avoid any microphonic noise. This had a disturbing effect at the lower frequency due to local capacity and charge changes owing to dynamic bending or compression and tension of the cable when not clamped.

3.6.2 Selection of An Optimum Number of Accelerometers

(i) Narrow Band Random Excitation

The structure was randomly excited and accelerometers fixed to the skin of the shell were removed one at a time. The space average output measured for different number of accelerometers are given in figure (3.20). This showed that between 200 Hz and 5K Hz an average of 5 accelerometers would be sufficient provided the exciting field is reasonably uniform. This was not so when the structure was mechanically excited and an average of at least 9 accelerometers were required to obtain the same accuracy. Below 200 Hz the accuracy of the measured result depended upon the number of points averaged while above 5K Hz at least 12 accelerometers were required.

(ii) Wide Band Random Excitation

The output from the accelerometers were analysed in 1/1 and 1/3 octave. The results are given in a table of figure (3.21) which showed that one accelerometer would be sufficient provided the exciting field is random and diffuse and the structure is uniformly stiffened.

3.6.3 Microphones

For the measurement of noise inside the cylinder, Bruel and Kjaer type condenser microphones were used. These microphones were attached to a central pole, one in the centre and two 0.45m away from it. The pole was arranged to slide through bushes in the cylinder end blanks and to provide traverse over one half of the cylinder length at any angle.

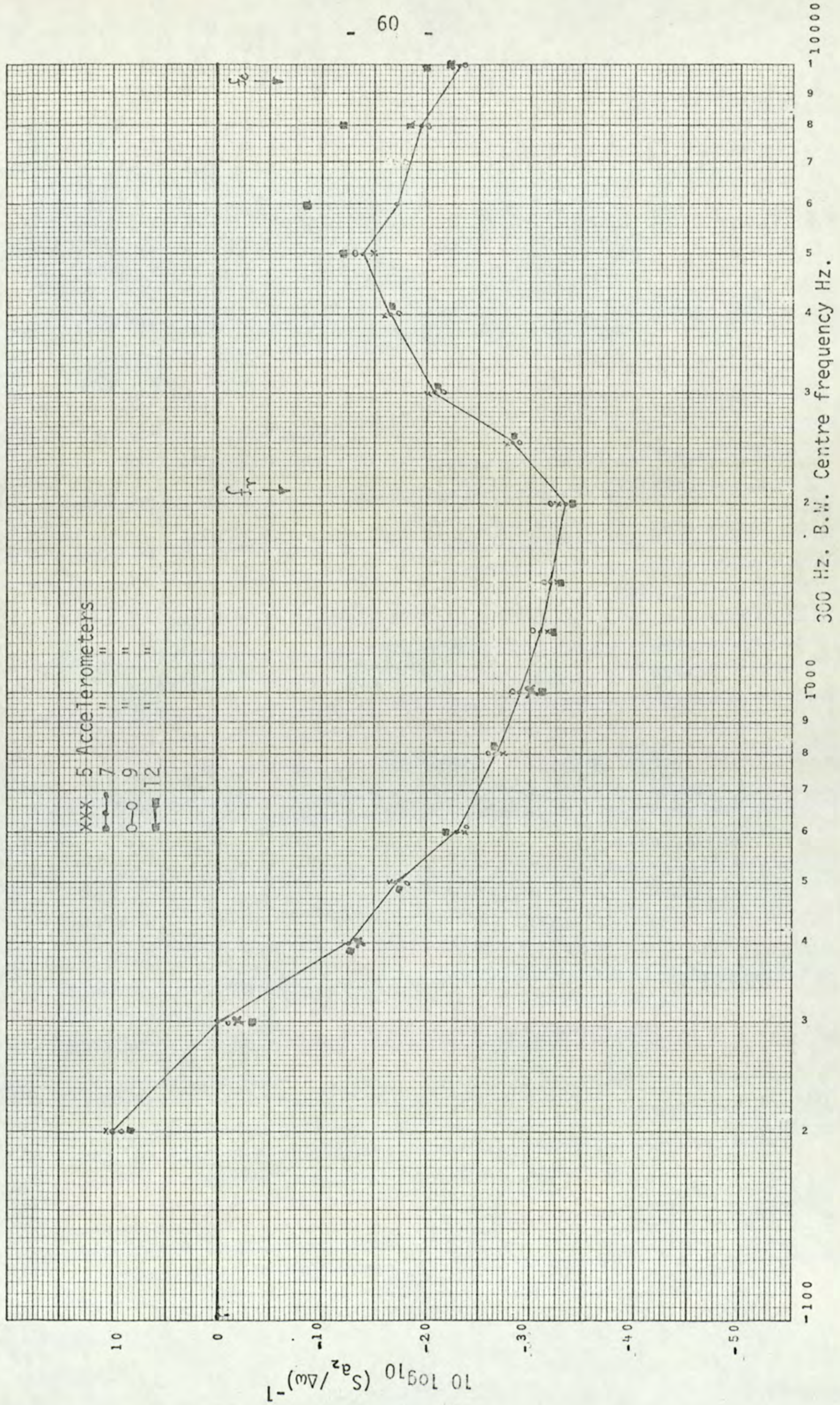

XXX 5 Accelerometers
7 " "
9 " "
12 " "
f_r
f_c
10 $\log_{10}$ $(S_{a_z}/\Delta\omega)^{-1}$
10
0
-10
-20
-30
-40
-50
100
2
3
4
5
6
7
8
9
1000
2
3
4
5
6
7
8
9
10000
300 Hz. B.W. Centre frequency Hz.

Fig. (3.20)

Position → f ↓	1	2	3	4	5	6	7	8	9	10	11	12
50	.14	.18	.16	.18	.16	.17	.18	.2	.19	.18	.19	.17
200	.11	.12	.14	.10	.10	.14	.13	.14	.10	.13	.12	.13
500	.32	.30	.31	.35	.32	.36	.35	.32	.33	.32	.34	.32
1000	3.6	3.8	3.8	3.7	3.9	3.8	3.6	3.8	3.6	3.7	3.4	3.2
1500	5.5	5.3	5.6	5.3	5.4	5.2	5.3	5.2	5.4	5.3	5.5	5.4
2000	9.5	9	9.5	9.5	9	9	9	9.5	9.5	9.5	9	9
3000	3.0	3.0	2.8	2.9	3.0	2.9	3.1	2.9	2.9	3.0	3.1	3.1
4000	1.4	1.4	1.3	1.5	1.3	1.4	1.4	1.3	1.4	1.5	1.5	1.4
5000	0.80	0.90	0.85	0.75	0.80	0.82	0.78	0.80	0.75	0.80	0.80	0.75
6000	1.1	1.0	1.2	1.2	1.3	1.2	1.0	0.95	1.2	1.0	1.2	0.95
8000	2.2	2.0	2.2	2.0	2.25	2.2	2.0	2.25	2.0	2.0	2.1	2.2
9000	3.4	3.0	3.0	2.9	2.9	3.2	2.9	2.80	3.0	3.0	3.1	2.9
10000	5.5	5.5	5.6	5.3	5.6	3.6	5.2	5.2	5.2	5.3	5.5	5.5

TABLE 3.21

Table showing acceleration levels (m/sec^2) measured at different positions of cylinder when subjected to wideband random acoustical excitation. Response analysed in 1/3 octave.

3.6.4 Selection of an optimum number of microphones

(i) Narrow band random excitation

The system was randomly excited and the space average output from different numbers of microphones were recorded. This was repeated for other positions along the cylinder length and radial directions. Results of one of such measurements is given in figure (3.22).

It was found that between 70 Hz and 3K Hz, space average of only three microphones would be sufficient provided they are not positioned too close (< 0.3m) to the ends. This was because noise reflection from the hard ends and noise absorption by the non-reverberant ends tended to upset the results. When the structure was excited in the frequency bandwidth narrower than 300 Hz, at least six microphones were required for the same accuracy.

In the frequency below 70 Hz, it was necessary to space average at least 12 positions for a reasonable accuracy. In the frequency above 3K Hz, it was difficult to make a reasonable assessment due to sound absorption in the room. Similar measurements were made when the system was mechanically excited. It was found that the conclusions drawn above did not hold because the exciting source was not uniform and space average of many positions in the enclosure were required.

(ii) Wide band random excitation

The system was excited in the wide band random and the output

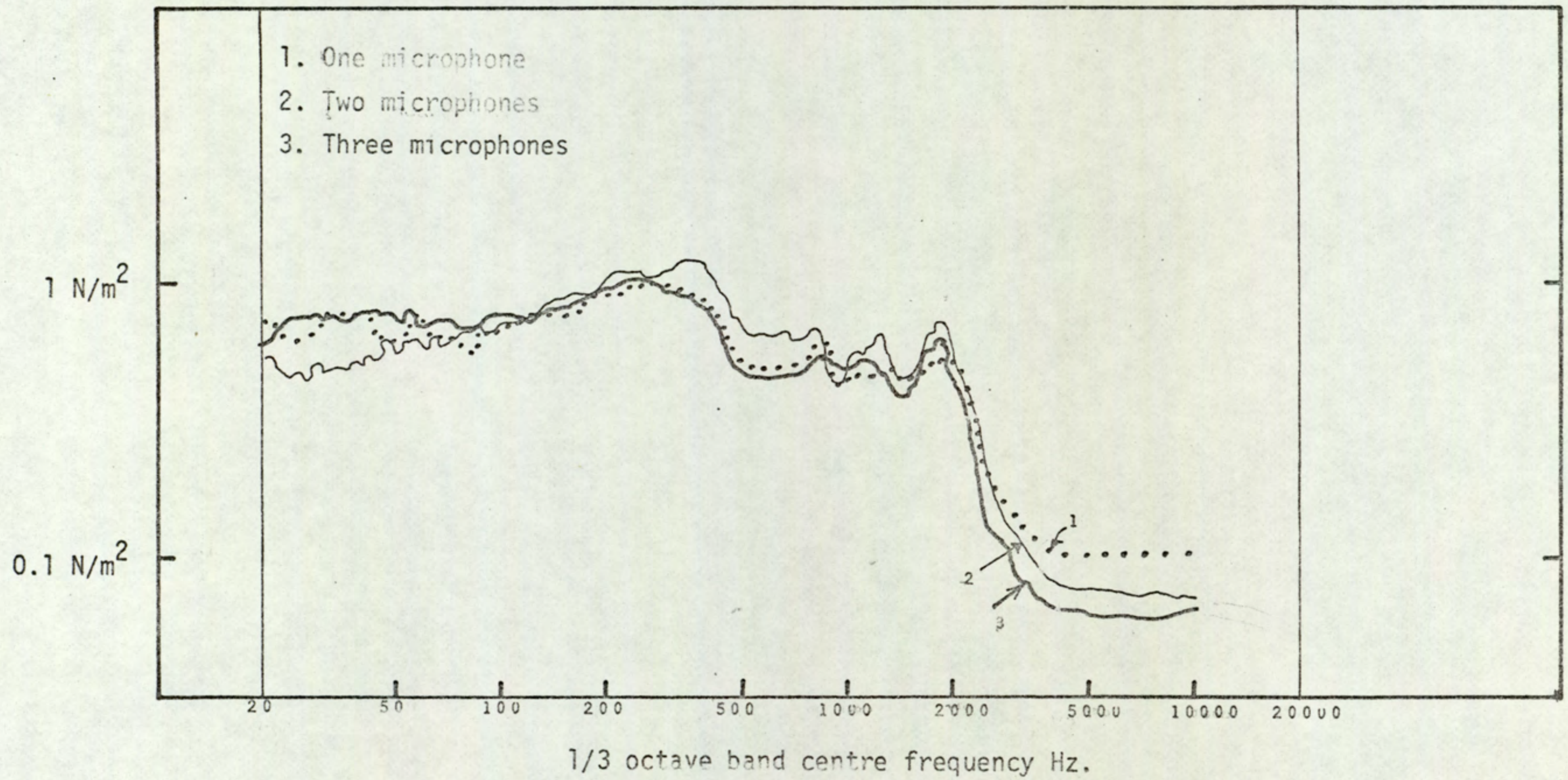

Fig. 3.22

Graph showing the effects of varying number of microphones.

from microphones placed at different positions and radial direction were analysed in 1/1 and 1/3 octave. It was found that only one microphone positioned in the centre of the enclosure was sufficient. The variation in the measurements along the length and radial direction of the enclosure was ± 0.5 dB. The system was also subjected to 1/1 and 1/3 octave excitation and it was found that space average of two microphones were sufficient.

This was not so when the system was subjected to mechanical excitation. Space average of six microphone positions were required when the system was excited in the wide band random and at least 12 positions were required to be sampled when the system was excited in 1/1 and 1/3 octave.

3.7 Determination of least area for the measurement

It is not always possible to take measurements on a structure as complex as a fuselage. Therefore, measurement is taken on either a scaled model or a part of the real structure. In this case, a model described in section (3.3) was used for determining the smallest area that could be used for this purpose. The results obtained from this could then be used for the whole structure. The areas considered for this test subjected to a particular type of excitation are given on the next page.

Type of Excitation	Area 1 (2.4mx1.8m) Whole Cylinder	Area 2 (0.3mx0.3m) Middle of Cylinder	Area 3 0.15mx0.15m Middle of Cylinder	Area 4 0.3mx0.3m End of Cylinder	Area 5 0.15mx0.15m End of Cylinder	Area 6 Radial	Area 7 Longitudinal	Area 8 0.3mx0.3m Between Stiffeners	Area 9 0.3mx0.3m Including Stiffeners
Wideband Random	✓					✓	✓		
1/3 Octave	✓	✓	✓	✓	✓	✓	✓		
Narrow Band Random	✓	✓	✓	✓	✓	✓	✓	✓	✓

3.7.1 Wideband Random Excitation

The output from each accelerometer was analysed in 1/3 octave and recorded on the level recorder. An example of one such recording is given in figure (3.23). It was found that the acceleration level was within ± 1 dB for any points sampled on the structure. This was perhaps because it was a uniformly stiffened model which was excited with diffused noise field. The test was then repeated for mechanical excitation when it was found that vibration level was different at every point tested on the skin of the cylinder.

It is clear, therefore, that only a point measurement would be sufficient provided the structure is uniformly stiffened and excited with a diffused source. An average of more than one point measurement on a larger area would be required where a structure is unevenly stiffened and exciting source is not diffused. This was not true when the structure was mechanically excited.

3.7.2 1/3 Octave excitation

The space average sound pressure level (Sp) of 3 microphones placed inside the cylindrical shell was measured first. Measurement of space average (Sa) of 12 accelerometers placed in areas shown in section (3.6) was then taken. In order to compare the results, and to show a relationship between the space average sound pressure level inside the cylindrical enclosure and shell skin space average acceleration level at different parts of the

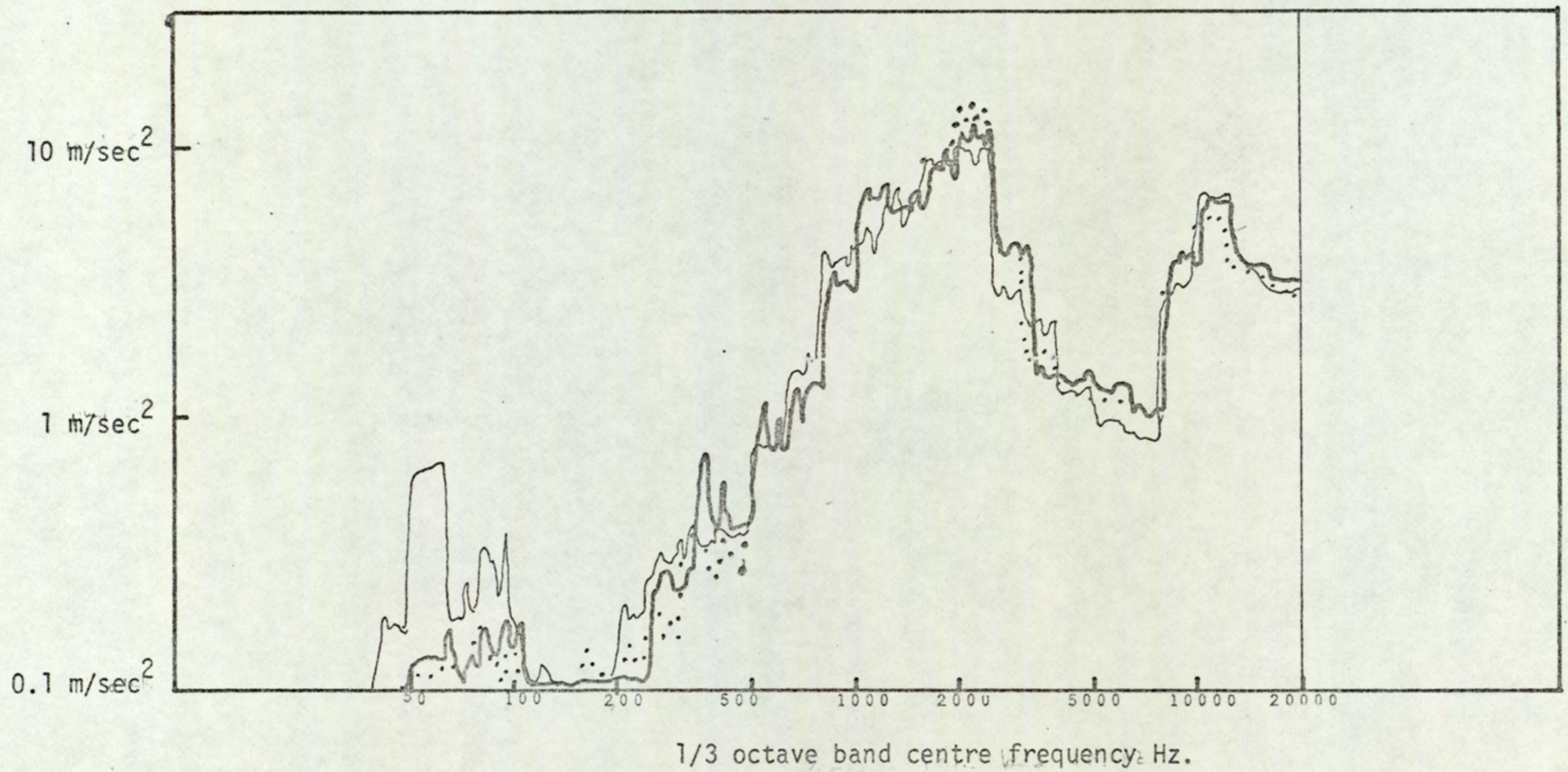

Fig. 3.23

Comparison of cylinder response measured at different points on the cylinder.

model, the S_{p_3}/S_{a_2} ratio was taken. An example of one such measurement is given in figure (3.24).

Between 350 Hz and 2.5K Hz there was a difference of only 1.5 dB between the measured results. This means that an area as small as 0.15m x 0.15m (6" x 6") would be sufficient. Above 2.5K Hz and below 350 Hz, an area not smaller than 0.3m x 0.3m (12" x 12") should give results closer to that measured on a large area. Again this was found not true for mechanical excitation.

3.7.3 Narrow band random excitation

The above experiment was repeated when the structure was acoustically excited in the narrow band. Measurements were once again taken in the areas shown in section (3.6). The result in figure (3.25) shows that there is a difference of approximately ± 3.5 dB between the measured results. This difference was even wider when the structure was excited in the frequency band narrower than 300 Hz. This variation in the results was consistent for other measurements not shown here.

The result shown in figure (3.26) clearly shows that a poor agreement exists between the overall measurement and the measurement taken between the stiffeners. Further result is shown in figure (3.27) from which it is concluded that between 350 Hz and the ring frequency, (It is the frequency at which the longitudinal wavelength in the cylinder material is equal to the circumference) of 2.1 K Hz, measurement could be taken either between the stiffeners or on an area including them.

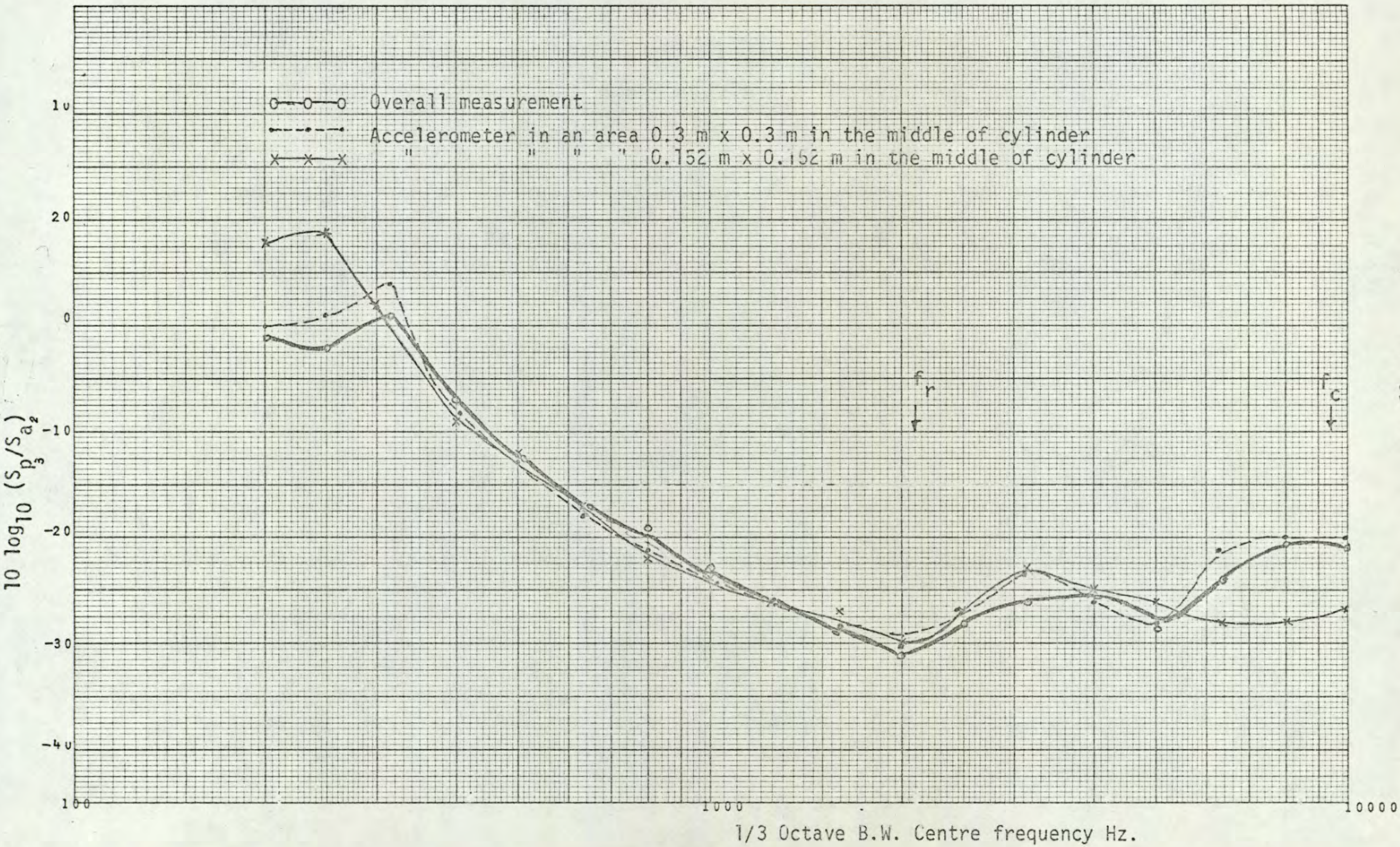
Overall measurement
Accelerometer in an area 0.3 m x 0.3 m in the middle of cylinder
" " " " 0.152 m x 0.152 m in the middle of cylinder
10
20
0
-10
-20
-30
-40
10 log10 (Sp3/Sa2)
100
1000
10000
1/3 Octave B.W. Centre frequency Hz.
fr
fc

Fig. (3.24)

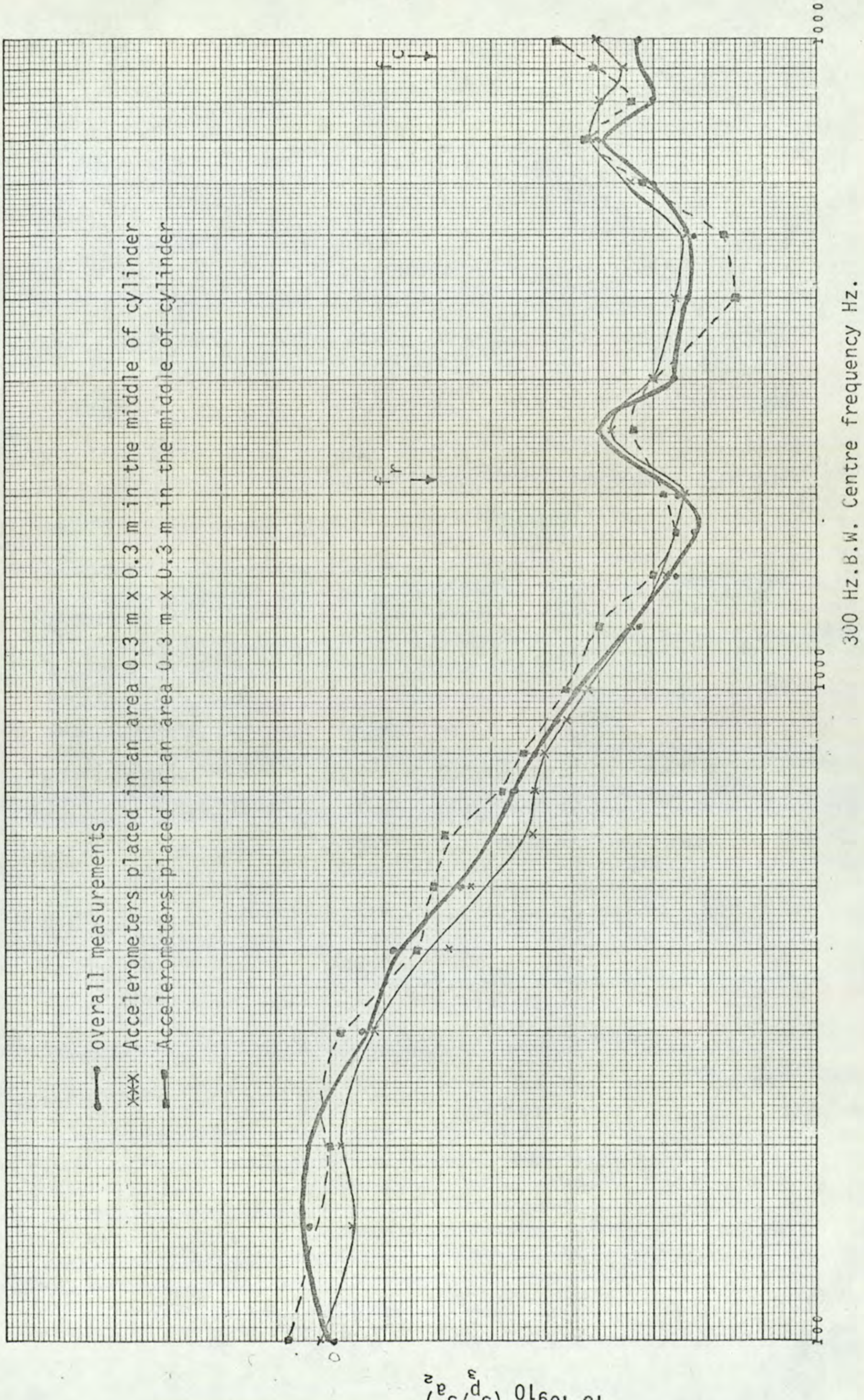
overall measurements
Accelerometers placed in an area 0.3 m x 0.3 m in the middle of cylinder
Accelerometers placed in an area 0.3 m x 0.3 m in the middle of cylinder
f_c
f_r
100
1000
10000
0
300 Hz.B.W. Centre frequency Hz.
$10 \log_{10} (S_p/S_{a_z})$

Fig. 3.25

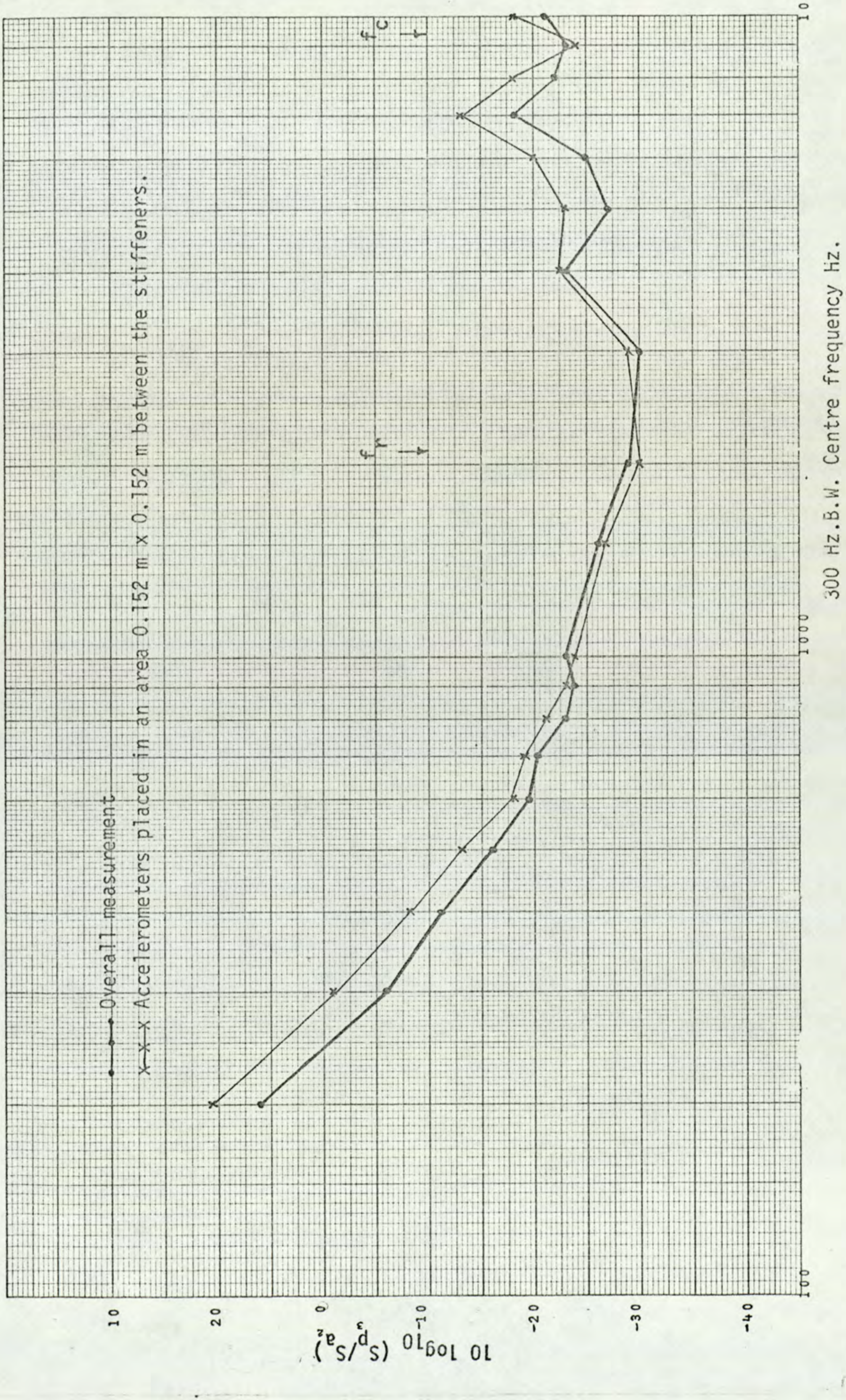

Overall measurement
x—x—x Accelerometers placed in an area 0.152 m x 0.152 m between the stiffeners.
f_c
f_r
100
1000
10000
10
20
0
-10
-20
-30
-40
$10 \log_{10} (S_p/S_{a^2}^3)$
300 Hz.B.W. Centre frequency Hz.

Fig. (3.26)

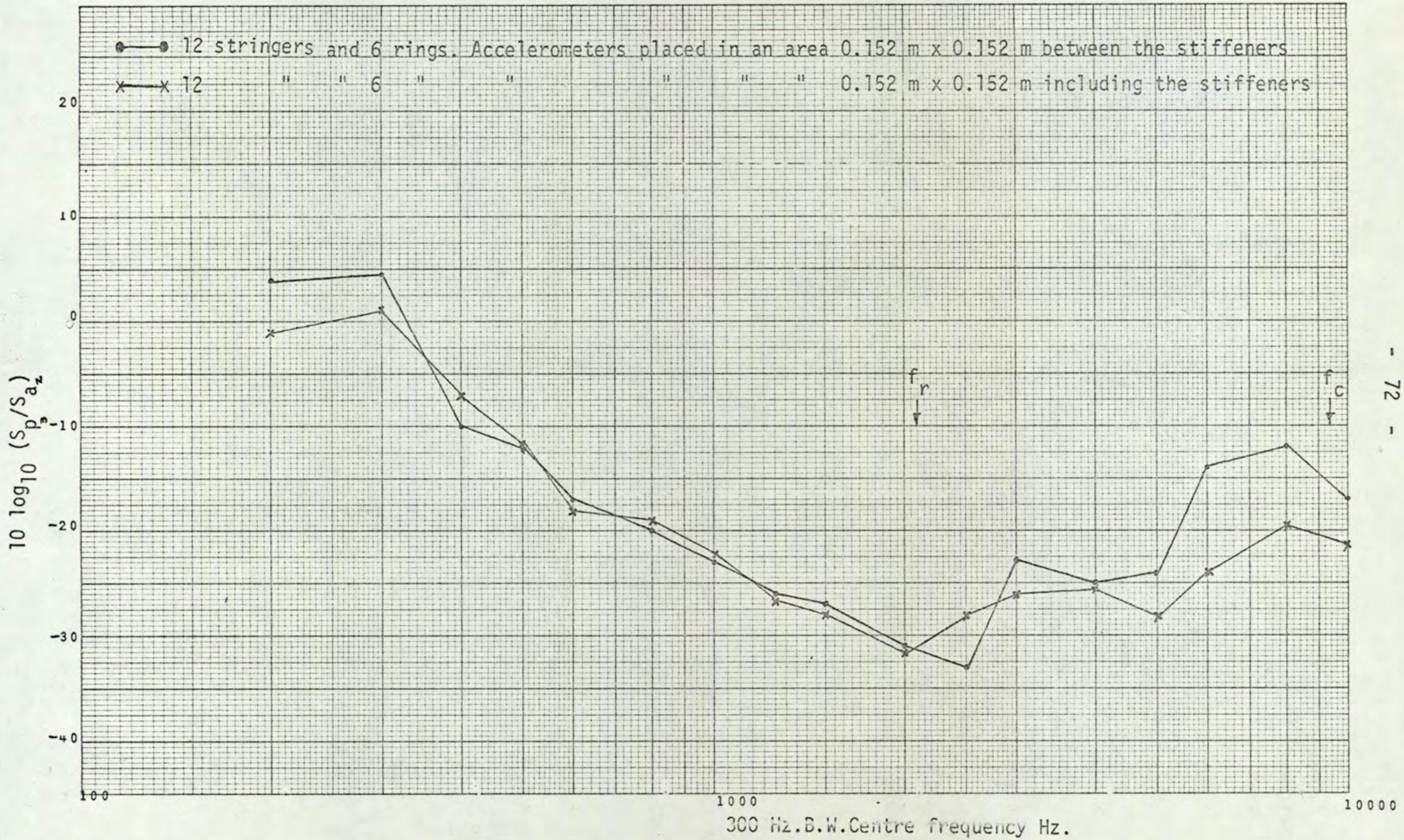
12 stringers and 6 rings. Accelerometers placed in an area 0.152 m x 0.152 m between the stiffeners
12 " " 6 " " " " " 0.152 m x 0.152 m including the stiffeners
f_r
f_c
20
10
0
-10
-20
-30
-40
$10 \log_{10} (S_p/S_{a_z})$
100
1000
10000
300 Hz.B.W.Centre frequency Hz.

Fig. (3.27)

3.8 Comparison of measurements obtained by acoustical and mechanical excitation of the cylindrical shell

In order to investigate the vibration properties of the experimental model approximating realistic fuselage, a uniform exciting facility was necessary. To achieve this and to meet one of the objectives of the contract, the investigations described in this section were carried out.

3.8.1 Effects of vibrators on overall cylindrical shell response

The cylindrical shell was suspended in the centre of the reverberant room and the overall space average acceleration were measured when the cylinder was excited with a vibrator mounted in the middle. The effects of the vibrators were measured by increasing the number of vibrators. The results of this test are shown in figure (3.28). The variation in the measured results between one vibrator and four vibrators are approximately 10 dB while this difference is not so much between two and four vibrators.

The cylinder was then acoustically excited and overall space average acceleration measured as before. A comparison of this result with that obtained by four vibrators is given in figure (3.29). The difference between the two results is quite obvious. On either side of the ring frequency (2.1K Hz), the cylinder does not appear to absorb energy due to weak coupling between the noise field and the cylinder skin. In the case of mechanical excitation the question of coupling between the exciting source and the structure is not critical because the structure is subjected to forced vibration.

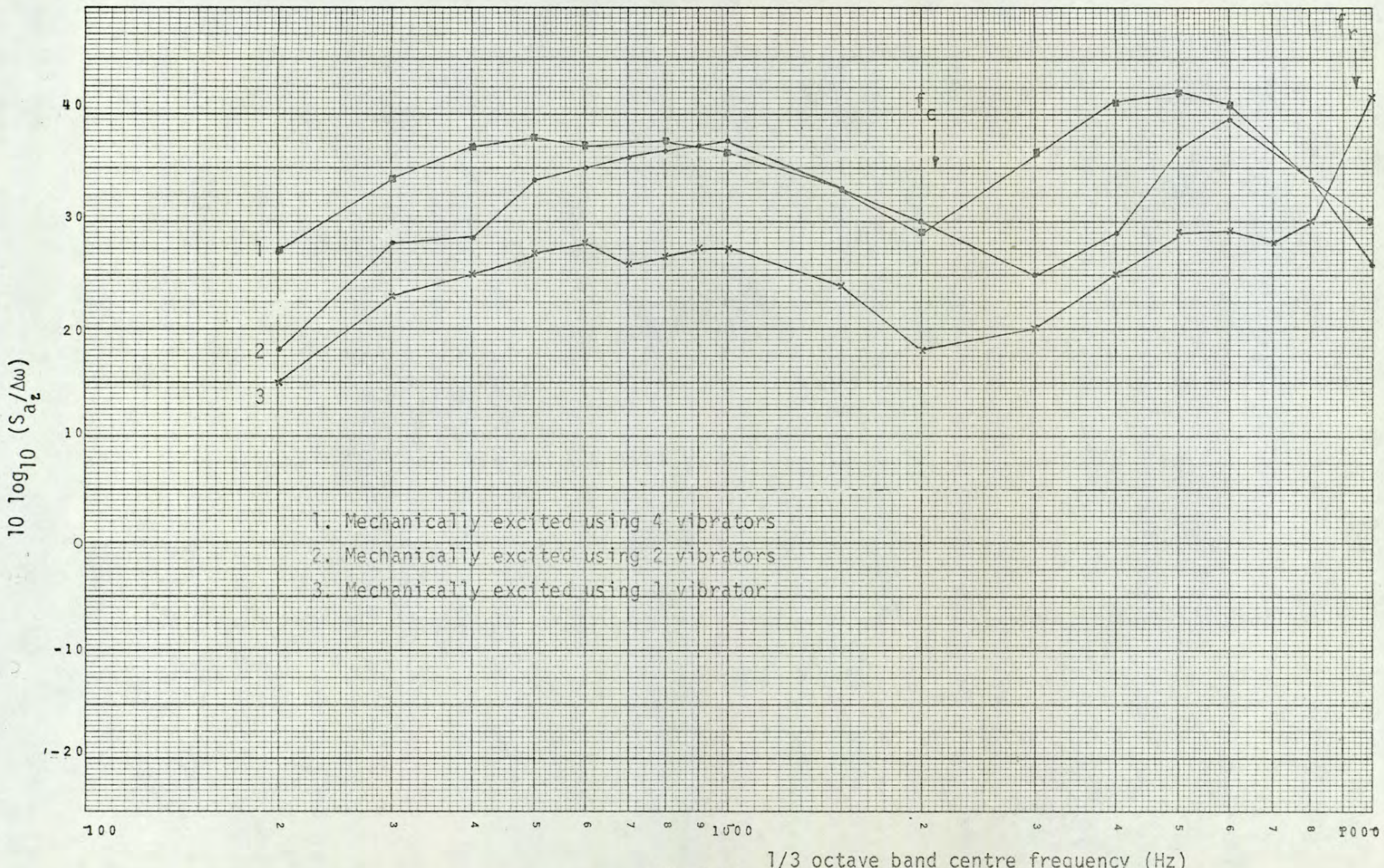
$10 \log_{10} (S_{a_z}/\Delta\omega)$
40
30
20
10
0
-10
-20
100
2
3
4
5
6
7
8
9
1000
10000
f_c
f_r
1
2
3
1. Mechanically excited using 4 vibrators
2. Mechanically excited using 2 vibrators
3. Mechanically excited using 1 vibrator
1/3 octave band centre frequency (Hz)

Fig.3.28

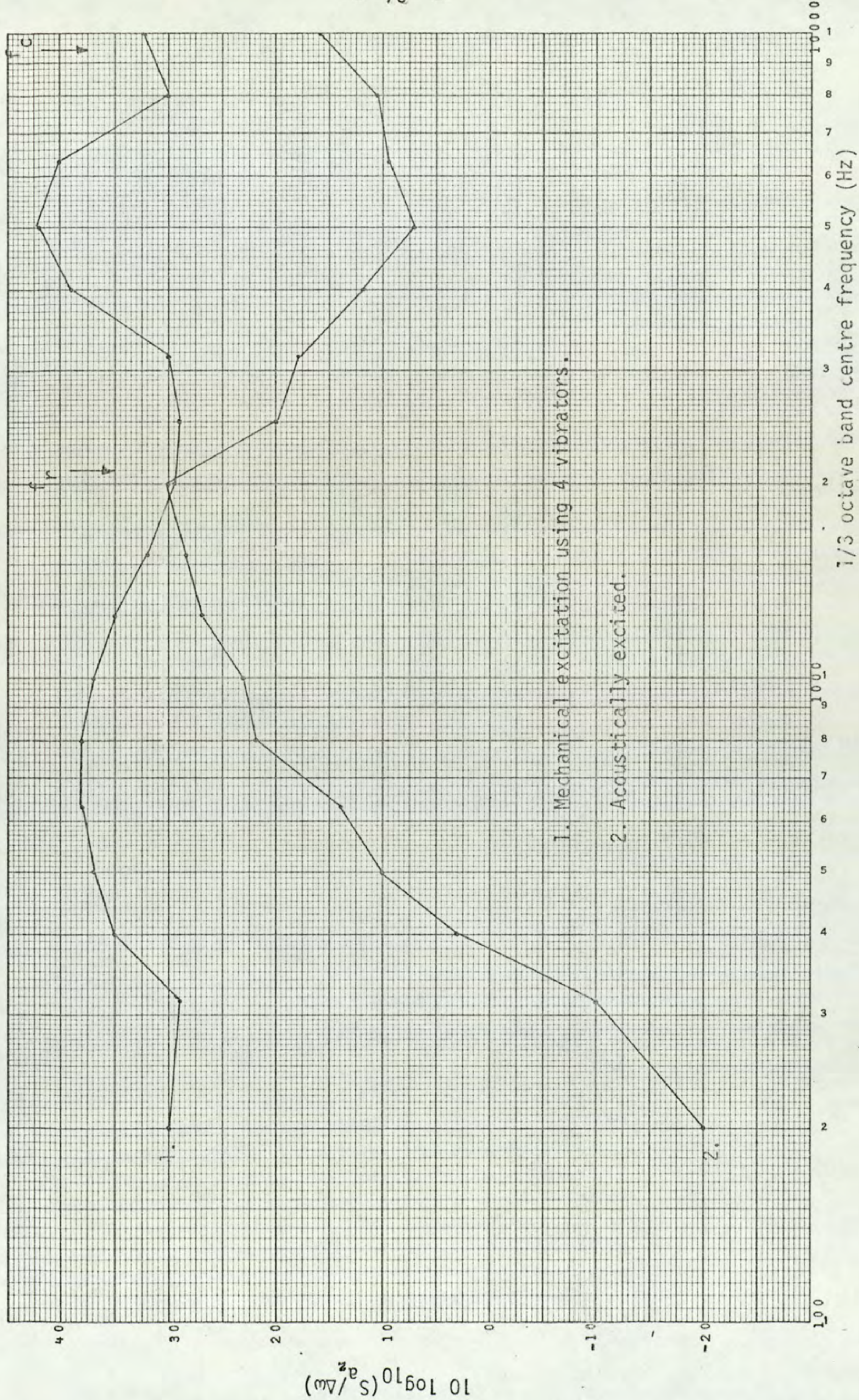
1. Mechanical excitation using 4 vibrators.
2. Acoustically excited.
1/3 octave band centre frequency (Hz)
10 log10(S_az/Δω)
f_c
f_r
40
30
20
10
0
-10
-20
100
1000
10000

Fig. 3.29)

A further test was carried out on the same system but the exciting source was limited to a 1/3 octave and 300 Hz band. The results of this measurement are shown in figure (3.30). Again the separation between the results measured by the two forms of excitation are in the same order.

One of the results shown in figure (3.31) was measured by one accelerometer placed on the cylinder skin. For this, the cylinder was acoustically excited with wideband random source and then repeated for mechanical excitation with the identical input to four vibrators. Measurements were made at a number of positions on the cylinder skin and it was found that in every case the measured results were the same as in figure (3.31). The separation between the two results were more than in figure (3.31) when less numbers of vibrations were used. Although the separation between the two measurements are as shown, there is a close similarity between them in frequency spectrum. Owing to the limitations set by the size of the room and the loudspeaker,anoise level of approximately 110 dB could only be produced in the room for this measurement. If the cylinder could have been excited with a noise level of approximately 140 dB to 160 dB then it is thought a better comparison would have been achieved.

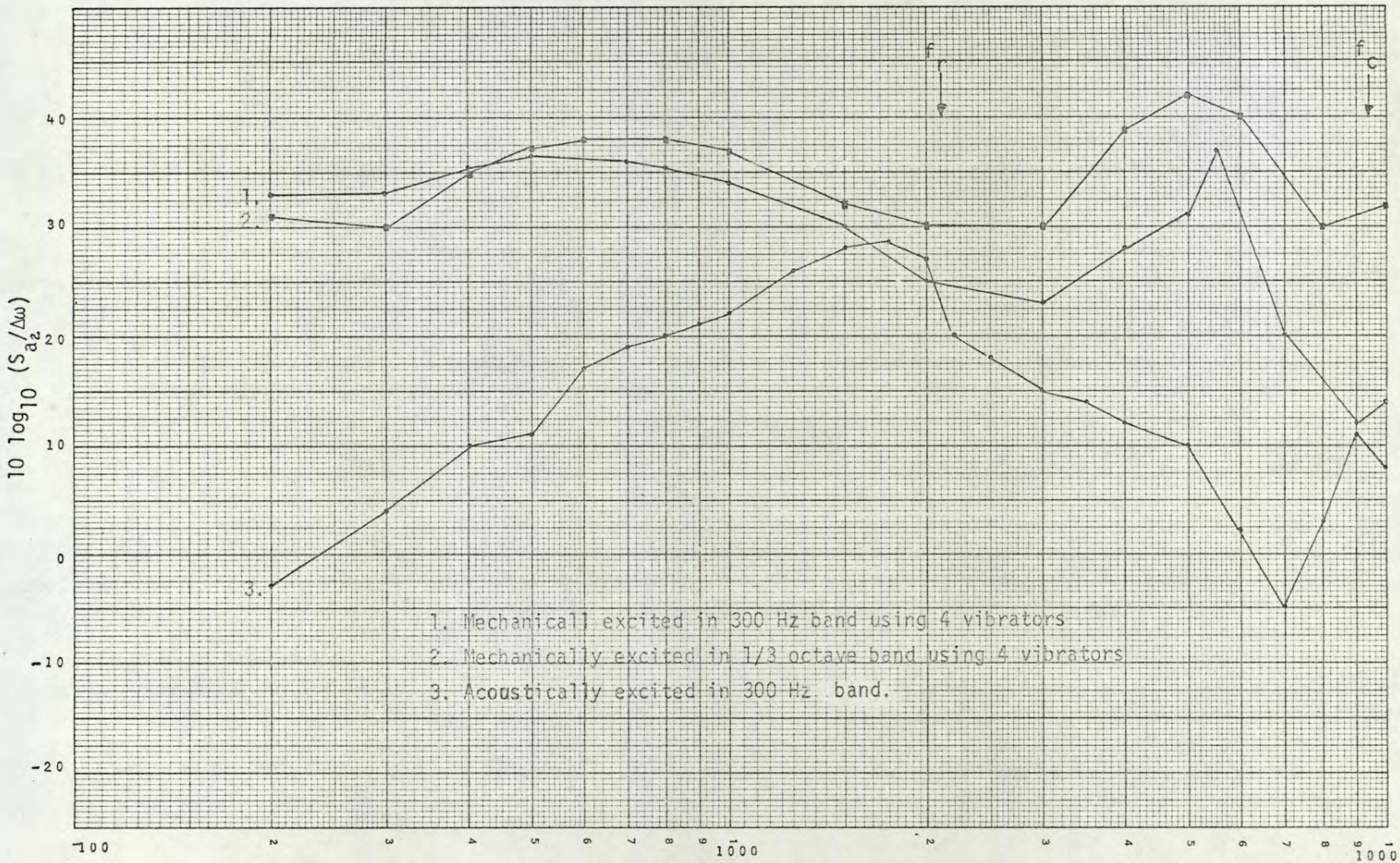

40
30
20
10
0
-10
-20
10 log10 (S_a2/Δω)
100
1000
10000
Filter band centre frequency (Hz)
f_r
f_c
1.
2.
3.
1. Mechanicall excited in 300 Hz band using 4 vibrators
2. Mechanically excited in 1/3 octave band using 4 vibrators
3. Acoustically excited in 300 Hz band.

Fig. 3.30)

f r
f c
1
2
30
20
10
0
-10
-20
10 log10 (S a z /Δω)
100
2
3
4
5
6
7
8
9
1000
2
3
4
5
6
7
8
9
10000
1. Mechanically excited in wide band random using 4 vibrators. Result analysed in 1/3 octave.
2. Acoustically excited in wide band random. Result analysed in 1/3 octave.
1/3 octave band centre frequency (Hz)

Fig.3.31

3.8.2 Effect of vibrations on limited area of cylindrical shell response

The previous experiment was repeated and the measurements were taken in an area 0.3 m x 0.3 m in the middle of the cylinder. The results are shown in figure (3.32). The measurement obtained when the cylinder was excited by 4 vibrators does not show a great deal of difference from that obtained from overall measurement. The result obtained when the cylinder was excited by one vibrator, however, is different above the ring frequency and maintains a trend in response closer to that obtained for acoustical excitation. This similarity was also true for the measurements taken at other parts of the cylinder not shown here.

The results shown in figure (3.33) were obtained when the cylinder was excited in the 1/3 octave using only one vibrator. Twelve accelerometers were placed in radial direction to the point source of excitation. The results show the trend and extent of the cylinder response away from the exciting source.

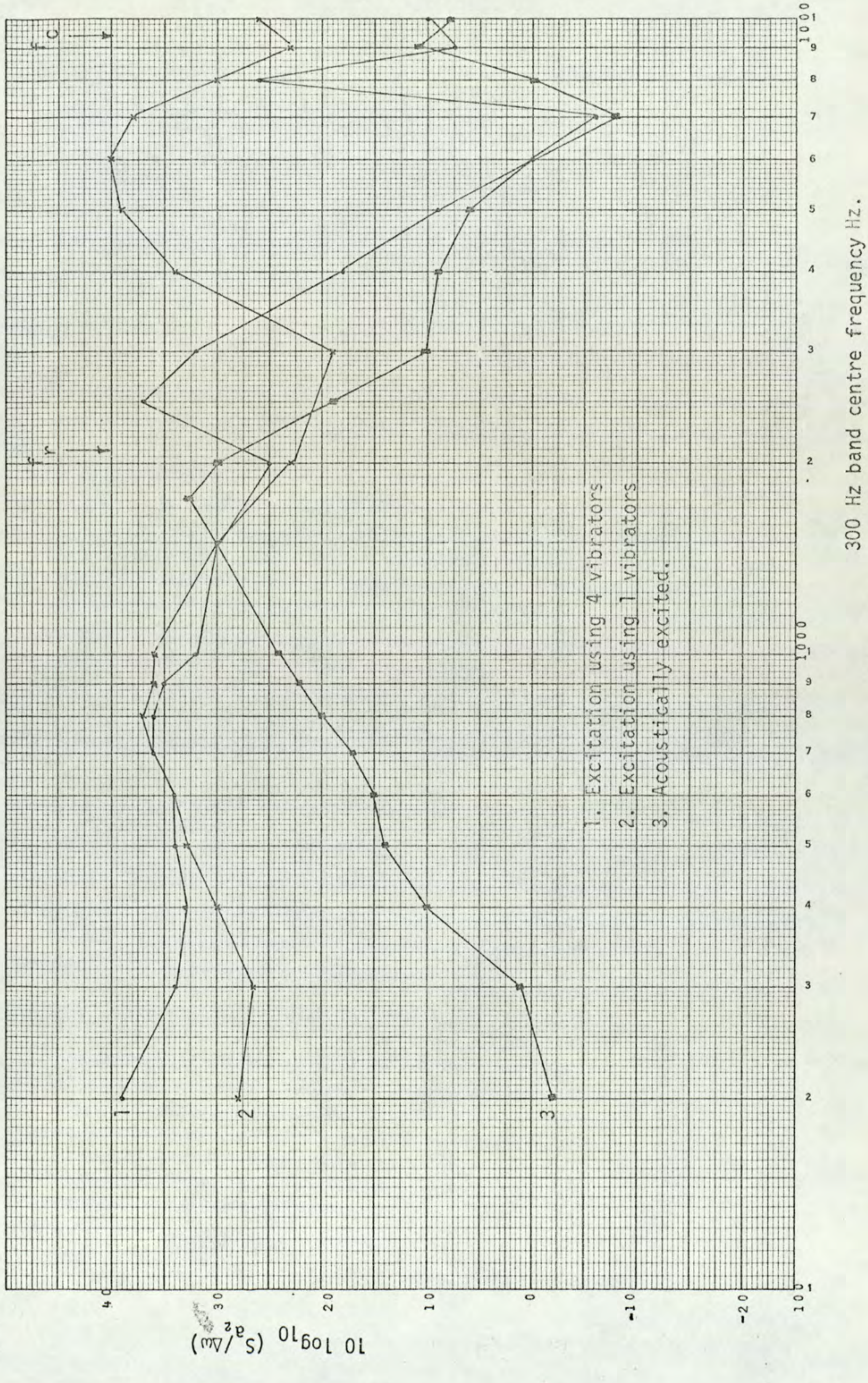

1. Excitation using 4 vibrators
2. Excitation using 1 vibrators
3, Acoustically excited.
f_c
f_r
1
2
3
40
30
20
10
0
-10
-20
1000
10000
300 Hz band centre frequency Hz.
$10 \log_{10} (S_{a^2}/\Delta\omega)$

Fig. 3.32

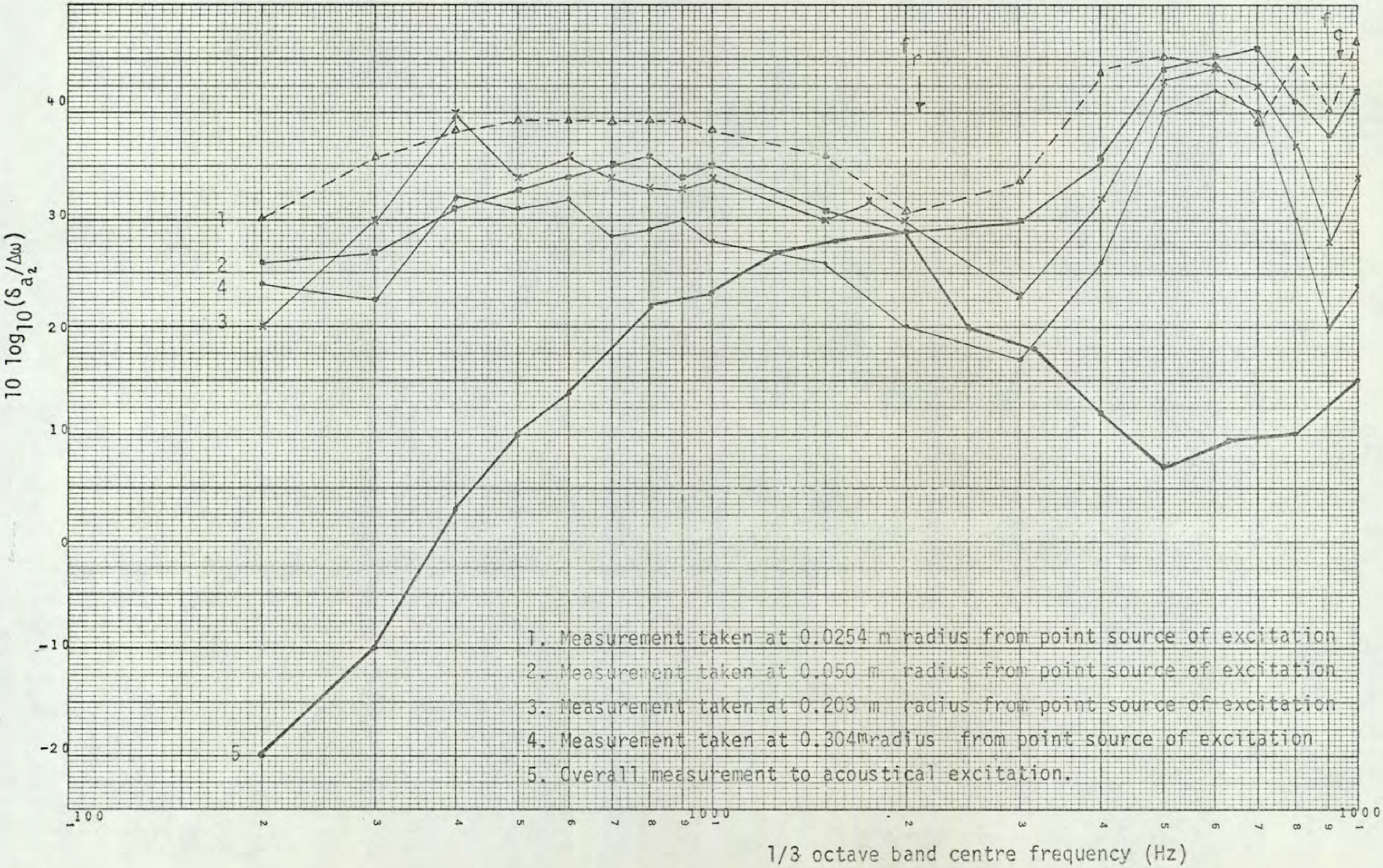
10 $\log_{10}(S_{a_2}/\Delta\omega)$
40
30
20
10
0
-10
-20
1
2
4
3
5
f_r
f_c
100
1000
10000
2
3
4
5
6
7
8
9
1. Measurement taken at 0.0254 m radius from point source of excitation
2. Measurement taken at 0.050 m radius from point source of excitation
3. Measurement taken at 0.203 m radius from point source of excitation
4. Measurement taken at 0.304m radius from point source of excitation
5. Overall measurement to acoustical excitation.
1/3 octave band centre frequency (Hz)

Fig. 3.33

3.8.3 Relationship between cylinder response and sound pressure contained in the enclosure due to different forms of excitation

This relationship is shown in the form of ratio between the space average sound pressure measured in the space enclosed by the cylinder and space average cylinder response.

The overall measured result given in figure (3.34) and that measured from a restricted cylinder surface given in figure (3.35) show the trend in the measured result. Again the separation between the results are minimum at and either side of the ring frequency. More results shown in figures (3.36) and (3.37) give further confirmation of the relationship. It is therefore clear that below the ring frequency, the cylinder response and the noise transmission due to this response should be treated separately depending upon the type of excitation - either mechanical or acoustical.

In figure (3.38) are shown results obtained by wideband random excitation of both forms. The results show that there is a good comparison above 1350 Hz. This is because the cylinder responded more efficiently to a wideband random source of excitation.

3.8.4 Measurement of resonant frequencies

Resonant frequencies were measured on plain cylindrical shell. The structure was excited by sinusoidal force fed to a loudspeaker in the case of acoustical excitation and to a vibrator in the case of

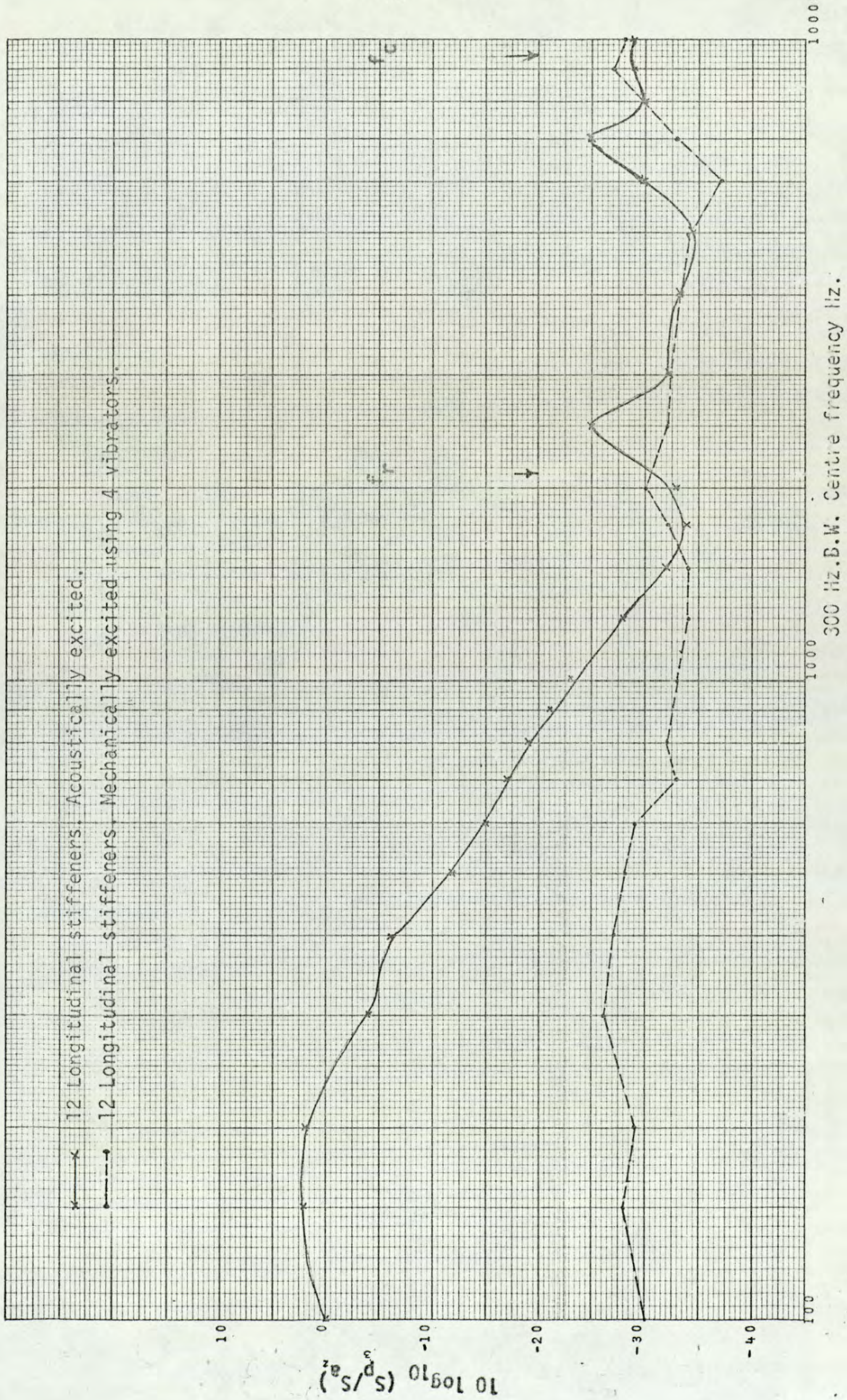
12 Longitudinal stiffeners. Acoustically excited.
12 Longitudinal stiffeners. Mechanically excited using 4 vibrators.
f_c
f_r
10
0
-10
-20
-30
-40
10 log10 (S_p^ω/S_{a_z})
100
1000
10000
300 Hz.B.W. Centre frequency Hz.

Fig. 3.34

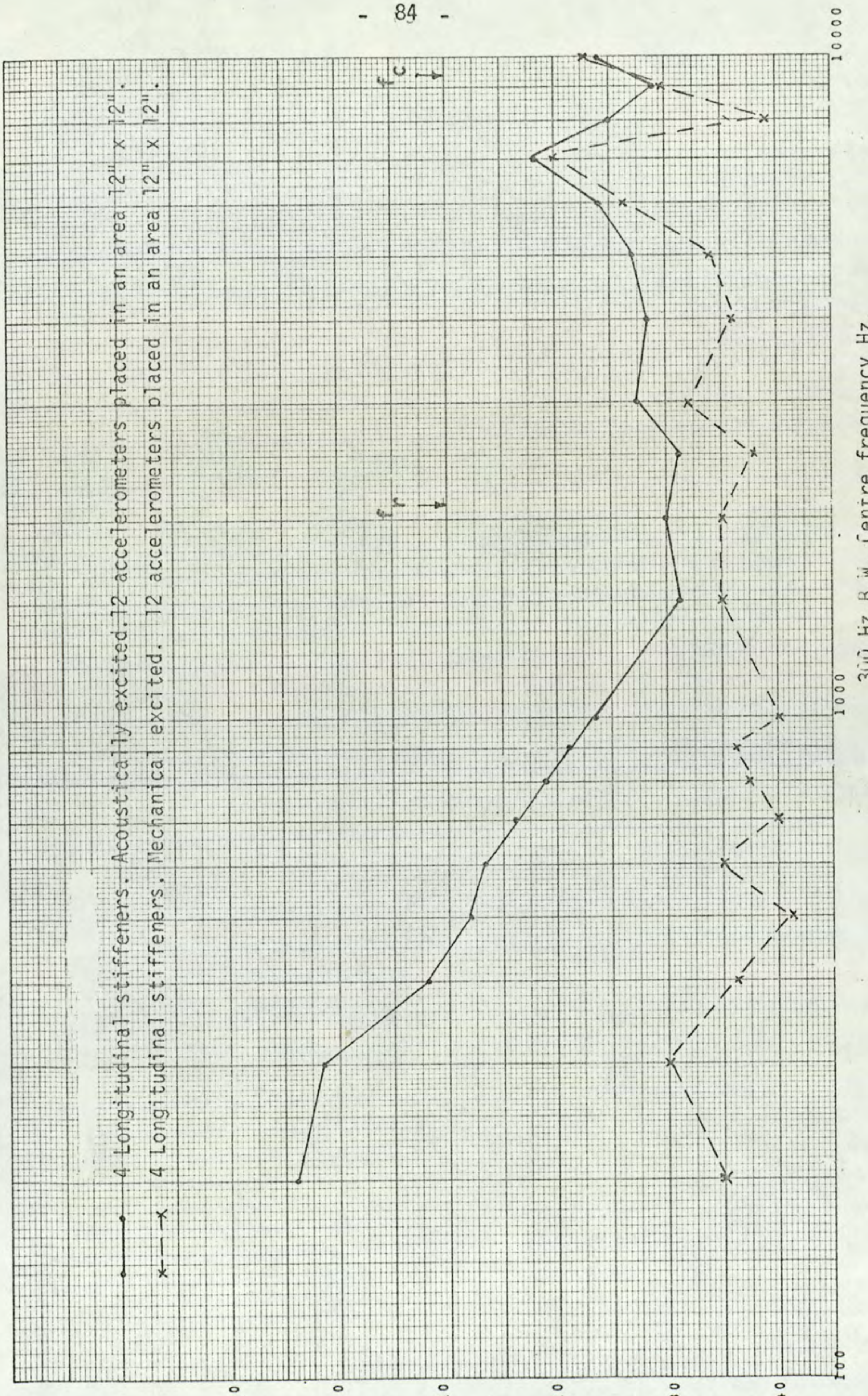
4 Longitudinal stiffeners. Acoustically excited. 12 accelerometers placed in an area 12" x 12".
4 Longitudinal stiffeners. Mechanical excited. 12 accelerometers placed in an area 12" x 12".
f_c
f_r
10
0
-10
-20
-30
-40
$10 \log_{10} (S_p/S_{a_z})$
100
1000
10000
300 Hz.B.W. Centre frequency Hz.

Fig. 3.35

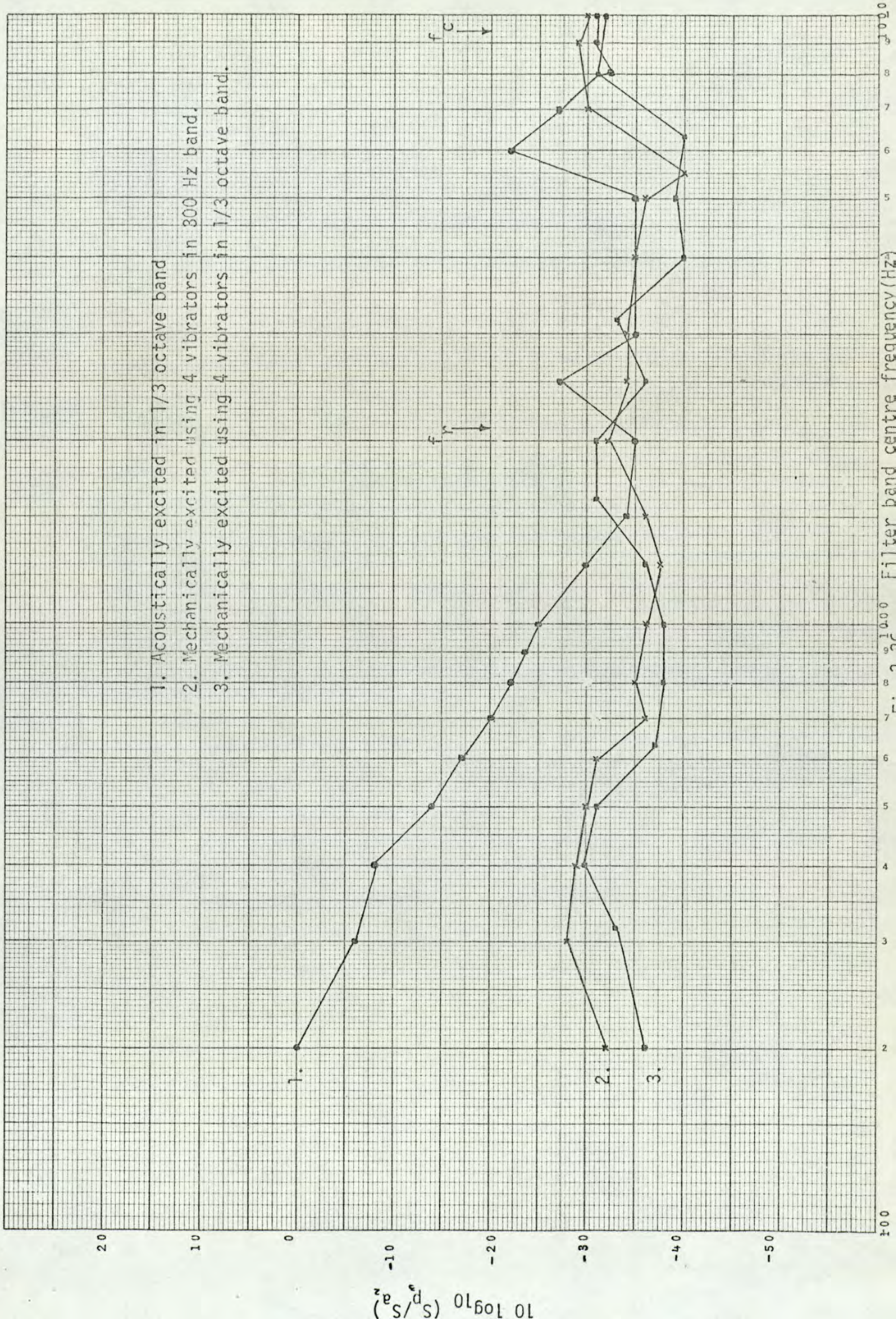
1. Acoustically excited in 1/3 octave band
2. Mechanically excited using 4 vibrators in 300 Hz band.
3. Mechanically excited using 4 vibrators in 1/3 octave band.
f_c
f_r
1.
2.
3.
20
10
0
-10
-20
-30
-40
-50
$10 \log_{10} (S_p/S_{a_2})$
100
1000
10000
Filter band centre frequency(Hz)

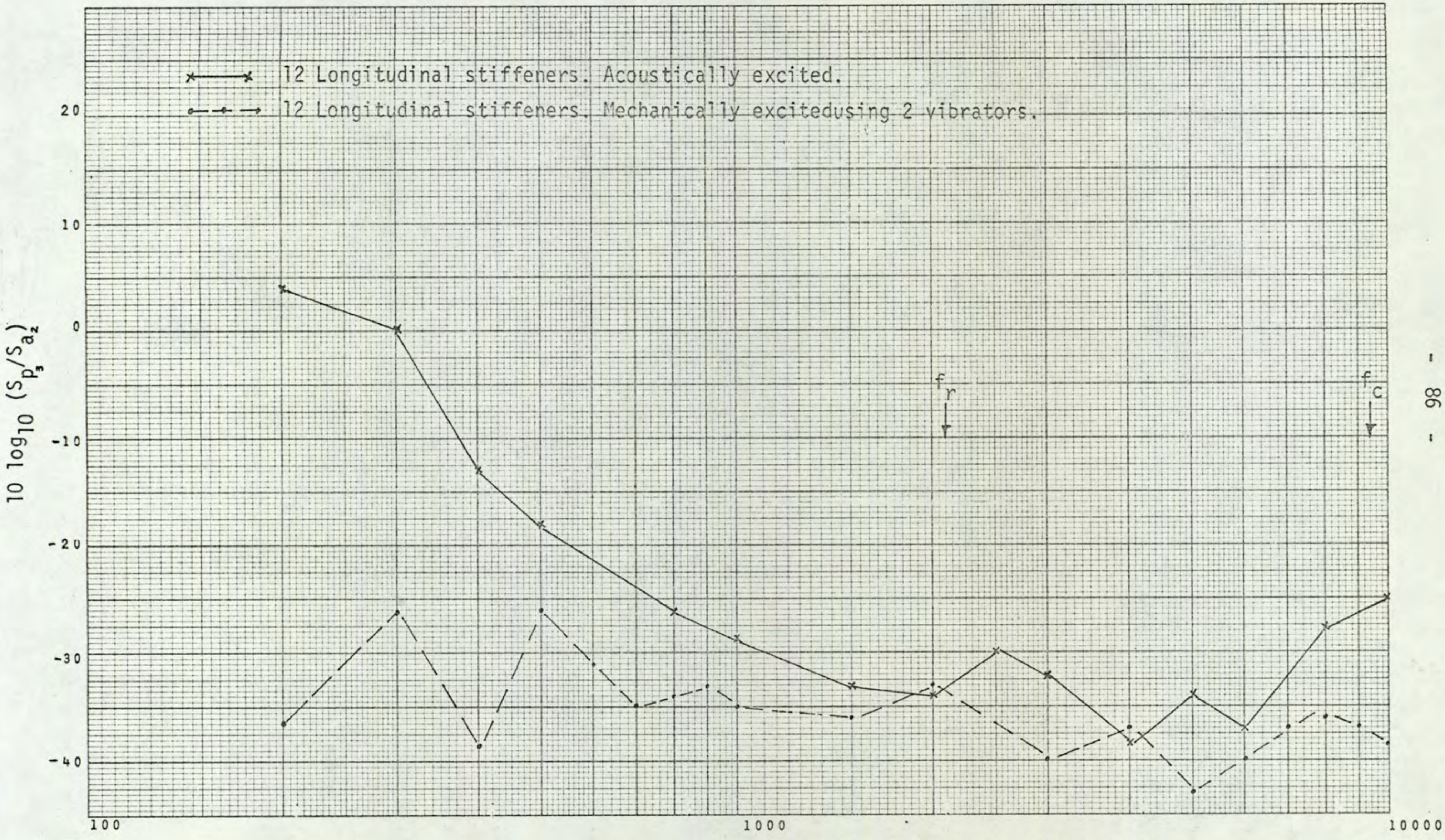
12 Longitudinal stiffeners. Acoustically excited.
12 Longitudinal stiffeners. Mechanically excitedusing 2 vibrators.
20
10
0
-10
-20
-30
-40
$10 \log_{10} (S_{p_3}/S_{a_z})$
f_r
f_c
100
1000
10000
1/3 Octave B.W. Centre frequency Hz.

Fig. 3.37

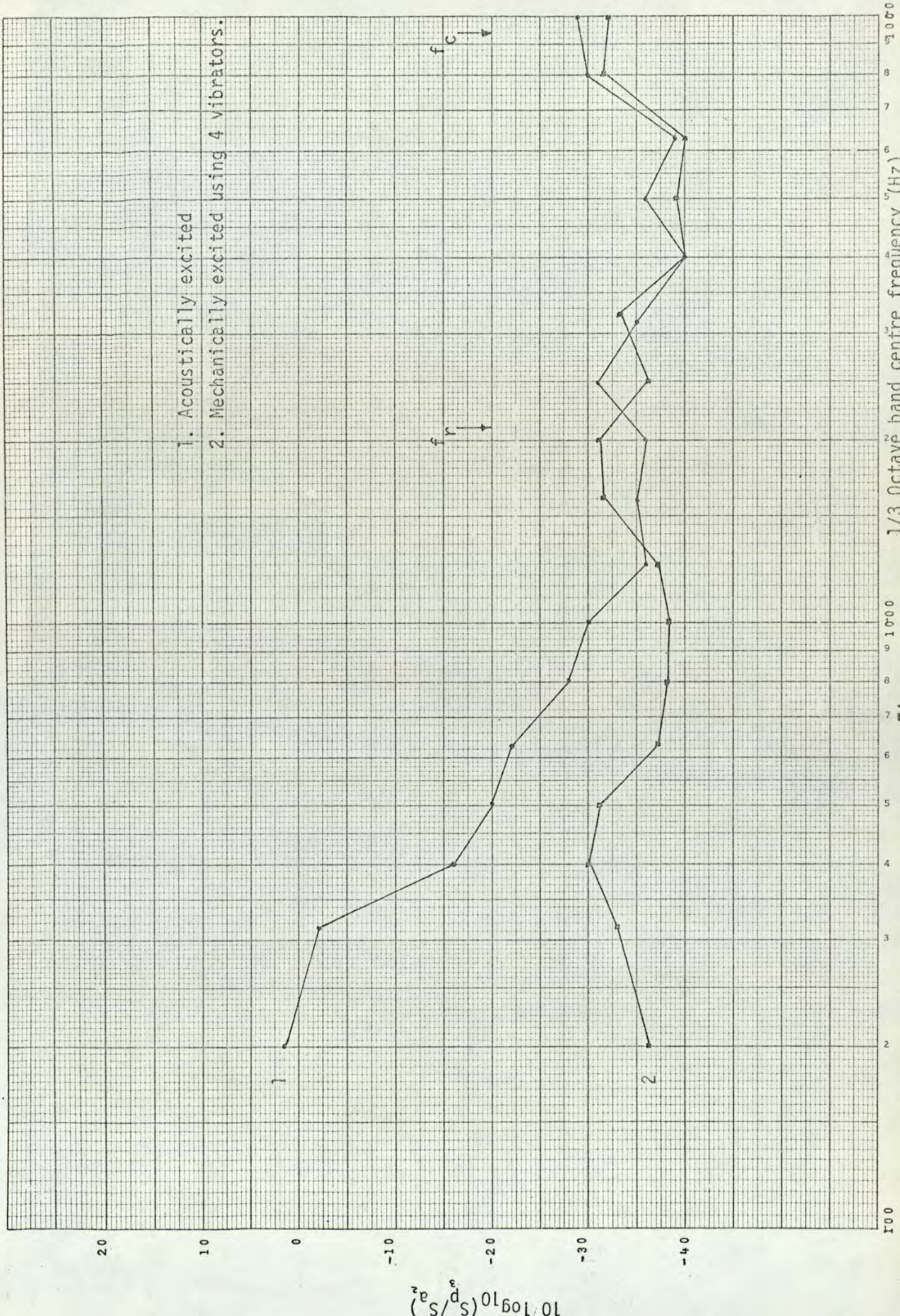
1. Acoustically excited
2. Mechanically excited using 4 vibrators.
f_c
f_r
1
2
20
10
0
-10
-20
-30
-40
$10 \log_{10}(S_p^3/S_a^2)$
100
2
3
4
5
6
7
8
9
1000
2
3
4
5
6
7
8
9
10000
1/3 Octave band centre frequency (Hz)

mechanical excitation. The cylinder response was measured by an accelerometer placed on the skin. The result of one such measurement is shown in figure (3.39). Measurements were made at other frequencies for similar excitation not shown here and the difference between the resonant frequencies counted for the two types of excitation were in the same order.

3.9 Stiffener Effect

The effect on the relationship between the noise contained in the cylinder enclosure and the skin response was measured by increasing the number of stiffeners. The results are shown in figures (3.40) and (3.41). At and either side of ring (fr) and coincidence (fc) frequency, the effect of the stiffener is very small. This could be because of efficient coupling between the structure and the noise field and therefore transfer of energy between System 2 to System 3 is rather balanced. At other frequencies the stiffener effect is very obvious and this may be because of poor coupling.

3.10 Effects of end blanks

The results shown in figures (3.42) and (3.43) were measured when aluminium plates were used as reverberant ends and 0.1m thick rocksil for non-reverberant ends. With the aluminium end blanks the noise field inside the enclosure was more uniformly distributed. This was not so in the lower frequencies when reflections from the ends influenced the level of distribution. When non-reverberant ends were used, however, measurements in the middle of the enclosure were found to be more uniform. This is because of absorption of noise fields at the ends. The lack of uniformity in the results shown above must have been influenced by this.

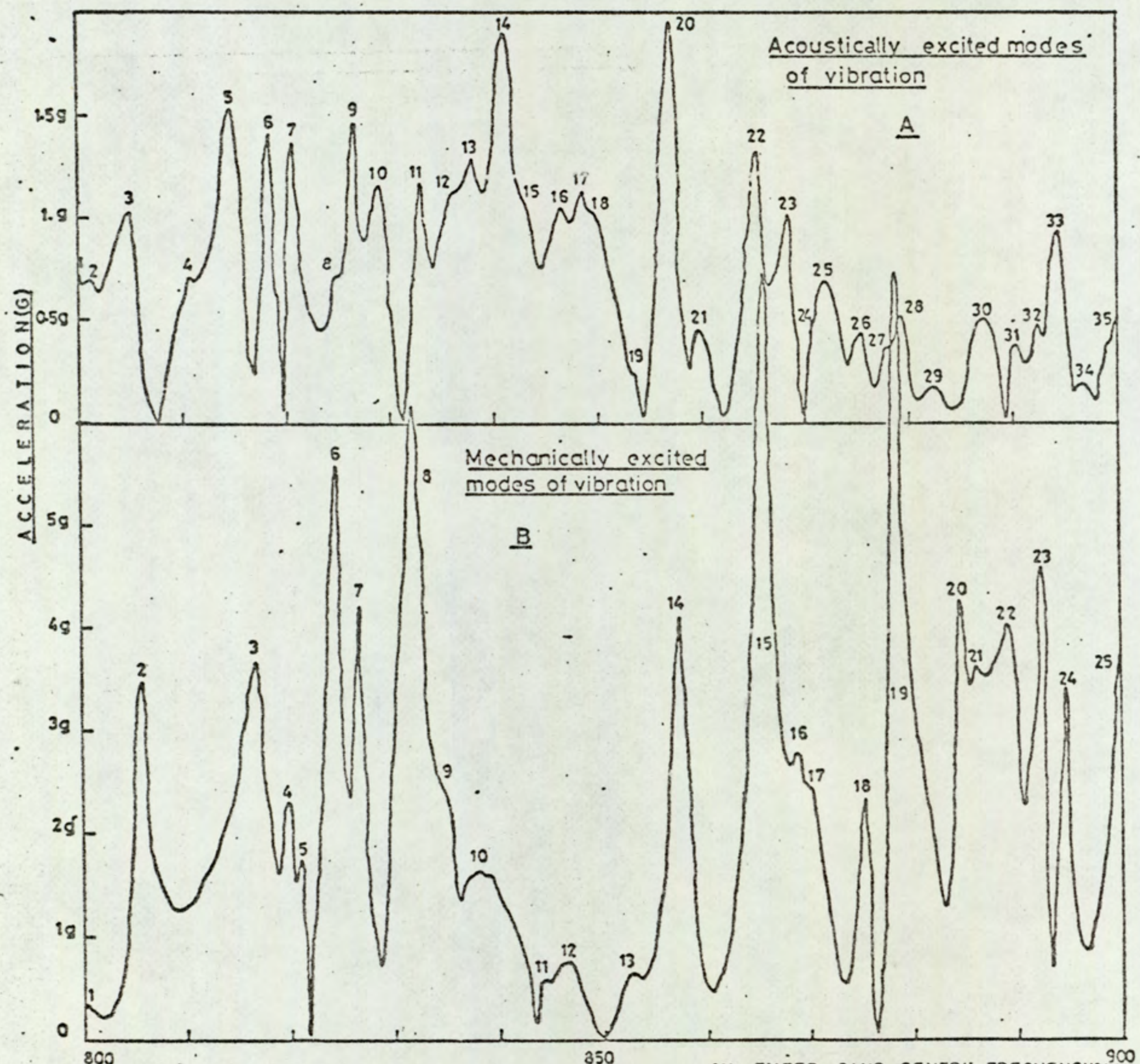

Modes of vibrations of freely supported cylindrical shell.

Fig. 3.39

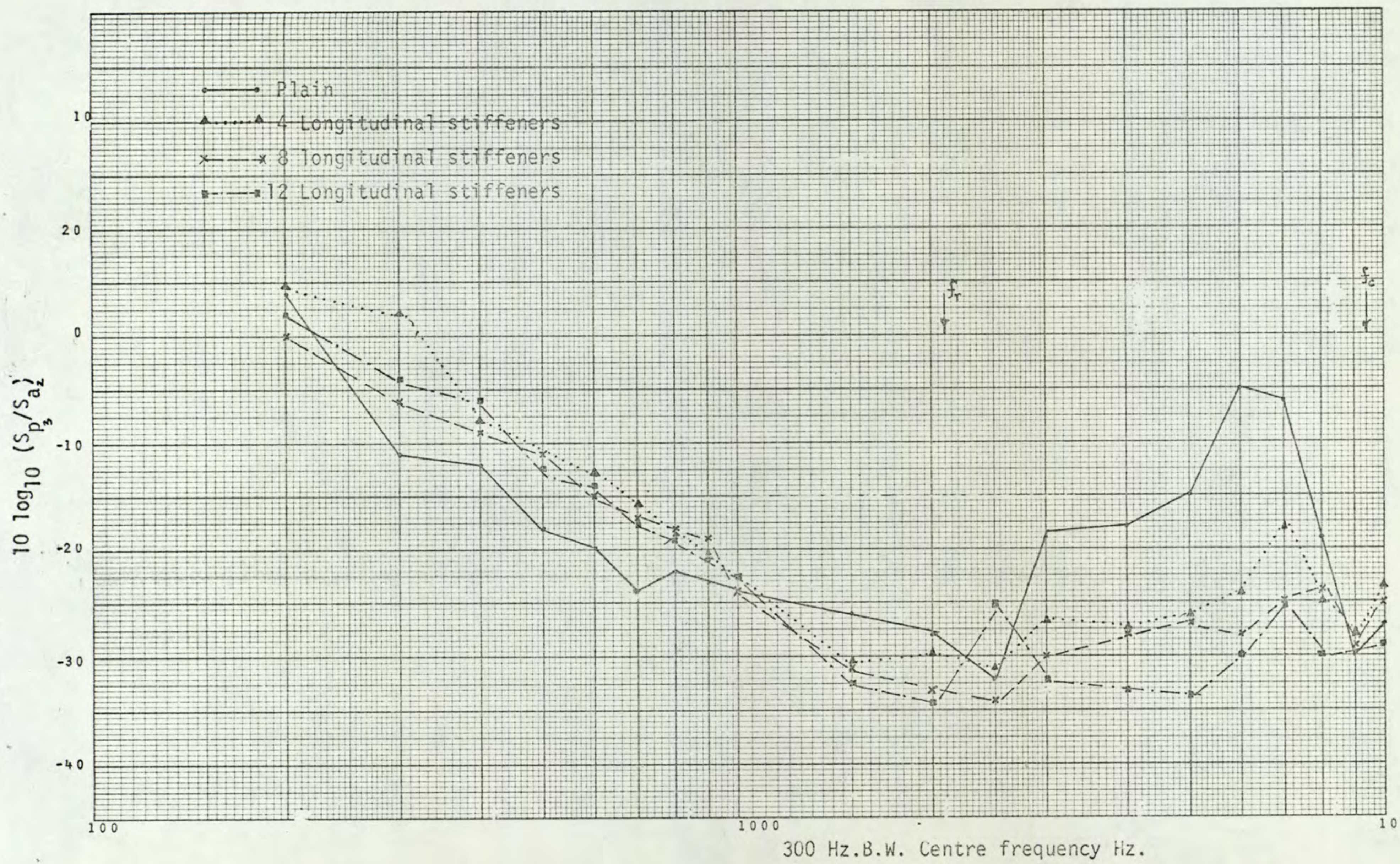
Plain
4 Longitudinal stiffeners
8 longitudinal stiffeners
12 Longitudinal stiffeners
f_r
f_c
10
20
0
-10
-20
-30
-40
$10 \log_{10} (S_{p_3}/S_{a_z})$
100
1000
10000
300 Hz.B.W. Centre frequency Hz.

Fig. (3.40)

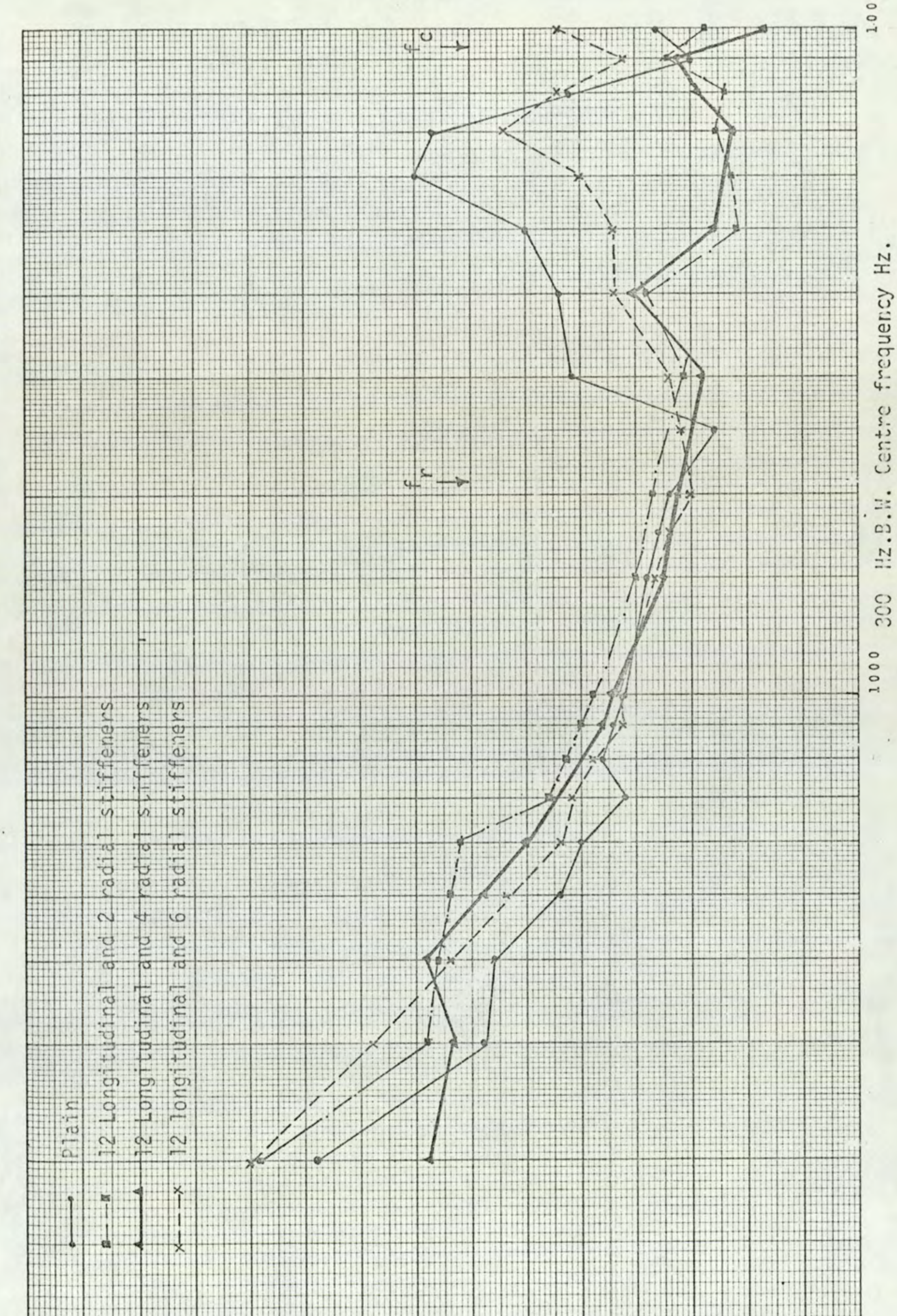
Plain
12 Longitudinal and 2 radial stiffeners
12 Longitudinal and 4 radial stiffeners
12 longitudinal and 6 radial stiffeners
f_r
f_c
100
1000
10000
300 Hz.B.W. Centre frequency Hz.
10
20
0
-10
-20
-30
-40
10 log10 (S_p/S_a)

Fig. (3.41)

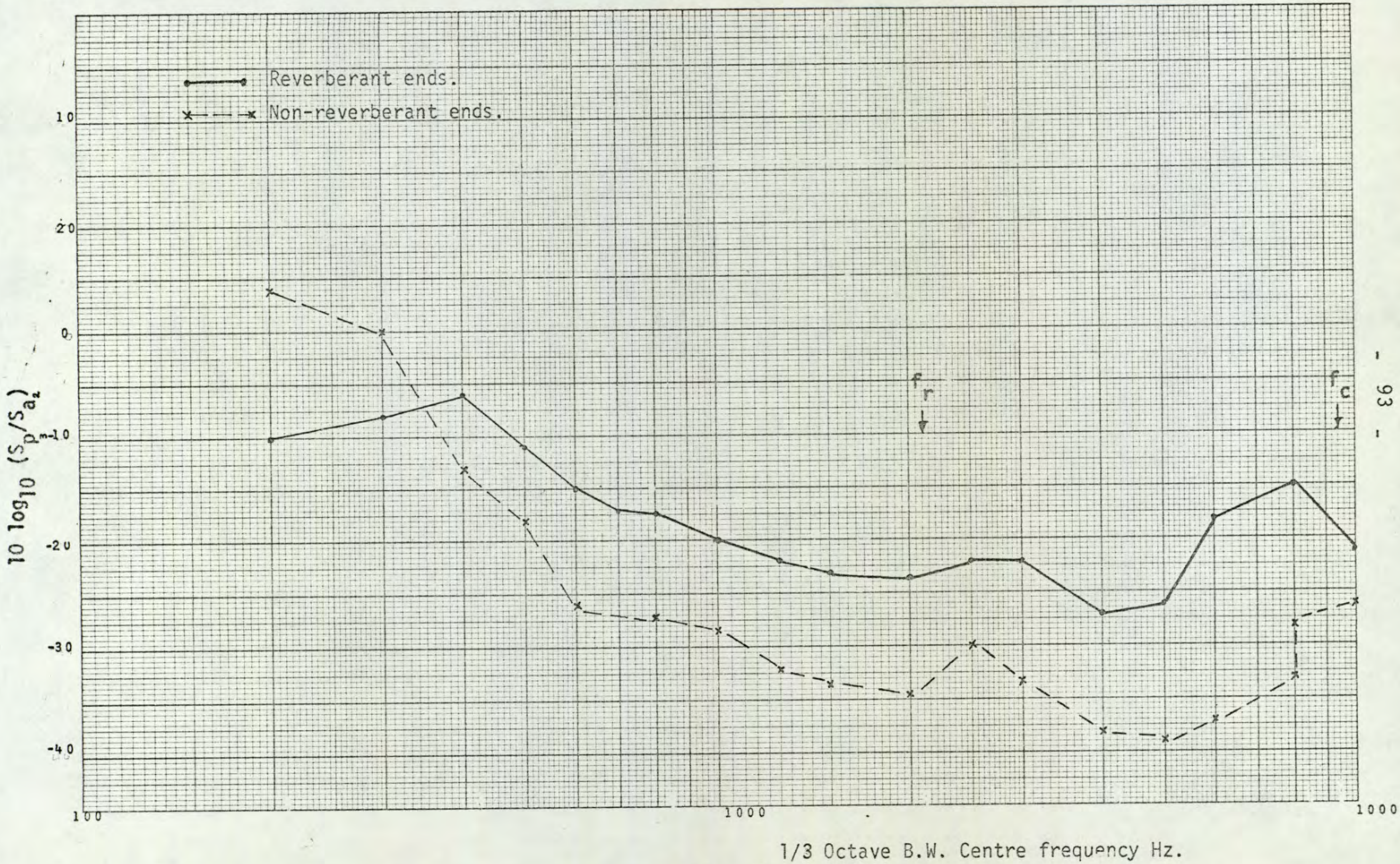
Reverberant ends.
Non-reverberant ends.
10
20
0
-10
-20
-30
-40
$10 \log_{10} (S_p/S_{a_2})$
f_r
f_c
100
1000
10000
1/3 Octave B.W. Centre frequency Hz.

Fig. (3.42)

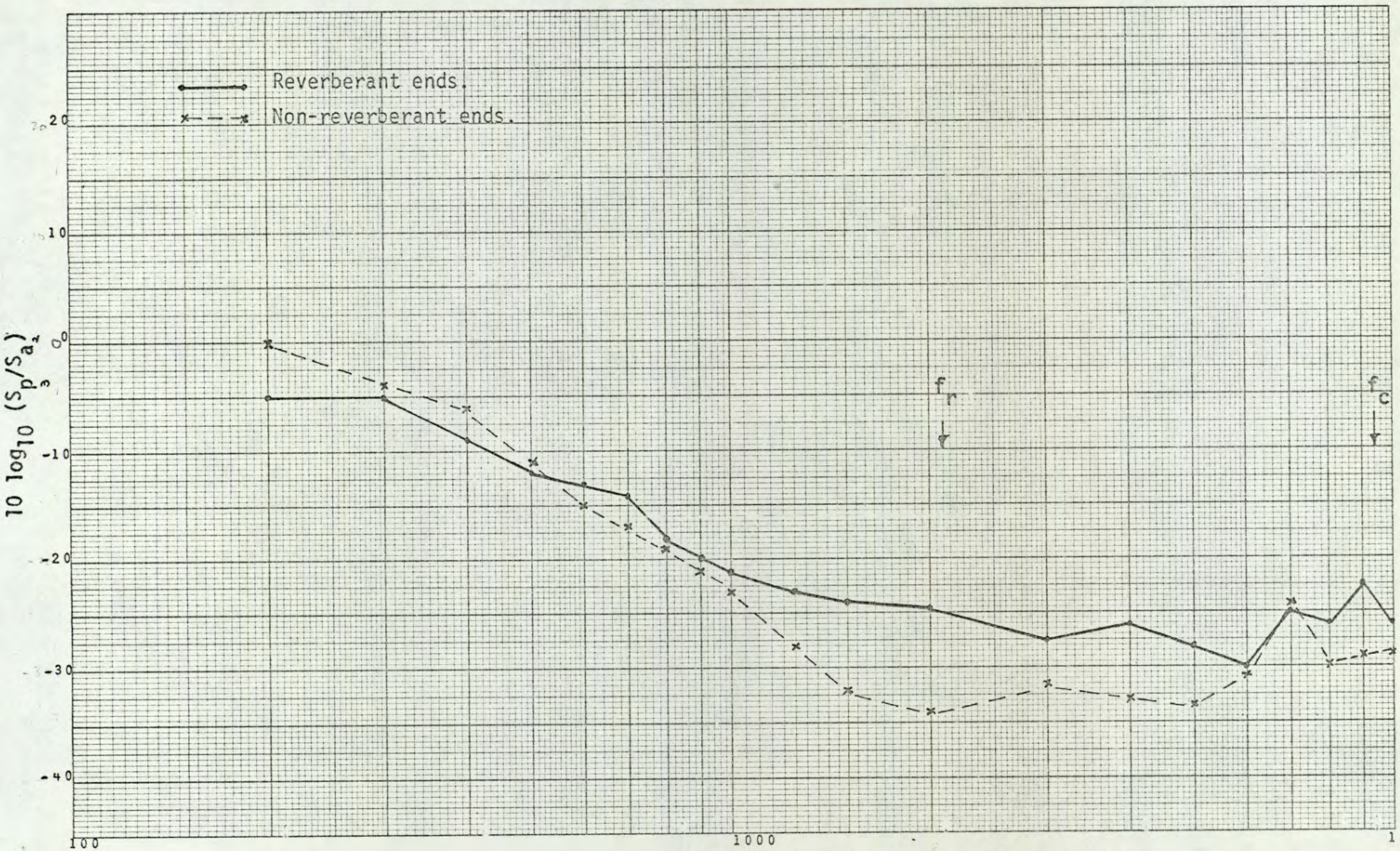

Reverberant ends.
Non-reverberant ends.
$10 \log_{10} (S_p/S_{a_2})$
20
10
0
-10
-20
-30
-40
f_r
f_c
100
1000
10000
300 Hz B.W. Centre frequency Hz.

(Fig. 3.43)

CHAPTER FOUR

CHAPTER FOUR

CALCULATION OF NATURAL FREQUENCIES OF CYLINDRICAL SHELLS AND PLATES

4.1 INTRODUCTION

Natural frequencies are one of the important parameters required for the calculation of noise transmission properties. It was not possible to obtain these experimentally with reasonable accuracy in the frequency range of interest,therefore there was no alternative but to resort to theoretical calculations.

Calculations using theoretical formulae were made on the computer. Using the large number of calculated frequencies, graphs and tables were also produced on the computer. For this small computer programs were developed initially and then combined to form one large program.

4.2 Formulae for Frequencies

Formulae were taken from papers by Arnold and Warburton(12) and Mikulas and McElman(10), the main arguments from which are summarised in Appendix [C]. Arnold and Warburton's paper does not deal with stiffened cylinders or with plates.(Detailed analysis of Arnold and Warburton methods for unstiffened cylindrical shell was given in reference (11).

The formulae considered are summarised in the following table:

	Arnold and Warburton	Mikulas & McElman.
UNSTIFFENED CYLINDRICAL SHELL	✓	✓
STIFFENED CYLINDRICAL SHELL		✓
STIFFENED PLATES		✓
UNSTIFFENED PLATES		✓

It can be seen that it enabled a comparison to be made between Arnold and Warburton and Mikulas and McElman expressions for unstiffened cylindrical shells.

4.2.1 Unstiffened Cylindrical Shells

(i) Arnold and Warburton Method

The formula given by Arnold and Warburton;

$$\Delta^3 - k_2\Delta^2 + k_1\Delta - k_o = 0 \qquad (4.1)$$

where $$f = \frac{1}{2\pi R}\left[\frac{Eg\Delta}{\rho\,(1-\mu^2)}\right]^{\frac{1}{2}} \qquad (4.2)$$

$$\lambda = \frac{m\pi R}{a}, \ \beta = h^2/12R^2, \ \alpha = t/R$$

and the values of the coefficients are,

$$K_o = \tfrac{1}{2}(1-\mu)^2(1+\mu)\lambda^4+\tfrac{1}{2}(1-\mu)\beta[(\lambda^2+n^2)^4-2(4-\mu^2)\lambda^4n^2-8\lambda^2n^4-2n^6+4(1-\mu^2)\lambda^4$$
$$+4\lambda^2n^2+n^4]$$

$$K_1 = \tfrac{1}{2}(1-\mu)(\lambda^2 n^2)^2+\tfrac{1}{2}(3-\mu-2\mu^2)\lambda^2+\tfrac{1}{2}(1-\mu)n^2+\beta[\tfrac{1}{2}(3-\mu)(\lambda^2+n^2)^3$$
$$+2(1-\mu)\lambda^4-(2-\mu^2)\lambda^2n^2 -\tfrac{1}{2}(3+\mu)n^4+2(1-\mu)\lambda^2+n^2] \qquad (4.3)$$

$$K_2 = 1 + \tfrac{1}{2}(3-\mu)(\lambda^2+n^2)+\beta[(\lambda^2+n^2)^2+2(1-\mu)\lambda^2+n^2]$$

Values of the frequencies can be calculated from this formula for different values of m and n. This calculation is summarised in figure (4.1).

(ii) Formula given by Mikulas and McElman

For this method the formula given by Mikulas and McElman for stiffened cylindrical shells was used with the stiffener parameters set to zero. (See Section 4.2.2.).

4.2.2 Stiffened Cylindrical Shells

Mikulas and McElman give the following formula for the frequency. (Mikulas and McElman refer to a as length of cylindrical shell and plate and R as the radius of the cylinder).

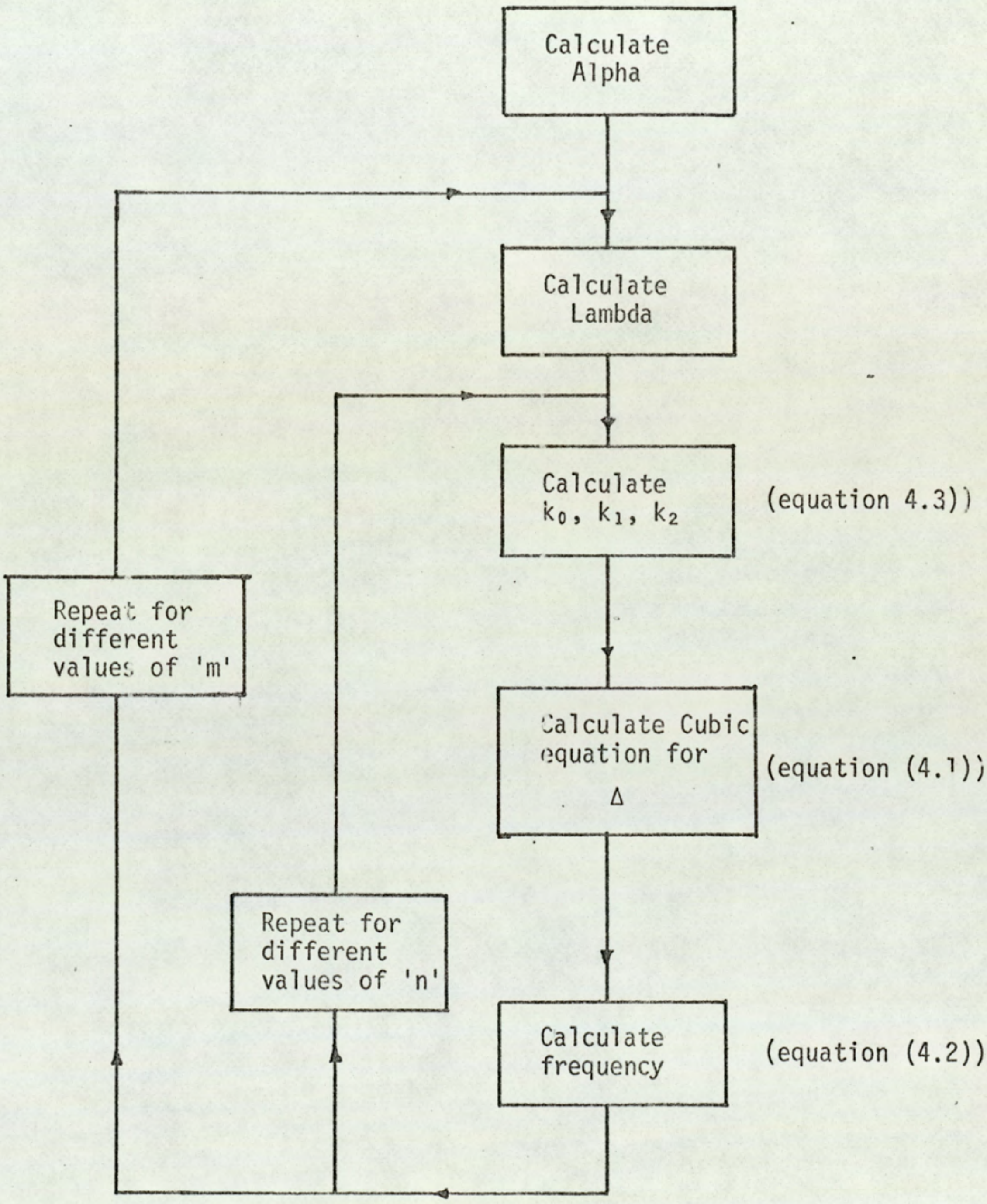
Calculate Alpha
Calculate Lambda
Calculate k_0, k_1, k_2
(equation 4.3))
Repeat for different values of 'm'
Calculate Cubic equation for Δ
(equation (4.1))
Repeat for different values of 'n'
Calculate frequency
(equation (4.2))

Fig. (4.1)

$$\frac{Ma^2\omega^2}{\pi^4 D} = m^4(1+\beta^2)^2+m^4\left[\frac{E_sI_s}{Dd}+\beta^2\left(\frac{G_sJ_s}{Dd}+\frac{G_rJ_r}{D\ell}\right)+\beta^4\frac{E_rI_r}{D\ell}\right]$$

$$+\frac{12Z^2}{\pi^4}\left(\frac{1+\bar{S}\Lambda_s+\bar{R}\Lambda_r+\bar{S}\bar{R}\Lambda_{rs}}{\Lambda}\right) \tag{4.4}$$

where

$$\Lambda_s = 1+2\alpha^2\left(\frac{\bar{z}_s}{R}\right)(\beta^2-\mu)+\alpha^4\left(\frac{\bar{z}_s}{R}\right)^2(1+\beta^2)^2 \tag{4.5a}$$

$$\Lambda_r = 1+2n^2\left(\frac{\bar{z}_r}{R}\right)(1-\beta^2\mu)+n^4\left(\frac{\bar{z}_r}{R}\right)^2(1+\beta^2)^2 \tag{4.5b}$$

$$\Lambda_{rs} = n^2\alpha^2[\beta^2(1-\mu^2)+2(1+\mu)]\left(\frac{\bar{z}_s}{R}\right)^2+n^4[1-\mu^2+2\beta^2(1+\mu)]\left(\frac{\bar{z}_s}{R}\right)^2$$

$$+2n^2(1-\mu^2)\left(\frac{\bar{z}_s}{R}\right)+2n^2(1-\mu^2)\left(\frac{\bar{z}_r}{R}\right)+2n^4(1+\mu)^2\left(\frac{\bar{z}_r}{R}\right)\left(\frac{\bar{z}_s}{R}\right)+1-\mu^2 \tag{4.5c}$$

$$\Lambda = (1+\beta^2)^2+2\beta^2(1+\mu)(\bar{R}+\bar{S})+(1-\mu^2)[\bar{S}+\beta^4\bar{R}+2\beta^2\bar{R}\bar{S}(1+\mu)] \tag{4.5d}$$

and

$$z^2 = a^4\frac{(1-\mu^2)}{R^2t^2} \tag{4.5e}$$

The non-dimensional parameters are defined as follows:

$$\beta = \frac{na}{m\pi R}, \quad \bar{S} = \frac{E_sA_s}{Etd}$$

$$\alpha = \frac{m\Lambda R}{a} \quad \bar{R} = \frac{E_rA_r}{Et\ell}$$

As before the separate values of $\omega = 2\pi f$ can be computed for different m and n values and also for different spacings of radial stiffeners and longitudinal stiffeners or both. This is summarised in figure (4.2).

4.2.3 Unstiffened Plate

Mikulus and McElman's stiffened plate formula was used to give some results for unstiffened plate by setting stiffener parameters to zero (See Section (4.2.4)).

4.2.4 Stiffened Plates

Mikulas and McElman give the following formula for natural frequencies for stiffened plate:

$$\frac{Ma^4\omega^2}{\pi^4 D} = m^4(1+\quad) + m\left[\frac{E_sI_s}{Dd} + \left(\frac{G_sJ_s}{Dd} + \frac{G_rJ_r}{D\ell}\right) + \frac{E_rI_r}{D\ell}\right]$$

$$+ 12(1-\mu^2)m^4 \left\{ \frac{\bar{S}(1+\beta^2)^2\left(\frac{\bar{z}_s}{t}\right)^2 + \bar{R}\beta^4(1+\beta^2)^2\left(\frac{\bar{z}_r}{t}\right) + \bar{R}\bar{S}C}{(1+\beta^2)^2 + 2\beta^2(1+\mu)(\bar{R}+\bar{S}) + (1-\mu^2)[\bar{S}+\beta^4\bar{R}+2\beta^2\bar{R}\bar{S}(1+\mu)]} \right\} \quad (4.6)$$

where

$$C = \beta^2\ [\beta^2(1-\mu^2)+2(1+\mu)]\left(\frac{\bar{z}_s}{t}\right)^2 + 2\beta^4(1+\mu)^2\left(\frac{\bar{z}_s}{t}\right)\left(\frac{\bar{z}_r}{t}\right)$$

$$+\ \beta^4\ [1-\mu^2+2\beta^2(1+\mu)]\ \left(\frac{\bar{z}_r}{t}\right)^2 \quad (4.7)$$

and the following non-dimensional parameters are defined:

$$\beta = \frac{na}{mb}, \quad \bar{S} = \frac{E_sA_s}{Etd}, \quad \bar{R} = \frac{E_rA_r}{Et\ell}$$

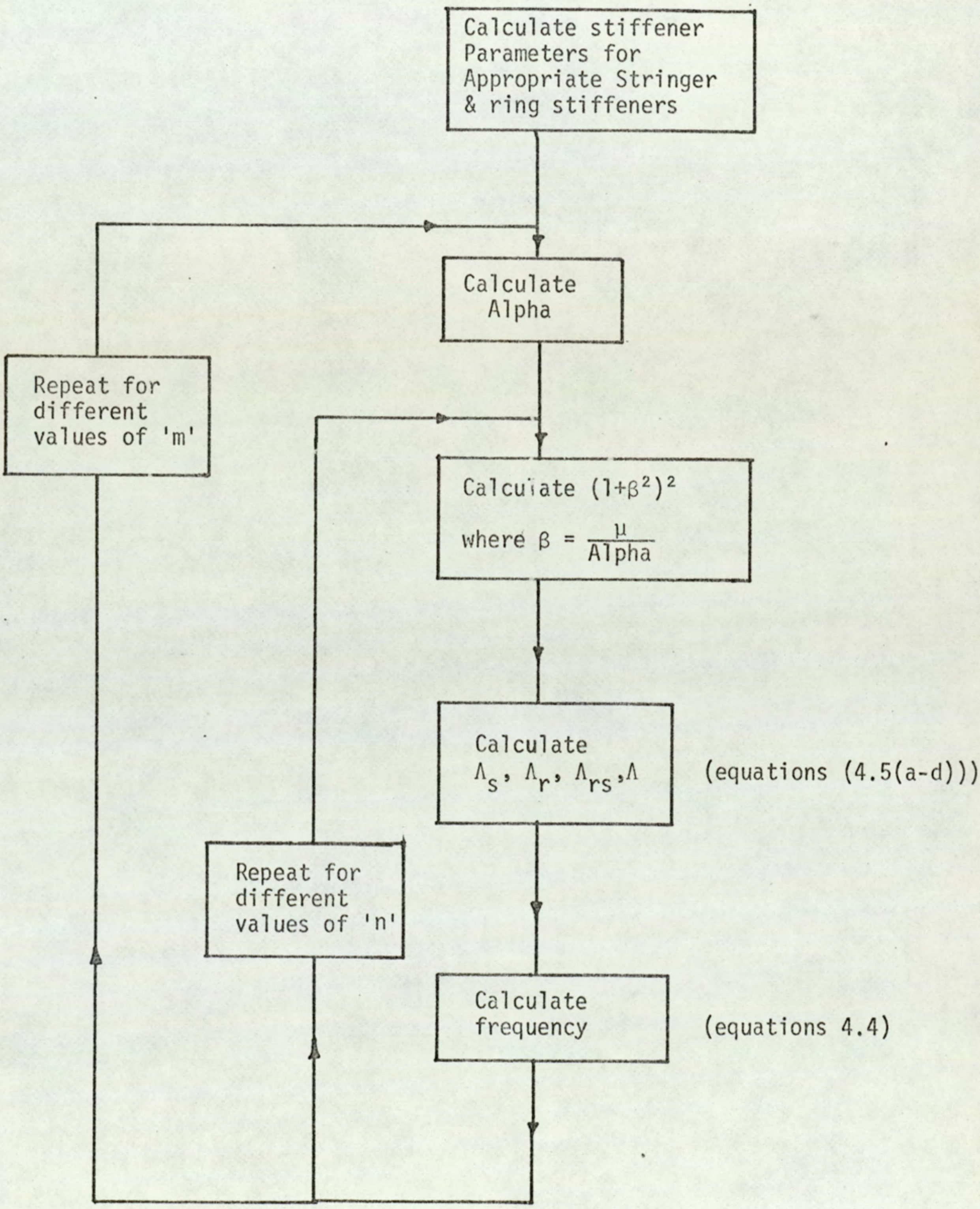

Calculate stiffener Parameters for Appropriate Stringer & ring stiffeners
Calculate Alpha
Repeat for different values of 'm'
Calculate $(1+\beta^2)^2$
where $\beta = \frac{\mu}{\text{Alpha}}$
Calculate Λ_s, Λ_r, Λ_{rs}, Λ
(equations (4.5(a-d)))
Repeat for different values of 'n'
Calculate frequency
(equations 4.4)

Fig. (4.2)

Separate values of ω can be computed for different values of m and n and also for different spacings of stiffeners. For flat plates m and n are the numbers of half waves in the x and y directions, respectively. This is summarised in figure 4.3.

4.3 Producing tables of frequencies

It is clear that these computations are all very complicated, thus in order to perform the calculations many times with different parameters, it was necessary to use the computer.

4.3.1 Unstiffened Cylindrical Shells

Tables of frequencies for successive values of m and n where computed using (separately) the Arnold and Warburton formulae (See Section (4.2.1)) and the Mikulas and McElman formulae (See Section 4.2.2.)). The program in each case following the lines of the flow diagrams already given. Values of m between 1-59 were considered together with n values of 2-148 in each case. An example of output from the smaller of these values is reproduced in figure (4.4).

Although these tables are useful, it is clear that much more information regarding modal densities can be obtained if the frequencies are sorted into order and the number of resonances defined in a given bandwidth. The computer programs were therefore modified to give this. An extract from the output indicates the results of this and is given in figures (4.5) and (4.6).

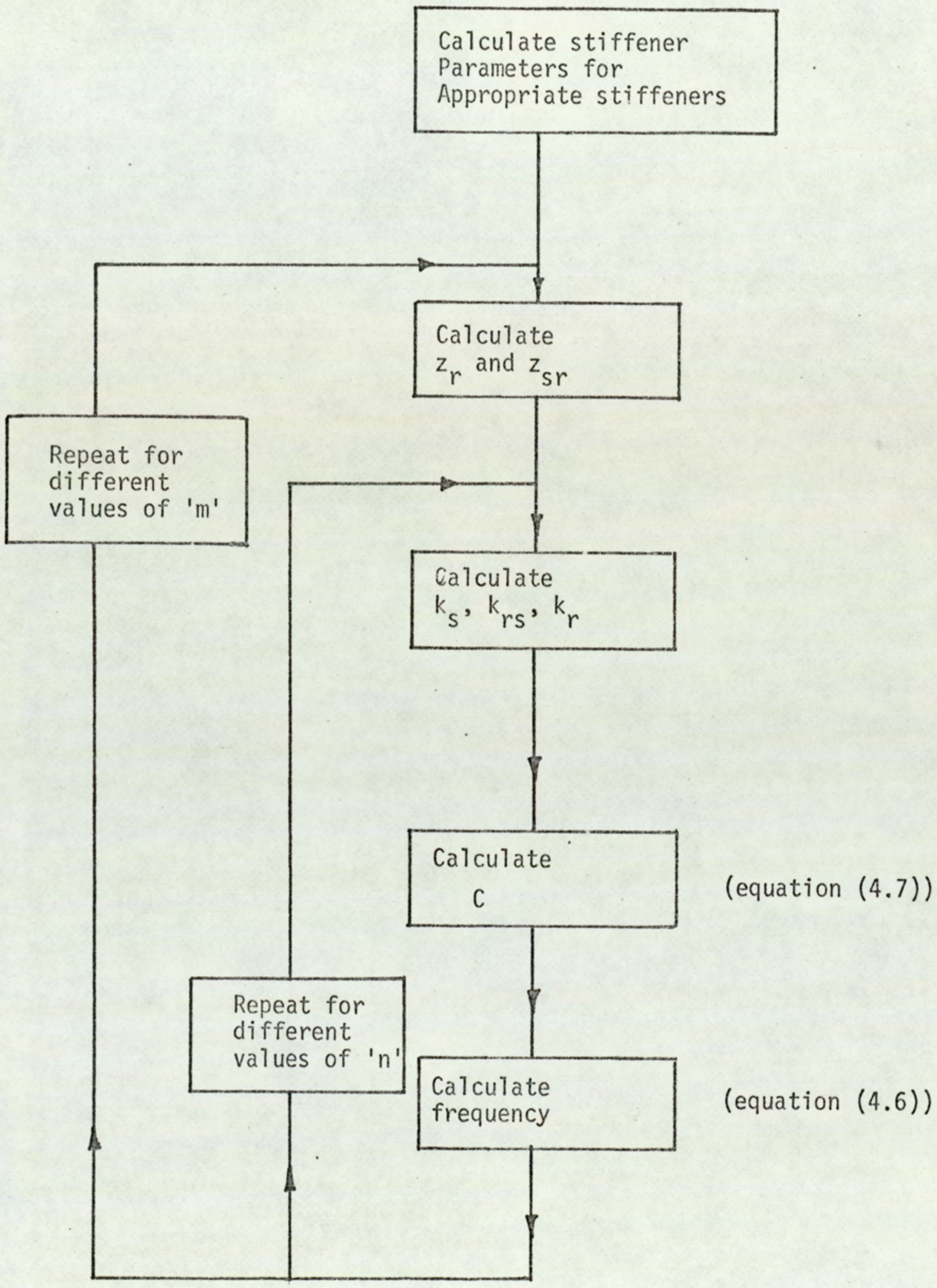
Calculate stiffener Parameters for Appropriate stiffeners
Calculate z_r and z_{sr}
Repeat for different values of 'm'
Calculate k_s, k_{rs}, k_r
Calculate C
(equation (4.7))
Repeat for different values of 'n'
Calculate frequency
(equation (4.6))

Fig. (4.3)

n ↓	m → 1	2	3	4	5	6	7	8	9	10	11	12
2	119	422	816	1225	1606	1938	2216	2443	2626	2774	2893	2989
3	72	271	453	728	1016	1299	1564	1803	2016	2202	2364	2503
4	91	155	290	471	679	898	1118	1332	1534	1722	1894	2051
5	138	162	233	347	492	656	830	1008	1185	1356	1520	1675
6	200	210	244	310	405	523	656	798	945	1094	1241	1384
7	274	280	297	333	391	471	567	677	795	919	1045	1172
8	360	364	374	395	431	482	549	629	720	819	924	1033
9	458	461	468	482	505	538	584	641	709	786	870	960
10	567	570	576	586	602	626	658	699	749	807	873	946
11	687	690	696	704	717	735	759	789	827	872	924	982
12	820	822	827	835	846	860	880	904	934	969	1011	1058
13	963	966	971	978	987	1000	1017	1037	1062	1091	1126	1164
14	1118	1121	1126	1132	1141	1153	1168	1186	1208	1233	1262	1296
15	1285	1288	1292	1299	1307	1318	1332	1349	1368	1391	1417	1446
16	1463	1466	1470	1477	1485	1496	1509	1524	1542	1563	1587	1614
17	1653	1655	1660	1666	1674	1685	1697	1712	1729	1749	1771	1797
18	1854	1856	1861	1867	1875	1885	1898	1912	1929	1948	1969	1993
19	2066	2069	2073	2080	2088	2098	2110	2124	2140	2158	2179	2202
20	2290	2293	2297	2304	2312	2322	2334	2347	2363	2381	2401	2424
21	2526	2529	2533	2539	2547	2557	2569	2583	2598	2616	2636	2658
22	2773	2776	2780	2786	2794	2804	2816	2820	2845	2862	2882	2903
23	3031	3034	3039	3045	3053	3063	3074	3088	3103	3120	3140	3161
24	3302	3304	3309	3315	3323	3333	3344	3358	3373	3390	3409	3430
25	3583	3586	3590	3596	3604	3614	3626	3630	3654	3671	3690	3711

EXAMPLE OF NATURAL FREQUENCY - NOT IN ASCENDING ORDER (Arnold and Warburton Expression)

FIG. 4.4

72	91	119	138	155	162	200	210	221	233
244	274	280	290	297	310	333	347	360	364
374	391	395	405	422	431	453	458	461	468
471	471	402	482	492	505	523	538	549	567
567	570	576	584	586	602	626	629	641	656
656	658	677	679	687	690	696	699	704	709
717	720	728	735	749	759	786	789	795	798
807	816	819	820	822	827	827	830	835	846
860	870	872	873	880	898	904	919	924	924
934	945	946	960	963	966	969	971	978	982
987	1000	1008	1011	1016	1017	1024	1033	1037	1045
1046	1054	1058	1062	1091	1094	1106	1110	1114	1118
1118	1121	1126	1126	1132	1141	1144	1151	1153	1164
1167	1168	1172	1185	1186	1187	1192	1208	1208	1225
1229	1233	1241	1249	1254	1256	1252	1263	1279	1285
1288	1292	1294	1296	1298	1299	1299	1307	1309	1318
1332	1332	1333	1342	1348	1349	1356	1363	1365	1365
1368	1368	1375	1384	1391	1417	1420	1421	1423	1425
1435	1446	1447	1458	1463	1466	1469	1470	1473	1477
1480	1485	1489	1496	1505	1508	1509	1516	1520	1522
1522	1524	1534	1541	1542	1544	1548	1555	1557	1563
1564	1578	1590	1584	1587	1588	1600	1606	1614	1623
1637	1638	1641	1644	1647	1653	1654	1655	1657	1660
1661	1666	1671	1674	1675	1677	1684	1685	1694	1697
1698	1699	1712	1714	1722	1727	1729	1736	1740	1749
1751	1753	1755	1763	1766	1768	1771	1780	1785	1796
1797	1803	1807	1815	1819	1820	1824	1829	1830	1839
1840	1842	1854	1855	1856	1861	1866	1867	1875	1875
1883	1885	1889	1891	1894	1898	1899	1899	1899	1903
1912	1915	1920	1923	1925	1927	1929	1938	1942	1948
1955	1965	1969	1969	1977	1977	1979	1989	1991	1991
1993	1996	2006	2007	2009	2011	2016	2019	2041	2048
2051	2052	2053	2056	2059	2066	2068	2068	2069	2073
2073	2075	2080	2080	2080	2088	2088	2096	2098	2100
2110	2112	2114	2114	2116	2124	2124	2139	2140	2146
2151	2151	2157	2157	2158	2168	2170	2174	2179	2180
2188	2191	2192	2193	2195	2202	2202	2204	2215	2216
2219	2224	2227	2233	2237	2239	2242	2252	2255	2256
2259	2263	2263	2264	2278	2285	2290	2293	2297	2300
2301	2302	2303	2304	2308	2312	2317	2318	2319	2320
2322	2324	2326	2332	2334	2336	2340	2341	2344	2347
2353	2363	2364	2370	2376	2377	2380	2381	2381	2391
2395	2399	2400	2401	2403	2410	2412	2417	2422	2422
2424	2428	2431	2433	2439	2439	2443	2448	2459	2460
2474	2475	2477	2478	2480	2483	2484	2489	2491	2494
2499	2499	2503	2503	2504	2510	2519	2526	2529	2533
2536	2536	2539	2539	2540	2540	2547	2555	2555	2555
2557	2560	2566	2569	2569	2569	2570	2573	2573	2573
2575	2582	2593	2598	2599	2606	2616	2616	2618	2620
2624	2626	2627	2628	2628	2632	2636	2637	2637	2644

TABLE OF NATURAL FREQUENCIES OF UNSTIFFENED CYLINDER (Arnold and Warburton Expression)

FIG. 4.5

80	99	135	146	163	170	208	219	236	241
252	283	288	302	306	318	342	358	369	373
383	400	404	414	439	466	470	477	478	480
481	489	491	491	505	514	534	547	558	575
577	578	585	593	595	611	635	639	650	667
668	672	688	696	699	703	704	708	713	718
726	730	744	758	768	771	796	799	807	812
817	828	830	831	836	837	844	850	855	869
880	882	883	889	913	920	928	932	934	936
943	956	961	971	972	975	979	979	986	992
996	1009	1020	1026	1030	1034	1045	1046	1056	1059
1065	1067	1071	1074	1101	1111	1117	1120	1124	1127
1130	1134	1135	1141	1150	1154	1156	1162	1162	1174
1177	1177	1186	1195	1197	1202	1209	1217	1218	1239
1242	1259	1261	1266	1267	1272	1274	1290	1294	1296
1301	1304	1305	1307	1313	1316	1319	1327	1341	1343
1352	1358	1360	1363	1365	1371	1373	1375	1377	1378
1379	1382	1385	1400	1403	1426	1430	1433	1436	1437
1445	1456	1458	1469	1472	1474	1479	1479	1485	1487
1489	1494	1499	1505	1515	1518	1519	1526	1532	1533
1542	1547	1551	1556	1557	1559	1565	1566	1573	1574
1588	1593	1595	1597	1599	1610	1624	1633	1634	1648
1649	1653	1654	1657	1661	1664	1668	1672	1673	1674
1675	1682	1683	1687	1694	1697	1702	1704	1706	1708
1710	1721	1724	1738	1738	1748	1750	1753	1758	1761
1762	1763	1766	1774	1777	1781	1784	1798	1799	1806
1806	1817	1827	1830	1834	1841	1841	1846	1850	1850
1852	1862	1865	1865	1869	1871	1876	1876	1884	1891
1894	1896	1899	1901	1907	1909	1909	1914	1918	1921
1926	1932	1933	1934	1935	1938	1938	1952	1957	1975
1978	1979	1980	1980	1990	1992	2000	2001	2002	2002
2007	2017	2017	2021	2029	2029	2051	2058	2063	2064
2067	2070	2075	2076	2078	2079	2079	2081	2082	2084
2087	2088	2089	2090	2097	2099	2104	2107	2107	2110
2119	2123	2124	2124	2133	2134	2135	2149	2150	2156
2161	2161	2168	2168	2169	2181	2182	2184	2188	2192
2199	2201	2204	2211	2214	2218	2226	2230	2232	2234
2237	2243	2248	2250	2254	2260	2262	2265	2270	2270
2274	2274	2275	2288	2295	2299	2302	2306	2310	2312
2313	2313	2320	2323	2324	2327	2328	2330	2330	2336
2336	2336	2342	2343	2347	2350	2350	2354	2354	2356
2363	2372	2381	2386	2387	2390	2390	2392	2401	2410
2410	2411	2414	2415	2419	2420	2427	2427	2433	2433
2434	2438	2441	2450	2450	2458	2461	2470	2471	2484
2484	2488	2491	2492	2493	2495	2501	2505	2508	2510
2511	2514	2514	2520	2529	2535	2537	2542	2543	2545
2548	2548	2549	2550	2550	2556	2561	2565	2565	2566
2568	2571	2577	2578	2579	2580	2580	2583	2584	2585
2590	2592	2592	2607	2609	2615	2625	2627	2628	2630
2637	2641	2641	2645	2647	2648	2651	2654	2654	2658

TABLE OF NATURAL FREQUENCIES OF UNSTIFFENED CYLINDER (Mikulas and McElman Expression)

FIG. 4.6

A comparison of them shows that the resonant frequencies are all somewhat about 10% higher than using the Arnold and Warburton formula. It was not attempted to examine these experimentally because from the previous work (reference 11) it was found that accurate mode counting in the frequency range of interest was not possible. The tables also show that at some frequency band the resonances not only lay very close together but there are more than one at a given frequency and it would be virtually impossible to separate and count them.

In figure (4.7) is given an example of the output sorted in a given bandwidth. These results were later produced on graph. The results produced in this form were used in calculating noise transmission for a given cylinder.

4.3.2 Stiffened Cylindrical Shells

The Mikulas and McElman formula which was used for unstiffened cylinders was obtained by setting the stiffener parameters to zero. Thus the parameters for stiffened cylinders were already catered for in the computer program using Mikulas and McElman formula. Many computer runs were made using various values for the stiffener parameters. Thus copious quantities of computer outputs were produced which, it is not practical to produce here. However, for illustration purposes, a matrix of frequencies is given below for various diameter and stiffening conditions. Similar matrices can be produced simply by reading values from the output.

Δf	$n_s(f)$	$n_s(f)/\Delta f$	$n_s(\omega)$	$\frac{1}{n_s(\omega)}$
0 - 50	0	0,0000	0.0000	
50 - 100	2	0,0400	0.0064	157.08
100 - 150	2	0,0400	0.0064	157.08
150 - 200	2	0,0400	0.0064	157.08
200 - 250	5	0,1000	0.0159	62.83
250 - 300	4	0,0800	0.0127	78.54
300 - 350	3	0,0600	0.0095	104.72
350 - 400	5	0,1000	0.0159	62.83
400 - 450	3	0,0600	0.0095	104.72
450 - 500	9	0,1800	0.0286	34.91
500 - 550	4	0,0800	0.0127	78.54
550 - 600	6	0,1200	0.0191	52.36
600 - 650	4	0,0800	0.0127	78.54
650 - 700	9	0,1800	0.0286	34.91
700 - 750	7	0,1400	0.0223	44.88
750 - 800	5	0,1000	0.0159	62.83
800 - 850	10	0,2000	0.0318	31.42
850 - 900	6	0.1200	0.0191	52.36
900 - 950	7	0,1400	0.0223	44.88
950 - 1000	8	0.1600	0.0255	39.27
1000 - 1050	10	0.2000	0.0318	31.42
1050 - 1100	5	0.1000	0.0159	62.83
1100 - 1150	11	0.2200	0.0350	28.56
1150 - 1200	10	0.2000	0.0318	31.42
1200 - 1250	7	0.1400	0.0223	44.88
1250 - 1300	13	0.2600	0.0414	24.17
1300 - 1350	9	0.1800	0.0286	34.91
1350 - 1400	9	0.1800	0.0286	34.91
1400 - 1450	8	0.1600	0.0255	39.27
1450 - 1500	11	0.2200	0.0350	28.56
1500 - 1550	13	0.2600	0.0414	24.17
1550 - 1600	9	0.1800	0.0286	34.91
1600 - 1650	9	0.1800	0.0286	34.91
1650 - 1700	17	0.3400	0.0541	18.48
1700 - 1750	8	0.1600	0.0255	39.27
1750 - 1800	11	0.2200	0.0350	28.56
1800 - 1850	11	0.2200	0.0350	28.56
1850 - 1900	17	0.3400	0.0541	18.48
1900 - 1950	11	0.2200	0.0350	28.56
1950 - 2000	12	0.2400	0.0382	26.18
2000 - 2050	8	0.1600	0.0255	39.27
2050 - 2100	19	0.3800	0.0605	16.53
2100 - 2150	11	0.2200	0.0350	28.56
2150 - 2200	15	0.3000	0.0477	20.94
2200 - 2250	12	0.2400	0.0382	26.18
2250 - 2300	12	0.2400	0.0382	26.18
2300 - 2350	21	0.4200	0.0668	14.96
2350 - 2400	12	0,2400	0.0382	26.18
2400 - 2450	16	0,3200	0.0509	19.63
2450 - 2500	14	0,2800	0.0446	22.44
2500 - 2550	15	0.3000	0.0477	20.94
2550 - 2600	18	0,3600	0.0573	17.45
2600 - 2650	18	0,3600	0.0573	17.45
2650 - 2700	12	0,2400	0.0382	26.18
2700 - 2750	16	0.3200	0.0509	19.63
2750 - 2800	22	0,4400	0.0700	14.28
2800 - 2850	14	0,2800	0.0446	22.44
2850 - 2900	20	0,4000	0.0637	15.71
2900 - 2950	15	0,3000	0.0477	20.94

EXAMPLE OF NATURAL FREQUENCIES IN A GIVEN BANDWIDTH

FIG. 4.7

Diameter of Un-stiffened Cylinder	First 10 natural frequencies (Hz)
(18") 0.45m	80, 99, 135, 146, 163, 170, 208, 219, 236, 241
(24") 0.61m	68, 83, 86, 118, 138, 142, 158, 169, 170, 177
(30") 0.76m	63, 64, 79, 97, 103, 123, 126, 133, 145, 145
(120") 3.05m	30, 31, 31, 33, 34, 36, 36, 40, 42, 44
(144") 3.66m	28, 28, 29, 29, 30, 31, 32, 35, 35, 38

The above results show the effect of diameter on the calculated resonant frequencies. It is clear from this that as the diameter is increased the natural frequencies get closer.

No.of stiffeners	10 natural frequencies (Hz) either side of ring frequency (2.1K Hz)
12 Long. & 6 radial	1578,1701,1831,1979,2013,2152,2164,2213,2309,2330
6 " 6 "	1785,1817,1953,2098,2099,2152,2161,2192,2263,2339
4 " 4 "	1775,1898,1964,2080,2083,2085,2743,2335,2383,2387
2 " 3 "	1999,2011,-023,2063,2071,2137,2161,2233,2299,2299
Un-stiffened Cylinder	2099,2101,2101,2101,2103,2104,2105,2105,2106,2106

The effect of stiffening on calculated natural frequencies is shown above. The separation between the calculated natural frequencies becomes larger as the number of stiffeners are increased.

4.3.3 Plates (Stiffened and Unstiffened)

Tables similar to that produced for the cylinder described on the previous page were obtained for the plates. An extract from the "sorted" tables for unstiffened plate is given in figure (4.8). Tables similar to this were also obtained for the stiffened plate.

The calculated lowest natural frequency of the plate, (3 Hz) (same in dimension to a cylinder when unfolded.) is not the same as that in figure (4.6) which is (80 Hz). This must be because of curvature effects. Many of the natural frequencies calculated for the cylinder above the ring frequency were found to be identical to those of the plate. This is because the cylinder behaves like a plate above this frequency as shown in figures (4.14) to (4.17).

4.4 Producing graphs

4.4.1 Unstiffened Cylinders

The results tabulated in figure (4.4) were expressed graphically by producing on one graph a set of curves of frequencies at successive values of n for each of the values of m (i.e. one curve for each value of m). Graphs were also produced for successive values of m for each of the values of n (i.e. one curve for each value of n). These were produced on computer, use being made of standard software concerned with graph plotting. Specimen graphs of 'n' curves for a shell cylinder of .457 m diameter are given in figure (4.9) and graphs of 'm' curves of an aluminium cylinder of 0.762 m diameter

3	6	9	9	10	12	14	17	19	21
21	22	23	23	26	27	29	34	34	36
36	37	38	39	41	42	43	43	45	49
50	52	55	56	57	57	58	59	60	62
63	65	66	66	68	70	70	75	76	77
77	81	82	82	82	86	86	86	88	88
90	91	92	95	97	97	100	101	101	103
104	108	110	110	110	111	112	114	115	116
116	119	120	121	122	123	123	128	129	129
132	134	135	136	138	138	139	142	144	144
145	146	147	149	149	150	151	152	152	156
156	158	160	162	163	164	165	167	170	170
170	173	174	178	180	181	181	182	182	183
185	185	186	187	188	189	190	190	193	194
195	197	197	198	199	206	206	207	207	209
211	211	213	215	217	218	219	224	225	226
227	227	227	227	229	230	230	231	232	232
234	234	237	238	238	240	242	245	247	248
248	249	249	251	252	256	258	259	261	262
264	264	270	270	271	272	272	273	273	273
275	277	277	279	280	280	283	283	284	285
285	288	289	291	292	293	293	295	296	299
300	302	303	303	304	305	306	309	311	315
317	318	321	322	323	324	324	324	325	325
327	328	328	329	330	333	333	334	334	336
339	342	343	343	344	344	346	347	350	350
352	352	353	354	354	354	359	361	364	366
366	367	369	369	369	375	377	378	378	378
380	381	382	382	383	384	387	388	389	389
390	390	390	394	394	396	398	400	401	403
403	404	405	405	408	410	412	412	413	413
416	417	419	420	421	421	424	425	428	431
432	434	435	435	436	438	438	439	440	441
441	444	444	445	445	446	449	449	451	453
453	456	457	459	460	462	462	463	464	465
465	465	467	469	473	474	474	475	476	476
480	483	486	486	487	488	489	492	493	493
494	494	495	496	501	502	503	503	505	506
506	507	508	509	511	511	513	513	515	515
516	516	518	520	521	523	524	526	528	530
530	531	533	533	533	536	538	539	540	542
542	544	544	547	549	551	551	557	557	557
557	559	562	565	565	566	566	568	568	571
571	572	574	574	576	577	577	577	580	580
581	582	582	584	586	586	588	590	593	593
594	594	594	596	597	598	598	601	601	602
602	604	607	610	614	614	615	615	616	616
621	624	624	624	625	629	630	630	631	632
634	636	636	636	641	642	644	645	647	649
650	650	651	651	651	652	655	655	655	656

TABLE OF NATURAL FREQUENCIES OF UNSTIFFENED PLATE (1.8 m x 2.38 m)

FIG. 4.8

THEORETICAL FREQUENCY CURVES

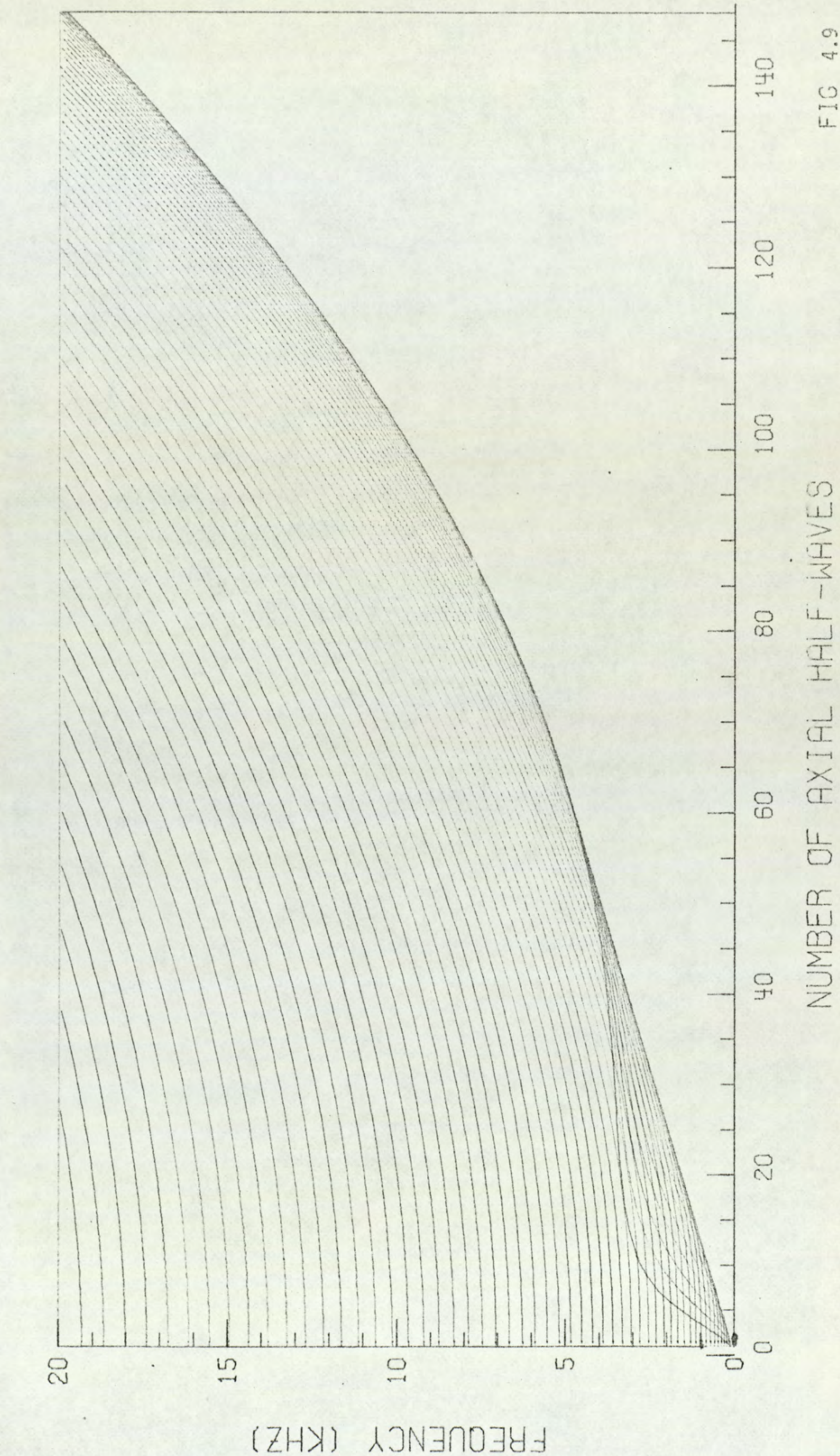

FIG 4.9

are given in figure (4.10). These were produced from frequency output calculated using two different formulae.

The two graphs show frequencies as a function of mode shapes. Natural frequencies could easily be obtained from these by counting the number of m and n crossings. For a closer inspection of mode shapes, the graph was drawn in small frequency steps so that each m or n curve was clearly identified.

The tables of counts of numbers of frequencies within specific bandwidth were also represented graphically again on the computer. These graphs indicate either number of modes per radian per second or a total number of modes in a given bandwidth. Specimen graphs are given in figure (4.11) and (4.12).

The calculations were repeated for different bandwidth and different cylinder dimensions. A sample of the results are presented in figures (4.13) to (4.17).

The effect of constant bandwidth filters are clearly shown in the graphs. A meaningful trend in the results are produced when sampled in filter band wider than 200 Hz. Results presented in frequency bands narrower than 200 Hz (figures (4.11) to (4.14); although appear to give more details in the frequency spectrum, will be difficult to interpret. Analysis in a frequency band too wide (i.e. 500 Hz) is seen in figure (4.17) to produce a smooth graph but

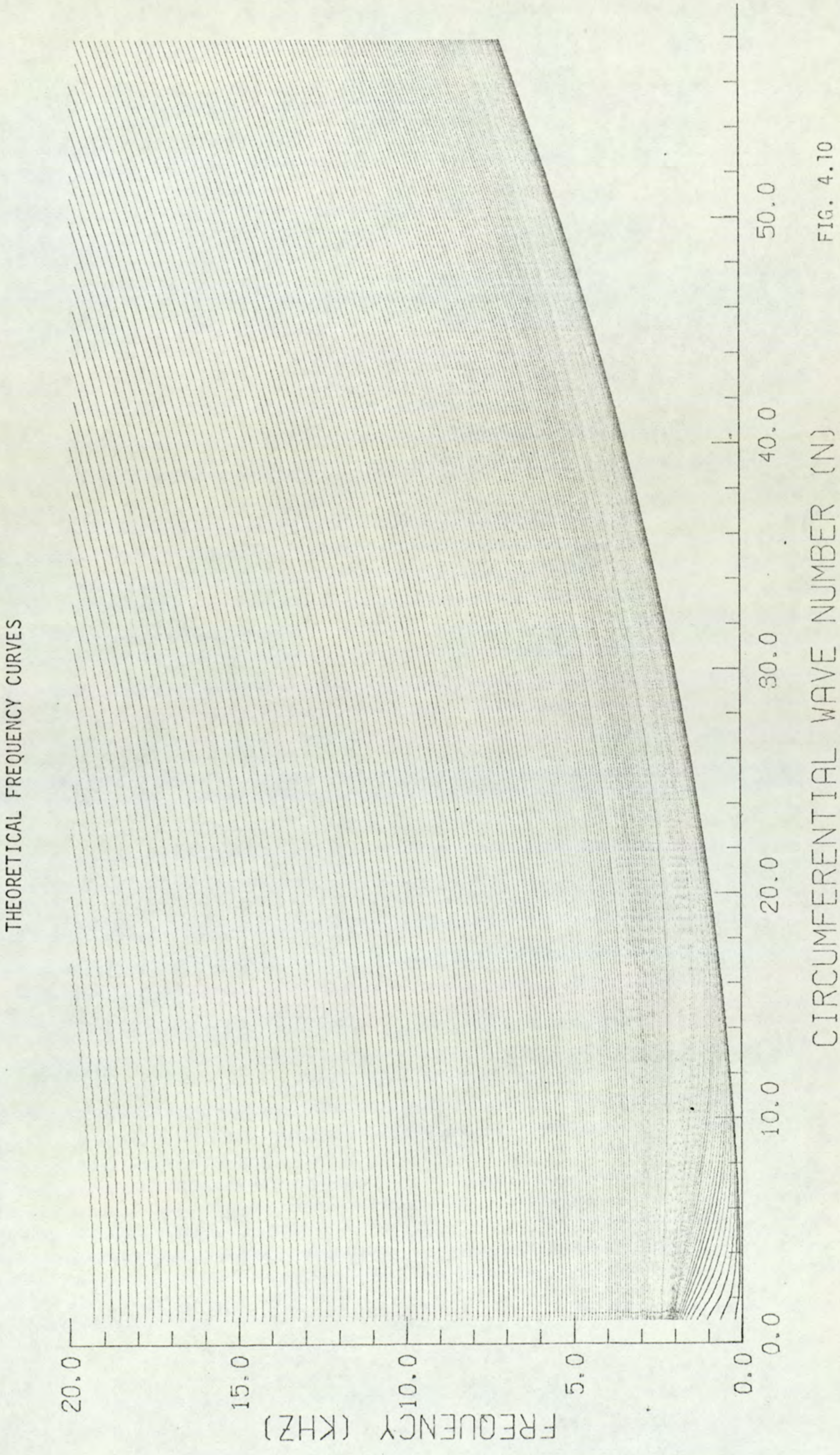
THEORETICAL FREQUENCY CURVES
FREQUENCY (KHZ)
0.0
5.0
10.0
15.0
20.0
CIRCUMFERENTIAL WAVE NUMBER (N)
0.0
10.0
20.0
30.0
40.0
50.0

FIG. 4.10

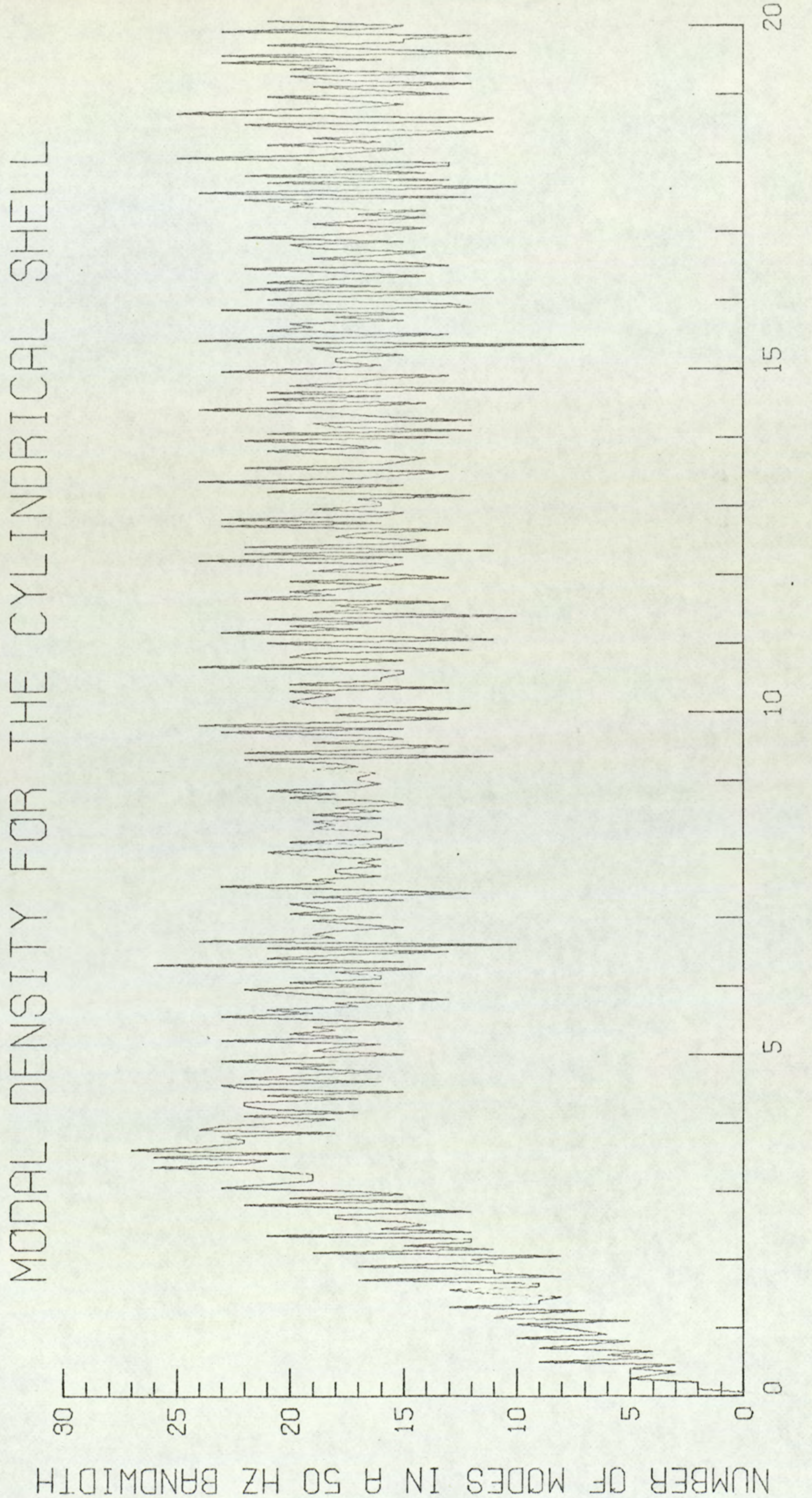
MODAL DENSITY FOR THE CYLINDRICAL SHELL
NUMBER OF MODES IN A 50 HZ BANDWIDTH
0
5
10
15
20
25
30
FREQUENCY (KHZ)
0
5
10
15
20

FIG 4.11

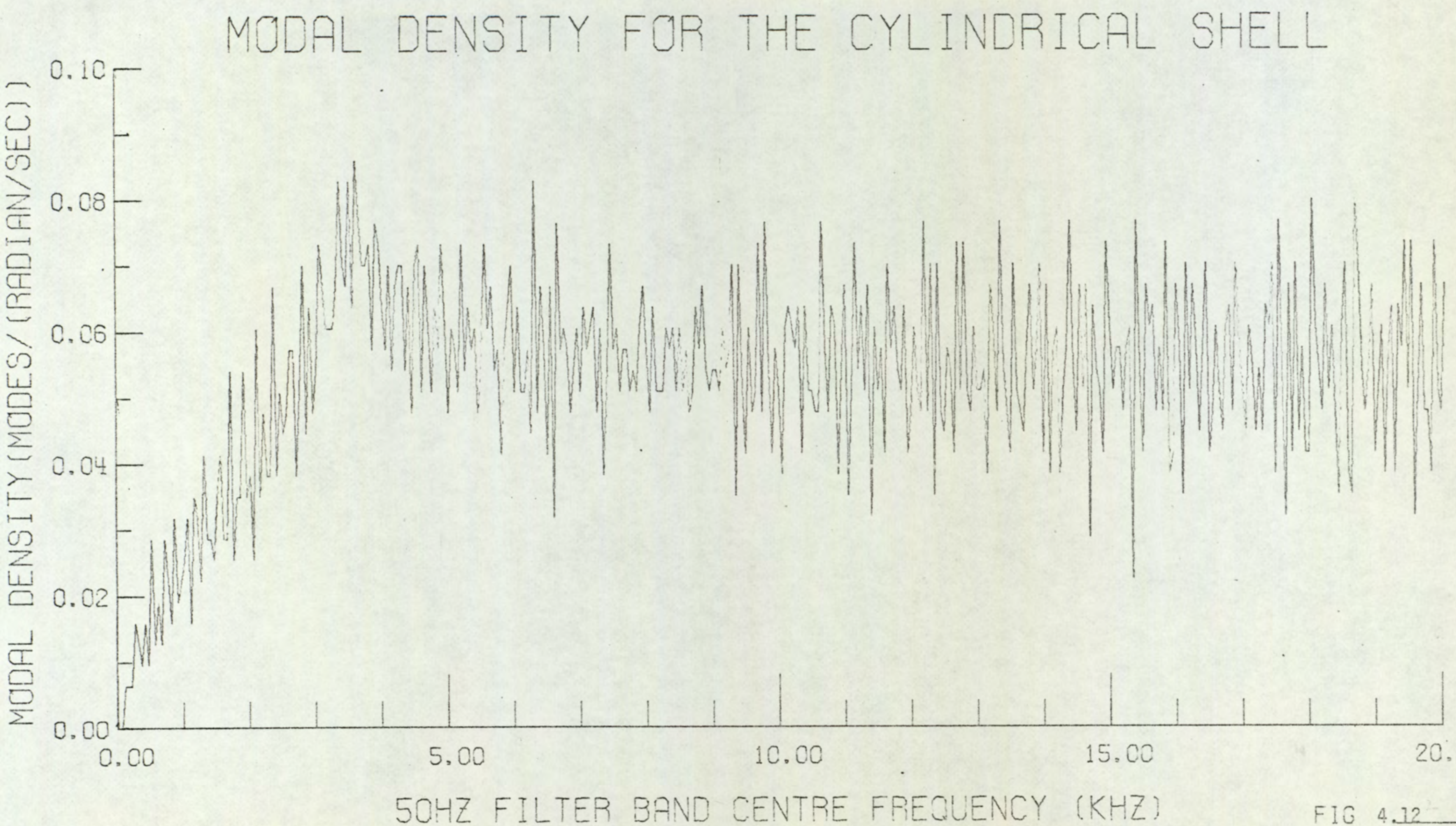
MODAL DENSITY FOR THE CYLINDRICAL SHELL
MODAL DENSITY(MODES/(RADIAN/SEC))
0.10
0.08
0.06
0.04
0.02
0.00
0.00
5.00
10.00
15.00
20.00
50HZ FILTER BAND CENTRE FREQUENCY (KHZ)

FIG 4.12

MODAL DENSITY FOR THE CYLINDRICAL SHELL

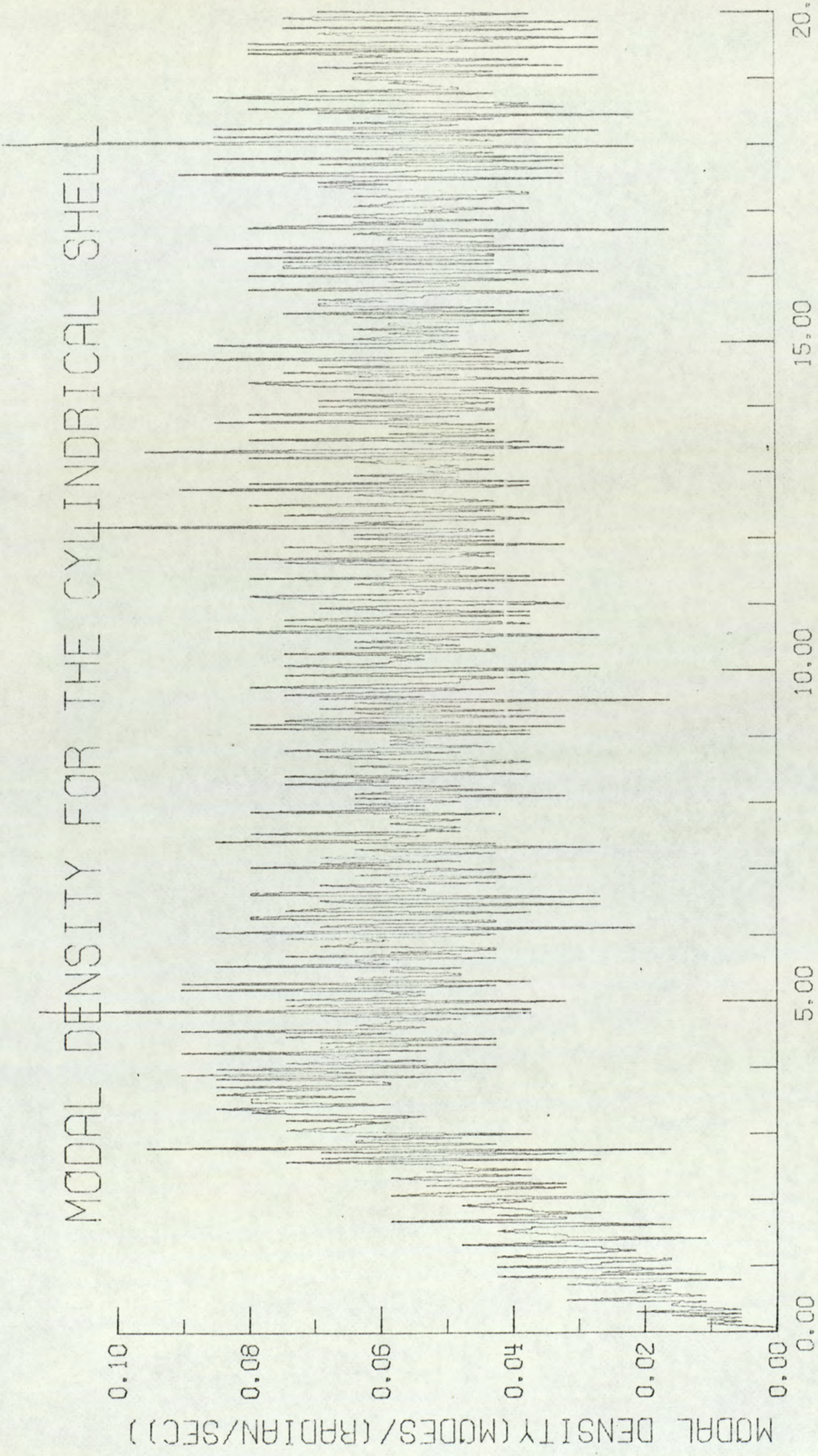

FIG 4.13

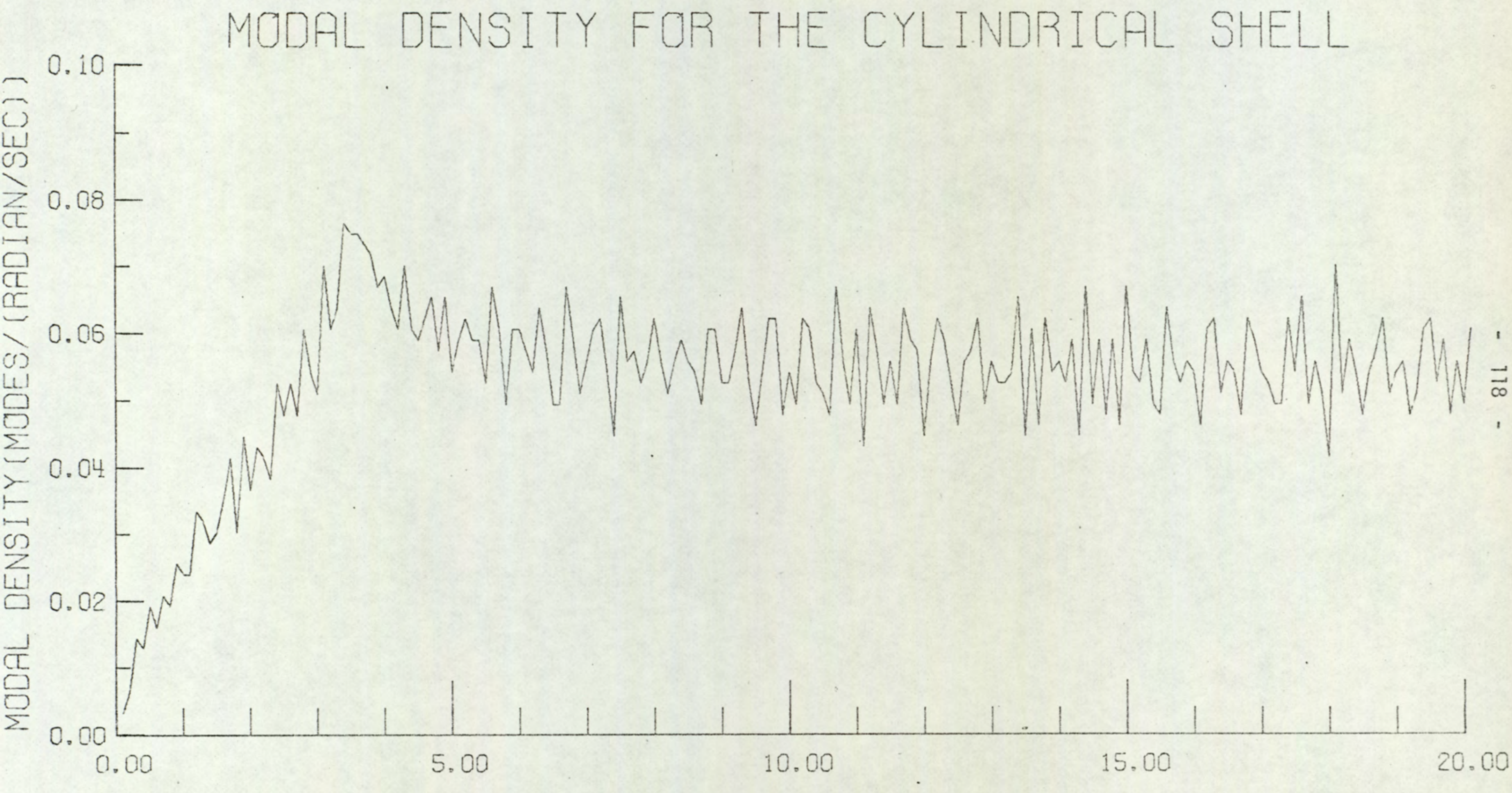
MODAL DENSITY FOR THE CYLINDRICAL SHELL
MODAL DENSITY(MODES/(RADIAN/SEC))
0.10
0.08
0.06
0.04
0.02
0.00
0.00
5.00
10.00
15.00
20.00
100HZ FILTER BAND CENTRE FREQUENCY (KHZ)

FIG 4.14

MODAL DENSITY FOR THE CYLINDRICAL SHELL

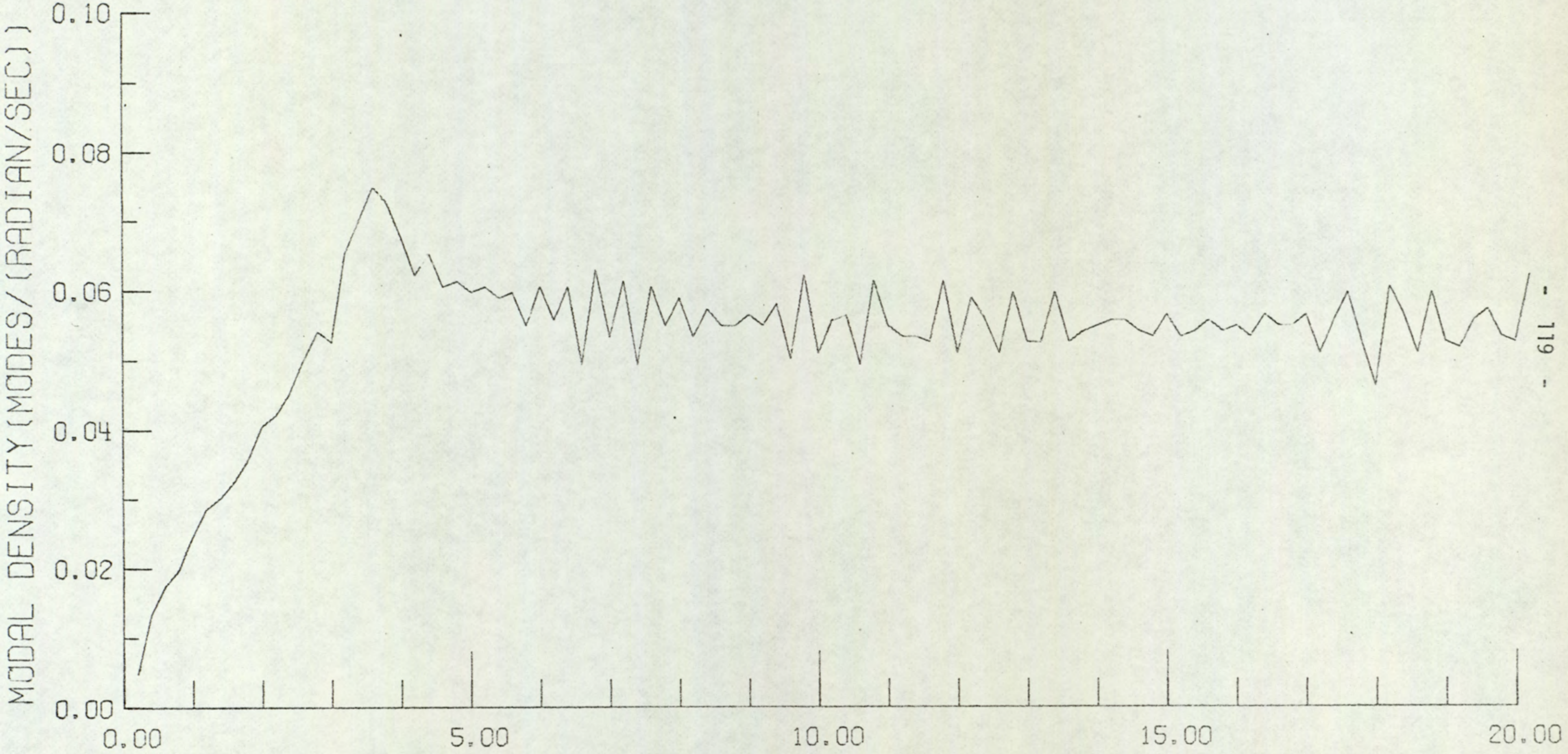

FIG 4.15

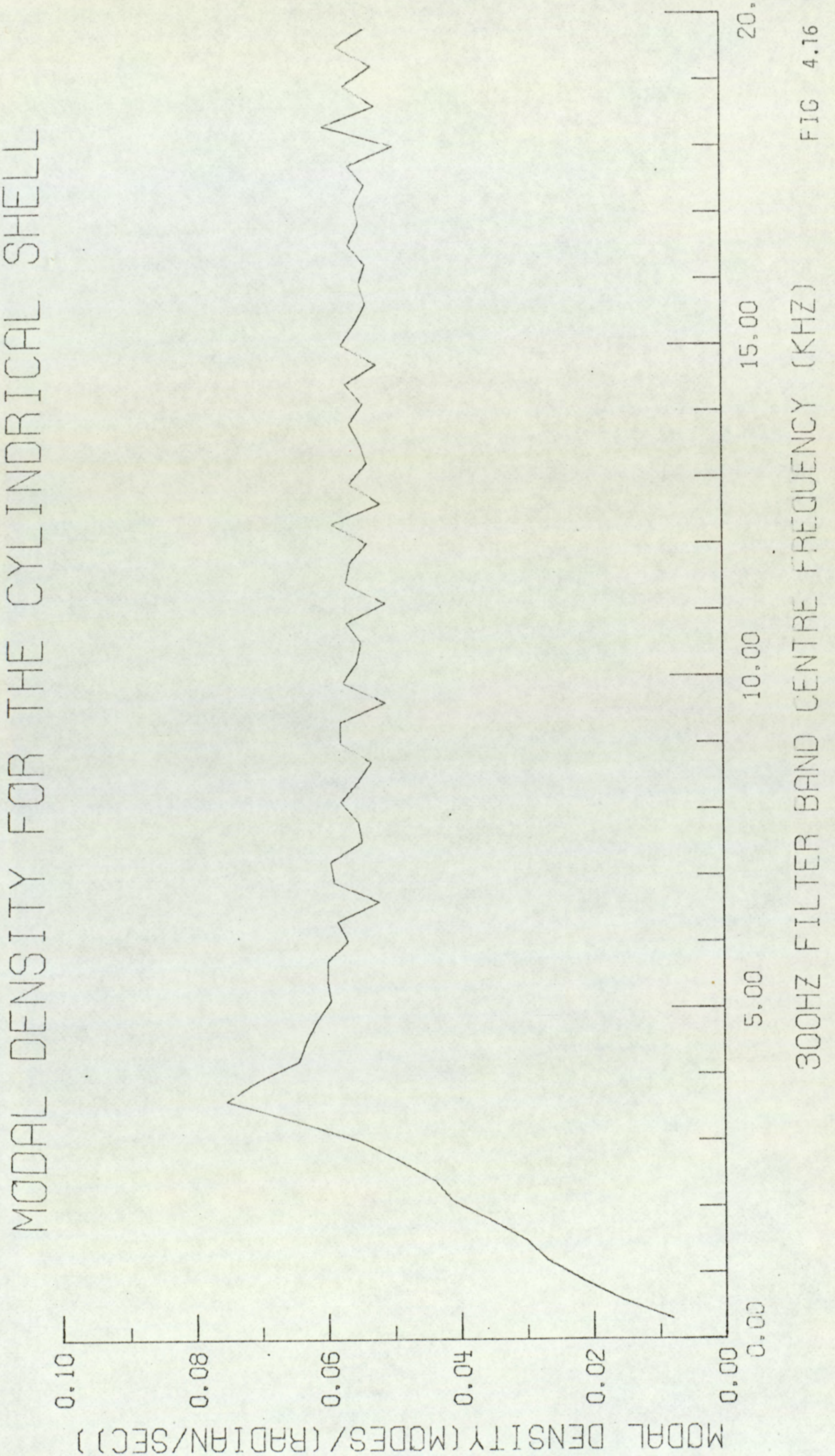
MODAL DENSITY FOR THE CYLINDRICAL SHELL
MODAL DENSITY(MODES/(RADIAN/SEC))
0.10
0.08
0.06
0.04
0.02
0.00
0.00
5.00
10.00
15.00
20.00
300HZ FILTER BAND CENTRE FREQUENCY (KHZ)

FIG 4.16

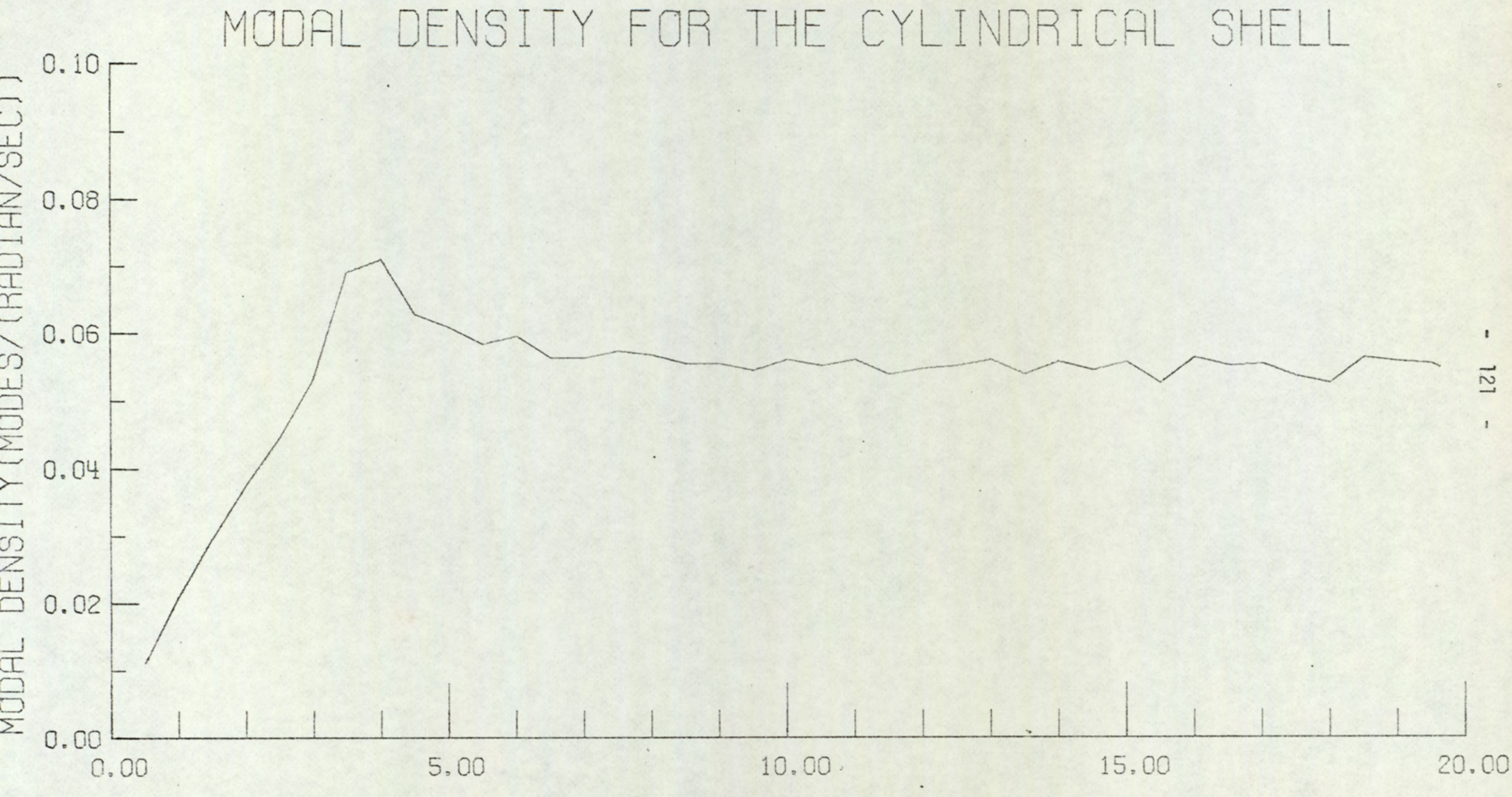
MODAL DENSITY FOR THE CYLINDRICAL SHELL
MODAL DENSITY(MODES/(RADIAN/SEC))
0.10
0.08
0.06
0.04
0.02
0.00
0.00
5.00
10.00
15.00
20.00
500HZ FILTER BAND CENTRE FREQUENCY (KHZ)

FIG 4.17

the peak at the ring frequency (3778 Hz) has been averaged. This trend was almost repeated when analysis was made in 1/1 and 1/3 octave band.

Experimental results discussed in section (3.4) of the previous chapter confirms this. It is clear therefore that analysis in a particular frequency band will depend on the accuracy of data required.

4.4.2 Stiffened Cylindrical Shells

Similar graphs as those produced for unstiffened cylinders were produced for cylinders with various combinations of stiffeners. A selection of these graphs of mode shapes and tables of resonant frequencies are given in figures (4.18) to (4.21).

4.4.3 Stiffener effects

In figures (4.18 to (4.21), the mode shapes and tables of resonant frequencies as obtained from equation (4.4) are given for a cylinder which is stiffened with both rings and stringers. The lowest natural frequency for the cylinder stiffened with 12 stringers and 6 rings occur at 405 Hz which is higher than for a cylinder stiffened with only 12 stringers and 3 rings which is 298 Hz. These are much higher than 80 Hz for a plain cylinder with the same physical properties. This situation for a cylinder which is stiffened with both rings and stringers is due to the coupling term Λ_{rs} in equation (4.4).

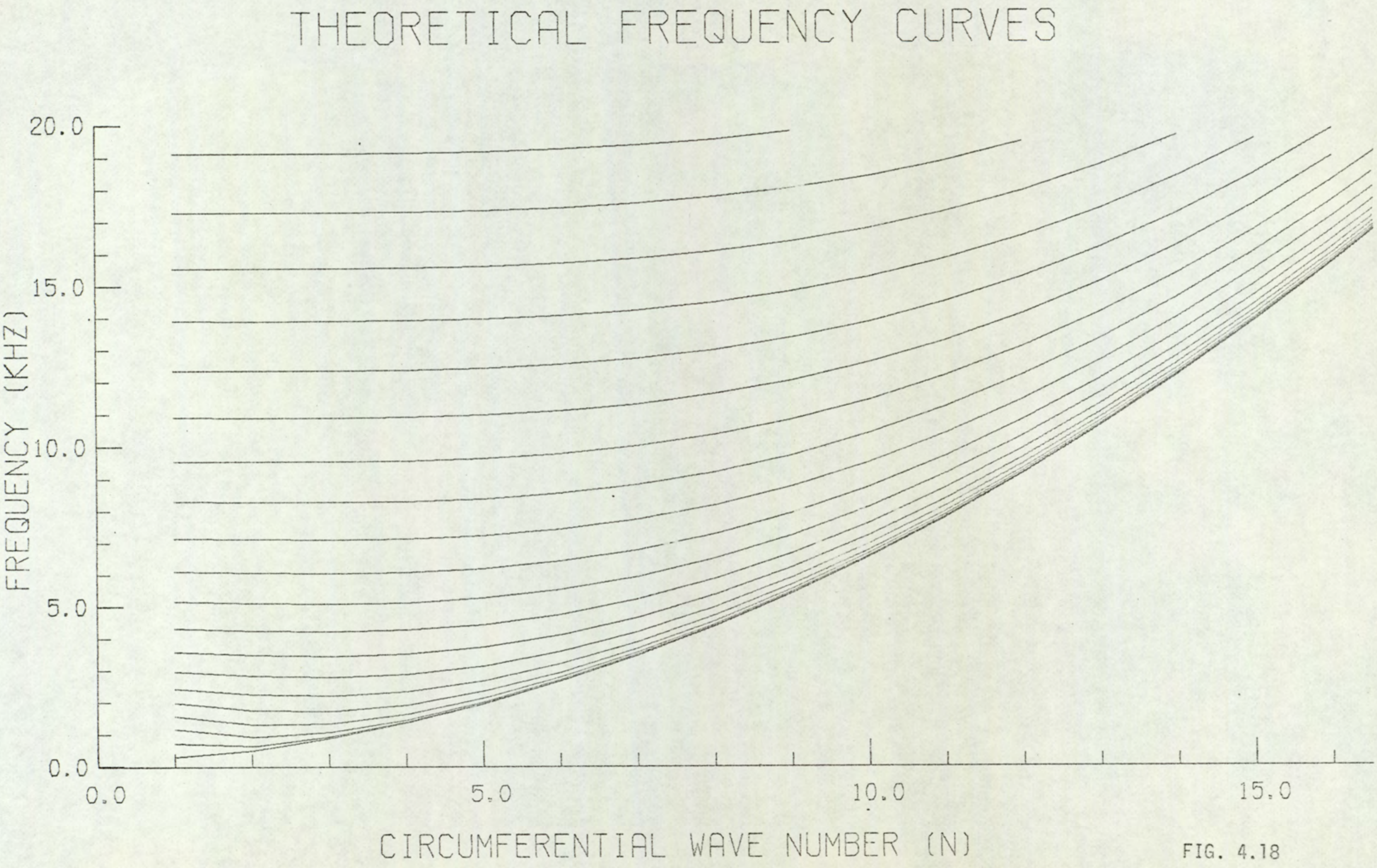
THEORETICAL FREQUENCY CURVES
FREQUENCY (KHZ)
20.0
15.0
10.0
5.0
0.0
0.0
5.0
10.0
15.0
CIRCUMFERENTIAL WAVE NUMBER (N)

FIG. 4.18

298	496	597	671	815	867	892	973	1068	1076
1114	1300	1332	1352	1361	1381	1392	1459	1515	1568
1576	1622	1718	1752	1818	1827	1900	1946	1950	1965
1999	2011	2023	2063	2071	2137	2161	2253	2299	2299
2347	2404	2472	2479	2618	2648	2651	2653	2659	2680
2704	2710	2719	2749	2785	2884	2974	2974	2998	3021
3057	3070	3200	3290	3370	3383	3426	3438	3445	3459
3461	3466	3480	3507	3553	3626	3653	3699	3730	3806
3812	3853	3871	3876	4023	4055	4063	4285	4285	4285
4315	4350	4378	4379	4383	4393	4397	4412	4447	4502
4518	4565	4583	4695	4802	4806	4820	4824	4845	4867
4895	5019	5036	5273	5278	5293	5363	5370	5379	5405
5405	5408	5416	5427	5431	5458	5501	5560	5566	5566
5656	5712	5779	5814	5898	5938	5967	5977	5979	6031
6139	6157	6198	6288	6383	6385	6540	6540	6543	6549
6561	6583	6615	6617	6623	6625	6670	6676	6680	6732
6734	6744	6792	6846	6979	6998	7026	7150	7228	7305
7311	7316	7320	7361	7364	7425	7470	7617	7659	7777
7783	7783	7785	7790	7800	7818	7847	7877	7890	7921
7953	7955	8037	8038	8041	8049	8094	8151	8192	8276
8296	8365	8377	8383	8478	8637	8654	8701	8810	8813
8823	8865	8942	8955	8967	9028	9115	9134	9134	9136
9140	9145	9149	9164	9188	9225	9278	9282	9350	9366
9447	9554	9572	9625	9626	9638	9646	9659	9677	9727
9729	9761	9909	9923	10063	10140	10157	10216	10228	10435
10475	10481	10481	10493	10531	10532	10593	10593	10595	10598
10606	10609	10619	10639	10671	10716	10745	10760	10779	10851
10865	10932	10959	10971	11056	11108	11135	11271	11278	11377
11377	11389	11425	11484	11497	11526	11561	11624	11634	11697
11730	11823	12020	12039	12112	12160	12161	12162	12165	12171
12183	12201	12228	12254	12266	12268	12313	12316	12322	12326
12356	12359	12395	12427	12490	12510	12545	12572	12610	12730
12741	12760	12942	12952	12999	13032	13159	13160	13176	13290
13291	13303	13334	13371	13398	13419	13508	13565	13580	13691
13720	13801	13836	13836	13837	13840	13845	13855	13861	13871
13895	13930	13931	13978	14042	14068	14126	14207	14232	14279
14307	14309	14320	14349	14364	14409	14464	14482	14496	14512
14526	14672	14721	14739	14803	14908	14910	14952	15223	15233
15246	15325	15364	15366	15376	15404	15408	15453	15460	15537
15557	15619	15620	15621	15623	15628	15637	15651	15665	15672
15703	15707	15745	15802	15876	15896	15927	15959	15971	16048
16089	16158	16218	16233	16233	16303	16408	16460	16462	16473
16499	16552	16564	16616	16639	16642	16759	16783	16860	16903
16918	16990	17145	17160	17224	17267	17277	17469	17511	17511
17512	17514	17519	17526	17539	17558	17585	17597	17599	17609
17623	17634	17659	17674	17684	17731	17741	17769	17809	17825
17828	17840	17901	17931	17938	18060	18095	18151	18217	18258
18365	18405	18443	18597	18625	18706	18725	18726	18767	18773
18775	18785	18809	18855	18882	18935	19060	19111	19179	19191
19243	19244	19497	19511	19511	19512	19514	19515	19517	19518

TABLE OF NATURAL FREQUENCIES FOR CYLINDER STIFFENED WITH 12 STRINGERS AND 3 RINGS (Diameter = 0.762 m, Length = 1.8 m)

FIG. 4.19

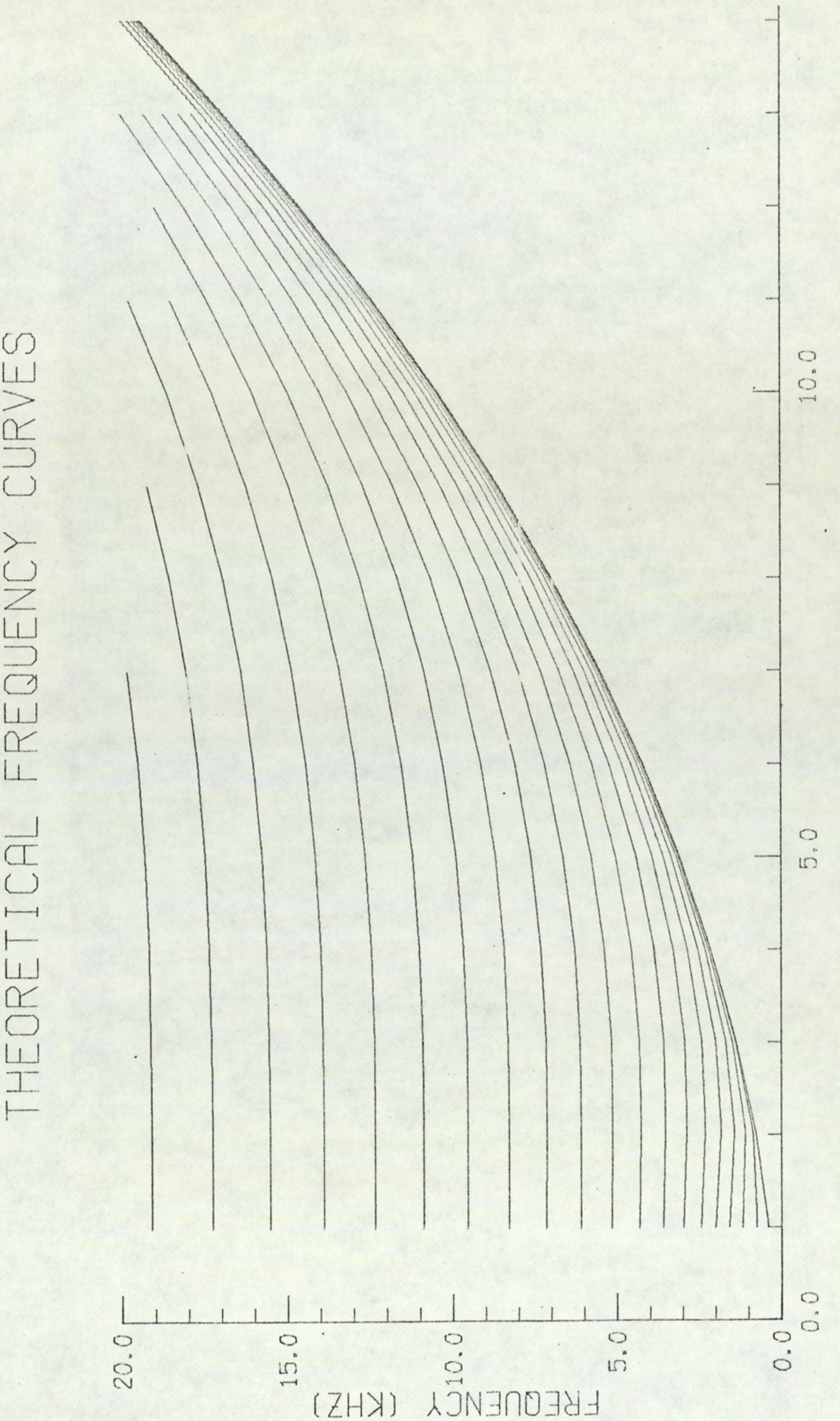
THEORETICAL FREQUENCY CURVES
FREQUENCY (KHZ)
20.0
15.0
10.0
5.0
0.0
0.0
5.0
10.0
CIRCUMFERENTIAL WAVE NUMBER (N)

FIG. 4.20

405	751	782	869	1094	1177	1379	1406	1425	1502
1578	1701	1831	1979	2013	2152	2164	2213	2309	2330
2426	2435	2543	2869	2871	2951	2965	3099	3106	3135
3209	3320	3356	3520	3574	3599	3600	3891	3959	4217
4222	4242	4269	4294	4302	4338	4399	4442	4581	4582
4863	5054	5118	5136	5180	5259	5386	5508	5512	5526
5564	5644	5731	5784	5791	6006	6068	6077	6125	6302
6328	6434	6651	6765	6971	6974	6985	7015	7077	7119
7121	7172	7187	7216	7325	7328	7365	7627	7628	7992
8022	8125	8268	8271	8320	8454	8472	8607	8609	8617
8641	8691	8719	8780	8848	8925	9078	9142	9157	9447
9517	9522	9567	9687	9803	9814	9855	9920	10307	10379
10414	10416	10423	10442	10483	10557	10677	10683	10858	10866
10873	10885	10915	11021	11028	11115	11227	11463	11571	11683
11807	11916	12089	12314	12322	12360	12394	12395	12401	12417
12451	12456	12484	12513	12614	12640	12719	12767	12813	12947
12986	13177	13284	13412	13676	13763	13860	13868	13904	13990
13999	14068	14155	14174	14431	14545	14546	14551	14565	14594
14647	14733	14787	14851	14864	14939	14954	15052	15310	15445
15505	15512	15524	15545	15624	15650	15773	16021	16043	16087
16245	16390	16401	16629	16869	16870	16874	16886	16911	16941
16956	17031	17144	17244	17253	17263	17284	17287	17307	17355
17389	17490	17531	17671	17716	17829	18060	18069	18213	18521
18555	18614	18694	18979	19082	19091	19119	19185	19222	19281
19308	19365	19366	19370	19380	19402	19441	19506	19513	19604
19747	19786	19826	19944	19985	20022	20092	20206	20277	20545
20812	20891	20972	21016	21025	21051	21111	21182	21197	21224
21411	21498	21694	21698	21766	22033	22034	22037	22046	22065
22100	22110	22131	22157	22243	22369	22506	22543	22675	22708
22775	22852	22880	23047	23055	23076	23080	23135	23238	23410
23418	23457	23673	23751	23928	23948	24052	24072	24360	24498
24573	24750	24873	24874	24877	24885	24902	24932	24983	25060
25171	25173	25177	25181	25204	25255	25260	25326	25350	25425
25508	25520	25533	25750	25802	25880	25971	26100	26136	26143
26566	26581	26888	26911	27080	27144	27217	27221	27395	27403
27424	27472	27560	27696	27706	27885	27886	27889	27896	27911
27929	27932	27938	27983	28033	28052	28151	28252	28290	28420
28475	28528	28540	28697	28716	29023	29047	29106	29260	29288
29405	29713	29720	29741	29785	29866	29871	30001	30047	30071

TABLE OF NATURAL FREQUENCIES OF CYLINDER STIFFENED WITH 12 STRINGERS AND 6 RINGS (Diameter = 0.762 m, Length = 1.8 m)

FIG. 4.21

The experimental results measured for space average acceleration given in section (3.8) of Chapter 3 show that due to lack of coupling between the noise field and the cylinder, it was not possible to freely excite it below about 400 Hz. On the other hand when a vibrator was used as an exciter, the response of the cylinder in this frequency range is quite high because it was being forced to vibrate. This shows that there is a general confirmation between the theory and experiment.

4.4.4 Plates (Unstiffened and stiffened)

The corresponding graphs were also produced and a specimen is given in figure (4.22). These results were not verified experimentally.

4.5 Combining the Computations

It can be seen that the number of possible combinations of formulae, cylinder/plate, stringer/no stringer, graph/no graph etc., is large. The number of computer programs required to cater for all these combinations is large. At an early stage of the work it was therefore decided to combine all these possible options in one program. The flow diagram for this program is given in pages 133-137; a description of its use is outlined below:

4.5.1 Control Cards

The options required are indicated by control cards which precede the data proper. These control cards have the following

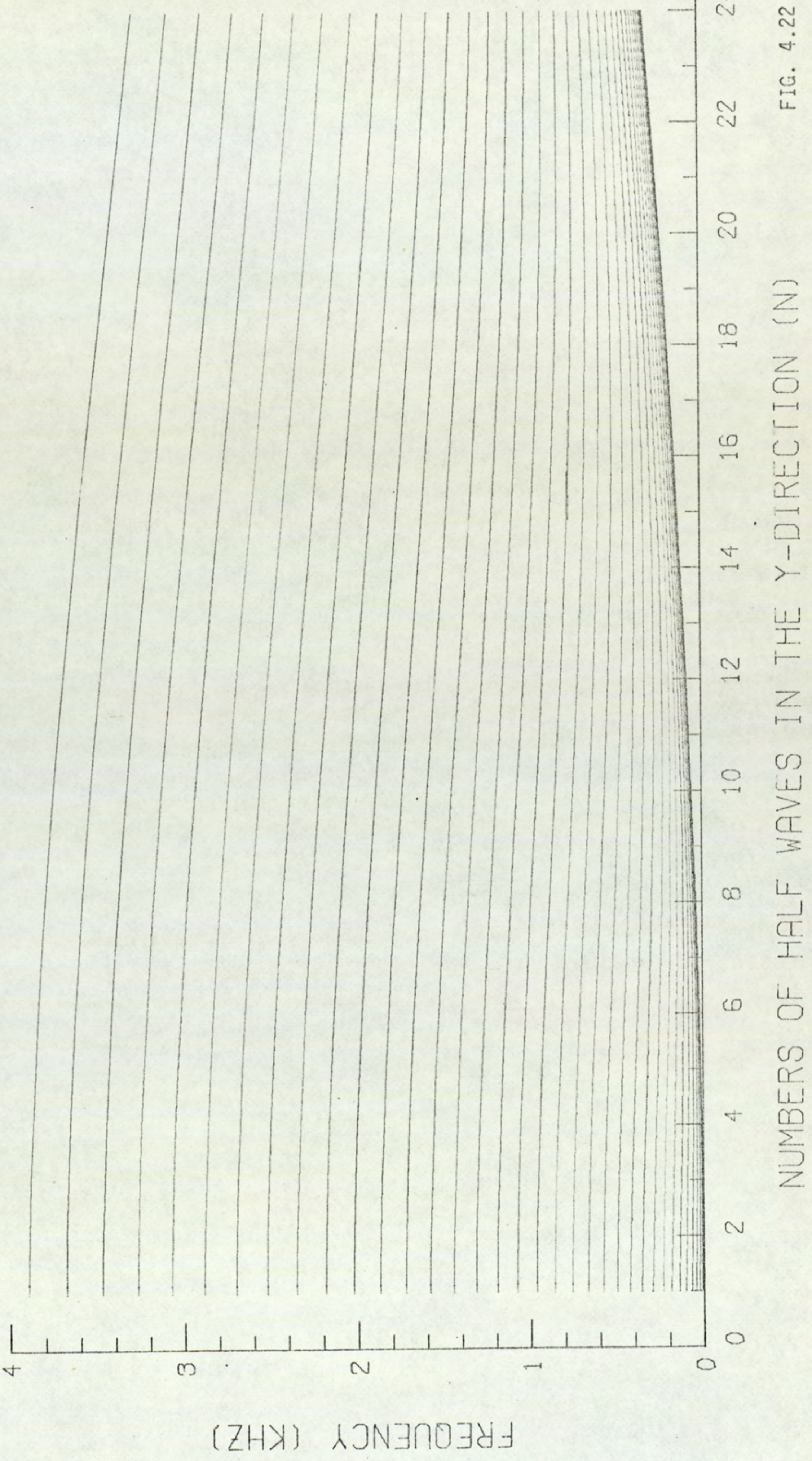
FREQUENCY (KHZ)
0
1
2
3
4
0
2
4
6
8
10
12
14
16
18
20
22
24
NUMBERS OF HALF WAVES IN THE Y-DIRECTION (N)

FIG. 4.22

meanings if present.

ARNOLD	Use the Arnold and Warburton formulae.
MIKULAS	Use the Mikulas and McElman formulae.
CYLINDER	Data presented will be for a cylinder and the formulae for a cylinder should therefore be used.
PLATE	Data presented will be for a plate and the formulae for a plate should therefore be used.
GRAPH	Graphical output is required.
TABLES	Tables of frequencies are required to be printed out on the lineprinter.
RINGS	Allowance is to be made for ring stiffeners in accordance with the data supplied.
STRINGERS	Allowance is to be made for stringer stiffeners in accordance with the data supplied.
DENSITIES	Any tables output are required to be of the form where the frequencies have been sorted into ascending order first and any graphical output should be of the form where modal density is plotted against frequency.
NATURALS	Any tables output are required to be of the form where the frequencies are given for each value of m and n and any graphical output should be of the form where frequency is plotted against m for each n (i.e. 'n' curves on the one graph).
END	The control cards are terminated by the control card END.

As the Arnold and Warburton formulae apply only to unstiffened cylinders, if ARNOLD is specified then STRINGERS, RINGS and PLATE must not be specified. Also, if GRAPH is specified then one of DENSITIES and NATURALS must be specified, but not both. ARNOLD and MIKULAS cannot both be specified in the same run and neither can CYLINDER and PLATE.

4.5.2 Data Parameters

Detailed data on the properties of the cylinder or plate, frequency bandwidth to be considered and specific requirements on size and annotation of any graphical output required is presented in the following order (in free format).

(a) Always required

The density of the cylinder or plate.

The length of the cylinder or plate.

The width of the plate or the radius of the cylinder.

Poisson's Ratio.

The acceleration due to gravity.

Young's modulus for the material of the cylinder or plate.

The range of harmonics:

lower m

higher m

lower n

higher n

The highest frequency of interest.

(b) Required if STRINGERS specified

The stringer spacing.

Young's modulus for the material of the stringers.

Shear modulus for the material of the stringers.

Distance from middle surface of cylinder or plate to centroid of stringer.

Cross-sectional area of stringer.

The width of the (I or Z shaped) stringer (I_b)

The depth of the stringer (I_d)

The height of the stringer (I_h)

The thickness of the material of the stringer (I_t)

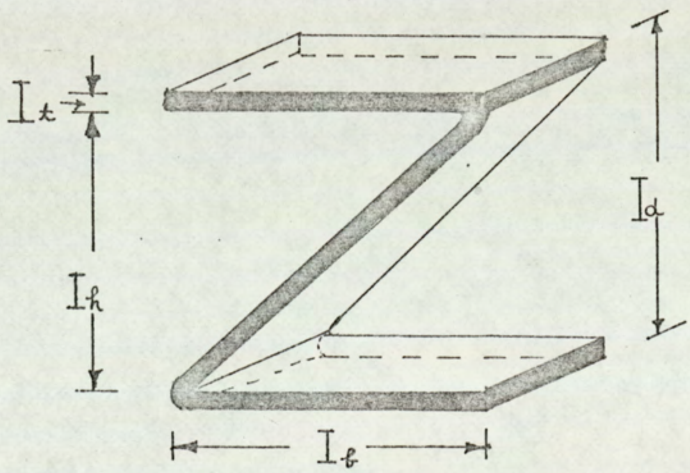

(c) Required if RINGS specified

Same information as for stringer (see above).

(d) Required if GRAPH specified

The X and Y coordinates of the point where the axes are to intersect.

The length in inches of the "negative" and "positive" parts of the X axis.

The lengths in inches of the "negative" and "positive" parts of the Y axis.

The lengths in inches of the small tickmarks on the X and the Y axes respectively.

The lengths in inches of the larger tickmarks on the X and the Y axes respectively.

The X and Y coordinates of the bottom left hand corner of the surrounding box.

The height and width of the box.

The number of decimal places before and after the decimal point on the numbering of the axes.

The distance between numbers (in inches) on the X and Y axes respectively.

The size (height) of the numbers.

The X axis scale in problem units per inch.

The Y axis scale in problem units per inch.

The X and Y coordinates of the midpoint of the graph title.

The X and Y coordinates of the midpoint of the labels for the X-axis and the Y-axis respectively.

The size (height) of the lettering of the title, X-axis label, and Y-axis label respectively.

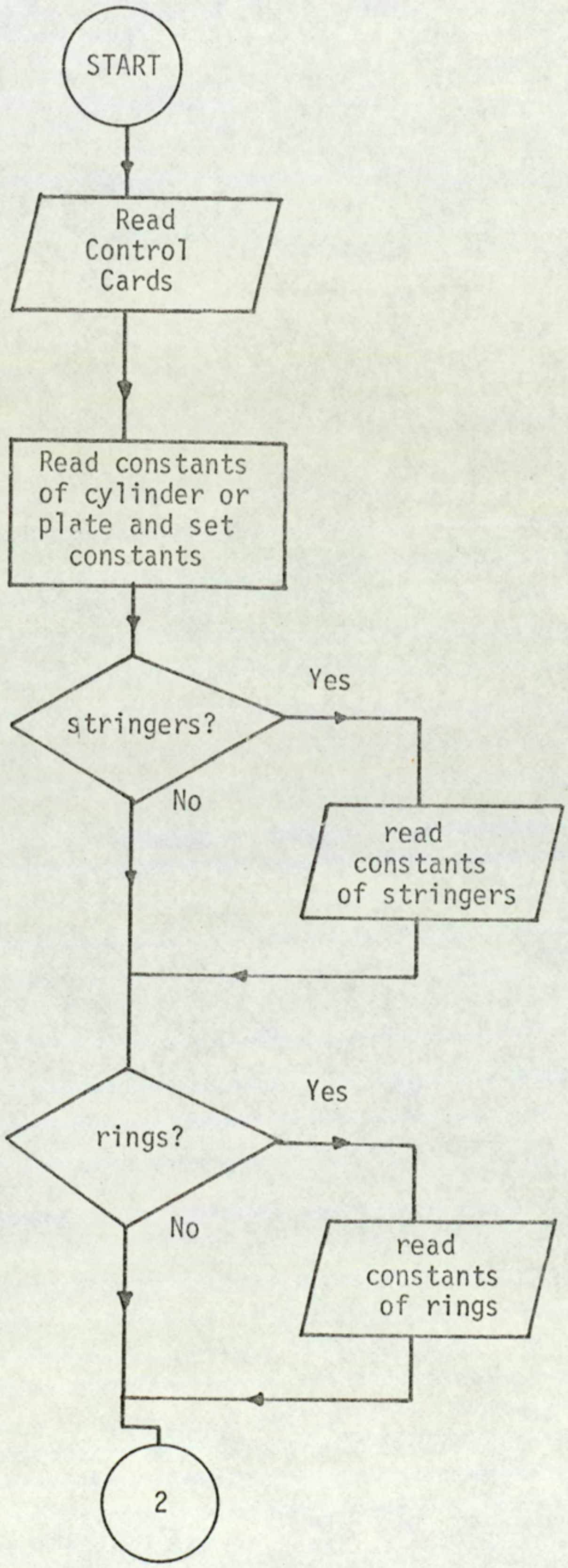
START
Read Control Cards
Read constants of cylinder or plate and set constants
stringers?
Yes
No
read constants of stringers
rings?
Yes
No
read constants of rings
2

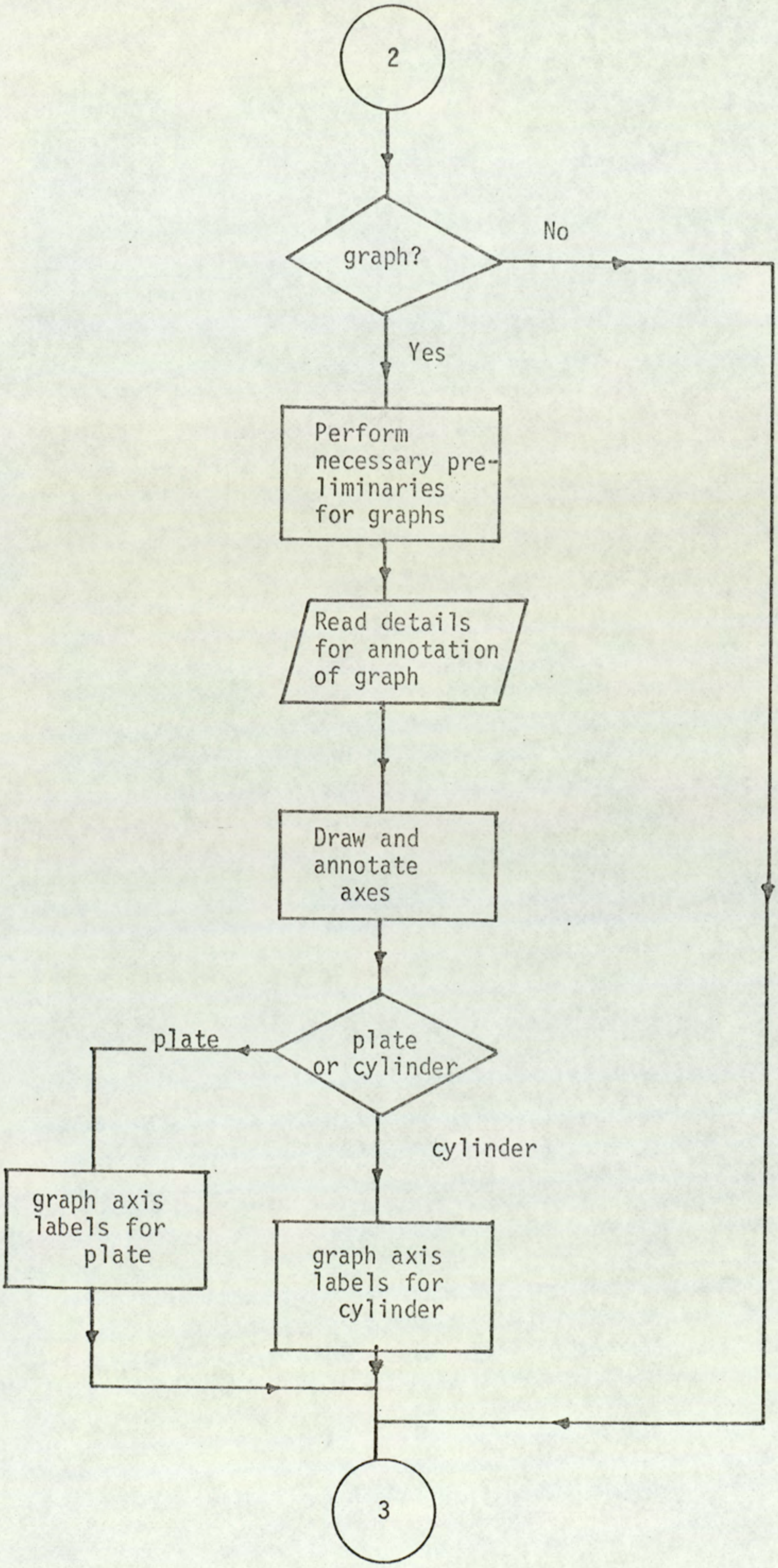
2
graph?
No
Yes
Perform necessary pre-liminaries for graphs
Read details for annotation of graph
Draw and annotate axes
plate or cylinder
plate
cylinder
graph axis labels for plate
graph axis labels for cylinder
3

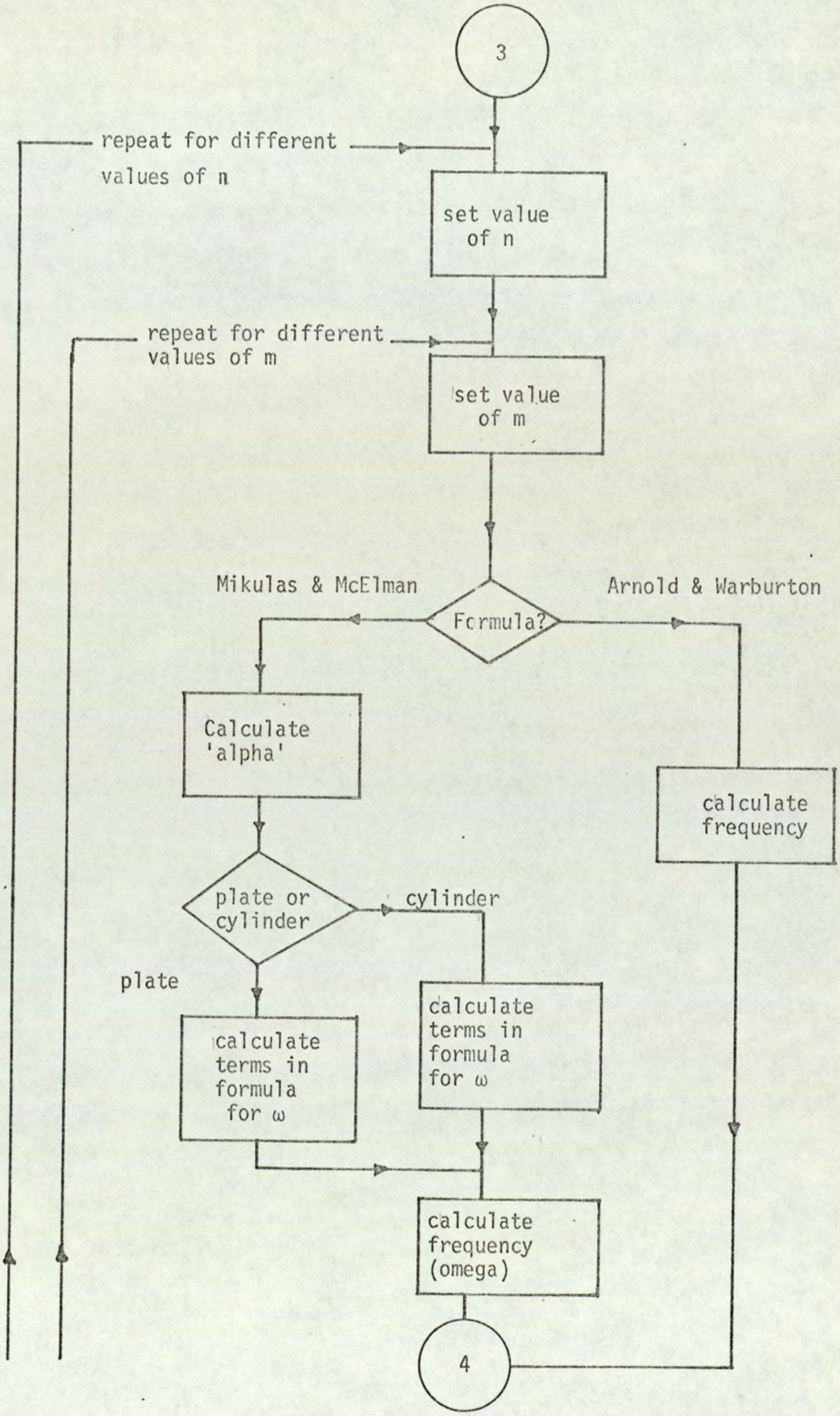
3
repeat for different values of n
set value of n
repeat for different values of m
set value of m
Mikulas & McElman
Formula?
Arnold & Warburton
Calculate 'alpha'
calculate frequency
plate or cylinder
cylinder
plate
calculate terms in formula for ω
calculate terms in formula for ω
calculate frequency (omega)
4

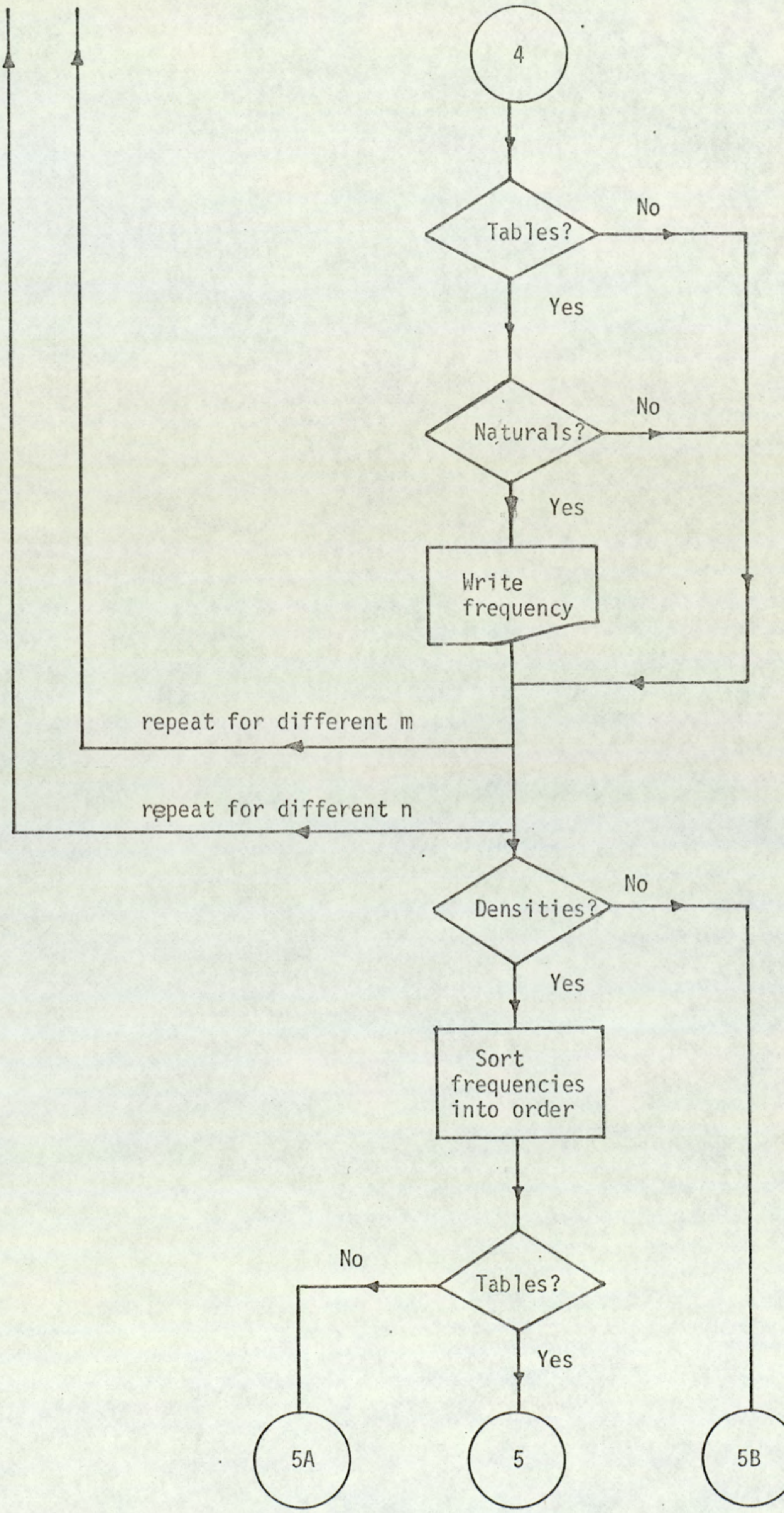
4
Tables?
No
Yes
Naturals?
No
Yes
Write frequency
repeat for different m
repeat for different n
Densities?
No
Yes
Sort frequencies into order
Tables?
No
Yes
5A
5
5B

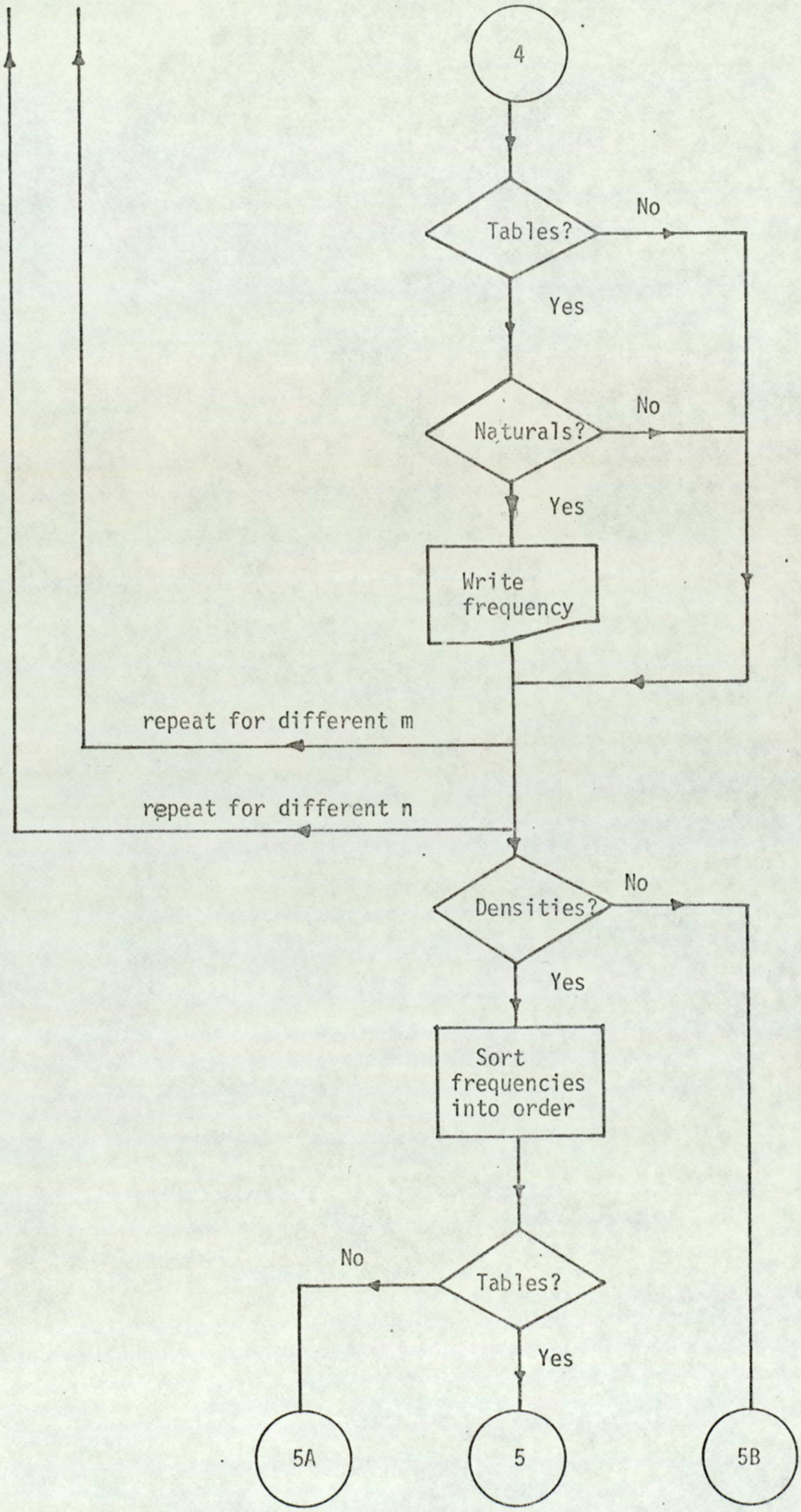
4
Tables?
No
Yes
Naturals?
No
Yes
Write frequency
repeat for different m
repeat for different n
Densities?
No
Yes
Sort frequencies into order
Tables?
No
Yes
5A
5
5B

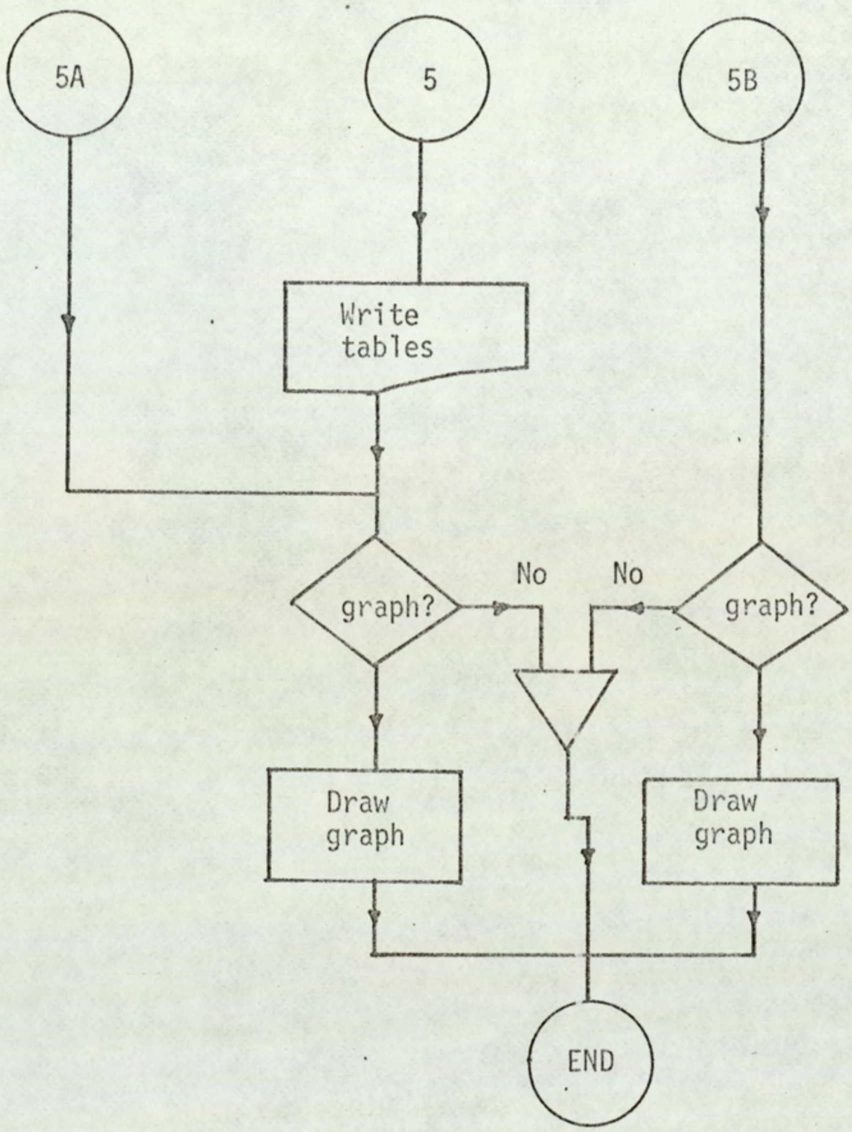
5A
5
5B
Write tables
graph?
No
No
graph?
Draw graph
Draw graph
END

CHAPTER FIVE

CHAPTER FIVE

ANALYSIS OF RESULTS OF VIBRATION AND SOUND TRANSMISSION STUDY

5.1 Introduction

In the previous chapters an experimental and theoretical study of the important parameters and their effects on vibration and sound transmission characteristics is made. The results obtained from this study is further analysed in this chapter and used in calculations.

Statistical energy analysis described in Chapter (2) is applied to give theoretical predictions of radiation resistance, average energy ratios between the systems and sound transmission loss. Inter-system coupling parameters are also calculated. The internal loss factor (η_{int}) is determined from measured total loss factor and the calculated coupling loss factor.

Since the effects of stiffener and cylinder configurations have already been dealt with in Chapter 4, and the work covered in this chapter is therefore based on cylinders stiffened with 12 stringers and 6 rings. Where necessary a comparison with unstiffened cylinders is made to emphasise a valid point.

5.2 Modal density of cylinddr wall and receiving spaces

[Transmission room and space enclosed by cylinder wall]

5.2.1 Cylinder Wall

For theoretical prediction of system energy and sound transmission properties, the modal density of the cylinder wall computed in Chapter (4) was used. In the frequency range below 400 Hz, the modal density of a plain cylinder was used when making theoretical calculations for the stiffened cylinders. This is because, due to stiffening, the first natural frequency for a freely vibrating cylinder was recorded above this frequency (figure (4.21)).

5.2.2 Transmission room and space enclosed by cylinder wall

The modal density was calculated using the equation given in section (3.4.3) of Chapter 3. The computed results used for the calculations was from figure (3.10).

5.3 Radiation Resistance

The expression for radiation resistance was obtained from equation (2.16) (Chapter 2).

$$R_{2rad} = \frac{\omega^2}{S_{a_2}(\rho_a C_a{}^2)} \quad [V_1 S_{p_1} \beta_1 + V_3 S_{p_3} \beta_3] \tag{5.1}$$

For the transmission room and enclosed space, $\beta_i = 13.8/T_i$ where $i = 1$ and 3 (Equation 2.15).

The cylinder wall was excited by 4 vibrators in 1/3 octave band. The space average sound pressure levels of transmission room and the enclosed space together with that of the cylinder wall was measured. The measured values of S_{p_1}, S_{p_3}, S_{a_2} and T_i were used in equation (5.1) to calculate radiation resistance. The result of this calculation is given in figure (5.1) as normalised radiation resistance. It is to be noted that R_{2rad} is the total radiation resistance of the cylinder and that this includes radiation on both sides of the cylinder. It is also noted that radiation resistance above concidence frequency (9.4 kHz) is greater than one because it is essentially radiation controlled.

5.3.1 Total Resistance

This quantity is defined by,

$$P_d = \left(\frac{S_a}{\omega^2}\right) R_{TOT} = \frac{S_a}{\omega^2} (R_{rad} + R_{int}) \tag{5.2}$$

where P_d is the total power dissipated by the cylinder wall including radiation.

The total energy stored in the system is given by,

$$E_T = M_c \frac{S_a}{\omega^2} + M_r \frac{S_{a_r}}{\omega^2} \tag{5.3}$$

where M_c is the total mass of plain cylinder and M_r is the total mass of stiffeners.

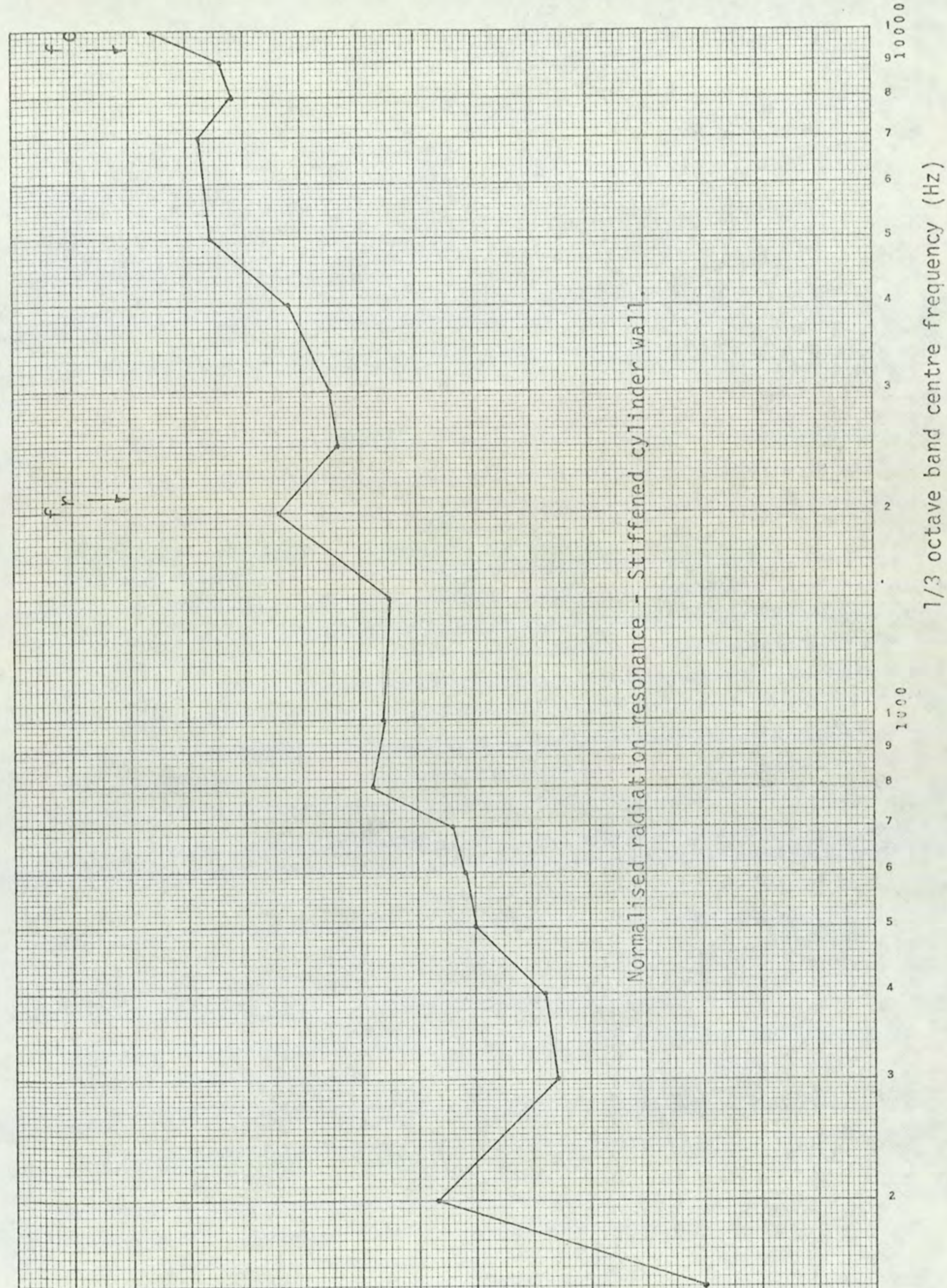
Normalised radiation resonance - Stiffened cylinder wall
f_c
f_r
10 log$_{10}$ ($R_{rad}/2A_z\rho_a C_a$)
10
0
-10
-20
-30
-40
-50
1/3 octave band centre frequency (Hz)
100
2
3
4
5
6
7
8
9
1000
2
3
4
5
6
7
8
9
10000

Fig. 5.1

The rate of energy dissipation by the structure is given by,

$$P_b = \beta_s E_T \qquad \text{where } \beta_s = 13.8/T_s$$

where T_s is the energy decay time of the structure, and hence for the cylinder wall in consideration;

$$R_{2_{TOT}} = (13.8/T_2)M_2 \, [1 + M_r \, (\frac{S_{a_r}}{\omega^2}) \Big/ M_2(\frac{S_a}{\omega^2})] \tag{5.4}$$

Total radiation resistance was determined from the measured values of cylinder wall decay time and equation (5.4). In calculating this, total mass of the cylinder and stiffeners were taken. Since T_2 was measured on the stiffened cylinder, the terms in the brackets of equation (5.4) were ignored. The result of this calculation is given in figure (5.2). From this it is seen that a trend similar to that of $R_{2_{rad}}$ is obtained. The straight line drawn through the curve shows that damping of the cylinder above coincidence frequency (9.4 kHz) is radiation controlled ($R_{2_{rad}} > R_{2_{int}}$).

5.4 Cylinder wall coupling factor

The formula for the coupling factor of the cylinder wall was obtained by combining equations (2.22) and (2.23) (Chapter 2) and is given below,

$$\mu = [S_{a_2} \,/ (S_{p_1} + S_{p_3})] \, [2\pi^2 (n_2/M_2) \, \frac{c_a}{\rho a}]^{-1} \tag{5.5}$$

In calculating μ, the appropriate correction for the total mass and modal density due to stiffeners were made.

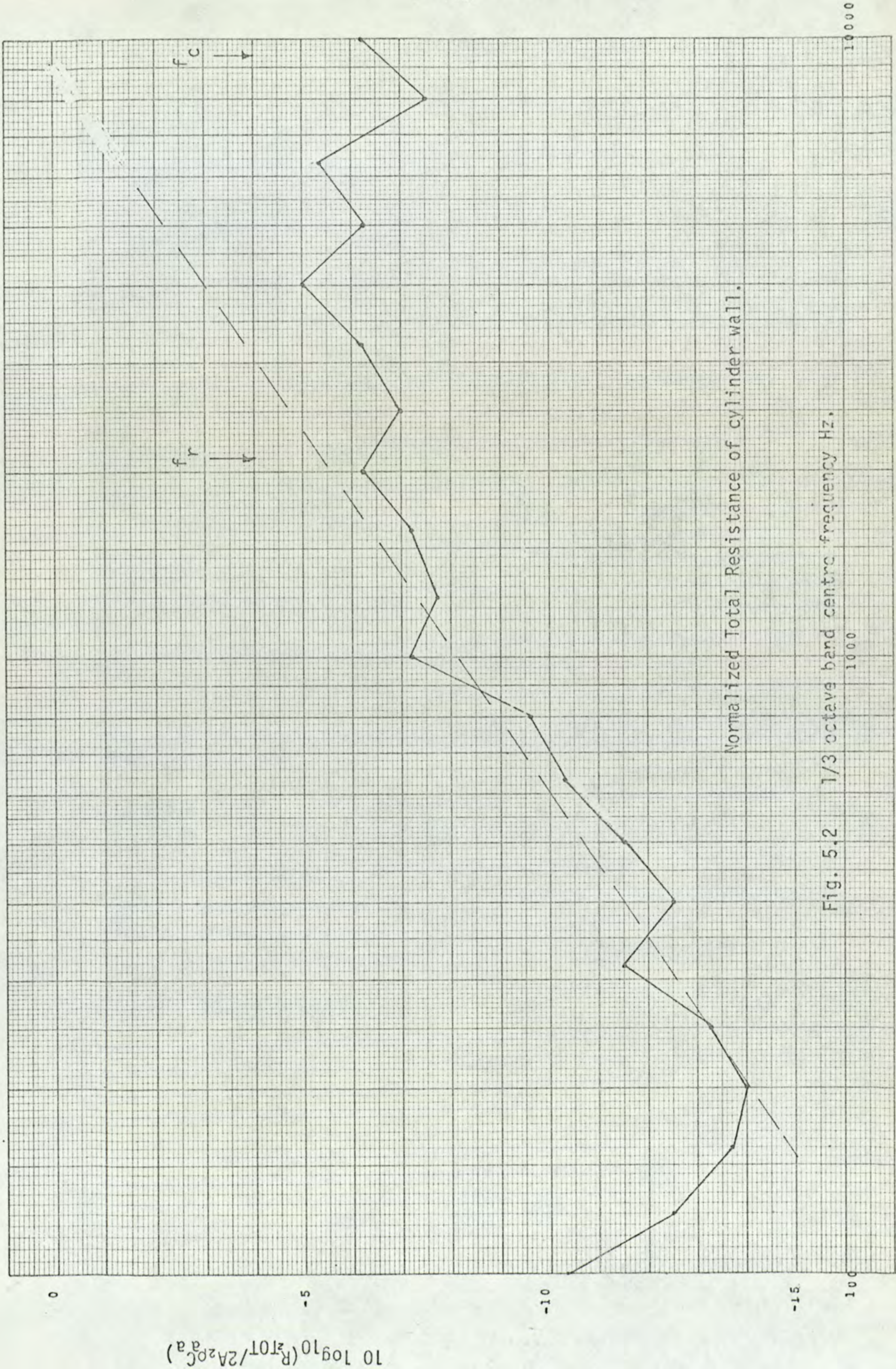

Fig. 5.2 Normalized Total Resistance of cylinder wall.

The transmission room and the space enclosed by the cylinder wall was acoustically excited in 1/3 octave band and space average sound pressure and acceleration levels were measured. The measured values of S_{p_1}, S_{p_3}, S_{a_2} and the computed values of n_2 were used in equation (5.5) to calculate the coupling factor. The result of this calculation is given in figure (5.3).

It is seen that between 700 Hz to 2.8 kHz and above 5.4 kHz the coupling is radiation controlled [$\mu > 1$]. This is not quite in agreement with the measurement of $R_{2_{TOT}}$.

The coupling factor was also calculated from equation (2.21) (Chapter 2),

$$\mu = \frac{\eta_{rad}}{\eta_{int} + \eta_{rad}} \qquad (5.6)$$

where η_{rad} is the total radiation loss factor and that includes radiation on both sides of the cylinder. The result of this calculation is compared with that calculated from equation (5.5) and is shown in figure (5.4). The data for internal loss factor (η_{int}) used for this calculation was extracted from the total loss factor (η_{TOT}).

Below 3 kHz, the large difference in the results could be due to η_{int} because this was determined from the measured value of η_{TOT}. A repeat of this calculation with improved values of η_{int} determined emphirically should be attempted for a better accuracy.

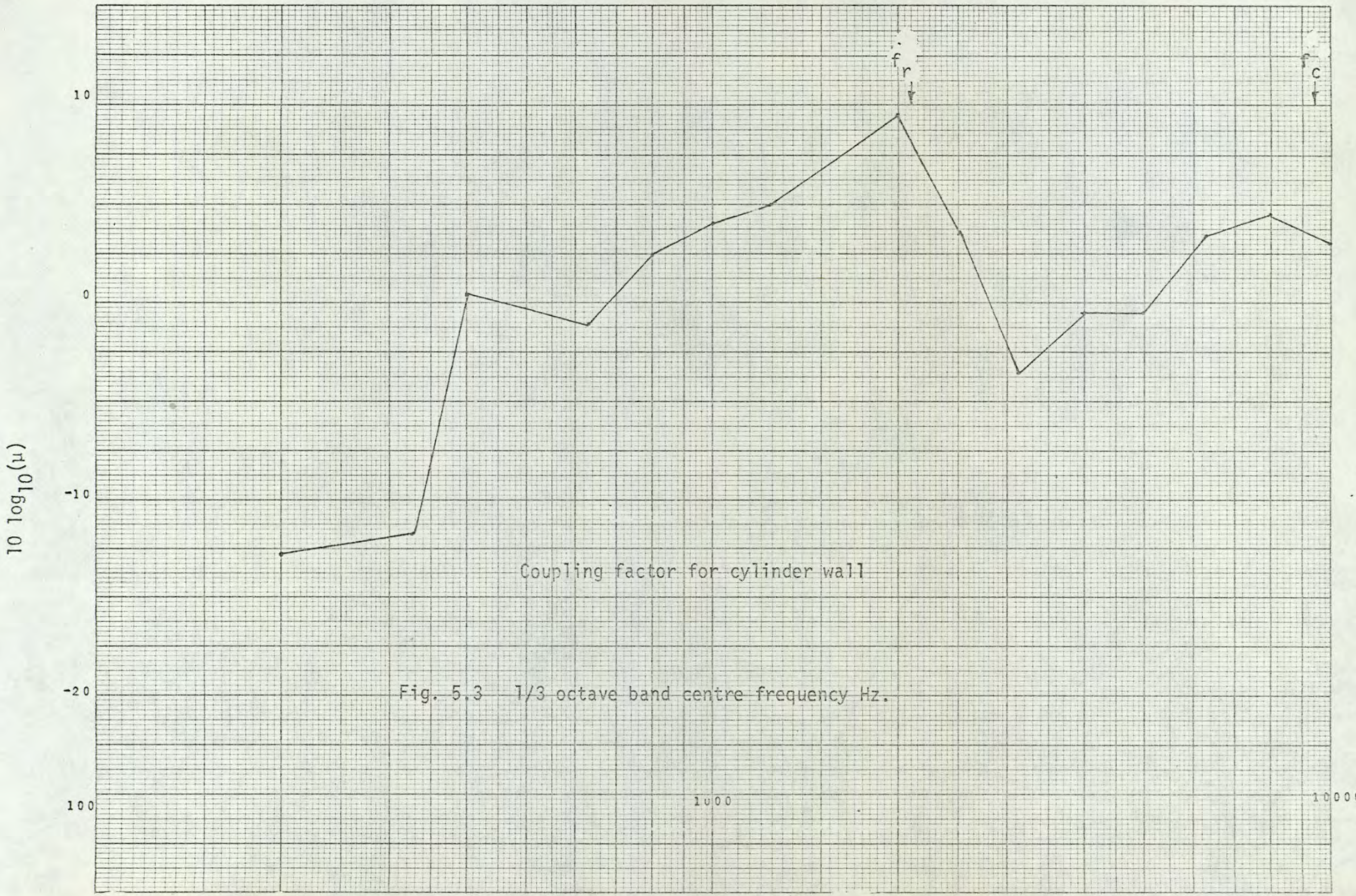

Coupling factor for cylinder wall

Fig. 5.3 1/3 octave band centre frequency Hz.

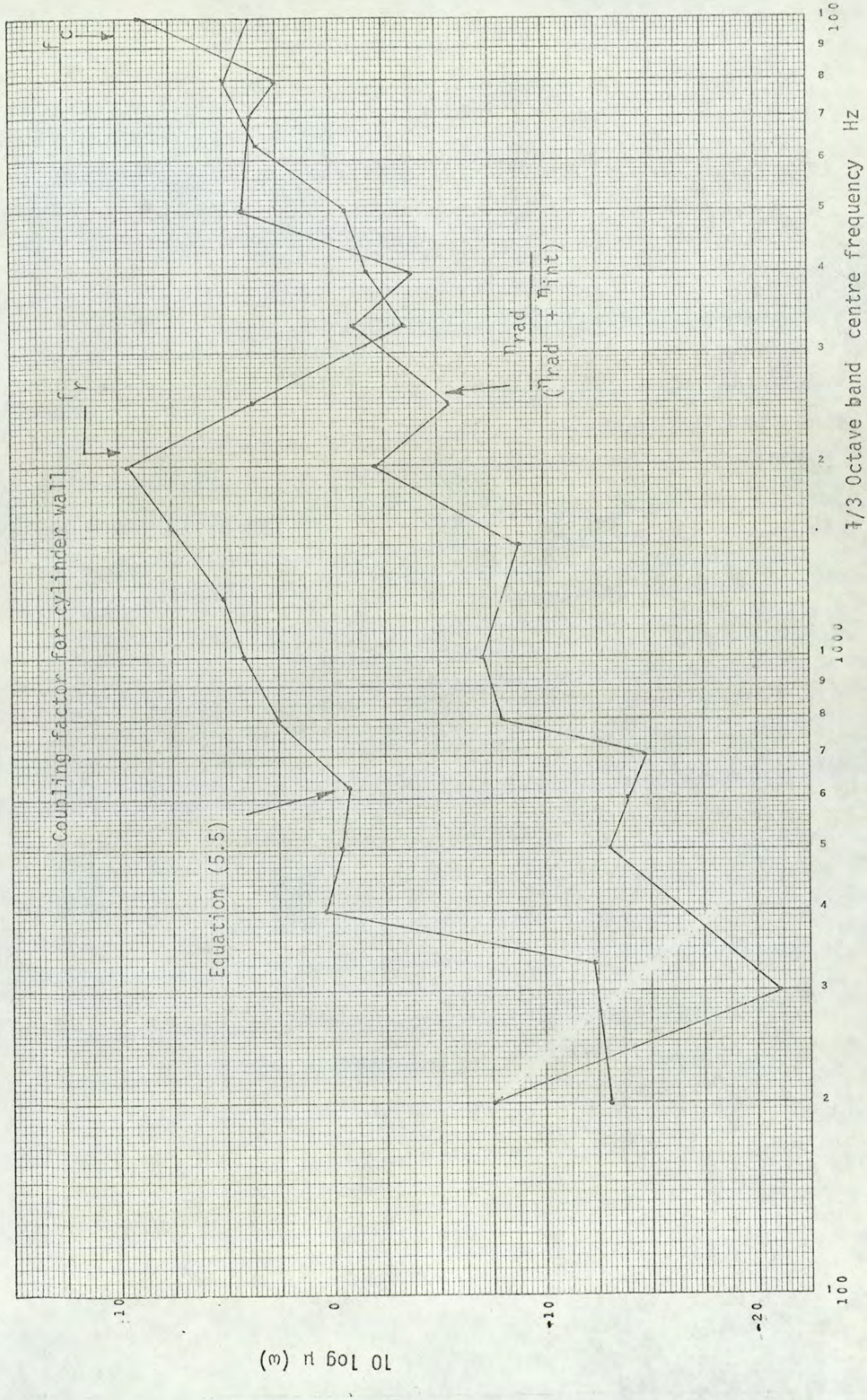

Coupling factor for cylinder wall
f_c
f_r
Equation (5.5)
η_rad / (η_rad + η_int)
10 log μ (ω)
1/3 Octave band centre frequency Hz
10
0
-10
-20
100
1000
10000

Fig. 5.4

5.5 Loss factors for Systems 1, 2 and 3

5.5.1 Total loss factor

The total loss factor for the systems 1, 2 and 3 were calculated from equation (2.15) (Chapter 2) and is given by,

$$\eta_{TOT} = \frac{2.2}{T_{if}} \qquad \text{where } i = 1,\ 2 \text{ and } 3. \tag{5.7}$$

The reverberation time of the systems against frequency was measured in 1/3 octave and used in equation (5.7) to calculate the loss factors. The results of this calculation are shown in figure(5.5) and Table (5.6). It is interesting to note that above 1 kHz, there is very small difference between the total loss factors of the systems.

A comparison of the total loss factor determined for unstiffened and stiffened cylinders is shown in figure (5.7) and Table (5.8) An increase in damping below the ring frequency for stiffened cylinder is clearly shown.

5.5.2 Coupling loss factor

The coupling loss factor was calculated using equation (2.32) (Chapter 2) and is given by,

$$\eta_{rad} = R_{2_{rad}}/\omega M_2 \tag{5.8}$$

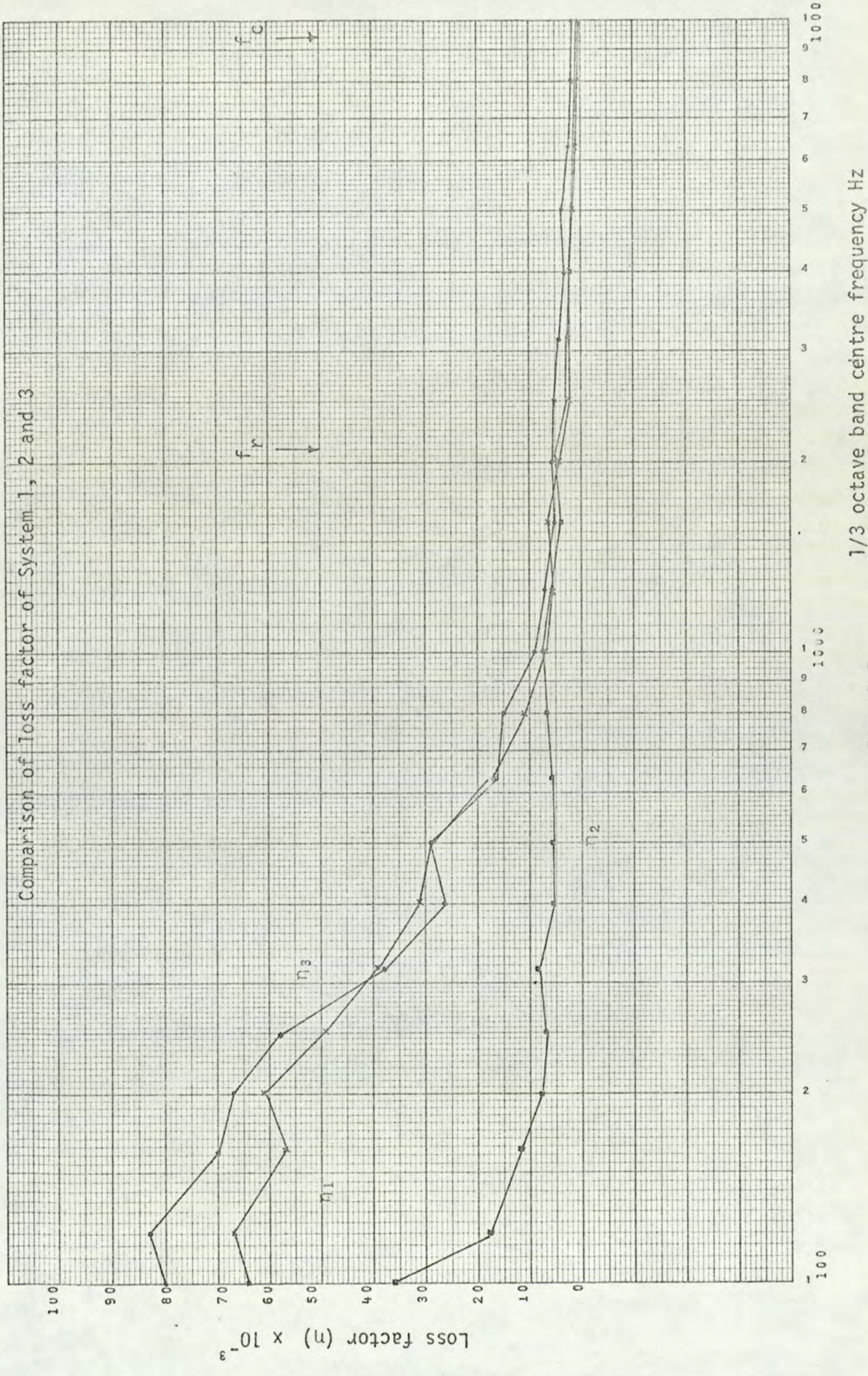

Comparison of loss factor of System 1, 2 and 3

Fig. 5.5

TABLE 5.6

f	η_1	η_2	η_3
100	64.32×10^{-3}	36.6×10^{-3}	80.29×10^{-3}
125	67.15×10^{-3}	17.6×10^{-3}	83.25×10^{-3}
160	57.28×10^{-3}	10.57×10^{-3}	70.39×10^{-3}
200	$61.3. \times 10^{-3}$	7.85×10^{-3}	73.25×10^{-3}
250	49.58×10^{-3}	7.33×10^{-3}	58.45×10^{-3}
315	39.12×10^{-3}	8.73×10^{-3}	38.39×10^{-3}
400	31.22×10^{-3}	5.5×10^{-3}	26.36×10^{-3}
500	29.46×10^{-3}	5.5×10^{-3}	29.43×10^{-3}
630	17.23×10^{-3}	5.82×10^{-3}	16.49×10^{-3}
800	11.35×10^{-3}	6.87×10^{-3}	15.29×10^{-3}
1000	7.61×10^{-3}	7.33×10^{-3}	9.16×10^{-3}
1250	7.33×10^{-3}	5.33×10^{-3}	7.32×10^{-3}
1600	6.55×10^{-3}	4.04×10^{-3}	5.16×10^{-3}
2000	4.5×10^{-3}	4.58×10^{-3}	5.2×10^{-3}
2500	2.44×10^{-3}	3.25×10^{-3}	4.9×10^{-3}
3150	2.58×10^{-3}	2.88×10^{-3}	4.6×10^{-3}
4000	2.29×10^{-3}	3.05×10^{-3}	3.31×10^{-3}
5000	1.83×10^{-3}	1.83×10^{-3}	3.4×10^{-3}
6300	1.45×10^{-3}	1.83×10^{-3}	2.16×10^{-3}
8000	1.31×10^{-3}	0.88×10^{-3}	1.7×10^{-3}
10000	0.85×10^{-3}	0.91×10^{-3}	1.46×10^{-3}

Loss factor of Systems 1, 2 and 3 determined from $(\frac{2.2}{T_i f})$

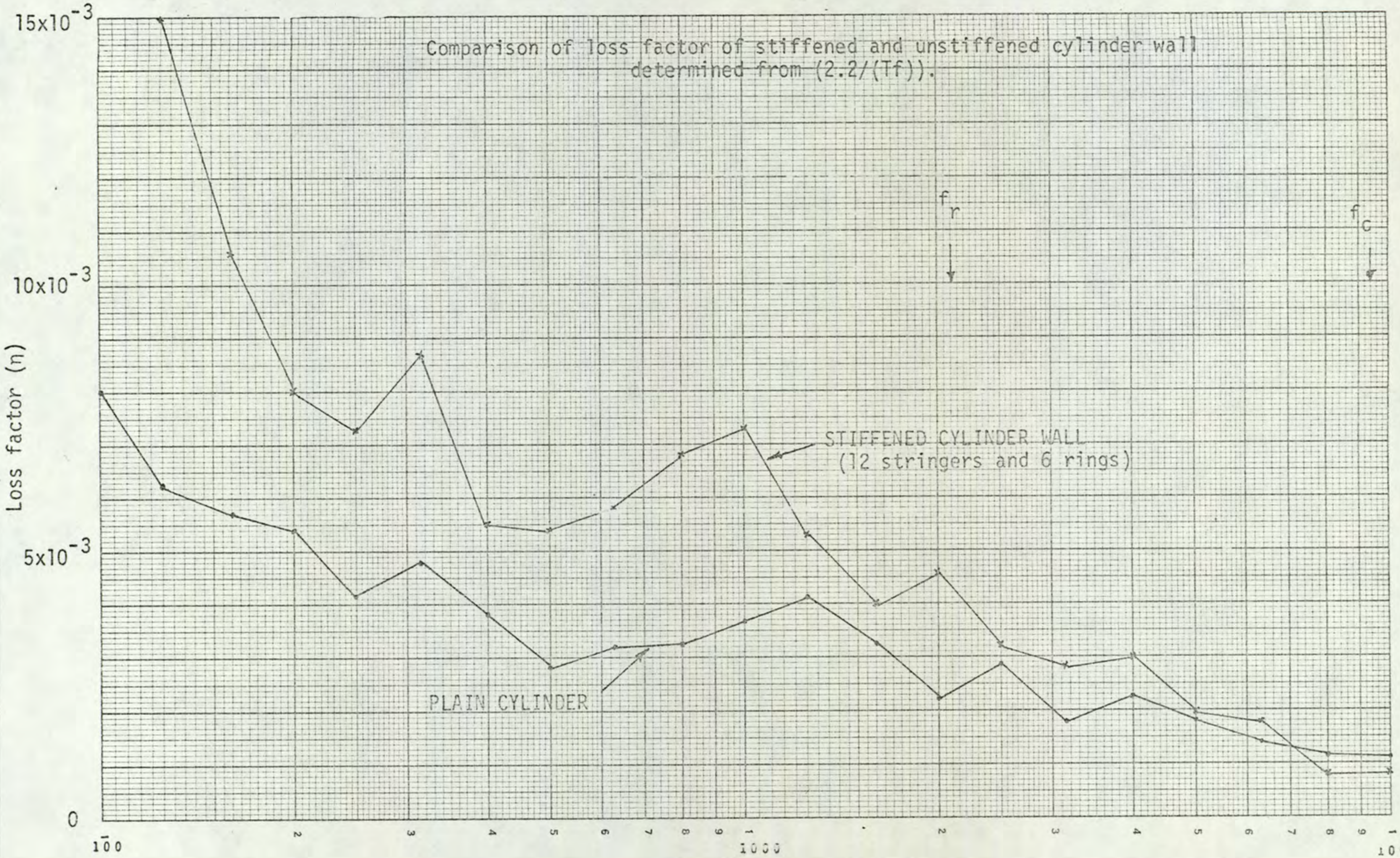

1/3 octave band centre frequency Hz.

Fig. 5.7

TABLE 5.8

	Plain Cylinder	Stiffened Cylinder (12 stringers and 6 rings)
f	Loss factor (2.2/Tf)	Loss factor (2.2/Tf)
100	7.8×10^{-3}	36.6×10^{-3}
125	6.28×10^{-3}	17.6×10^{-3}
160	5.58×10^{-3}	10.57×10^{-3}
200	5.39×10^{-3}	7.85×10^{-3}
250	4.19×10^{-3}	7.33×10^{-3}
315	4.85×10^{-3}	8.73×10^{-3}
400	3.87×10^{-2}	5.5×10^{-3}
500	2.82×10^{-3}	5.5×10^{-3}
630	3.23×10^{-3}	5.12×10^{-3}
800	3.27×10^{-3}	6.87×10^{-3}
1000	3.66×10^{-3}	7.33×10^{-3}
1250	4.19×10^{-3}	5.33×10^{-3}
1600	3.27×10^{-3}	4.04×10^{-3}
2000	2.29×10^{-3}	4.58×10^{-3}
2500	2.93×10^{-3}	3.25 c 10^{-3}
3200	1.90×10^{-3}	2.86×10^{-3}
4000	2.29×10^{-3}	3.05×10^{-3}
5000	1.83×10^{-3}	1.83×10^{-3}
6300	1.45×10^{-3}	1.83×10^{-3}
8000	1.1×10^{-3}	0.88×10^{-3}
10000	1.1×10^{-3}	0.91×10^{-3}

Table showing loss factor calculated for plain and stiffened cylinders

The coupling loss factor of the cylinder wall to the adjacent spaces was taken to be the same, hence, $\eta_{21} = \eta_{23} = R_{2rad}/\omega M_2$ The result of this calculation is given in Table (5.9).

5.5.3 Determination of internal loss factor

The internal loss factor was determined from the total and radiation loss factor using the following equation:

$$\eta_{TOT} = \eta_{rad} + \eta_{int} \tag{5.9}$$

$$\eta_{int} = \eta_{TOT} - \eta_{rad} \tag{5.10}$$

where η_{rad} = Radiation loss factor to whole space.

Figure (5.10) gives the result obtained by application of equation (5.10). The accuracy of internal loss factor determined this way will depend upon the accuracy of energy decay time measured for the cylinder wall. From the result, it is seen that above 2.4 kHz the loss factor determined is negative. This is because the energy radiated into the space was higher than that dissipated by the cylinder wall.

5.6 Relationship between energy ratio of Systems 1, 2 and 3

5.6.1 Energy equations

The total energy contained in each system was derived from the response equation given in section (2.4.2) (Chapter 2). These are summarised as follows:

TABLE 5.9

f	$R_{2_{rad}}$	$\eta_{21} = \eta_{23}$
150	0.129	$.00913\ 10^{-3}$
200	26.23	$1.392\ 10^{-3}$
300	2.19	$.07749\ 10^{-3}$
400	3.17	$.08413\ 10^{-3}$
500	11.27	$.239278\ 10^{-3}$
600	12.57	$.222349\ 10^{-3}$
700	13.76	$.208675\ 10^{-3}$
800	91.36	$1.2123\ 10^{-3}$
1000	88.17	$.93598\ 10^{-3}$
1500	77.26	$.54678\ 10^{-3}$
2000	564.37	$2.99559\ 10^{-3}$
2500	196.84	$.8358\ 10^{-3}$
3150	676.21	$2.3928\ 10^{-3}$
4000	469.43	$1.2458\ 10^{-3}$
5000	2293.71	$4.869\ 10^{-3}$
7000	2810.52	$4.262\ 10^{-3}$
8000	1240.76	$1.712\ 10^{-3}$
9000	1781.52	$2.101\ 10^{-3}$
10000	7449.37	$7.903\ 10^{-3}$

Coupling loss factor $\eta_{21} = \eta_{23} = R_{2_{rad}}/2\omega M_2$

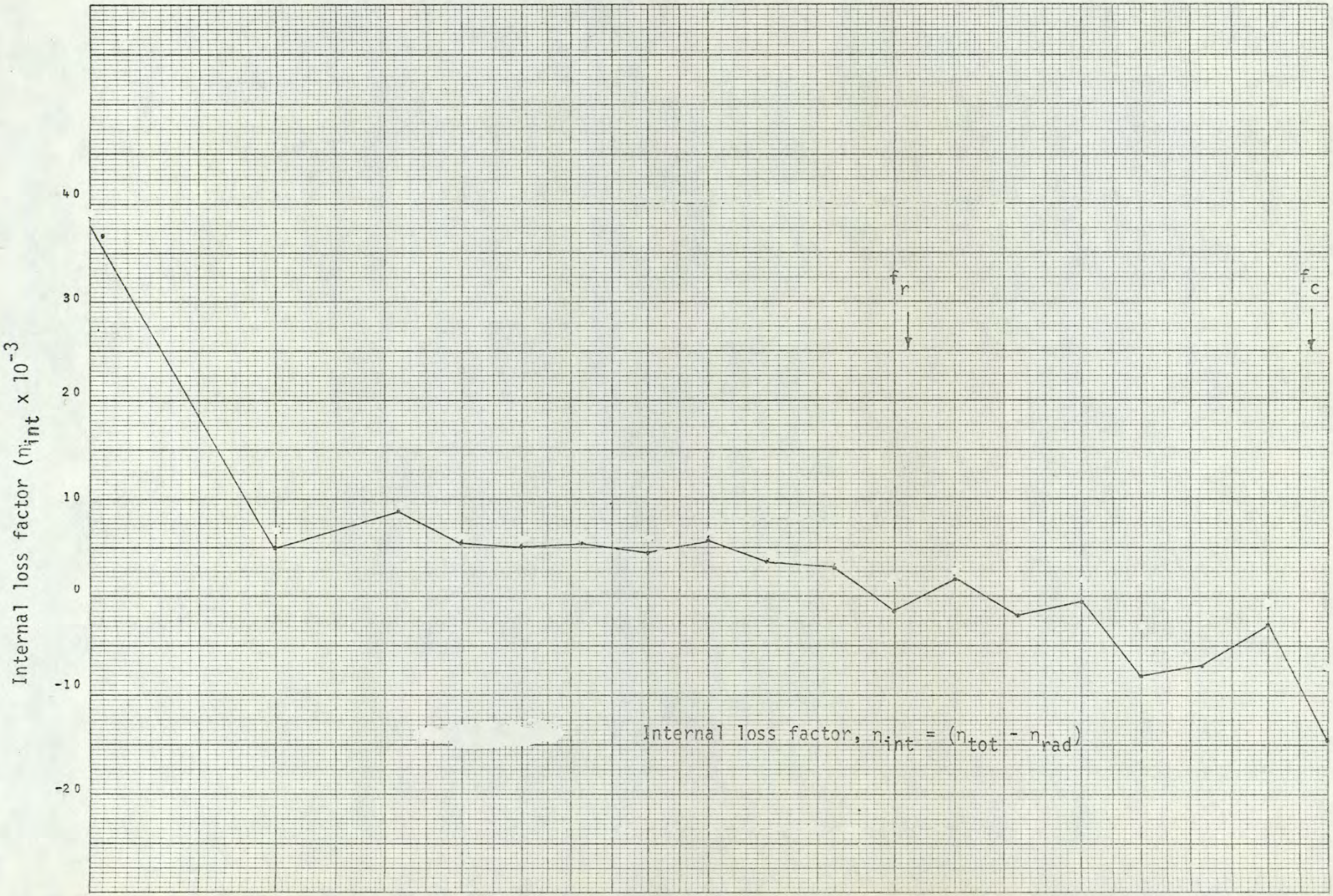

Fig. 5.10 1/3 octave band centre frequency (Hz)

$$E_1 = S_{p_1} V_1/(\rho_a C_a^{\,2}); \tag{5.11}$$

Total energy (E_2) in System 2 (cylinder wall) is given by:

$$E_2 = M_2\, S_{a_2}/\omega^2 \tag{5.12}$$

Total energy (E_3) in System 3 (space enclosed by cylinder wall) is given by:

$$E_3 = S_{p_3} V_3/(\rho_a C_a^{\,2}) \tag{5.13}$$

5.6.2 Energy ratio between the transmission room and cylinder wall

The energy ratio is obtained by application of equations (5.11) and (5.12),

$$\frac{E_1}{E_2} = \left[\frac{S_{p_1}}{S_{a_2}}\right]\left[\frac{V_1\omega^2}{\rho_a C_a^2 M_2}\right] \tag{5.14}$$

The transmission room was acoustically excited in 1/3 octave band. The space average sound pressure and acceleration levels were measured and used in equation (5.14) for calculating the energy ratio. The result of this calculation is given in figure (5.11)

In figure (5.12) is shown the result when system 2 (cylinder wall) was mechanically excited using 4 vibrators.

It is clearly seen from the graphs (figures (5.11) and (5.12))

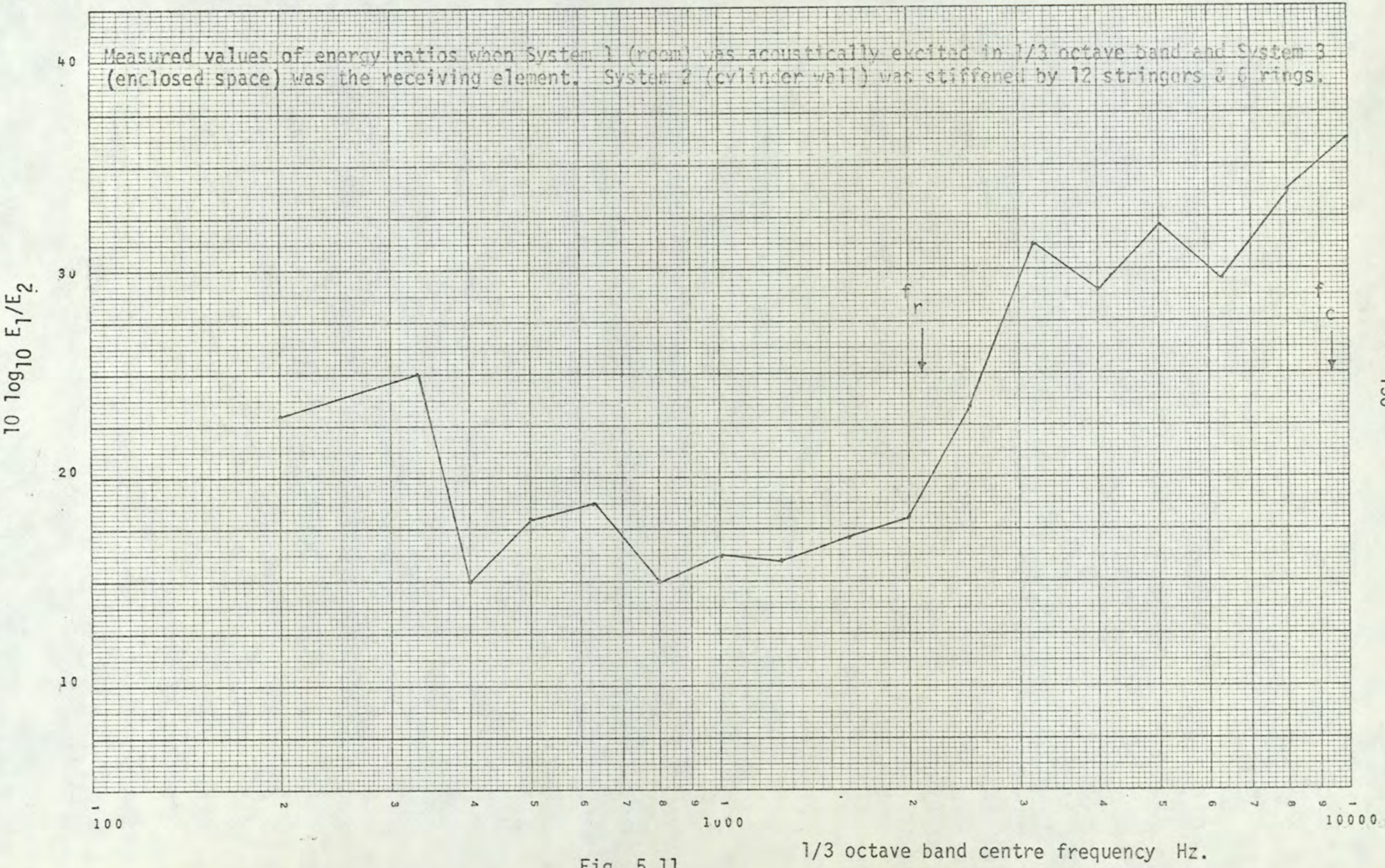

Measured values of energy ratios when System 1 (room) was acoustically excited in 1/3 octave band and System 3 (enclosed space) was the receiving element. System 2 (cylinder wall) was stiffened by 12 stringers & 6 rings.
10 log10 E1/E2
40
30
20
10
f r
f c
100
1000
10000
1/3 octave band centre frequency Hz.

Fig. 5.11

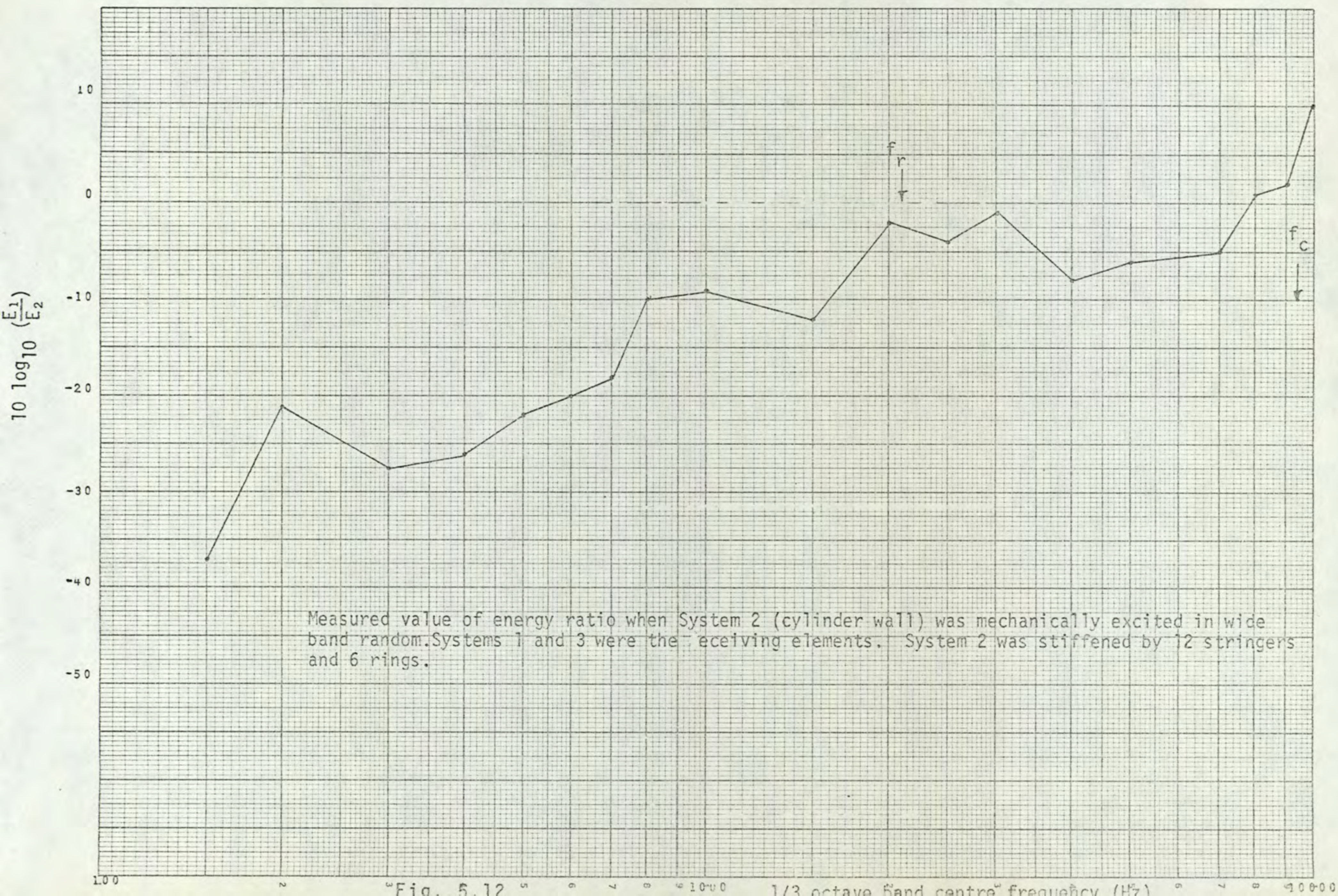

Fig. 5.12

Measured value of energy ratio when System 2 (cylinder wall) was mechanically excited in wide band random. Systems 1 and 3 were the eceiving elements. System 2 was stiffened by 12 stringers and 6 rings.

that the energy flow between the systems depends to a great extent on the type of excitation - either acoustical or mechanical. The energy flow from System 1 to System 2, when excited acoustically, shown in figure (5.11) is a function of frequency. This is because of coupling between the exciting source and the cylinder wall. This is not so when the system 2 (cylinder wall) was mechanically excited as is shown in figure (5.12). The energy radiated into the space is quite small. Further, it is not so much a function of frequency.

5.6.3 Energy ratio between Systems 3 and 2

The energy ratio is derived from equations (5.13) and (5.12).

$$\frac{E_3}{E_2} = \left[\frac{S_{p_1}}{S_{a_2}}\right] \left[\frac{V_3\omega^2}{\rho_a C_a^2}\right] \tag{5.15}$$

The transmission room was excited as before and space average sound pressure and acceleration were measured and used in equation (5.15). The result of this calculation is given in figure (5.13). As before, the energy flow between cylinder wall and enclosed space is a function of frequency (figure (5.13)). The energy flow from System 2 to System 3 is very small compared to that received by System 2.

In figure (5.14) is shown the result when System 2 (cylinder wall) was mechanically excited by 4 vibrators. It is of interest to note that the trend in energy flow between Systems 2 to 3 and 2 to 1 is very similar. The peak shown at 200 Hz in figure (5.14) could be

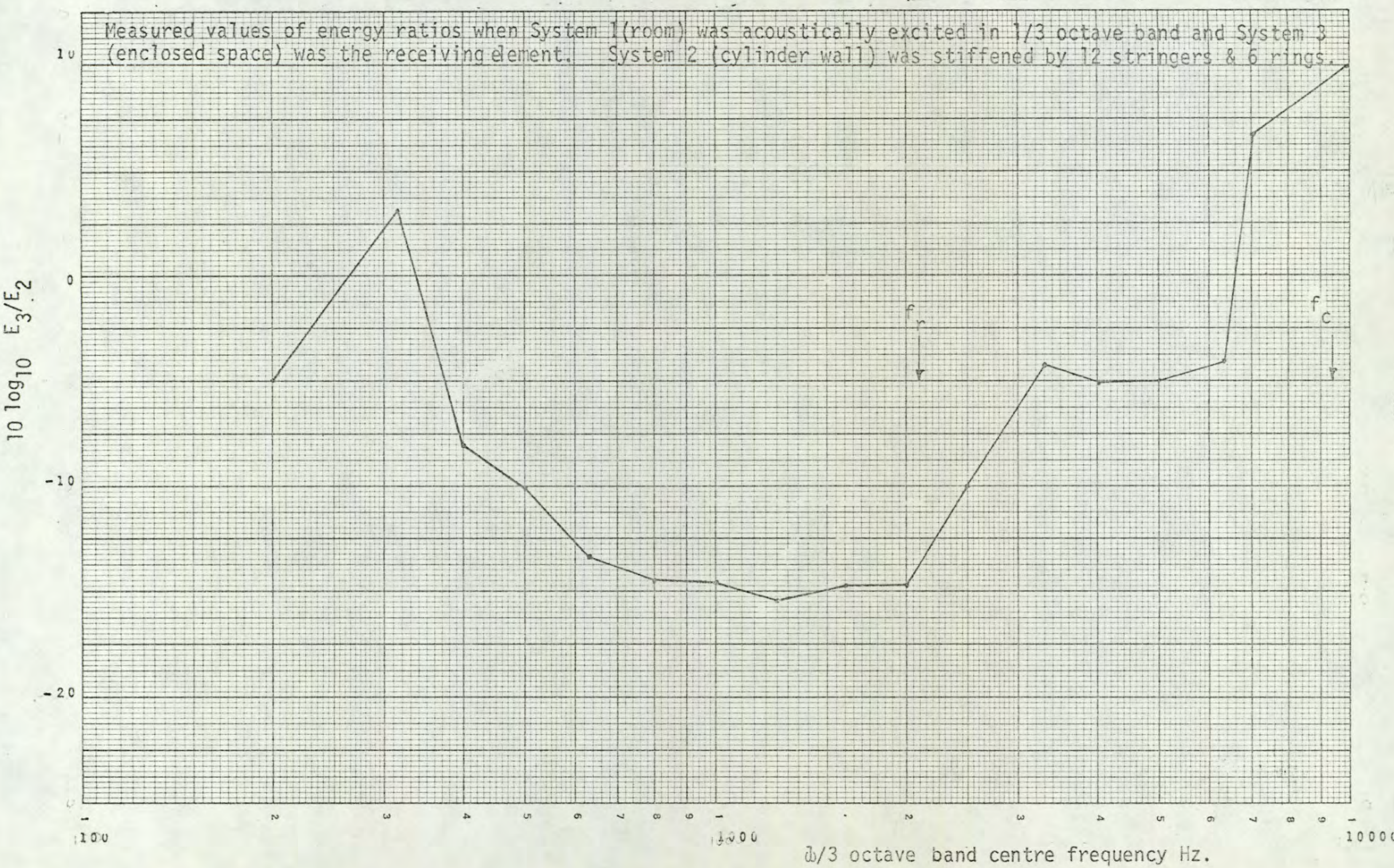
Measured values of energy ratios when System 1(room) was acoustically excited in 1/3 octave band and System 3 (enclosed space) was the receiving element. System 2 (cylinder wall) was stiffened by 12 stringers & 6 rings.
10
0
-10
-20
10 log10 E3/E2
fr
fc
100
1000
10000
1/3 octave band centre frequency Hz.

Fig. 5.13

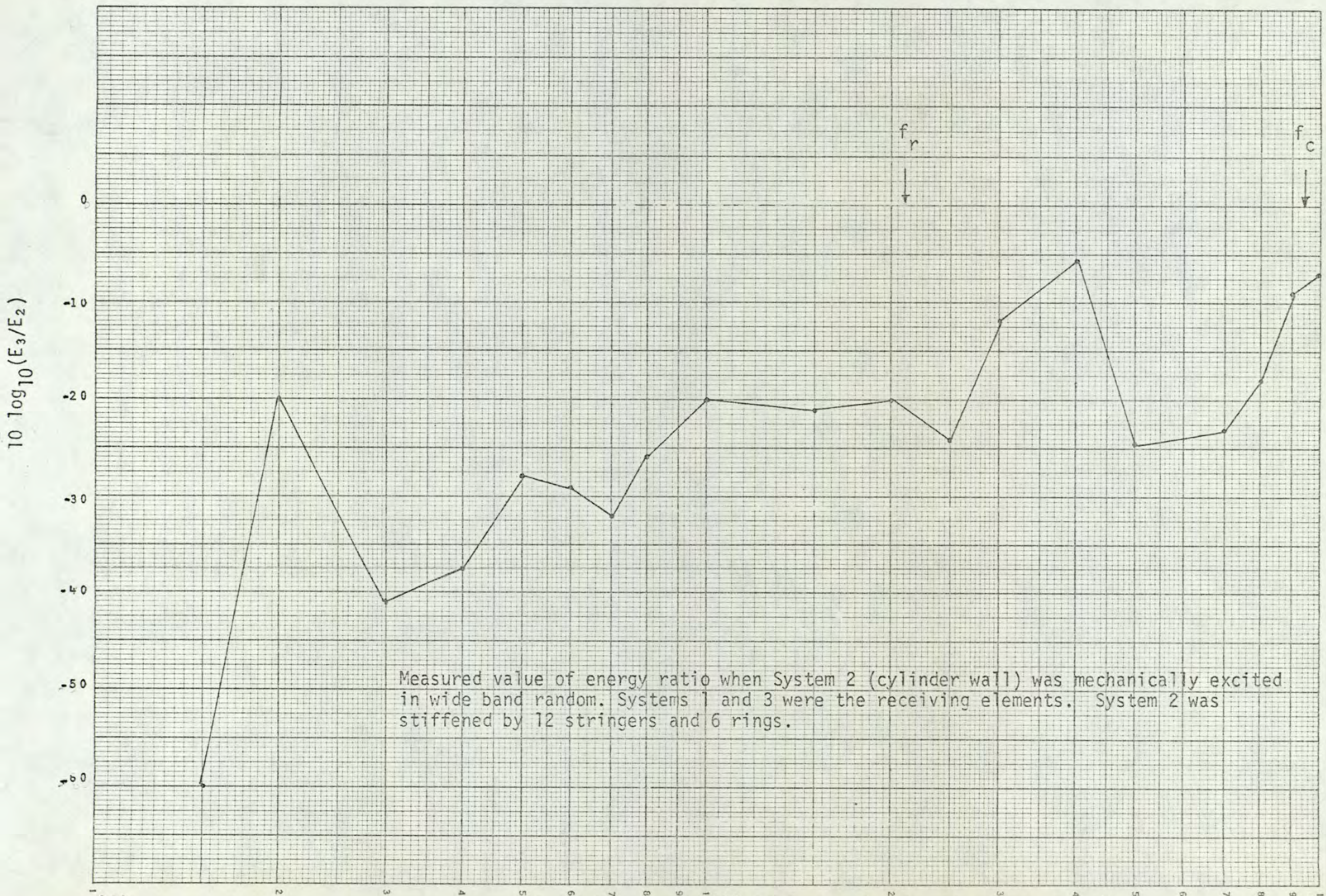

Measured value of energy ratio when System 2 (cylinder wall) was mechanically excited in wide band random. Systems 1 and 3 were the receiving elements. System 2 was stiffened by 12 stringers and 6 rings.

Fig. 5.14 1/3 octave band centre frequency (Hz) due to standing waves inside the cylinder. A comparison of these results is shown in figure (5.15). The trend in the energy flow is clearly demonstrated when System 2 (cylinder wall) was excited and it is in the order of 6 dB/octave.

A direct comparison is drawn between the energy ratios ($\frac{E_2}{E_3}$) when the systems were excited by two different methods. This is shown in figure (5.16). At the ring frequency, the difference in the energy flow is only 2 dB and below and above this frequency the difference is large. Below 400 Hz - where the cylinder responds to a forced vibration - this difference is even larger. Above the ring frequency there is a similarity in the trend of energy flow. This is perhaps because the cylinder behaves like a plate and the number of modes excited would be almost the same.

5.7 Response of Cylinder Wall

The response equation given below is from equation (2.34) (Chapter 2).

$$\frac{S_{a_2}}{S_{p_1}} = \frac{n_2\omega^2}{M_2}\left[V_1/\rho_a C_a^2 n_1)\mu\right] \qquad (5.16)$$

where $$\mu = \frac{\eta_{rad}}{(\eta_{int} + 2\eta_{rad})} \quad \text{is the coupling factor} \qquad (5.17a)$$

or $$\mu = [S_{a_2}/(S_{p_1} + S_{p_3})]\,[2\pi^2(n_2/M_2)C_{a/\rho_a}\,]^{-1} \qquad (5.17b)$$

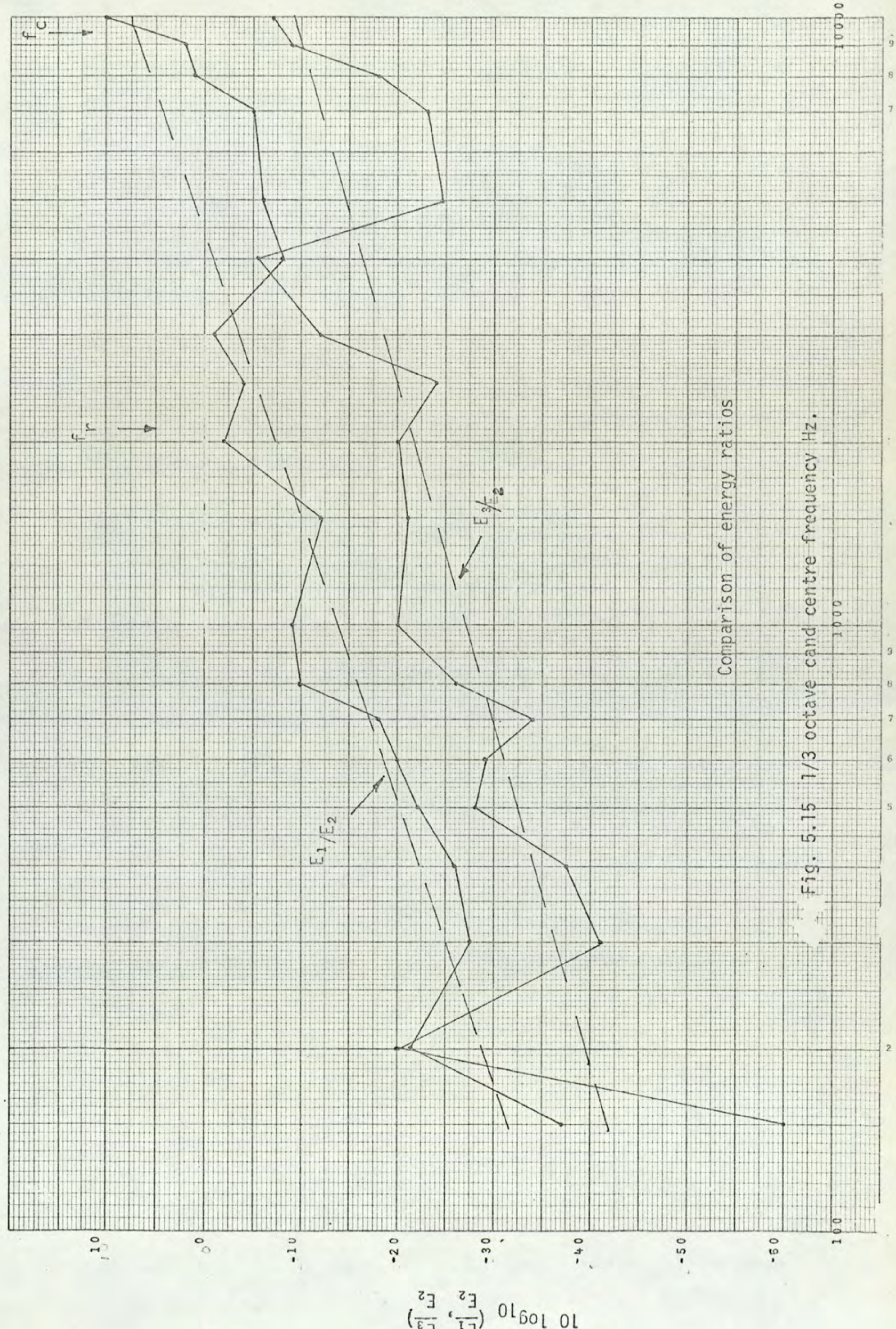

Fig. 5.15 1/3 octave cand centre frequency Hz.
Comparison of energy ratios

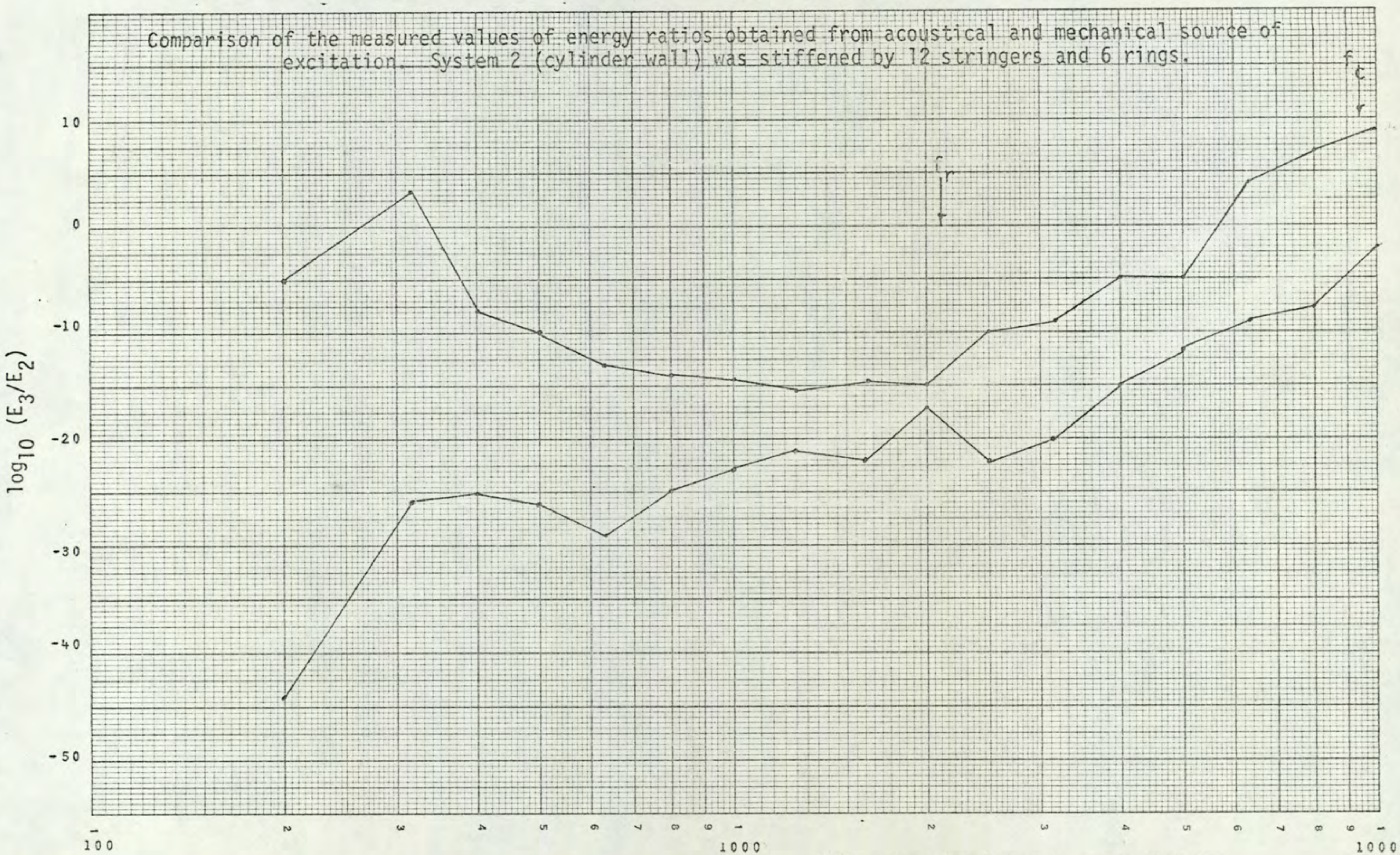
Comparison of the measured values of energy ratios obtained from acoustical and mechanical source of excitation. System 2 (cylinder wall) was stiffened by 12 stringers and 6 rings.
f_c
f_r
10
0
-10
-20
-30
-40
-50
$\log_{10} (E_3/E_2)$
100
1000
10000
1/3 octave band centre frequency Hz.

Fig. 5.16

The calculated values of modal density (n_2) of the cylinder wall and n_1 of the transmission room was used.

The results of this calculation are compared with the experimental measurement and are shown in figures (5.17) and (5.18).

The calculated result using $\eta_{rad}/(2\eta_{rad} + \eta_{int})$ for the coupling factor shows that below 3 kHz there is a difference of approximately 11 dB with that obtained experimentally. This points to inaccuracy in determining η_{int} from measured values of η_{TOT}. When the coupling factor given in equation (5.17b) was used for calculating the response, the experimental and calculated results are in absolute agreement (see figure (5.18)). This confirms that internal loss factor determined in this way could lead to an inaccurate result.

5.8 Noise reduction and transmission loss

5.8.1 Noise reduction

For this measurement the transmission room was acoustically excited in 1/3 octave and space average sound pressure levels (S_{p_1}) in the room and (S_{p_3}) in the space enclosed by the cylinder wall were recorded. A plot of experimental noise reduction, $S_{p_1} - S_{p_3}$ is given in figure (5.19), together with the theoretical noise reduction calculated using equation (2.29b),(Chapter 2) . The percentage error calculated between the results is given in Table (5.20).

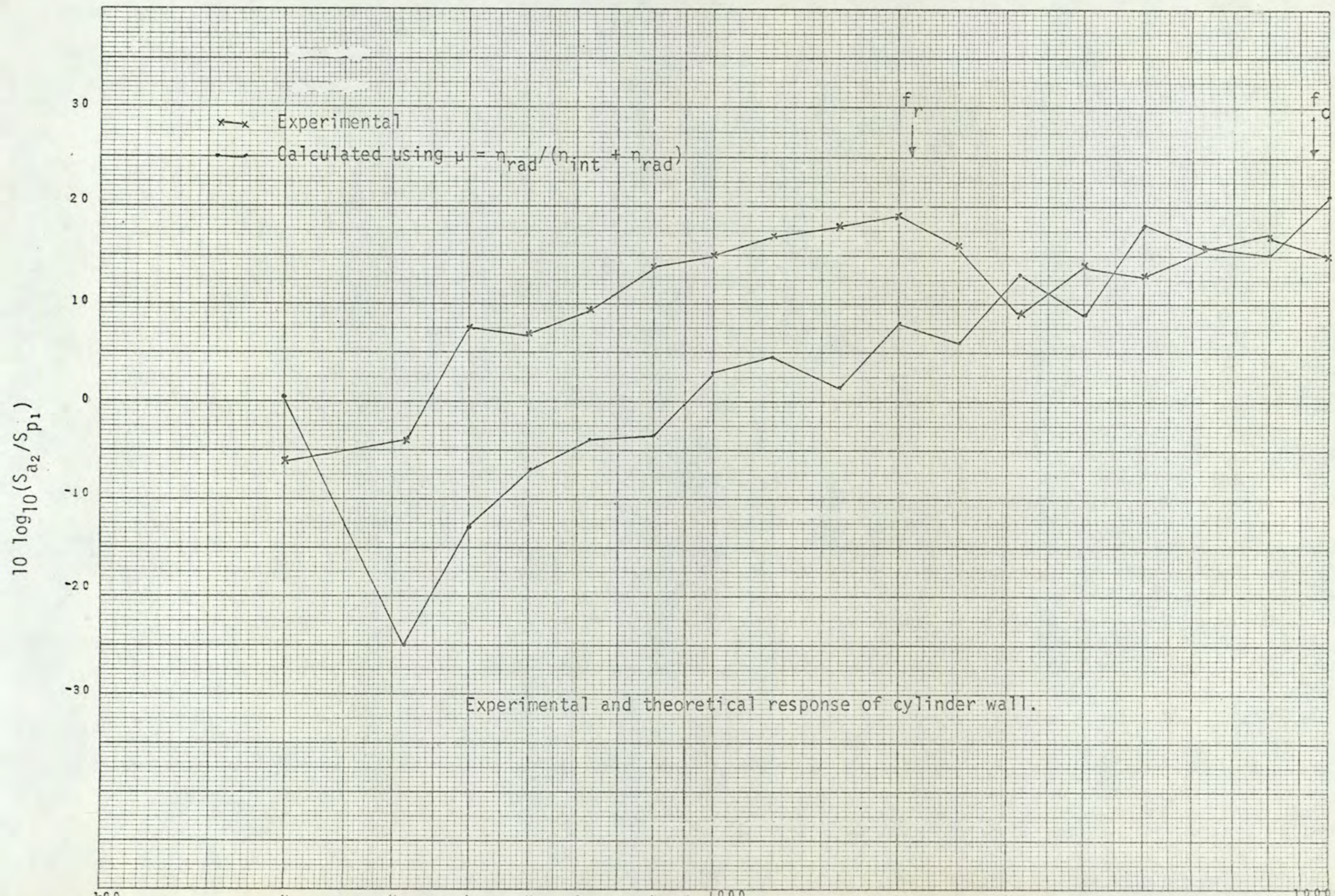

Experimental and theoretical response of cylinder wall.

Fig. 5.17

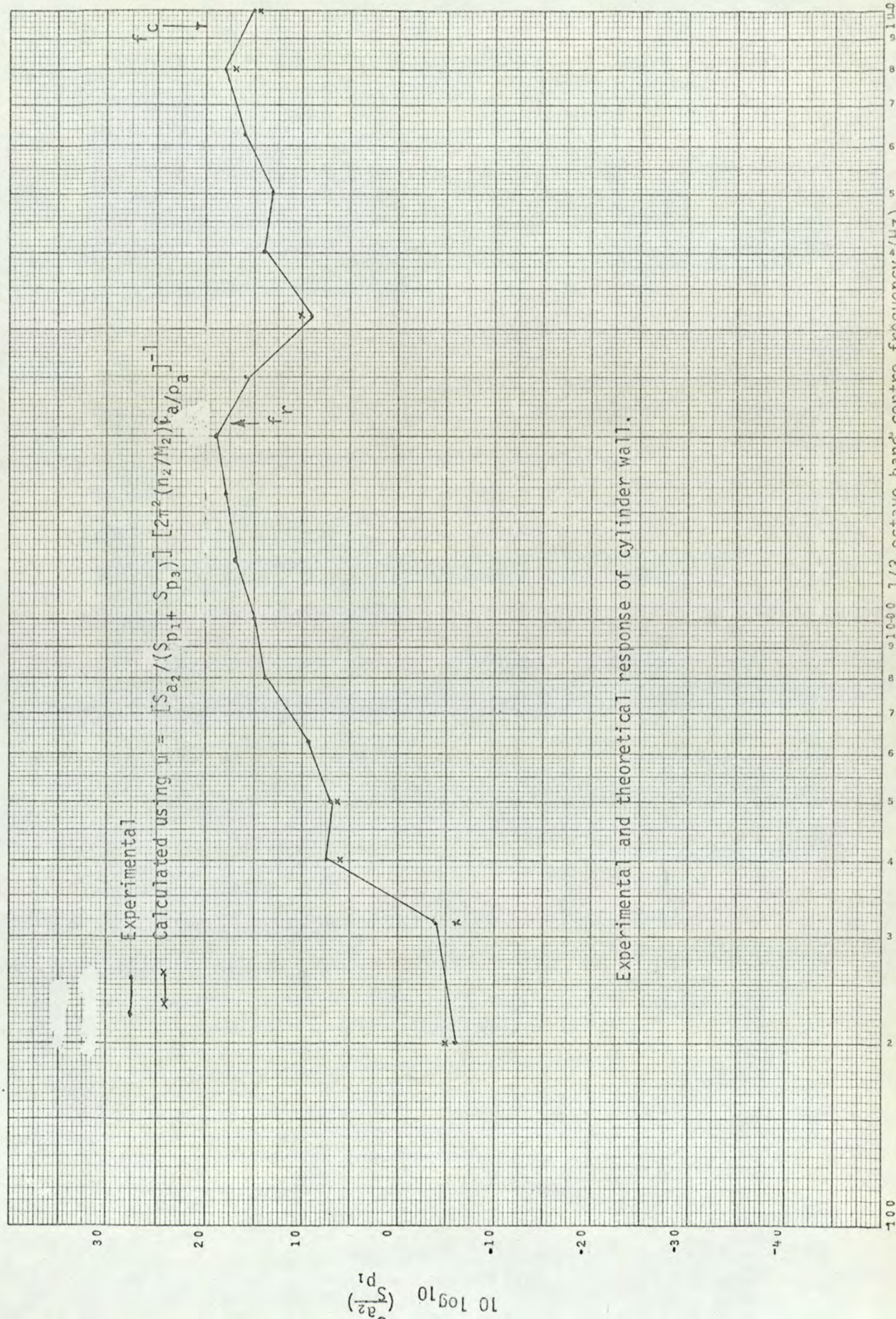

Experimental and theoretical response of cylinder wall.

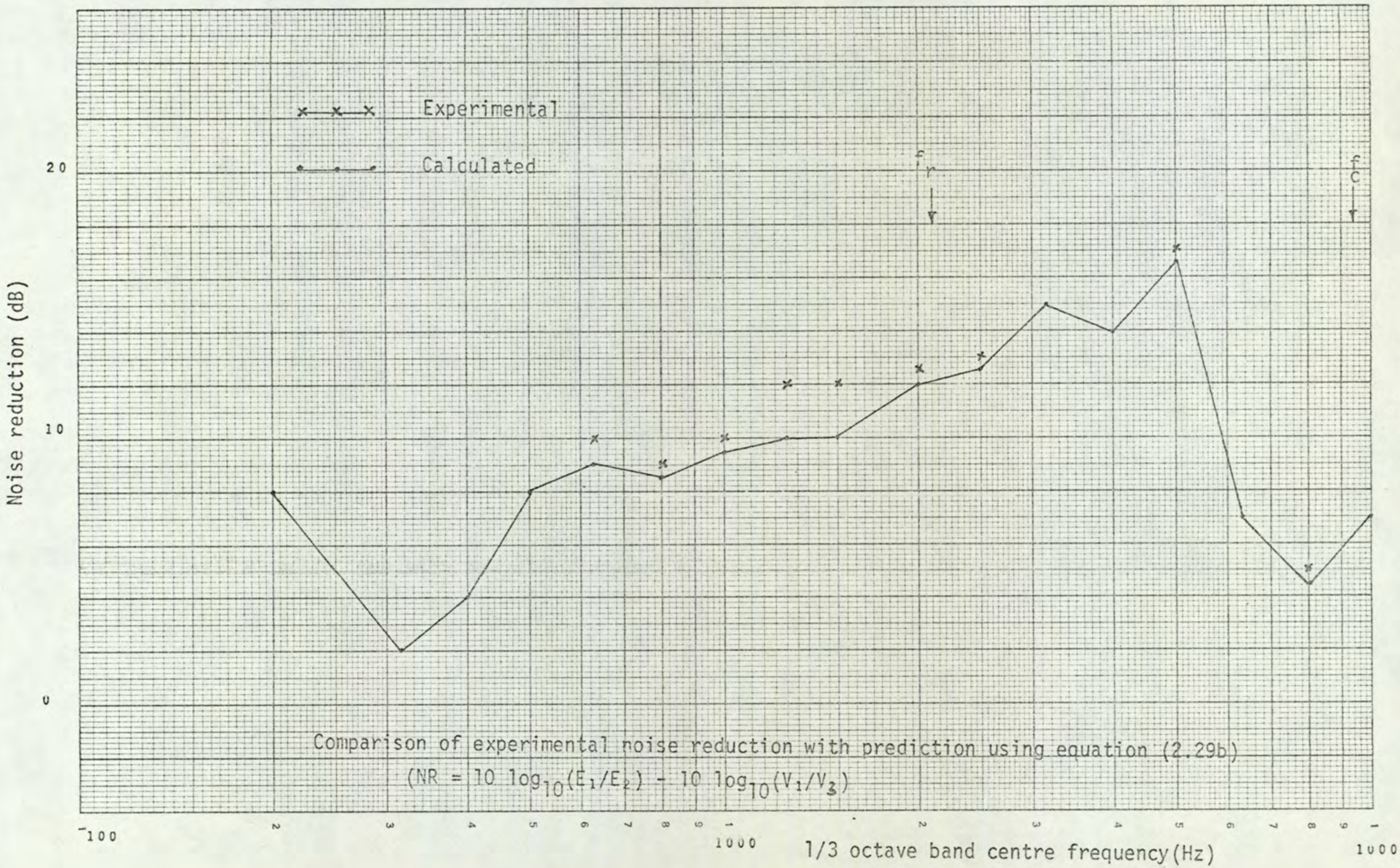

Comparison of experimental noise reduction with prediction using equation (2.29b)

$(NR = 10 \log_{10}(E_1/E_2) - 10 \log_{10}(V_1/V_3))$

Fig. 5.19

TABLE 5.20

f	Prediction of Noise reduction in dB using Equation $10 \log_{10}(E_1/E_3) - 10 \log_{10}(V_1/V_3)$	Experimental (dB)	Error in dB	% error using prediction as ref.
200	8	8	0	0
315	2	2	0	0
400	4	4	0	0
500	8	8	0	0
630	9.5	10	0.5	5
800	8.5	9	0.5	5
1000	9.5	10	0.5	5
1250	10	12	2.0	20
1600	10	12	2.0	20
2000	12	12.5	0.5	5
2500	12.5	13	0.5	5
3150	15	15	0	0
4000	14	14	0	0
5000	16.5	17	0.5	5
6300	7	7	0	0
8000	4.5	5	0.5	5
10000	7	7	0	0

Comparison of experimental noise reduction with prediction

% error is shown using prediction as reference.

There is a very good agreement between the results. This is because the amount of error involved was small in the measuring space average sound pressure levels and calculating $E_1/E_3 = (S_{p_1}V_1)/(S_{p_3}V_3)$, assuming $\rho_a C_a$ to be the same for the transmission room and enclosed space.

5.8.2 Transmission Loss

The transmission loss was computed from the noise reduction data and equation (2.28) (Chapter 2). This was related to the transmission loss by;

$$T_L = NR + 10 \log_{10} \left[\frac{A_2 C_a T_3}{24 V_3 \ln (10)} \right] \qquad (5.18)$$

The result of this calculation and that obtained experimentally is given in figure(5.21) & Table (5.22). Again, the agreement between the results is very good except in the region between 600 Hz and 2.5 kHz. This is perhaps due to measurement error.

A comparison of the results calculated using equations (2.27) and experimental values are given in fig.(5.23). The two results have the same trend in the frequency spectrum but agreement between the results is not all that good. This is because the error involved in extracting loss factors [η_3, η_{rad}, η_{int}] from measurement.

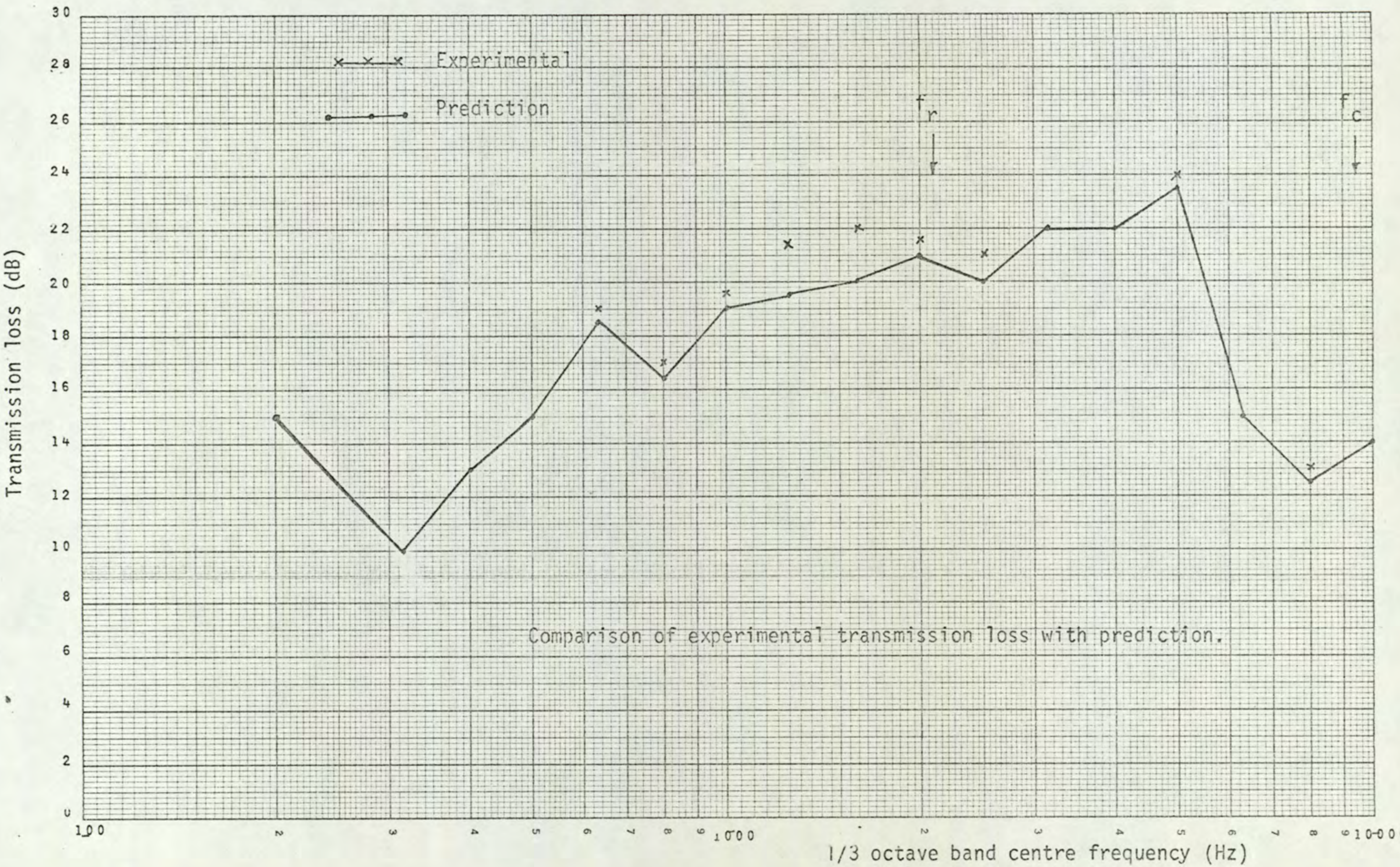
Experimental
Prediction
f_r
f_c
Comparison of experimental transmission loss with prediction.
Transmission loss (dB)
1/3 octave band centre frequency (Hz)
0
2
4
6
8
10
12
14
16
18
20
22
24
26
28
30
100
2
3
4
5
6
7
8
9
1000
2
3
4
5
6
7
8
9
10000

Fig. 5.21

TABLE 5.22

f	Transmission loss (dB) Prediction	Transmission loss (dB) Experimental
200	15.0	15
315	10.0	10
400	13.0	13
500	15.0	15
630	18.5	19
800	16.5	17
1000	19.0	19.5
1250	19.5	21.5
1600	20.0	22
2000	21.0	21.5
2500	20.5	21
3150	22.0	22
4000	22.0	22
5000	23.5	24
6300	15	15
8000	12.5	13
10000	14	14

Comparison of experimental transmission loss with prediction.

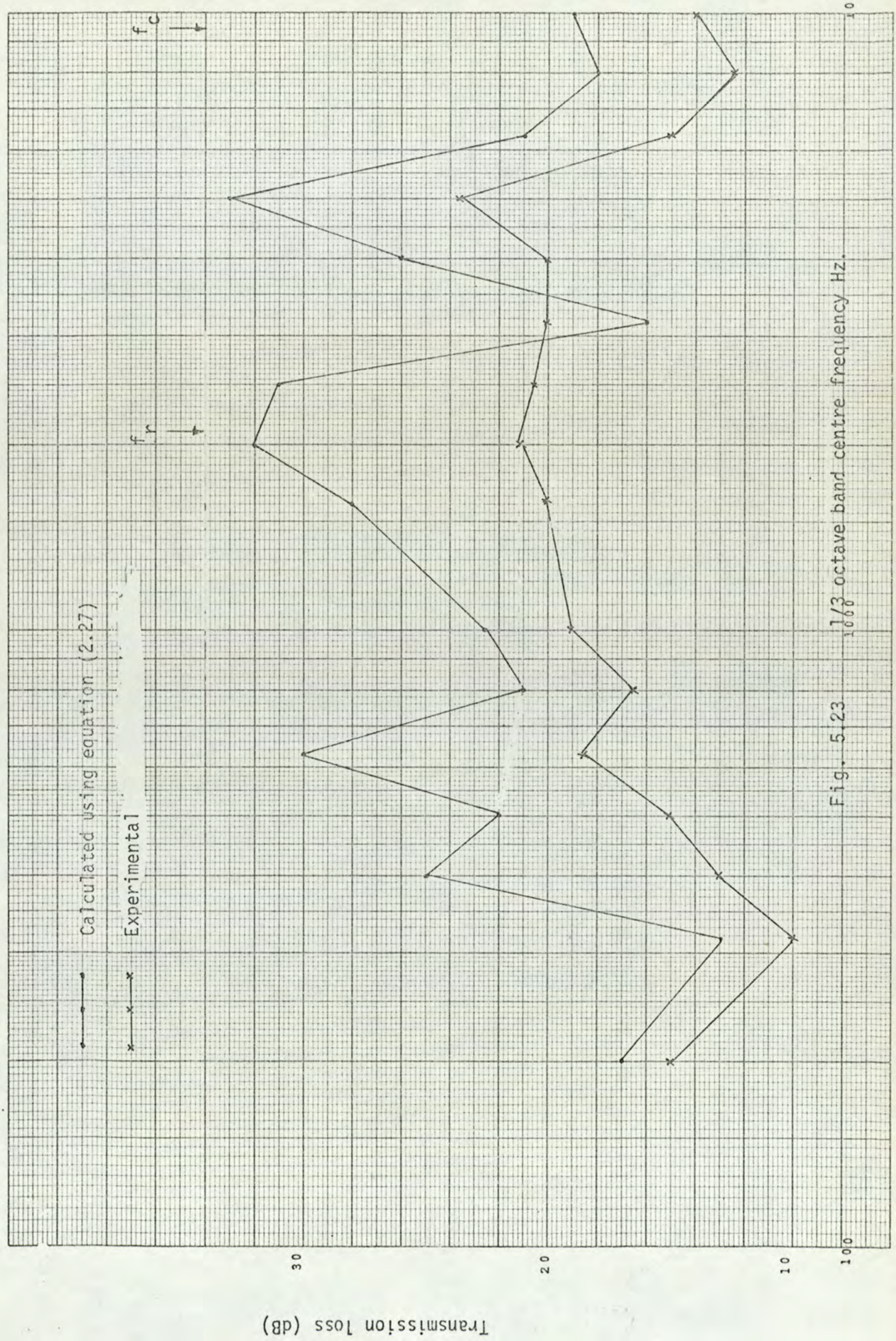
Calculated using equation (2.27)
Experimental
f_c
f_r
30
20
10
Transmission loss (dB)
100
1000
10000
1/3 octave band centre frequency Hz.

Fig. 5.23

5.8.3 Nonresonant Transmission

Nonresonant mass-law noise reduction was calculated from equation (2.39) (Chapter 2) and, hence, transmission loss after applying equation (2.40) was evaluated. The result of this calculation is shown in figure (5.24).

The nonresonant mass-law transmission loss is in the upper bounds since the resonant cylinder wall modes that result in a greater transmission of energy are neglected. This was not verified experimentally.

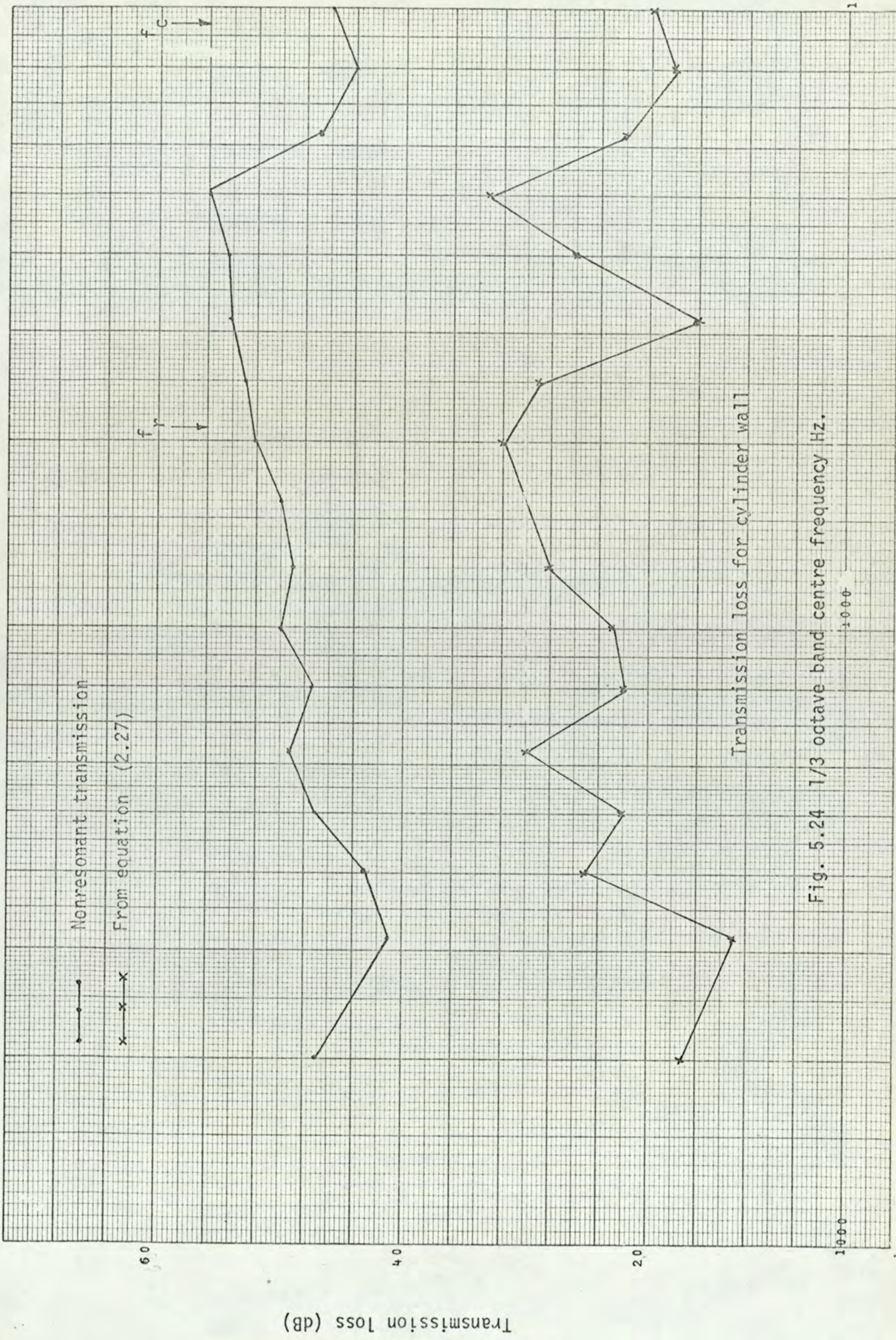

Fig. 5.24 Transmission loss for cylinder wall

CHAPTER SIX

CHAPTER SIX

DISCUSSION OF RESULTS, CONCLUSIONS AND RECOMMENDATIONS FOR FURTHER WORK

6.1 Discussion of Results

The uniformly stiffened cylindrical shell model (0.762 m in diameter), approximating to an aircraft fuselage (3.66 m in diameter) was chosen to be a suitable model for experimental and theoretical study. Other cylinders were used for experimental investigations to show the effects of change in diameter and thickness. In practice, a real fuselage is built with various combinations of stiffeners, fixtures and fittings and could not be classed as a uniformly stiffened shell. It would be an interesting exercise, therefore, to test a real fuselage either on the ground or in flight. The results obtained from this exercise could then be compared with that of the model. This comparison is important in that a correction factor could be derived for relating the results from a model to a real structure. This will also form a firm basis upon which to draw conclusions in the relationship between the vibration level and as a result noise transmission loss.

The test chamber used for the experimental study was not an ideal reverberant room. The walls were lined with hard material and in order to break any standing wave pattern, aluminium reflectors were hung from the ceiling. A reasonable reverberant condition around the cylinder that was horizontally suspended from the ceiling in the middle of the room was achieved. It was observed that above 7 kHz, because of the limitations set by the room size, the noise level could not be maintained due to absorption in the room. Tests in a reverberant chamber of the type available at the Institute of Sound and Vibration Research, University of Southampton would have been preferable. Since a relationship between the vibrational energy and that contained in the space enclosed by it is shown as a ratio, this limitation did not matter all that much in showing a trend. The damping of the reverberant room and the enclosed space is shown in figure (3.6). Above the ring frequency, the sound energy in the enclosure is seen to decay at a faster rate than the room. This is because of the absorption in the end blanks.

The standard noise and vibration equipment selected for the experimental work were compatible to this type of measurement and analysis. The 'Automatic Space and Time Averaging System' has a limitation in its dynamic range but by careful test procedure, this was overcome. In selecting the best type of analyser for this kind of work, the experimental work described in section (3.5) was carried out. It was found that selection of an analyser, whether constant bandwidth, constant percentage bandwidth, narrow band or wideband depended upon the quality of data required. For the type of analysis discussed in this thesis where a trend in the result was more desirable than a closer study, analysis in the 1/3 octave was found to be sufficient. However, where a closer study was necessary, analysis in the narrow band was made.

Selection of an optimum number of transducers for vibration and noise transmission study depended not only upon the type of excitation, whether pure tone, narrow band random or wideband random but on the complexity of the structure (whether uniform or not). The experimental investigation carried out to determine this together with the results are described in section (3.6). For obtaining a reliable estimate of any parameter it was found important to sample many positions spread over a large area when the structure is subjected to a narrow band excitation. Only a few positions need be sampled when the excitation is in wideband random and reasonably diffused. In practice, this may not be possible and therefore an average result from a number of positions sampled should give a reasonable indication. For the uniformly stiffened cylinder wall, only one position was good enough to show a trend in the result with good accuracy. This was limited to a wideband random excitation only.

Determination of a least area for the measurement once again depended upon the size of structure, whether uniform or not and the type of excitation that it may be subjected to. Experimental investigation carried out to determine this is discussed in section (3.7). The results obtained from this test on the model show that a very small area could be used for test but this may not be true on a real structure because of its size and complexity. Determination of an area for test, whether large or small will, therefore, depend upon the type of structure and the form of excitation.

In order to study the vibration and sound transmission characteristics of the cylinder subjected to different forms of excitation, the experimental investigation described in section (3.8) was carried out. The effects of vibration on the cylinder response is shown in figure (3.28) which clearly indicates that the number of vibrators and its positions of excitation are important in that the response levels are different. This points to the fact that it is not possible to excite a structure uniformly using this technique unless an infinite number of vibrators are used. Further limitation observed when using vibrators was that due to mechanical and electrical characteristics, the vibration amplitude induced by vibrators varied although identical electrical inputs were supplied to each. The required space average acceleration levels obtained by mechanical and acoustical forms of excitation is shown in figure (3.29). The separation in the response either side of the ring frequency is clearly shown. Other measured results shown in this section show similar trends. The relationship between S_{p_3}/S_{a_2} is shown in figure (3.34). Again the separation between the results measured by two forms of excitation are shown. All the measured results point to the fact that below and above the ring frequency, the measured results should be considered separately. This is important in drawing a relationship between the vibration level and noise transmission as a result of this.

The effects of stiffeners on the overall measured ratio (S_{p_3}/S_{a_2}), is shown in figures (3.40) and (3.41). At the ring and coincidence frequencies this effect is a minimum due to efficient coupling between the noise field and the structure, hence the cylinder wall response and as a result sound transmission is high. The effect of stiffness on the calculated natural frequencies are shown on page (109). The effect of end blanks are shown in figures (3.42) and (3.43). This difference is caused by different absorption property of the end blanks.

The effect of change in cylinder diameter on the calculated natural frequencies are shown on page (109). Increasing the diameter by 4 times has given the lowest natural frequency which is 52% lower than the lowest natural frequency of the original cylinder. The ring frequency of the cylinder is also dependent upon the diameter. It is the frequency at which the longitudinal wavelength in the cylinder material is equal to the circumference and is given by;

$$f_r = \frac{1}{2\pi R} \left[\frac{E}{\rho} \right]^{\frac{1}{2}}$$

It can be seen that for a given material, it depends on the diameter. The measured ratio (S_{p_3}/S_{a_2}), obtained from cylinders of different diameter are given in figure (6.1). It is interesting to note that a reduction in diameter has only lowered the total energy in the enclosed space but the trend in the measured results did not change.

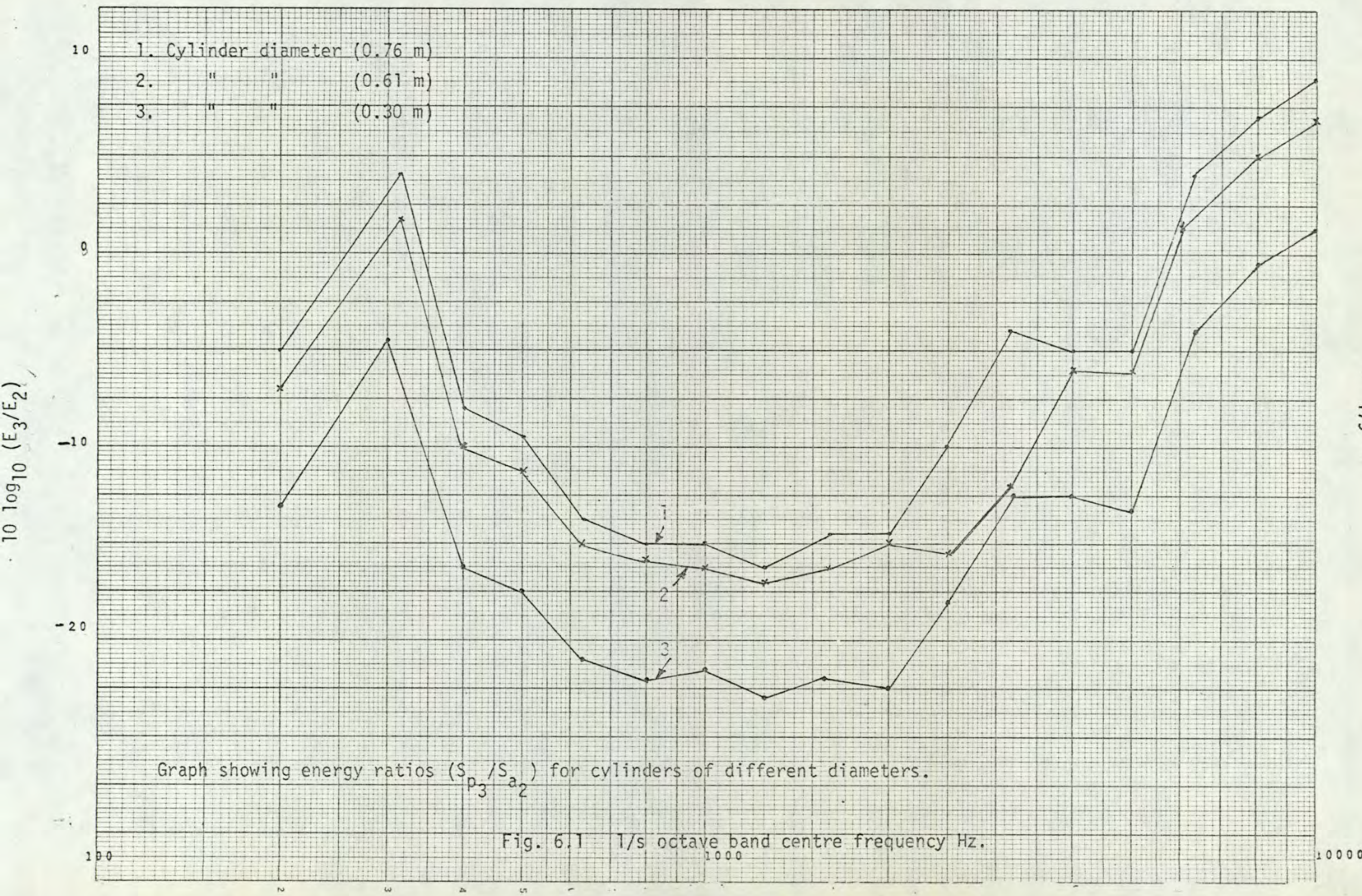

Graph showing energy ratios (S_{p_3}/S_{a_2}) for cylinders of different diameters.

Fig. 6.1 1/3 octave band centre frequency Hz.

An attempt was made to show the effect of thickness on the measured results when a cylinder having the same diameter as the model but different in thickness (.0006 m) was tested. The difference in the measured result was negligible. Theoretically, the coincidence frequency $(f_c) = \frac{Ca^2}{2\pi t} \left[\frac{12\rho(1-\mu^2)}{E} \right]^{\frac{1}{2}}$ depends on the material thickness, therefore, some effect on the measured result should have been noticed. It is the frequency where the trace velocity of the sound wave is equal to the bending wave velocity. It seems that the change in the thickness was too small to detect any change in the measured result.

Natural frequencies of the cylindrical shell model was one of the important parameters required in calculating the vibration level and the sound transmission loss. Since it was not possible to obtain this experimentally in the frequency range of interest, resort had to be made to theoretical analysis of the form discussed in Chapter 4. An extended computer program was developed for this and it is now possible not only to obtain the natural frequencies but to study vibration characteristics of plain cylinders, stiffened cylinders, plain plates and stiffened plates using the combined program. The samples of the results given indicate the usefulness of this program.

The radiation resistance of cylinder wall (figure 5.1) shows that above coincidence frequency it is greater than one because it is essentially radiation controlled. This is in close agreement with the value measured on stiffened plates by Maidanik(3). The total resistance (figure 5.2) is the sum of the internal resistance and the radiation resistance. At low frequency, where the radiation resistance is small, the resistance of the cylinder wall is mostly due to internal resistance. The measured values of the total resistance does not confirm that at the coincidence frequency it is mostly due to radiation resistance. This may be due to inaccuracy in the measurement. A straight line drawn through the graph (figure 5.2) shows a correction to this measurement.

The coupling of the panel with the room and the space enclosed by cylinder wall is shown in figures (5.3) and (5.4). The coupling factor calculated using equation (5.5) shows that between 700 Hz to 2.8 kHz and above 5.4 kHz, the coupling is radiation controlled, ($\mu > 1$). The agreement between the values of μ given in figure (5.4) calculated from equation (5.5) and that determined from experimental values of R_{2rad} and R_{2TOT} is not satisfactory below 3 kHz. It is thought that this considerable disagreement is due to inaccuracy in determining the internal resistance.

The loss factors determined from the decay time measurement for Systems 1, 2 and 3 are shown in figures (5.5) and Table (5.6). It is interesting to note that above 1 kHz, there is very small difference in the damping of the systems. The results shown in figure (5.7) and Table (5.8) give comparison of damping in stiffened and plain cylinders. As expected, the stiffened cylinder is heavily damped. The coupling loss factor of the cylinder wall to the adjacent spaces are given in Table (5.9). This was calculated from the radiation resistance values and it was assumed that radiation either side of the cylinder wall was the same. In figure (5.10) is shown the internal loss factor determined from $\eta_{int} = \eta_{TOT} - 2\eta_{rad}$. Above 2.4 kHz, the loss factor determined is negative. This points to inaccuracy in the measured values of total loss factor.

The general relationship drawn between the energy contained in systems discussed in section (5.6) suggest that the energy transfer and vibration levels in fairly complex systems may be estimated reasonably reliably from a few experimentally and/or theoretically determined energy-flow coefficients, i.e. the appropriate coupling - and interval loss factors, space average acceleration and sound pressure levels. In particular, this estimation method appears to be applicable in the present system where energy is transmitted through the cylinder wall. This method could be applicable in engineering situations where energy is transmitted through trusses or structural columns between various substructures. No applications of the method have been made in such practical cases during the course of this investigation, but such applications would seem appropriate.

It is interesting to note the difference in the energy ratios (E_1/E_2) shown in figures (5.11) and (5.12) when different systems were excited. The energy ratios E_3/E_2 shown in figures (5.13) and (5.14) also point to a similarity in the energy transfer trend.

A comparison of energy ratios (E_1/E_2, and E_3/E_2) shown in figure (5.15) indicate that it is in the order of 6 dB/octave below 4 kHz. A comparison of energy flow E_3/E_2 shown in figure (5.16) confirms that the energy transfer depends on the type of excitation and results obtained from each should be treated separately.

A comparison between the responses of cylindrical shell calculated and that measured are shown in figures (5.17) and (5.18). The calculated results using $\eta_{rad}/(2\eta_{rad} + \eta_{int})$ as the coupling factor give a difference of 11 dB with that obtained by measurements. This difference is only below 3 kHz (figure 5.17). A very good comparison between the measured cylinder response and that calculated was achieved (figure 5.18) when the value of μ was calculated from equation (5.17(b)).

The experimental noise reduction and hence the transmission loss for the cylinder has produced a curve (figure 5.21) which shows a predominantly non-resonant mass controlled transmission over the frequency range considered. This is in good agreement with that calculated from the energy flow equations where the measured values of S_{p_1} and S_{p_3} were used. Noise reduction and the percentage error from the measurement using this method is shown in figure (5.19) and Table (5.20). Sound transmission loss calculated using equations (2.27) where the measured values of loss factors (η_3,η_{rad} and η_{int}) were used produced a curve that is approximately 11 dB higher in values than the measured transmission loss (figure 5.23). It is felt that this difference is due to error in the determined values of the loss factor.

Since it was not possible to predict the actual resonant transmission, only the predictable mass-low transmission was considered for estimating the total transmission loss. Increase in transmission loss at a rate 6 dB/octave (figure 6.2), is predicted between 400 Hz and 5 kHz. Below 400 Hz, no reliable prediction seems possible. This is the region which is stiffness controlled. Above 5 kHz, the curve breaks away from the mass law curve at frequencies below f_c, and then rises towards the mass law curve above f_c because of large damping (figure 6.2).

6.2 Conclusions

Experimental techniques have been developed to study vibration and sound transmission characteristics of cylindrical shells. These were extended to investigate the effects of individual characteristics and to obtain experimental data. Using this method it was experimentally shown that the results obtained using different forms of excitation could not be compared directly. The techniques developed here can now be applied with confidence to study similar problems in a real structure.

A theoretical analysis for calculating the natural frequencies of cylindrical shells and plates with and without stiffeners has been implemented for digital computer solutions. This program is capable of presenting the results in either graphical form or tables. With the aid of this computer program, it is possible to study vibration characteristics of cylinders and plates.

Statistical energy analysis of the type used for studying sound transmission through plates was applied in the case of the cylinder considered in the present investigation. The method appears to be equally valid in the study of sound transmission providing accurate data is obtained for the loss factor.

An approximate prediction of sound transmission loss for the stiffened cylinder is given in figure (6.2). A more reliable prediction will only be possible when the results presented here are compared with those obtained from a real structure.

6.3 Recommendations for further work

This work could be extended to investigate the effects of introducing trimmings on the structureal response and sound transmission characteristics. Thus, by introducing trimmings with different characteristics it would be possible to select the type most suitable for aircraft fuselage.

Further work is required in determining total and internal loss factors more accurately. Application and accuracy of statistical energy method depends upon the accuracy of this data. It is recommended that an emphirical approach is attempted in determining

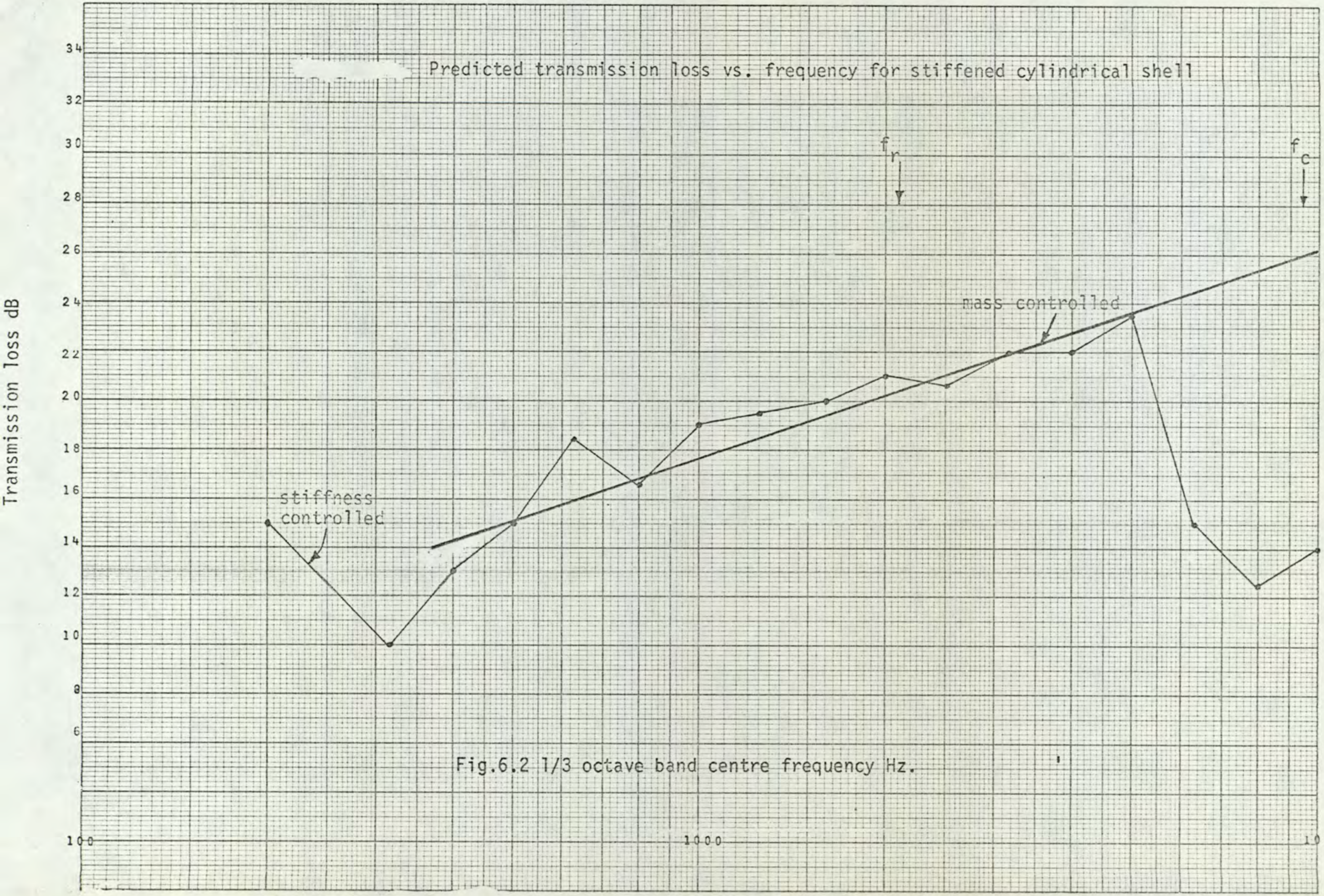

Predicted transmission loss vs. frequency for stiffened cylindrical shell

Fig.6.2 1/3 octave band centre frequency Hz.

the internal loss factor values.

The techniques developed and applied for the measurement of various parameters could now be tried on a real structure. The results could then be compared and corrections applied where necessary. This is essential in order that a reliable prediction could be made.

The present form of investigation should be extended to frequencies up to 20 kHz. This would be possible using a high frequency sound source such as an air jet.

REFERENCES

1. P.W. SMITH, Jr., Response and radiation of structural modes excited by sound, J.Acoust.Soc.Am. 34, (640-647),(1962).

2. R.H. LYON and G. MAIDANIK, Power flow between linearly coupled oscillators, J.Acoust.Soc.Am.34, (623-639), (1962)., and Statistical methods in vibration analysis, A.I.A.A.Journal, vol.2, No.6, (1962).

3. G. MAIDANIK, Response of ribbed panels to reverberant acoustic fields, J.Acoust.Soc.Am. 34, (809-826), (1962).

4. R.H. LYON and T.D. SCHARTON, Vibrational-energy transmission in a three-element structure, J.Acoust.Soc.Am. 38, (253-261), (1965).

5. M.J. CROCKER and A.J. PRICE, Sound transmission using statistical energy analysis, J.Sound Vib. 9(3), (469-486), (1969), Sound transmission through double panels using statistical energy analysis, J.Acoust.Soc.Am., (683-693), (1969).

6. R.H. LYON, Lecture notes from Belt, Beranek and Newman Inc. Program for advanced study - Aerospace Noise and Vibration, Los Angeles, Ch.1X. (1966-67).

7. R.H. LYON, Random noise and vibration in space vehicle, shock and vibration, information centre, United States Department of Defence, Monography SVM-1. (1967).

8. E.E. UNGAR and T.D. SCHARTON, Analysis of vibration distributions in complex structures, Shock vibration, Bull.36, Pt.5, 41.(1967).

9. R.H. LYSON. et al., Low-frequency noise reduction of spacecraft structures, NASA CR-589, (1966).

10. M.M. MIKULAS, Jr., and JOHN A. McELMAN, On free vibrations of eccentrically stiffened cylindrical shells and flat plates, Langley Research Centre.

11. A.V. SWAMY, Response of cylindrical shells to random acoustic excitation, M.Sc. Thesis, Aston University, (1970).

12. R.N. ARNOLD and G.B. WARBURTON, Flexural vibration of thin cylindrical shells having freely supported ends. Proc.Roy.Soc.(A). Vol. 197 (1949), and The flexural vibration of thin cylinders. Proc.Inst.Mech.Eng.(A), Vol.167, 1953.

13. C.M. HARRIS, Handbook of noise control, (McGraw-Hill Book Company), New York.

14. I. DYER, Response of space vehicle structures to rocket engine noise, Ch. 7 of random vibrations, Vol.2 ed. by S.H. Crandall, The MIT Press, Cambridge, Mass., (963).

15. L. RAYLEIGH, Theory of sound. The Macmillan Co., New York., (1894), 2nd ed., Vol. 1, p.409.

16. A.E.H. LOVE, Mathematical theory of elasticity, (Dover Publication. Inc., New York, (1944), 4th ed., (p.543-549).

17. M.R. SCHROEDER, New Methods of measuring reverberation time, J.Acoust.Soc.Am., Vol.37, (1965).

18. COOK AND ASSOCIATES , Measurement of correlation coefficients in reverberant sound fields. J.Acoust.Soc.Am., Vol.27,No.6(1965).

19. W. FLUGGE, Static und Dynamek der Schalen. (Julius Springer Verlog, Berlin, (1934) p.227 - 232.

20. A. VAN DER NEUT, The general instability of stiffened cylindrical shells under axial compression. Report S.314, Natl.Aeron.Res.Inst. (Amsterdam), 1947.

21. M. BARUCH and J. SINGER, Effect of eccentricity of stiffeners on the general instability of stiffened shells under hydrostatic pressure. J.Mech.Eng.Sci., Vol.5, No.9, (1963).p.23 - 27.

22. ANON: Theoretical and experimental analysis of orthotropic-shell stability. LMSC-A701014. Lockheed Missiles & Space Co., Sept.11. (1964).

23. JOHN M. HEDGEPETH and DAVID B. HALL, Stability of stiffened cylinders. Paper No.65-79. Am.Inst.Aeron. Astronaut., Jan.(1965).

24. DAVID L. BLOCK, MICHAEL F. CARD and M.M. MIKULAS, Jr., Buckling of eccentrically stiffened orthotropic cylinders. NASA TN D-2960, 1965.

25. MICHAEL F. CARD, Preliminary results of compression tests on cylinders with eccentric longitudinal stiffeners. NASA TM X-1004 (1964).

26. E. DOWNHAM, J.E.T. PENNY and A.V. SWAMY, The effect on a modern high rise building of a concorde sonic boom. Tech. report No. MECH/33, August 1971., The University of Aston in Birmingham.

APPENDIX (A)

RADIATION RESISTANCE OF A SIMPLY SUPPORTED PLATE

$$R_{rad}(\tfrac{1}{2}\ \text{space}) = A\rho_a C_a$$

$$\times\ [(\lambda_c\lambda_a/A)2(f/f_c)g_2+(P\lambda_c/A)g_2], f < f_c;$$

$$\times\ [(\ell_1/\lambda_c)^{\frac{1}{2}} + (\ell_3/\lambda_c)^{\frac{1}{2}}],\ f = f_c;$$

$$\times\ (1 - f_c/f)^{-\frac{1}{2}},\ f > f_c; \qquad (A1)$$

where

$g_1 \quad = (4/\pi^4)(1-2\alpha^2)/\alpha(1-\alpha^2)^{\frac{1}{2}},\ f < \tfrac{1}{2}f_c;$

$g_2 \quad = (2\pi)^{-2}\{\ (1-\alpha^2)\ \ n[(1+\alpha)/(1-\alpha)]\ \ +2\alpha\ \ /(1-\alpha^2)^{\frac{1}{2}};$

$\alpha \quad = (f/f_c)^{\frac{1}{2}}$

A = Surface Area of plate

f = frequency

f_c = critical frequency

ℓ_1,ℓ_3 = length and breadth of plate

λ_a = Acoustic wavelength

λ_c = Coincidence wavelength of panel

APPENDIX [B]

THEORY OF THE INTEGRATED IMPULSE METHOD

The basis of Schroeden's(17) "Integrated Impulse Method" is that the ensemble average of the square of the reverberation noise decay in an enclosure equals the time integral of the enclosure squared impulse response. To arrive at this result, it is considered that the room is excited by "stationary white noise" which is suddenly shut off. If the noise is stationary and white this can be mathematically stated by the equation,

$$< n(t_1) \times n(t_2) > = N \times \delta\ (t_2 - t_1) \qquad (B.1)$$

where

t_1 and t_2 are two arbitrary chosen instants of time.

$\delta(t_2 - t_1)$ is the Dirac δ-function.

$<n(t_1) \times n(t_2)>$ is the autocovariance function of the noise.

N is the noise power per unit bandwidth.

The response of any linear network to our arbitrary time function $n(\tau)$ is considered next;

$$s(t) = \int_{-\infty}^{t} n(\tau) \times r(t - \tau) d\tau \qquad (B.2)$$

Here $r(t - \tau)$ is the impulse response of the network at the time t, to a unit impulse occurring at time τ.

By considering the room a linear acoustic network and squaring equation (B.2) the double integral is obtained and shown as follows:

$$S^2(t) = \int_{-\infty}^{\tau=t} d\tau \int_{-\infty}^{\theta=t} d\tau \times n(\tau) \times n(\theta) \times r(t-\tau) \times r(t-\theta) \qquad \text{(B.3)}$$

The upper limit of integration should be taken to be 0, if this is chosen as the instant of time when the noise is shut off.

Averaging the above expression over the ensemble of noise signals and utilizing equation (B.1)

$$< n(\tau) \times n(\theta) > \ = N \times \delta(\theta - t)$$

the equation below is obtained:

$$<S^2(t)> \ = \int_{-\infty}^{0} \int N \times \delta(\theta - \tau) \times r(t - \tau) \times r(t - \theta) d\theta \delta\tau \qquad \text{(B.4)}$$

As $\delta(\theta - \tau)$ is zero except when $\theta = \tau$ and as the integral over the delta function equals unity, equation (B.4) finally becomes

$$< S^2(t) > \ = N \times \int_{-\infty}^{0} r^2 (t - \tau) \, d\tau \qquad \text{(B.5)}$$

From $\tau = 0$, the function $<S^2(t)>$ represents the ensemble average of the squared reverberation process. To obtain the function an "infinite" number of measurements would be necessary and the reverberation time determined according to normal procedures would be half the actual reverberation time due to the squaring.

On the other hand, the time integral $\int_{-\infty}^{0} r^2(t-\tau)\delta\tau$ represents, basically, a single measurement of the squared impulse response of the linear network integrated over an infinite time.

By definition $r(t-\tau)$ is the unit impulse response of the system under consideration. If such an impulse occurred at $\tau = -\infty$ then the above integration merely states that the squared response has to be theoretically considered and integrated over an infinite period of time. In practice, the response to unit impulse is only measurable over a certain, very finite, period of time. The meaning of the integral is thus to consider the integration as long as the response of the system to a unit impulse can be determined in practice, and the limits of integration are chosen accordingly.

The "unit impulse" is in practice often obtained by means of a pistol shot, a tone burst or other short lasting sound phenomena. Normally band-limited noise is used, to be able to determine the reverberation as a function of frequency. As soon as the noise is band-limited, equation (B.1) does not hold in a strict mathematical sense, because a certain time correlation is imposed upon the noise. If the effective correlation interval is small compared with any part of interest in the reverberation decay process, equation (B.1) is still valid in a practical sense.

To obtain the true impulse response, the length of the impulse used to determine the response of the filter room should be short compared to the period of the filter centre frequency.

APPENDIX [C]

FREE VIBRATION OF ECCENTRICALLY STIFFENED CYLINDRICAL SHELLS

Derivation of Basic Equations

The free vibration of a thin-walled circular cylindrical shell which is stiffened by evenly spaced uniform rings and/or stringers as shown in figure (C1) is considered in reference (10). In plane inertias are neglected, and it is assumed that the stiffener spacing is small compared with the vibration wavelength so that its effect on the behaviour of the cylinder may be averaged (smeared out). The strain energies of the cylinder and stiffeners are presented and the displacement of the stiffeners and the cylinder are required to be compatible. After formulating the potential energy of inertial loading, the equations of dynamic equilibrium and consistent boundary conditions are obtained by applying the method of minimum potential energy to the total energy of the system.

Strain Energy of Isotropic Cylinder

The strain energy of the unstiffened thin-walled isotropic cylinder is:

$$II_c = \frac{E}{2(1-\mu^2)} \int_{-t/2}^{t/2} \int_0^{2R} \int_0^{a} (e^2_{xT} + e^2_{yT} + 2\mu e_{xT} e_{yT} + \frac{1-\mu}{2} \gamma^2{}_{xyT}) dxdydz \quad (C1)$$

The linear Donnell-type strain-displacement relations are

$$e_{xT} = e_x - zw,_{xx} \tag{C2}$$

$$e_{yT} = e_y - zw,_{yy} \tag{C3}$$

$$\gamma_{xyT} = \gamma_{xy} - 2zw,_{xy} \tag{C4}$$

where the middle-surface strains are defined as

$$e_x = u,_x$$

$$e_y = v,_y + \frac{w}{R}$$

$$\gamma_{xy} = u,_y + v,_x$$

Substitution of equations (2), (3) and (4) into equation (1) and integration with respect to z yields the following expression for cylinder strain energy:

$$II_c = \frac{Et}{2(1-\mu^2)} \int_o^{2\pi R} \int_o^a [u^2,_x \quad (v_{,y} + \frac{w}{R})^2 \; [\; 2\mu u_x(v_y + \frac{w}{R}) +$$

$$\frac{1-\mu}{2}(u,y + v,x)^2]dx\, dy + \frac{D}{2} \int_o^{2\pi R} \int_o^a [w^2,_{xx} + w^2,_{yy} + 2\mu w,_{xx}\, w,_{yy} +$$

$$2(1-\mu)w^2,_{xy}]dx\, dy \tag{C5}$$

In this equation, $D = \dfrac{Et^3}{12(1-\mu^2)}$ is the flexural stiffness of the cylinder.

Strain Energy of Stiffeners

The strain energy of the stiffeners is derived on the basis that the displacements in the cylinder and stiffeners are equal at the point of attachment and stiffener twisting is accounted for in an approximate manner. In cases where both rings and stringers are attached to the same surface of the shell, the effect of joints in the stiffener framework is ignored.

Stringer Energy

The total strain energy of N stringers on the cylinder is written as

$$II_s = \sum_{j=1}^{N} \left(\int_0^a \int_{A_s} \frac{E_s}{2} \; e_{xT}^2 \; dA_s dx + \frac{G_s J_s}{2} \int_0^a w_{,xy}^2 \; dx \right) j \quad . \qquad (C6)$$

where the first term inside the parentheses of equation (6) is the strain energy of bending and extension in the stringer, and the second term is the strain energy involved in twisting of the stringer. The quantity dA_s is an element of the cross-sectional area of the stringer and $G_s J$ is the twisting stiffness of the stringer section. After substitution from equation (2), the first term inside the parentheses of equation (6) can be written as follows:

$$\int_0^a \frac{E_s}{2} (u^2{}_{,x} \int_{A_s} dA_s - 2u_{,x} \, w_{,xx} \int_{A_s} 2dA_s + w^2{}_{,xx} \int_{A_s} Z^2 dA_s) \, dx$$

The first integral inside the parentheses is the srea of the stringer cross scetion A_s, the second integral is the first moment of the area ($\bar{Z}_s A_s$) where $\bar{Z}_s$ is the distance from the middle surface of the isotropic shell ($Z = 0$) to the centroid of the stringer cross section, and the third integral is the moment of inertia of the stringer (I_{os}) about $Z = 0$.

NOTE that the centroidal distance $\bar{Z}_s$ is positive for stringers on the outer surface of the cylinder and negative for internal stringer. If the stringer spacing d is sufficiently small, the effect of the stringer can be averaged or smeared out, and an integral may be written instead of the finite sum. Equation (6), the total strain energy of the stringer, is now written as

$$II_s = \frac{1}{d} \int_0^{2\pi R} \int_0^a [\frac{E_s}{2} (A_s u_x^2 - 2\bar{Z}_s A_s u_x w_{xx} + I_{os} w^2{}_{xx}) + \frac{G_s J_s}{2} w^2{}_{xy}] dxdy \qquad (C7)$$

Ring Energy

By utilizing an approach similar to that used for stringer, the total strain energy of the rings is found as

$$II_r = \frac{1}{\ell} \int_0^{2\pi R} \int_0^a \{ \frac{E_r}{2} [A_r (v_y + \frac{w}{R})^2 - 2Z_r A_r (v_y + \frac{w}{R}) w_{yy} + I_{ox} w^2{}_{yy}]$$

$$+ \frac{G_r J_r}{2} w^2{}_{xy} \} dxdy \qquad (C8)$$

where ℓ is the ring spacing, A_r is the area of the ring cross section, $\bar{Z}_r$ is the distance from the middle surface of the isotropic shell ($Z = 0$) to the centroid of the ring, I_{or} is the moment of inertia of the ring cross section about $Z = 0$, and $G_r J_r$ is the twisting stiffness of the ring.

POTENTIAL ENERGY OF INERTIAL LOADING

If the stiffened cylinder is undergoing simple harmonic motion of circular frequency ω (inplane inertias neglected), and $w(x,y)$ is the deflection shape at the time of maximum deflection, the potential energy due to inertia load is written as in reference (10) as

$$\Pi_\omega = -\frac{1}{2} \int_0^{2\pi R} \int_0^a M\omega^2 w^2 \, dx \, dy \tag{9}$$

where $M = \rho_c t + \rho_s \frac{A_s}{d} + \rho_r \frac{A_r}{\ell}$ is the averaged smeared-out mass per unit area of the stiffened cylinder. The quantities ρ_c, ρ_s and ρ_r are the mass densities of the cylinder, stringers and rings, respectively.

EQUILIBRIUM EQUATION AND BOUNDARY CONDITIONS FOR STIFFENED CYLINDERS

The total potential energy Π of the system is the sum of the energies given by equations (5), (7), (8) and (9).

$$\Pi = \Pi_c + \Pi_s + \Pi_r + \Pi_\omega$$

The method of minimum potential energy ($\delta\Pi=0$) may now be applied to equation (10). By allowing the variation of three displacements δu, δv and δw to be arbitrary and by utilizing the fundamental lemma of the calculus of variations, the three differential equations of dynamic equilibrium for the stiffened cylinder are found to be

$$[1 + \frac{E_s A_s (1-\mu^2)}{Etd}]u_{xx} + \frac{1-\mu}{2} u_{yy} + \frac{1+\mu}{2} v_{xy} + \frac{M}{R} wx - \frac{Z_s E_s A_s (1-\mu^2)}{Etd} w_{xx} = 0 \quad (C11)$$

$$[1 + \frac{E_r A_r (1-\mu^2)}{Et\ell}]v_{yy} + \frac{1-\mu}{2} v_{xx} + \frac{1+\mu}{2} u_{xy} + [1 + \frac{E_r A_r (1-\mu^2)}{Et\ell}] \frac{w_y}{R}$$

$$- \frac{\bar{Z}_r E_r A_r (1-\mu^2)}{Et\ell} w_{yyy} = 0 \quad (C12)$$

$$D\nabla^4 w + \frac{Et}{R(1-\mu^2)} (v_y + \frac{w}{R} + \mu u_x) - \frac{\bar{Z}_s E_s A_s}{d} u_{xxx} + E_s \frac{(I_s + \bar{Z}_s^2 A_s)}{d} w_{xxxx}$$

$$+ \frac{E_r A_r}{R^2 \ell} w + E_r \frac{(I_r + \bar{Z}_r^2 A_r)}{\ell} w_{yyyy} + \frac{E_r A_r}{R\ell} v_y - \frac{\bar{Z}_r E_r A_r}{\ell} v_{yyy}$$

$$- \frac{2\bar{Z}_r E_r A_r}{R\ell} w_{yy} + (\frac{G_s J_s}{d} + \frac{G_r J_r}{\ell}) w_{xxyy} - M\omega^2 w = 0 \quad (C13)$$

Note that in equation (13), the moment of inertia of the stiffeners has been transferred by the following relations:

$$I_{os} = I_s + \bar{Z}_s^2 A_s$$

$$I_{or} = I_r + \bar{Z}_r^2 A_r$$

where I_s and I_r are the moments of inertia of the stringers and rings, respectively, about their centroidal axes.

In addition to the equilibrium equations, the method of minimum potential energy yields the appropriate boundary conditions. The homogeneous boundary conditions to be prescribed at each end of the cylinder are obtained from the energy variation ($\delta \Pi = 0$) as follows:

$$D(w,_{xxx} + \mu w,_{yyx}) + E_s \frac{(I_s+\bar{Z}_s^2 A_s)}{d} w,_{xxx} - \frac{\bar{Z}_s E_s A_s}{d} u,_{xxx}$$

$$+ \left(\frac{Gt^3}{3} + \frac{G_s J_s}{d} + \frac{G_r J_r}{\ell}\right) w,_{xyy} = 0 \qquad \text{(C14a)}$$

$$\text{or} \quad w = 0 \qquad \text{(C14b)}$$

$$D(w,_{xx} + \mu w,_{yy}) + E_s \frac{(I_s+\bar{Z}_s^2 A_s)}{d} w,_{xx} - \frac{\bar{Z}_s E_s A_s}{d} u,_{x} = 0 \qquad \text{(C15a)}$$

$$\text{or} \quad w_x = 0 \qquad \text{(C15b)}$$

$$\frac{Et}{1-\mu^2} [u,_x+\mu(v,_y+ \frac{w}{R})] + \frac{E_s A_s}{d} u,_x - \frac{Z_s E_s A_s}{d} w,_{xx} = 0 \qquad \text{(C16a)}$$

$$\text{or} \quad u = 0 \qquad \text{(C16b)}$$

$$G\,t(w,_y + v,_x) = 0 \qquad \text{(C17a)}$$

$$\text{or} \quad v = 0 \qquad \text{(C17b)}$$

The natural boundary conditions are given by equations (14a), (15a), (16a) and (17a) and the geometric boundary conditions are given in equations (14b), (15b), (16b) and (17b). The conditions in equation (14a) requires that a quantity comparable to the Kirchoff shear is prescribed and hence is a free-edge boundary condition. The three natural boundary conditions in equations (15a), (16a) and (17a) correspond to conditions in which the edge moment resultant, the normal stress resultant and the shearing stress resultant, respectively, are prescribed.

As a matter of interest the equilibrium equations (eqs.(11) to(13) and the boundary conditions (esq.(14) to (17) may also be written in terms of stress and moment resultants. In this form the equilibrium equations become

$$N_{x,x} + N_{xy,y} = 0 \tag{C18}$$

$$N_{y,y} + N_{xy,x} = 0 \tag{C19}$$

$$- M_{x,xx} - M_{xy,xy} + M_{yx,xy} - M_{y,yy} + \frac{N_y}{R} - M\omega^2 w = 0 \tag{C20}$$

and the boundary conditions which must be prescribed at each end of the cylinder become:

$$M_{x,x} - (M_{xy,y} - M_{yx,y}) = 0 \tag{C21a}$$

$$\text{or} \quad w = 0 \tag{C21b}$$

$$M_x = 0 \tag{C22a}$$

$$\text{or} \quad w,_x = 0 \tag{C22b}$$

$$N_x = 0 \tag{C23a}$$

$$\text{or} \quad u = 0 \tag{C 23b}$$

$$N_{xy} = 0 \tag{C 24a}$$

$$\text{or} \quad v = 0 \tag{C 24b}$$

where

$$M_x = -[D(w,_{xx} + \mu w,_{yy}) + E_s \frac{(I_s+\bar{Z}_s{}^2A_s)}{d} w,_{xx} - \frac{\bar{Z}_sE_sA_s}{d} u,_x]$$

$$M_y = -[D(w,_{yy} + \mu w,_{xx}) + E_r \frac{(I_r+\bar{Z}_r{}^2A_r)}{\ell} w,_{yy} - \frac{\bar{Z}_rE_rA_r}{\ell}(v,_y + \frac{w}{R})]$$

$$M_{xy} = (\frac{Gt^3}{6} + \frac{G_sJ_s}{d})w,_{xy} \tag{C25}$$

$$M_{yx} = -(\frac{Gt^3}{6} + \frac{G_rJ_r}{\ell})w,_{xy}$$

$$N_x = \frac{Et}{1-\mu^2}[u,_x + \mu(v,_y + \frac{w}{R})] + \frac{E_sA_s}{d}u,_x - \frac{\bar{Z}_sE_sA_s}{d}w,_{xx}$$

$$N_y = \frac{Et}{1-\mu^2}(v,_y + \mu u,_x) + \frac{E_rA_r}{\ell}(v,_y + \frac{w}{R}) - \frac{\bar{Z}_rE_rA_r}{\ell}w,_{yy} \tag{C26}$$

$$N_{xy} = Gt(u,_y + v,_x)$$

Equilibrium Equations and Boundary Conditions for Stiffened Flat Plates

Dynamic equilibrium equations and appropriate boundary conditions were derived by following the procedure already outlined for stiffened cylinders. For an isotropic plate, the middle-surface strain-displacement relations employed for the cylinder are replaced by

$$
\begin{aligned}
e_x &= u,_x \\
e_y &= v,_y \\
\gamma_{xy} &= u,_y + v,_x
\end{aligned}
\tag{C27}
$$

If the same procedure is followed, equilibrium equations identical to equations (11), (12) and (13) with R taken to be infinitely large are obtained as follows:

$$
1 + [\frac{E_s A_s (1-\mu^2)}{Etd}]\, u,_{xx} + \frac{1-\mu}{2}\, u,_{yy} + \frac{1+\mu}{2}\, v,_{xy} - \frac{\bar{z}_s E_s A_s (1-\mu^2)}{Etd}\, w,_{xxx} = 0 \tag{C28}
$$

$$
1 + [\frac{E_r A_r (1-\mu^2)}{Et\ell}]\, v,_{yy} + \frac{1-\mu}{2}\, v,_{xx} + \frac{1+\mu}{2}\, u,_{xy} - \frac{\bar{z}_r E_r A_r (1-\mu^2)}{Et\ell}\, w,_{yyy} = 0 \tag{C29}
$$

$$
D\nabla^4 w - \frac{\bar{z}_s E_s A_s}{d}\, u,_{xxx} + \frac{E_s (I_s + \bar{z}_s^2 A_s)}{d}\, w,_{xxx} + \frac{E_r (I_r + \bar{z}_r^2 A_r)}{\ell}\, w,_{yyy}
$$

$$
+ (\frac{G_s J_s}{d} + \frac{G_r J_r}{\ell})\, w,_{xxyy} - \frac{\bar{z}_r E_r A_r}{\ell}\, v,_{yyy} - M\omega^2 w = 0 \tag{C30}
$$

where $M = (\rho_p t + \rho_s \frac{A_s}{d} + \rho_r \frac{A_r}{\ell})$. The subscript s refers to the stiffeners in the x-direction and the subscript r refers to the cross stiffeners in the y-direction.

The appropriate homogensous boundary conditions obtained from the variational procedure are as follows:

For edges parallel to the y-axis,

$$D(w,_{xxx} + \mu w,_{yyx}) + \frac{E_s(I_s+\bar{z}_s^2A_s)}{d} w,_{xxx} - \frac{\bar{z}_sE_sA_s}{d} u,_{xx}$$

$$+ (\frac{Gt^3}{3} + \frac{G_sJ_s}{d} + \frac{G_rJ_r}{\ell}) w,_{xyy} = 0 \qquad \text{(C31a)}$$

$$\text{or } w = 0 \qquad \text{(C31b)}$$

$$D(w,_{xx} + \mu w,_{yy}) + \frac{E_s(I_s+\bar{z}_s^2A_s)}{d} w,_{xx} - \frac{\bar{z}_sE_sA_s}{d} u,_x = 0 \qquad \text{(C32a)}$$

$$\text{or } w,_x = 0 \qquad \text{(C32b)}$$

$$\frac{Et}{1-\mu^2}(u,_x+\mu v,_y) + \frac{E_sA_s}{d} u,_x - \frac{\bar{z}_sE_sA_s}{d} w,_{xx} = 0 \qquad \text{(C33a)}$$

$$\text{or } u = 0 \qquad \text{(C33b)}$$

$$Gt(u,_y + v,_x) = 0 \qquad \text{(C34a)}$$

$$\text{or } v = 0 \qquad \text{(C34b)}$$

and for edges parallel to the x-axis

$$D(w,_{yyy} + \mu w,_{xxy}) + \frac{E_r(I_r+\bar{z}_r^2A_r)}{\ell} w,_{yyy} - \frac{\bar{z}_rE_rA_r}{\ell} v,_{yy}$$

$$+ (\frac{Gt^3}{3} + \frac{G_sJ_s}{d} + \frac{G_rJ_r}{\ell}) w,_{yxx} = 0 \qquad \text{(C35a)}$$

$$\text{or } w = 0 \qquad \text{(C35b)}$$

$$D(w,_{yy}+\mu w,_{xx}) + \frac{E_r(I_r+\bar{z}_r^2A_r)}{\ell} w,_{yy} - \frac{\bar{z}_rE_rA_r}{\ell} v,_y = 0 \qquad \text{(C36a)}$$

$$\text{or } w,_y = 0 \qquad \text{(C36b)}$$

$$\frac{Et}{1-\mu^2}(v,_y+\mu u,_x) + \frac{E_r A_r}{\ell} v,_y - \frac{\bar{z}_r E_r A_r}{\ell} w,_{yy} = 0 \tag{C37a}$$

$$\text{or } v = 0 \tag{C37b}$$

$$Gt(u,_y + v,_x) = 0 \tag{C38a}$$

$$\text{or } u = 0 \tag{C38b}$$

In addition to these boundary conditions, the following relationships were to be satisfied at free corners

$$w,_{xy} = 0 \tag{C39}$$

Solution for Simply Supported Stiffened Cylindrical Shells

The co-ordinate system chosen has its origin located at one end of the cylinder shown in Appendix [C]. The simple-support boundary condition to be satisfied at each end $x = 0,a$ are

$$w = Mx = v = Nx = 0 \tag{C40}$$

The expressions for the displacements u, v and w which satisfy these boundary conditions, are given as:

$$\begin{aligned} u &= \bar{u} \cos \frac{m\pi x}{a} \cos \frac{ny}{R} \\ v &= \bar{v} \sin \frac{m\pi x}{a} \sin \frac{ny}{R} \\ w &= \bar{w} \sin \frac{m\pi x}{a} \cos \frac{ny}{R} \end{aligned} \tag{C41}$$

where m is the number of axial half waves and n is the number of circumferential full waves. After substitution of equations (41) into the equilibrium equations (11), (12) and (13), the following expression is obtained after some manipulation:

$$\begin{bmatrix} -[1+\bar{s}(1-\mu^2)+\beta^2(\frac{1-\mu}{2})] & -(\frac{1+\mu}{2}) & [\mu+\bar{s}(\frac{\bar{z}_s}{R})(1-\mu^2)\alpha^2] \\ -(\frac{1+\mu}{2}) & -[1+\bar{R}(1-\mu^2)+\frac{1-\mu}{2\beta^2}] & [1+\bar{R}(1-\mu^2)+(\frac{z_r}{R})\bar{R}(1-\mu^2)n^2] \\ [\mu+\bar{s}(\frac{\bar{z}_s}{R})(1-\mu^2)\alpha^2 & [1+\bar{R}(1-\mu^2)+(\frac{\bar{z}_r}{R})\bar{R}\,(1-\mu^2)n^2] & B_{33} \end{bmatrix} \begin{bmatrix} \bar{u} \\ \bar{v} \\ \bar{w} \end{bmatrix} = \begin{bmatrix} 0 \\ 0 \\ 0 \end{bmatrix} \tag{C42}$$

where

$$B_{33} = -D\alpha^4(1-\mu^2)(1+\beta^2)^2 - 1 - \bar{R}(1-\mu^2) + \frac{M\omega^2R^2(1-\mu^2)}{Et} - \frac{E_s\alpha^4(1-\mu^2)(I_s+z_s^2A_s)}{R^2dEt}$$

$$- \frac{E_rn^4(1-\mu^2)(I_r+\bar{z}_r^2A_r)}{R^2\ell Et} - 2\bar{R}n^2(\frac{\bar{z}_r}{R})(1-\mu^2)$$

$$- (\frac{G_sJ_s}{d} + \frac{G_rJ_r}{\ell}) \quad [\frac{\alpha^2n^2(1-\mu^2)}{EtR^2}]$$

and the following nondimensional parameters are defined:

$$\beta = \frac{na}{m\pi R}, \quad \bar{s} = \frac{E_sA_s}{Etd}$$

$$\alpha = \frac{m\pi R}{a}, \quad \bar{R} = \frac{E_rA_r}{Et\ell}$$

To obtain a nontrivial solution, the determinant of the coefficients of $\bar{u}$, $\bar{v}$ and $\bar{w}$ is set equal to zero. After more manipulation, the frequency equation (4.4) was obtained and is given in Chapter (4).

Solution for simply supported stiffened flat plate

A coordinate system is chosen having the origin at one corner of a plate of length 'a' and width 'b'. The simple-support boundary conditions which must be satisfied are

$$w(0,y) = w(a,y) = w(x,0) = w(x,b) = 0$$
$$M_x(0,y) = M_x(a,y) = M_y(x,0) = M_y(x,b) = 0$$
$$N_x(0,y) = N_x(a,y) = N_y(x,0) = N_y(x,b) = 0$$
$$v(0,y) = v(a,y) = u(x,0) = u(x,b) = 0$$

Expressions for the displacements u, v and w which satisfy that boundary conditions are:

$$\left.\begin{aligned} u &= \bar{u}\cos\frac{m\pi x}{a}\sin\frac{n\pi y}{b} \\ v &= \bar{v}\sin\frac{m\pi x}{a}\cos\frac{n\pi y}{b} \\ w &= \bar{w}\sin\frac{m\pi x}{a}\sin\frac{n\pi y}{b} \end{aligned}\right\} \qquad (C43)$$

where for flat plate m and n are the number of half waves in the x and y-directions, respectively.

Following a procedure similar to that used in the previous section, the frequency equation (4.6) was obtained and is given in Chapter (4).

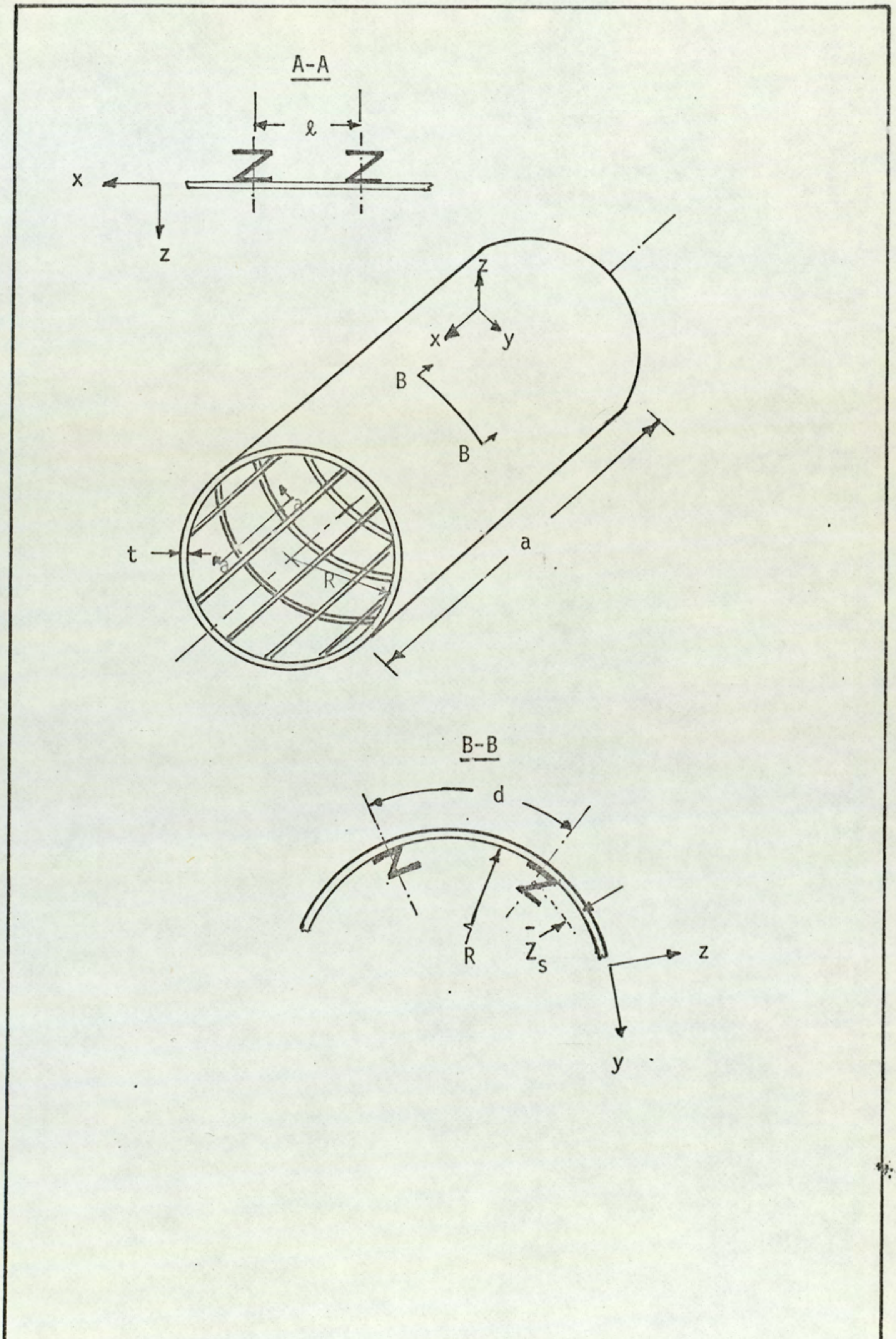

Geometry of stiffened cylinder

Fig. C1